Synthesis and Characterisation of Mononuclear and Dinuclear Rhenium Carbonyl Complexes.

by

Claire Brennan, BSc.

A Thesis presented to Dublin City University for the degree of Doctor of Philosophy.

Supervisor's Dr. Mary Pryce and Prof. J.G. Vos

School of Chemical Sciences

Dublin City University

August 2007

Authors Declaration

I hereby certify that this material, which I now submit for assessment on the programme of study leading to award of Doctor of Philosophy by research and thesis, is entirely my own work and has not been taken from the work of others, save and to extent that such work has been cited and acknowledged within the text of my work.

Signed: Claire Brennan

Claire Brennan

Student I.D. No.: 97565687

Date: 24/03/07.

Dedicated to my parents, Mary and Vivion

Abstract

Chapter One serves as an introduction to the Thesis. **Chapter Two** describes the synthesis and characterisation of a series of 3-(pyridin-2-yl)-1,2,4-triazole ligands and the corresponding rhenium(I) tricarbonyl. The structure of the complexes have been determined using NMR and IR spectroscopy. The complexes underwent [Re→π*(pyridyl-triazole)] transitions in the 295 – 360 nm region of the absorption spectrum. Emission was observed from all the complexes at 298 K and at 77 K. The absorption and emission properties of the pyridyl-triazole complexes were found to be pH dependent. The complexes underwent an irreversible Re(I)/Re(II) oxidation. The σ-donor nature of the triazole ligand results in a blue shift of both the absorption and emission spectra when compared to $[Re(CO)_3(bpy)Cl]$.

Chapter Three is discusses the synthesis of the rhenium(I) tricarbonyl complexes of 3-(pyrazin-2-yl)-1,2,4-triazoles, analogous to those described in Chapter Two. The complexes were characterised by NMR and IR spectroscopy. The carbonyl bands are observed at higher frequency compared to the corresponding pyridyl-triazole complexes. The UV/vis spectra exhibit [Re→π*(pyrazyl-triazole)] transitions between 390 and 410 nm. The protonated pyrazyl-triazole complexes are weak emitters at 298 K while emission was detected at room temperature from all of the deprotonated pyrazyl-triazole complexes. Emission was detected from all complexes at 77 K. The strongly π-accepting pyrazine results in a red shift of both the absorption and emission spectra when compared to the corresponding pyridyl-triazole complexes. Again, spectroscopic and electrochemical studies display a strong pH dependency.

Chapter Four describes the synthesis and characterisation of the homo-nuclear rhenium(I) dimer and the hetero-nuclear ruthenium(II)-rhenium(I) dinuclear complexes bridged by the triazole ligand Hbpt (3,5-bis(pyridin-2-yl)-1,2,4-triazole). The complexes have been studied using UV-vis and emission spectroscopy, lifetime studies and electrochemical measurements. For the ruthenium(II)-rhenium(I) complex, the absorption and emission properties indicate intercomponent energy transfer from the rhenium(I) metal centre to the ruthenium(II) metal centre.

Chapter Five discusses the methylation of the ruthenium(II) bipyridyl complex $[Ru(bpy)_2phpztr]^+$, (phpztr = 3-(pyrazin-2-yl)-5-phenyl-1,2,4-triazole). Selective deuteriation of the bipyridyl ligands and the triazole ligand was also employed. The photophysical and electrochemical properties of all complexes were also examined. Methylation of the pyrazyl-triazole ligand was found to quench emission from $[Ru(bpy)_2phpztr]^+$. Wavelength dependent ground-state resonace Raman measurements were also carried out in order to elucidate the electronic transitions in the absorption spectra. **Chapter Six** gives an overview of the experimental conditions used. **Chapter Seven** summaries results of the work undertaken with suggestions on further possible research directions.

Acknowledgements

First of all, I would like to thank my supervisors, Mary Pryce and Han Vos for their help, advice and patience during the last number of years. Special thanks to my family for their support over the years. My thanks also go to the HVRG past and present. To the Mary Pryce group, Tony and Nikki. To those that have moved on; Jennifer, Jonathan, Kieran and Karl for the laughs both inside and out of the lab. Thanks also to all the Chemistry postgrads new and old.

I must thank all my friends through the years for taking my mind off the chemistry and giving me some great memories; Aoife, Una, Deirdre, Anne-Marie, Martina and Ashlin. A big thanks to Fiona Lynch for all her help and counselling over the past few years!

Huge thanks to the technical staff in the department, Mick, Damien, Maurice, Ambrose, Vinnie, John, Veronica and Ann. Without your help this thesis would not have been possible. Thanks to Dr. Andrea Mc Nally and Dr. Fiona Killard for assistance with lifetime measurements. Special thanks to Dr. Wesley Browne and Prof. J.J. McGarvey for help with resonance Raman measurements in Belfast.

Finally I would like to thank Louth County Council for financial support.

Chapter 1

Introduction

Chapter 1 serves as an introduction to many of the subjects that are discussed in this thesis. Firstly, supramolecular chemistry is introduced. The development of this area of chemistry is outlined and its relevance to this thesis is highlighted. In order to understand the processes involved in a supramolecular species, it is important to first understand the fundamental properties of the simpler subunits of the supramolecular species. Hence an introduction to coordination chemistry and the photophysical pathways in transition metal complexes is outlined. The "reference" complex of many of the complexes discussed in this thesis, [Re(CO)$_3$(bpy)Cl], and its importance to the area of inorganic chemistry is highlighted. Finally, a summary of various polypyridyl briding ligands is given by discussing their structural and electronic properties and their influence on metal-metal interactions in hetero-nuclear ruthenium(II)-rhenium(I) dinuclear complexes

1.1 Introduction to supramolecular chemistry

Photosynthesis is an efficient biological process that converts solar energy into chemical energy. Photosynthesis is the link between the sun and the energy needs of the living world. Over the last few decades much attention has been focused on artificial photosynthesis. The aim of artificial photosynthesis is to synthesise complexes that follow nature's principle for water oxidation and to exploit the properties of these complexes to generate energy (e.g. H_2) from a sustainable and renewable source such as water.[1,2] These complexes are known as supramolecular complexes.

The most widely accepted definition of supramolecular chemistry is "the chemistry beyond the molecule, bearing on the organised entities of higher complexity that result from the association of two or more chemical species held together by intermolecular forces."[3,4] A chemical species can be described as a single unit (large molecule) or as made of distinct components (supramolecule). The difference between these two classes of compounds is based on the degree of interaction between the component units. When the interaction between subunits is small, the system can be viewed as a supramolecular system. The system is described as a large molecule if the interaction is strong.[5] Supramolecular systems are composed of individual components linked together through covalent bonds or through intermolecular forces such as Coulombic interactions or hydrogen bonds.[6] There are three types of supramolecular systems.[7] The first group involves second-sphere coordination compounds, i.e. complexes associated to other species by electrostatic interactions, hydrogen bonds or other intermolecular forces. The second group are cage-type coordination compounds, i.e. complexes in which a metal is encapsulated in a polydentate ligand. The third group involves molecular building blocks linked via bridging units by covalent or coordination bonds. The distinction between a large and a supramolecular species is based on the degree of interaction of the electronic

subsystems of the component units, regardless of the nature of intercomponent bonding.[8]

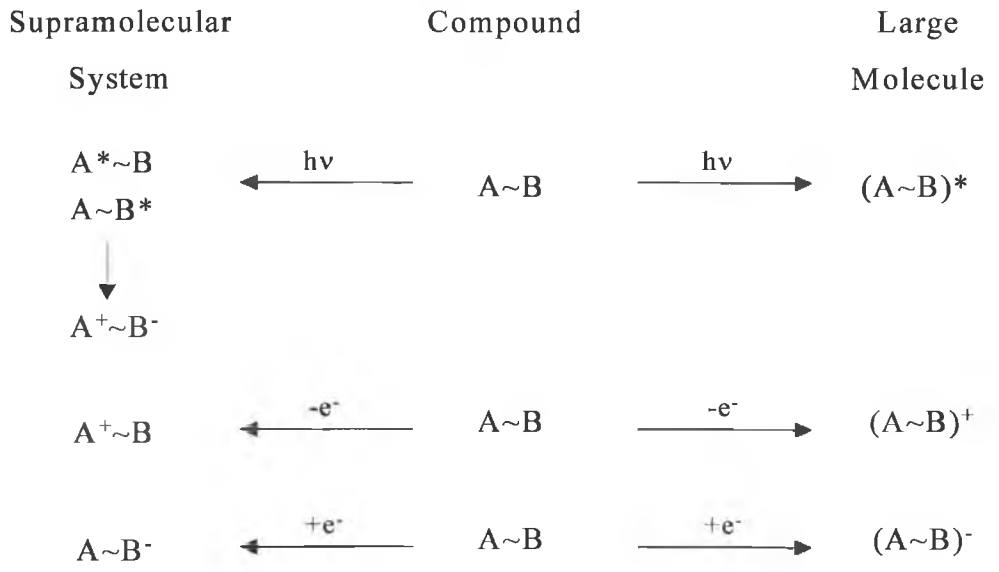

Figure 1. 1 *Schematic representation of the difference between a supramolecular system and a large molecule based on the effects caused by a photon or an electron input. The symbol "~" represents any type of bond that keeps the units A and B together i.e. coulombic or covalent.*

The above diagram (Figure 1. 1) aids in the definition of a supramolecular system. When A~B is irradiated and the excited states are delocalised on both A and B, the species is better considered as a large molecule. If the absorption of a photon by A~B leads to one of its subunits (A or B) forming an excited state rather than the whole molecule, this system can be classed as a supramolecular system. For the system A~B regardless of whether A or B is excited, the supramolecular system has two options. It may relax back to the ground state (with the release of energy as light or heat) or charge transfer may occur forming A^{+}~B^{-}. Charge recombination usually

occurs unless a quenching molecule is present to oxidise/reduce the charge separated species A^{+}~B^{-}.

Each component of a supramolecular species has its own individual properties, but when coupled together produce new photophysical and photochemical processes. In principle the properties of the molecular components of a supramolecular species can be obtained from the study of the isolated components.

1.2 Intercomponent processes in supramolecular complexes

The most important processes of supramolecular systems are those taking place between components. Of particular importance are the two processes that follow light excitation of a component. For example in a supramolecular species A~B, light excitation of A can be followed by energy or electron transfer processes as in Equations 1.1 to 1.3.

A~B + $h\nu$	→	*A~B	photoexcitation	1. 1
*A~B	→	A~B*	energy transfer	1. 2
*A~B	→	A^{+}~B^{-}	electron transfer	1. 3

The fundamental principles which govern photoinduced energy- and electron-transfer processes will be discussed in this section.

1.2.1 Energy transfer

Electronic energy transfer can occur via two mechanisms: the Förster-type mechanism[9] and the Dexter-type mechanism.[10]

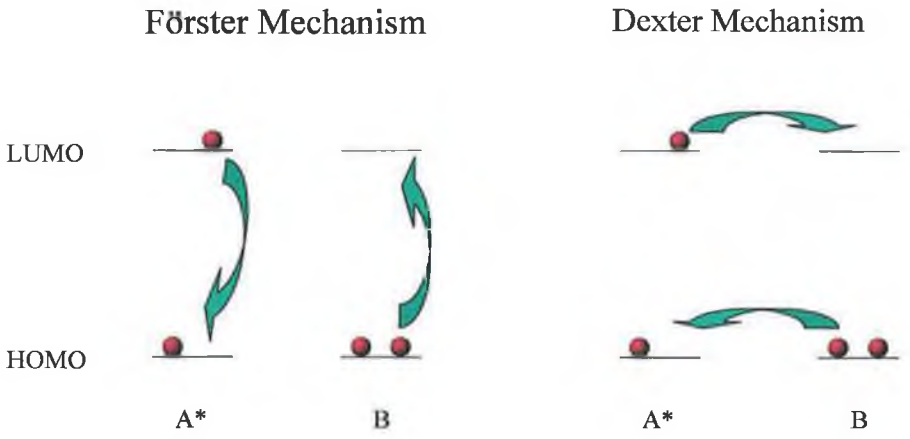

Figure 1. 2 *Schematic representation of energy transfer with a Förster-type or Dexter-type mechanism. A* is a component of supramolecular system (A~B) in the excited state.*[11]

The Förster-type mechanism takes place through a dipole-dipole interaction. In this mechanism (see Figure 1. 2) the excited state of a donor molecule (A*) behaves as an oscillating dipole, generating an electric field. When the other component B is in the collisional space of A* it will start to resonate, resulting in the formation of B* and A. No exchange of electrons occurs. The Förster-type mechanism is most effective when singlet excited states are involved i.e between large aromatic molecules. Since the only long-lived excited states in transition metal complexes are triplet excited states and transitions to the corresponding singlet ground-states are spin forbidden, this mechanism is not common among transition metal complexes. The dipole-dipole coulombic interaction maximises when the transition moments of the donor and acceptor are parallel and vanish when they are orthogonal.

The second energy transfer mechanism is known as a Dexter-type mechanism. The Dexter mechanism is a short-range mechanism that requires physical contact between the donor and acceptor components of a supramolecular system. The exchange interaction (*Figure 1. 2*) can be seen as the simultaneous exchange of two electrons between the donor (A) and the acceptor (B). For the Dexter contact exchange interaction, the donor and acceptor must be able to approach each other without being sterically hindered so as to allow spatial overlap of their molecular orbitals. Transfer of energy may only occur between states of similar multiplicity. When the donor and acceptor are covalently linked in supramolecular system, the presence of the bridging group is extremely important in determining donor acceptor interaction. The major factors influencing the rates of energy transfer in the Dexter mechanism are (i) energy gradient, (ii) distance, (iii) orientation of molecular components, (iv) electronic structure of the bridge and the number of intervening bonds.

1.2.2 Electron transfer

As illustrated in Figure Figure 1. 3, absorption of a photon of light by component "A" in the supramolecular species A~B, generates the excited state *A~B. It is well known that because of the higher energy content, an excited state is both a stronger reductant and stronger oxidant than the corresponding ground-state.[8,12] Hence an electron may now be transferred to the second component "B", generating the charge separated species A^{+}~B^{-}. This process is termed electron transfer. Note the charge separated species A^{+}~B^{-} may revert back to the ground-state by back electron transfer or may be used to carry out a desired function.

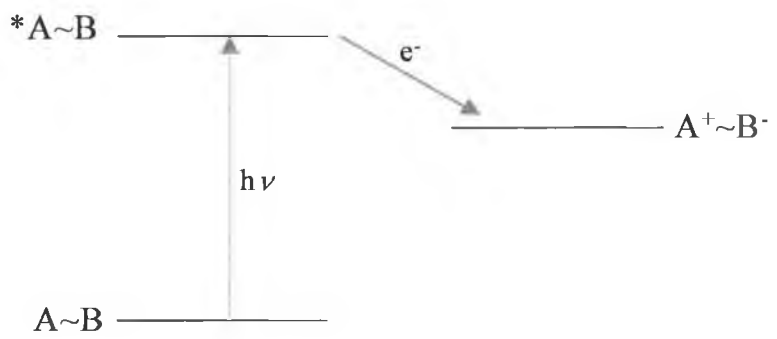

Figure 1. 3 *Schematic representation of energy levels for electron transfer in a supramolecular species A~B.*

The parameters that govern the extent of electron transfer between two components in a supramolecular system are orbital overlap and the energy gap between the units. Hence an understanding of bonding and excited state dynamics is essential in the design of useful supramolecular systems. This will be discussed in the following section.

1.3 Principles of molecular photophysics

Knowledge of the paths of energy degradation in inorganic systems is essential in the understanding of the spectroscopy and photochemistry of inorganic complexes as well as in the design of useful supramolecular systems. This knowledge requires understanding the dynamics, the pathways and the efficiencies of interconversion between different excited states and between excited states and the ground state.

1.3.1 The nature of light

The term "light" usually refers to electromagnetic radiation in the visible, near ultraviolet and near infrared spectral range. There are two models used to describe the nature of light. In the wave model, electromagnetic radiation is characterised by a wavelength (λ), a frequency (ν) and a velocity (c). The three quantities are related by the following relationship:

$$c = \nu\lambda \qquad 1.4$$

The velocity value is a constant (2.988 x 10^8 ms^{-1} in a vacuum) while the wavelength and frequency may vary.

In the quantum model a beam of radiation is described as a stream of *photons* or *quanta*. A photon has no mass but it has a specific energy (E) directionally proportional to the frequency (ν) of the radiation. This relationship is depicted in the following equation:

$$E = h\nu \qquad 1.5$$

The term h is termed Plancks constant (6.63 x 10^{-34} Js). This description of light as a stream of photons is essential to photochemistry. The interaction of light with molecular systems is generally an interaction between one molecule and one photon of light.

1.3.2 Electronic structures and transitions

It is necessary to understand some basic chemistry surrounding transition metal complexes before discussing the spectroscopic and photochemical properties of rhenium complexes. The following diagram (Figure 1. 4) shows a basic ligand field model for a transition metal octahedral complex. This simplified diagram illustrates the transitions responsible for the electronic absorption spectra of transition metal complexes. The various molecular orbitals (MO) can be classified according to their predominant atomic orbital contribution:

i) Strongly bonding, ligand-centred σ_L orbitals.

ii) Bonding, ligand-centred π_L orbitals.

iii) Essentially non-bonding $\pi_M(t_{2g})$, metal-centred *d* orbitals.

iv) Anti-bonding $\sigma^*_M(e_g)$, metal-centred *d* orbitals.

v) Ligand-centred, antibonding π^*_L orbitals.

vi) Strongly anti-bonding, metal-centred σ^*_M orbitals.

In the ground state configuration of the metal complex, the σ_L and π_L molecular orbitals are completely filled. The π_M molecular orbitals are either partially or completely filled depending on the number of d electrons in the transition metal ion. The higher orbitals (π_L^*, σ_M^*) are generally empty. There are many different allowed transitions between different molecular orbitals. These transitions are responsible for the various bands, which appear in absorption spectra.

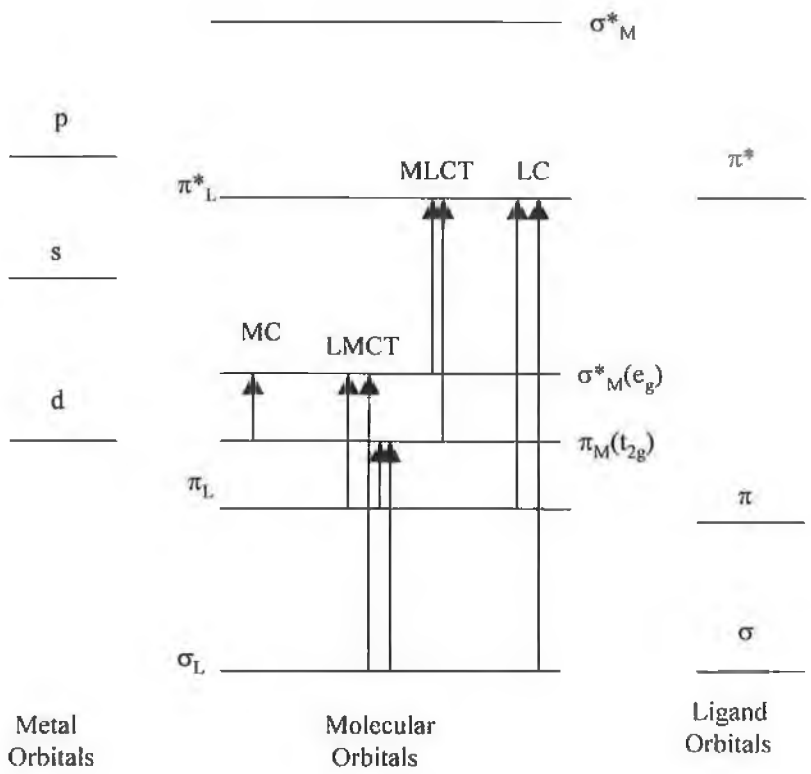

Figure 1. 4 *Molecular orbital diagram of an octahedral transition metal comlex, ML_6. The different types of electronic transitions are shown.*[13]

There are three basic types of electronic transitions:

i) Transitions localised on the central metal ion are termed metal-centred (MC) transitions. These types of transitions are also known as ligand-field or d-d transitions.

ii) Ligand-centred (LC) or intraligand transitions are transitions between molecular orbitals localised on the ligands.

iii) Charge-transfer (CT) transitions are between molecular orbitals of different localisation resulting in displacement of charge from the

ligands to the metal or vice-versa. These transitions can be divided into ligand-to-metal charge transfer (LMCT) and metal-to-ligand charge transfer transitions (MLCT).

There are two other less frequently encountered transitions that are not described in the above diagram. These transitions are ligand-to-ligand (LLCT) and metal-to-metal charge transfer (MMCT).[14]

1.3.3 Photophysical pathways in metal complexes

A molecule can be excited from the ground electronic state to an electronically excited state by the absorption of a quantum of light. In such a situation the photon energy ($h\nu$) corresponds to the energy gap between the ground and the excited state. When a molecule (A) absorbs light, an excited state A* is formed. The excited state is a high-energy unstable species with a number of different channels of deactivation open to it (Figure 1. 5). The deactivation pathways are:

i) Photochemical reaction, which results in the disappearance of the original molecule and the generation of new products.

ii) Radiative deactivation is termed luminescence.

iii) Radiationless deactivation causes the degradation of the excess energy into heat and a regeneration of the starting molecule A.

iv) The quenching process occurs when the excited state species interacts with other species present in solution.

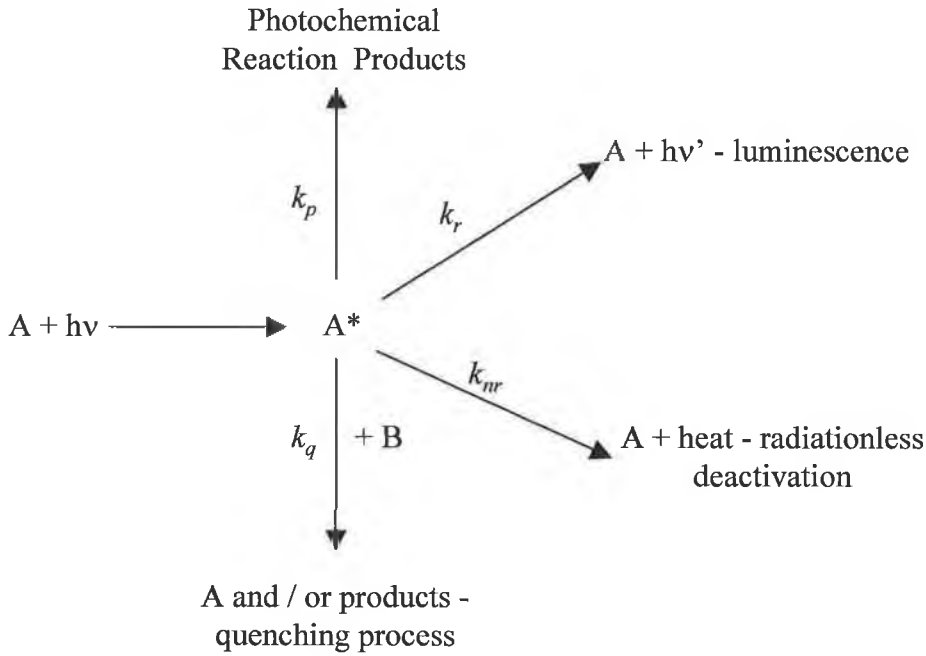

Figure 1. 5 *Schematic representation of excited state deactivation processes.*[15]

The above diagram (Figure 1. 5) sumarises the deactivation processes. Photochemical reaction, luminescence and radiationless deactivation are unimolecular processes. When a quencher (B) is added, a bimolecular process occurs.

Radiative deactivation is the reverse process of light absorption. In such a process electronically excited molecules return to the ground state by emitting a quantum of light. This observation will be explained with the aid of a Jablonski diagram (see Figure 1. 6). The Jablonski diagram illustrates the photophysical relaxation pathways for the decay of excited states. Singlet states are represented by S, while triplet states are described by T. The ground state is denoted by S_0 and excited states by S_1 and T_1.

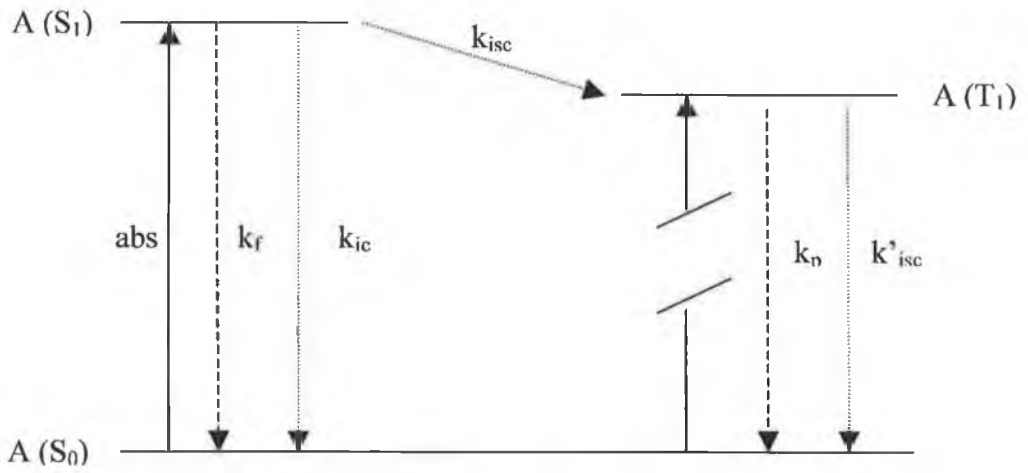

Figure 1. 6 *Schematic Jablonski Diagram showing the various deactivation processes. k_{ic}, k_{isc}, k_p and k'_{isc} are the unimolecular rate constants for fluorescence, internal conversion, $S_1 \rightarrow T_1$ intersystem crossing, phosphorescence and $T_1 \rightarrow S_0$ intersystem crossing, respectively.*[16]

In most transition metal complexes, the lowest excited state is a triplet state, which cannot be populated by light absorption. The triplet excited-state is obtained by deactivation of upper excited states. A nonradiative relaxation between two states of the same multiplicity (e.g. $S_1 \rightarrow S_0$) is termed internal conversion (IC). Relaxation between states of different multiplicity (e.g. $S_1 \rightarrow T_1$) is termed intersystem crossing (ISC). Intersystem crossing and internal conversion are examples of radiationless transitions (see). An emissive transition (luminescence) between states of the same multiplicities (e.g. $S_1 \rightarrow S_0$) is called fluorescence. Phosphorescence refers to an emissive transition involving a change of multiplicity (e.g. $T_1 \rightarrow S_0$).

In the absence of other processes, an excited state (A*) will decay according to first-order kinetics, with a lifetime (τ_{A^*}). This is represented by the following equation (Equation 1.6):

$$\tau_{A^*} = 1/\sum_i k_i \qquad \textbf{1.6}$$

Where k_i is the first order rate constant for a unimolecular process that causes the disappearance of the excited state. By taking into account the processes described in the Jablonski diagram, this equation may be rewritten in the following form:

$$\tau = \frac{1}{k_r + k_{nr} + k_p} \qquad \textbf{1.7}$$

For each process one can define the quantum yield. The quantum yield of a particular process is the number of photons that would be emitted per photon absorbed by the system. The quantum yield of emission (phosphorescence quantum yield, ϕ_p) from the lowest ^{3}MLCT is of particular interest in metal complexes. This can be expressed by the following equation:

$$\phi_p = \eta_{isc} k_p \tau_{T_1} \qquad \textbf{1.8}$$

The term η_{isc} is the efficiency of intersystem crossing. This is expressed in the following equation:

$$\eta_{isc} = k_{isc}/(k_{isc} + k_f + k_{ic}) \qquad \textbf{1.9}$$

Many inorganic complexes have unitary efficiency because of heavy atom (metal) induced spin orbit coupling. The term τ_{T_1} in Equation 1.10 is the lifetime of the emitting state and is defined by the following equation:

$$\tau_{T_1} = 1/(k_p + k'_{isc}) \qquad \textbf{1. 10}$$

So far only unimolecular processes have been discussed. If the lifetime of a particular complex is sufficiently long, the excited molecule may have a chance to encounter another species, B. In this situation an interaction between the two species may occur. This is called a bimolecular process.[15] The most important bimolecular processes are energy-transfer and electron-transfer (see Section 1.2.1 and Section 1.2.2). Electron-transfer may involve either oxidation or reduction of the excited state. Bimolecular energy and electron transfer process are essential components of supramolecular systems (Section 1.1). The kinetic aspects of bimolecular processes are beyond the scope of this thesis.

1.3.4 Non radiative transitions

Excited state deactivation of metal complexes may also occur via nonradiative decay paths. The nature and energy of these deactivation paths will be discussed in this section. It has been found that, in general, the non-radiative behaviour of most metal systems can be accommodated by the "energy gap law".[17,18,19] The energy gap law (EGL) shows that the rate of nonradiative decay (k_{nr}) is exponentially dependent on the energy difference between the ground state and the emissive excited state i.e. the energy gap. The form of the energy gap law adopted for this discussion is:

$$k_{nr} \propto \exp\left(\frac{-\mathrm{E}_0\gamma}{\hbar\omega_m}\right) \qquad \gamma = \ln\left(\frac{E_0}{S_m\hbar\omega_M}\right) \qquad \textbf{1. 11}$$

In Equation 1. 11, k_{nr} is the rate constant for nonradiative decay, E_0 is the energy difference between the excited and ground states in their lowest energy vibrational levels. The parameter ω_M is the angular frequency of the acceptor vibration in the ground state. A measure of the distortion of ω_M in the excited state is gauged by the Huang-Rhys factor (S_M):

$$S_M = \frac{1}{2}\left(\frac{M\omega_M}{\hbar}\right)(\Delta Q_e)^2 \qquad \textbf{1. 12}$$

In Equation 1. 12, M is the reduced mass of the oscillator and Q_e represents the difference between the ground and the excited state geometries with respect to the specified nuclear coordinate. The effect changes in both E_0 and ΔQ_e have on vibrational overlap (and therefore k_{nr}) is shown in Figure 1. 7.

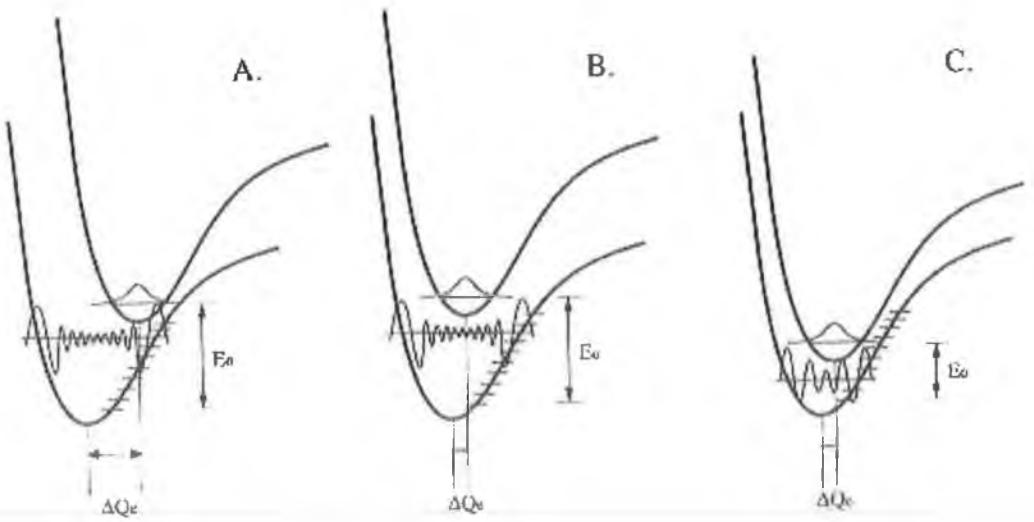

Figure 1. 7 *Illustration of the factors influencing vibrational overlap for nonradiative decay.*[20]

Starting with the central potential energy curve (B) in Figure 1. 7, a decrease in the energy gap (E_0) at constant ΔQ_e (C) results in an increase in the overlap between the lowest vibrational state of the excited state energy curve and the isoenergetic vibrational state of the ground state. Hence k_{nr} will increase. Note, increasing the energy gap has the opposite effect. An increase in the energy gap reduces the vibrational overlap, thus reducing k_{nr}. Changes in ΔQ_e at constant E_0 also influence k_{nr}. Large values of ΔQ_e (A) favour vibrational overlap. Consequently k_{nr} increases for C when compared to B.

1.4 Electronic and structural properties of mononuclear rhenium(I) complexes

The spectroscopy, photochemistry and photophysics of rhenium(I) tricarbonyl complexes of the general form *fac*-[$Re(CO)_3(L)X$] (where L is a polypyridyl ligand and X is a chloride/nitrogen donor) continue to attract much attention ever since their interesting excited state properties were first recognised in the 1970's.[21,22,23] Such rhenium(I) complexes are ideally suited to the design of luminescent sensors and materials for supramolecular devices.[24,25,26,2728] Their excited states have also demonstrated the potential to act as sensitisers in the photo and electrocatalytic reduction of CO_2 to CO.[29,30] The photochemical and photophysical properties of these complexes can be fine-tuned by adjusting the ligands coordinated to the rhenium(I) tricarbonyl moiety. This attribute of rhenium(I) complexes will be discussed in this section.

1.4.1 Syntheses

Rhenium(I) complexes of the form *fac*-[$Re(CO)_3(L)Cl$] where L is a polypyridine type ligand, can be readily synthesised by the reaction of the appropriate ligand with an equimolar amount of $Re(CO)_5Cl$ in a non-polar solvent (typically hexane or

toluene).[31,32] The synthesis of $[Re(CO)_3(bpy)Cl]$ is outlined in . The desired product often precipitates from solution and can be isolated and purified easily.

$$Re(CO)_5Cl + 2,2-bpy \xrightarrow{toluene\,/\,Ar} Re(CO)_3(bpy)Cl + 2CO \qquad \textbf{1. 13}$$

Two methods have been employed to substitute the chloride with a nitrogen donating ligand in complexes of the form $[Re(CO)_3(L)Cl]$ (see *Figure 1. 8*).[33,34,35]

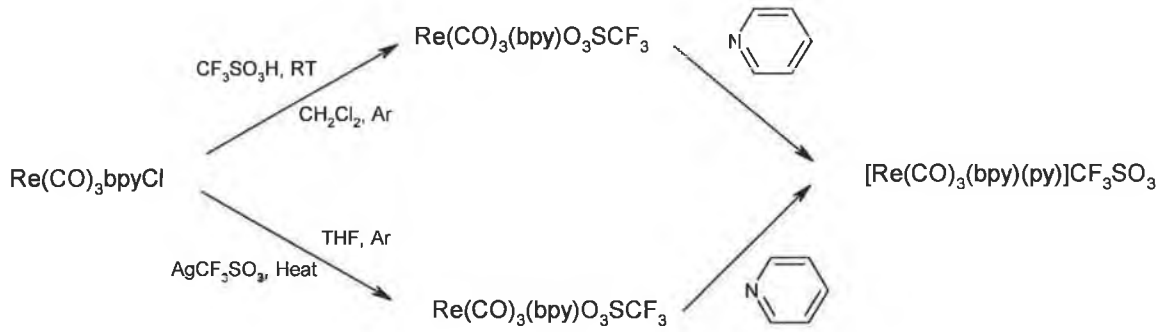

Figure 1. 8 *Synthetic scheme for the synthesis of $[Re(CO)_3(bpy)py]CF_3SO_3$ (bpy = 2,2'-bipyridine, py = pyridine).*[33]

When substituting the chloride ligand with a nitrogen donor, the electron donating abilities of the coordinated ligand influence the reactivity with either triflic acid or silver triflate.[33] This was evident in the synthesis of a series of $[Re(CO)_3(4,4'\text{-}X_2\text{-}bpy)Cl]$ complexes (X = NEt_2, CH_3, OCH_3, CH_3, H, Cl, Ph, CO_2CH_3 and NO_2).[33] When the coordinated ligand contained electron donating groups such as NEt_2, CH_3, OCH_3, CH_3 and H in the 4,4'-positions, the desired $[Re(CO)_3(4,4'\text{-}X_2\text{-}bpy)Et\text{-}py]^+$ (Et-py = 4-ethylpyridine) complex is formed in good yields. Electron accepting groups such as Cl, CO_2CH_3 and NO_2 result in low yields.

1.4.2 Infra-red spectroscopy

Rhenium tricarbonyl complexes with the following general configuration $[Re(CO)_3(L)X]$ posses C_s symmetry, with three infra-red (IR) active modes [A'(1) + A'(2) + A'']. [21,36] The IR spectrum of $[Re(CO)_3(bpy)Cl]$ (Figure 1. 9) is well understood. Three carbonyl bands are found at 2020, 1918 and 1893 cm^{-1}. This pattern corresponds to three carbonyls in a facial (fac) isomer arrangement (Figure 1. 10). The $\nu_{(CO)}$ bands are assigned to the A'(1), A'' and A' (2) vibrations respectively.[37] Note, there is no evidence in the literature for the formation of rhenium(I) tricarbonyl complexes in a *meridional* (*mer*-) isomeric form. A characteristic property of *mer*- isomers is the very low IR intensity of the highest frequency band with respect to the other two bands.[38]

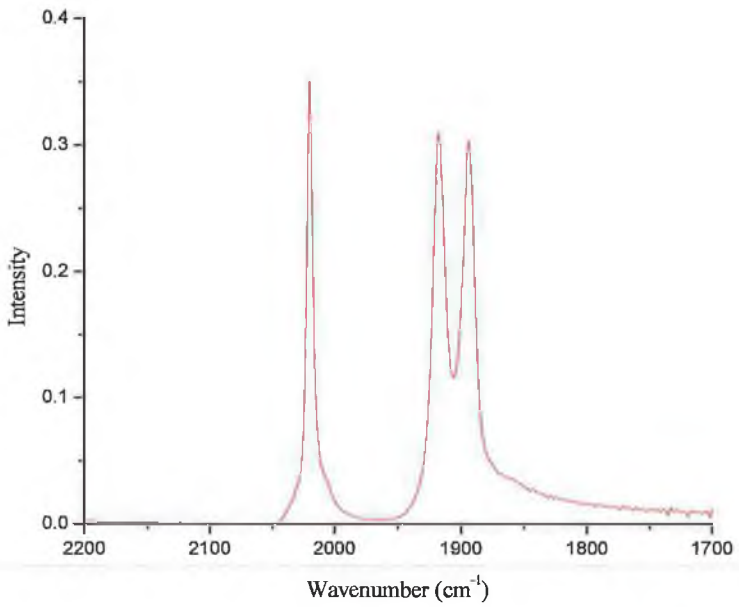

Figure 1. 9 *Infra-red spectrum of $[Re(CO)_3Cl(bpy)]$ in THF at 298 K.*

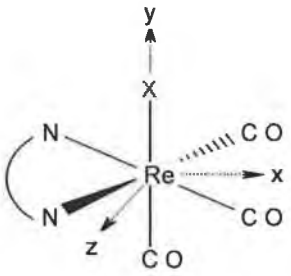

Figure 1. 10 *Coordination environment for the facial isomer of a rhenium tricarbonyl complex.*

In the IR spectra of $[Re(CO)_3(bpy)(4\text{-}Etpy)]^+$ (4-Etpy = 4-ethylpyridine) and $[Re(CO)_3(bpy)(CH_3CN)]^+$ only two carbonyl bands are observed (see Table 1. 1).[39,40] This in contrast to the IR spectra of $[Re(CO)_3(bpy)(Cl)]$ and $[Re(CO)_3(bpy)(PPh_3)]^+$ (PPh_3 = triphenylphosphine) where three resolved carbonyl bands are observed.[40] In complexes of the form $[Re(CO)_3(L)X]$, where the ancillary ligand X is pyridine based (i.e. when X is an N-bound pyridyl ligand) the local coordination around the metal centre is pseudo-C_{3v} symmetry, and only two bands appear in the ground-state IR spectrum. The higher energy band corresponds to an A_1 mode, while the broad lower energy band (E) is a convolution of the A'(2) and A'' bands of C_s symmetry. In $[Re(CO)_3(L)X]$ type complexes, the more dissimilar the bonding properties of the bidentate ligand (L) and X, the greater the splitting between the two low energy bands. For example in $[Re(CO)_3(bpy)(CH_3CN)]$, only two ν(CO) bands are observed at 2042 and 1938 cm^{-1}, whereas with $[Re(CO)_3(bpy)(Cl)]$ and $[Re(CO)_3(bpy)(PPh_3)]^+$ (PPh_3 = triphenylphosphine), three resolved CO stretches are observed (Table 1. 1).

Complex	$\nu_{(CO)}$ cm^{-1}		
$[Re(CO)_3(bpy)(4\text{-}Etpy)]^{+}$ [39]	2035	1927	—
$[Re(CO)_3(bpy)(CH_3CN)]^{+}$ [40]	2042	1938	—
$[Re(CO)_3(bpy)(PPh_3)]^{+}$ [40]	2042	1957	1927
$[Re(CO)_3(bpy)Cl]$ [40]	2024	1917	1900

Table 1. 1 *Carbonyl vibrational frequencies (ν_{CO}) for the series of complexes $[Re(CO)_3(bpy)(X)]$ in acetonitrile. 4-Etpy = 4-ethylpyridine, CH_3CN = acetonitrile and PPh_3 = triphenylphosphine.*

The positions of carbonyl bands in IR spectra are sensitive to the d_π electron density of the rhenium centre. This trend may be attributed to back-bonding between the rhenium metal centres and the carbonyl ligands. The bonding interaction of a carbonyl ligand with a transition metal has two major components (Figure 1. 11). Electron density is transferred from the carbon lone pair into a vacant metal orbital (d or p orbital) when a σ-bond is formed between the metal and the carbonyl. The metal is now "electron" rich. In order to compensate for the increased electron density, a filled metal d-orbital may interact with an empty π* orbital on the carbonyl ligand to relieve itself of the added electron density. This process is termed π-back bonding. The greater the σ donation by the carbonyl (or the other σ-donor ligands on the metal), the stronger the π-back bonding interaction. Back bonding causes the carbonyl bond to lengthen and weaken. IR spectra are consistent with the concept of π-back bonding. The better the σ donating capability (or the worse the π-acceptor ability) of the other ligands on the metal, the lower the ν_{CO} frequency.

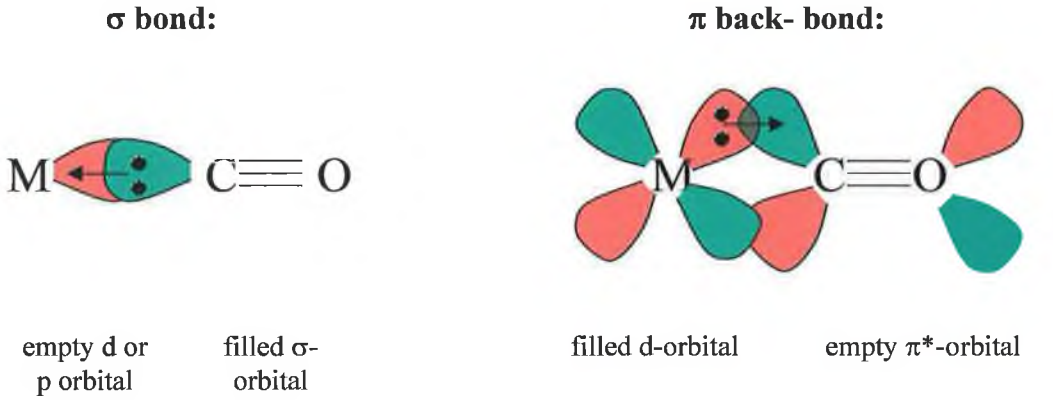

Figure 1. 11 *Bonding interaction of CO with transition metals.*

There are many examples of the π-acceptor capabilities of various ligands influencing the ν_{CO} on the tricarbonyl metal fragment. For instance, there is about a 10 cm^{-1} shift in carbonyl frequencies to higher energy for $[Re(CO)_3(bpm)Cl]$ (bpm = 2,2-bipyrimidine) complexes compared to $[Re(CO)_3(Mebpy\text{-}Mebpy)Cl]$ (Mebpy-Mebpy = 4,4'-dimethyl-2,2'-bipyridine).[41] This due to the weaker π-acceptor ability of 4,4'-dimethyl-2,2'-bipyridine compared to 2,2-bipyrimidine. $[Re(CO)_3(bpy)Cl]$ exhibits three carbonyls bands at 2020, 1918 and 1893 cm^{-1} whereas $[Re(CO)_3(bpz)Cl]$ (bpz = 2,2'-bipyrazine) exhibits three carbonyl bands at 2033, 1932 and 1909 cm^{-1}.[39,42] Pyrazine type ligands have much lower lower π* energy levels than 2,2'-bipyridine.[39,42] This leads to a more favourable back-bonding interaction between the d_π orbitals of rhenium(I) and the 2,2'-bipyrazine π* orbitals compared to $[Re(CO)_3(bpy)Cl]$. This interaction leaves less electron density available for back-bonding between the rhenium d_π orbitals and the CO π* orbitals. As a result the carbonyl bonds in $[Re(CO)_3(bpz)Cl]$ are shorter compared to the carbonyl bonds in $[Re(CO)_3(bpy)Cl]$. This explains the observed increase in CO stretching frequencies for the $[Re(CO)_3(bpz)Cl]$ compared to $[Re(CO)_3(bpy)Cl]$.

There is also an effect on the carbonyl frequencies when the chloride is exchanged with another halide. Kaim and co-workers have synthesised a series of rhenium tricarbonyl complexes of the form $[Re(CO)_3(abpy)X]$ (X = F, Cl, Br and I, abpy = 2,2'-azobispyridine).[43,44] All of these complexes exhibited three CO bands, but the bands were at lower values by about 20 cm^{-1} for $[Re(CO)_3(abpy)F]$. This was due to the effect of the highly electronegative flouride on rhenium carbonyl back bonding.

1.4.3 Absorption spectroscopy

The photochemical and photophysical properties of rhenium(I) complexes can be fine-tuned by adjusting the ligands coordinated to the rhenium(I) tricarbonyl moiety. It is therefore worth examining the ground state absorption properties of such complexes. The absorption spectra of rhenium tricarbonyl complexes display a number of different absorption bands as shown in the absorption spectrum of $[Re(CO)_3(bpy)Cl]$ (see Figure 1. 12) The higher energy feature at 295 nm in the absorption spectrum of $[Re(CO)_3(bpy)Cl]$ is associated with a bipyridyl based (π-π^*) transition.[21,22,23] This ligand centred transition in the free ligand is found at similar energy and shows very little change on complexation to the rhenium metal. The broad band observed at 390 nm is assigned to an $[Re\rightarrow\pi^*(bpy)]$ metal to ligand charge transfer (MLCT) transition. The exact electronic structure of this absorption band will be discussed at a later stage. The MLCT absorption band for rhenium tricarbonyl complexes shifts to lower energy with decreasing solvent polarity due to a characteristic solvatochromism.[45]

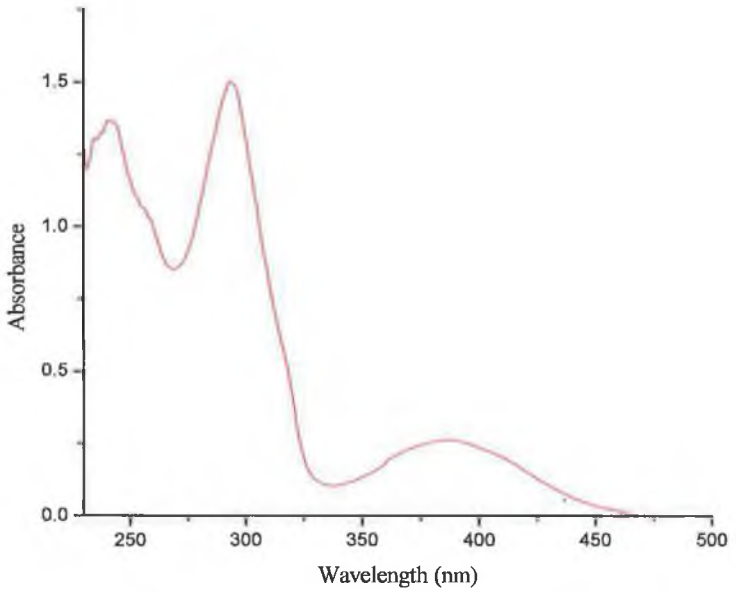

Figure 1. 12 *UV-vis absorption spectrum of [Re(CO)$_3$(bpy)Cl] in dichloromethane at 298 K.*

MLCT transitions in absorption spectra of rhenium tricarbonyl complexes exhibit band shifts that correlate with the electron-donating/withdrawing nature of the ligand substituents. This is reflected in Table 1. 2. The electron-donating substituents on bipyridyl increase the energy of the π* acceptor to a greater degree than they do the dπ (Re) orbitals. For example the presence of an electron-donating NH_2 group on the bipyridyl ligand substantially shifts the λ_{max} from 387 nm to 360 nm. Conversely the presence of an electron-withdrawing group (Cl) stabilises the π* level of the bipyridyl ring causing the λ_{max} to shift to 410 nm.

	λ_{max} (nm)	
Ligand (L)	**CH_2Cl_2**	**CH_3CN**
2,2-bipyridyl (bpy) [22]	387	370
4,4'-$(CH_3)_2$-bpy [22]	380	364
4,4'-$(phenyl)_2$-bpy	396[46]	384[47]
4,4'-$(NH_2)_2$-bpy [47]	360	350
4,4'-$(NO_2)_2$-bpy [47]	475	448
4,4'-$(COOCH_3)_2$-bpy	433[47]	—
4,4'-$(Cl)_2$-bpy [47]	410	390

Table 1. 2 *Absorption maxima data for the complexes [Re(CO)$_3$(4,4'-X$_2$-bpy)Cl] at 298 K, (bpy = 2.2'-bipyridine). For [Re(CO)$_3$(4,4'-(COOCH$_3$)$_2$-bpy)Cl], data was only available in dichloromethane.*

Recent theoretical calculations have afforded a thorough insight in to the electronic structure of $[Re(CO)_3(bpy)Cl]$ and related complexes.[48,49] In these contributions density functional theory (DFT) was applied to $[Re(CO)_3(bpy)Cl]$ and related complexes containing the electron-donating ligands such as 4,4'-dimethyl-bpy along with the electron-withdrawing ligand 5,5'-dibromo-bpy. These studies found that the highest occupied molecular orbital (HOMO) is mainly composed of chloride p_z orbitals that form antibonding interactions with metal d_{xz} orbitals. The lowest unoccupied molecular orbital (LUMO) and two subsequent unoccupied orbitals are π^* orbitals localised on the bipyridyl moieties. The higher unoccupied orbitals show considerable carbonyl character. In these complexes the low energy part of the absorption spectra originates in an electronic transition that corresponds to excitation from the mixed orbitals of rhenium and chloride character into a π^* orbital localised on the bipyridyl. Since the HOMO is composed of chloride p_z and metal d_{xz} orbitals, the lowest excited has mixed $[Re\rightarrow\pi^*(bpy)]$ MLCT and $[Cl\rightarrow\pi^*(bpy)]$ LLCT

character.[50] The intense bands at higher energy in the absorption spectra were found to correspond to π-π* excitations. Feng and co-workers found that the band character is identical for each of the complexes but $|\Delta E$ (HOMO – LUMO)$|$ decreases with increasing electron withdrawing character of the substituents on the 2,2'-bipyridyl. These results complement earlier studies by Stufkens and co-workers.[51]

There has been extensive work carried out in synthesising rhenium tricarbonyl complexes of the form $[Re(CO)_3(L)X]$ where L = 2,2'-bipyridine, 1,10-phenanthroline, or 2,3-di(2-pyridyl)pyrazine and X = substituted pyridine or quinoline.[64,19] The replacement of a chloride with a pyridine or substituted pyridine had a small effect on the absorption maxima. For the series of complexes $[Re(CO)_3(L)X]$ where L = 2,3-di(2-pyridyl)quinoxaline and X = Cl, pyridine or substituted pyridine, the absorption maximum shifted from 449 nm (X = Cl) to 380 nm (X = pyridine or methyl-pyridine).[52] This shift was attributed to the replacement of the weak field Cl^- with a stronger ligand field pyridine.

1.4.4 Excited state behaviour of rhenium(I) tricarbonyl complexes

1.4.4.1 Rhenium(I) complexes exhibiting charge transfer excited states

Rhenium tricarbonyl complexes are one of the few classes of metal carbonyl complexes that emit in fluid solution. Hence they are candidates for effecting energy and or electron transfer. As previously discussed in Section 1.4.1, the presence of a halide (chloride, bromide or fluoride) in the axial position of complexes of the general configuration $[Re(CO)_3(L)X]$ (where L is a polypyridyl ligand and X is a halide) allows great synthetic freedom in the synthesis of rhenium tricarbonyl complexes. The ability to synthetically manipulate rhenium tricarbonyl complexes gives rise to interesting excited state behaviour. In the mid 1970s $[Re(CO)_3(bpy)Cl]$

was found to emit at room temperature with a λ_{max} at 610 nm.[22] An example of the broad structureless emission observed by Wrighton and co-workers is shown in Figure 1. 9.

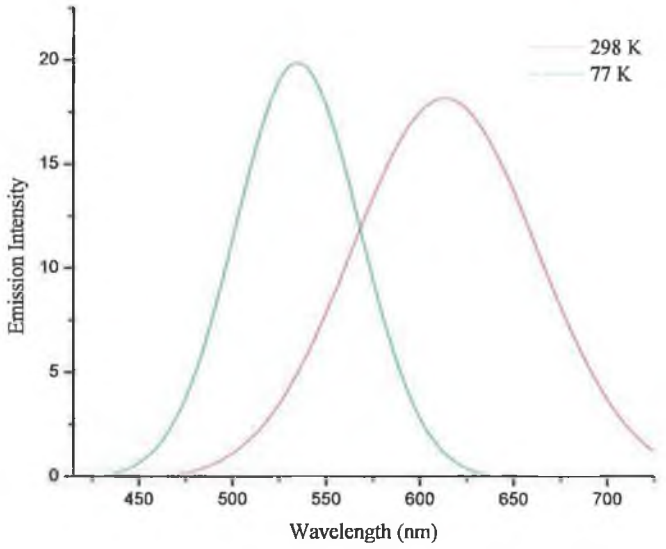

Figure 1. 13 *Emission spectra of [Re(CO)$_3$Cl(bpy)] at 298 K and 77 K.*

Emission from [Re(CO)$_3$(bpy)Cl] has been found to originate from a ^{3}MLCT. The emission λ_{max} of [Re(CO)$_3$(bpy)Cl] shifts from 610 nm to 535 nm on going from 298 K to 77 K (Figure 1. 13). This rigidochromic shift is characteristic of emission originating from a ^{3}MLCT state. In the case of [Re(CO)$_3$(bpy)Cl] emission from the ^{3}MLCT at 298 K decays with a life time of 51 ns and increases to 2.68 μs on cooling to 77 K.[53] In the alcoholic glass formed at 77 K, the solvent dipoles are immobile on the time scale of the excited state and consequently they cannot respond to the change in electronic configuration between the ground and excited state that accompanies an excitation. The result is an increase in the emission energy, i.e. a blue shift in the emission spectrum of [Re(CO)$_3$(bpy)Cl] from 610 nm to 535 nm. Another

observation at low temperature is the increase in emission intensity and longer lifetime of the excited state of $[Re(CO)_3(bpy)Cl]$ i.e. the lifetime is in the μs range. At low temperature, the complex and its environment are rigid, making it less susceptible to vibronic coupling to low frequency, high amplitude Re-N vibrations, which contribute to radiationless decay.[54] Solvent interactions, which may contribute to radiationless decay are also considerably reduced in the frozen matrix, as too is quenching of the excited state by the presence of oxygen, since diffusion of oxygen is restricted. These factors contribute to the increase in emission lifetime and blue shift in the emission maximum of $[Re(CO)_3(bpy)Cl]$ on cooling to 77 K.

	λ_{max} (nm)	
Ligand (L)	**298 K**	**77 K**
2,2-bipyridyl (bpy) [22]	610 [a]	535 [b]
4,4'-$(CH_3)_2$-bpy [41]	601 [c]	510 [b]
4,4'-$(phenyl)_2$-bpy [47]	647 [d]	560 [b]
4,4'-$(COOCH_3)_2$-bpy [55]	600 [e]	555 [f]
4,4'-$(Cl)_2$-bpy [47]	700 [d]	580 [b]
4,4'-$(NCH_3)_2$-bpy [55]	532 [e]	472 [f]

Table 1. 3 *Emission maxima data for the complexes $[Re(CO)_3(4,4'\text{-}X_2\text{-}bpy)Cl]$ at 298 K and 77K. [a] dichloromethane. [b] ethanol:methanol (4:1) v/v). [c] Acetonitrile. [d] Methyl THF. [e] DMF. [f] DMF/CH_2Cl_2 (9:1) v/v)*

There are many examples of rhenium(I) tricarbonyl complexes displaying ^{3}MLCT based emission at room temperature and 77 K. The emission maxima are sensitive to the nature of the polypyridine ligand at 298 K and 77 K (see Table 1. 3). For example, at 77 K $[Re(CO)_3(bpy)Cl]$, $[Re(CO)_3(4,4'\text{-dimethyl-bpy})Cl]$ and $[Re(CO)_3(4,4'\text{-dichloro-bpy})Cl]$ exhibit emission maxima at 535, 510 and 580 nm

respectively. The emission maxima (compared to $[Re(CO)_3(bpy)Cl]$) are blue shifted when in the presence of an electron donating group ($-CH_3$) and are red shifted in the presence of an electron withdrawing group (-Cl). An electron donating group leads to a blue shift in the emission maximum due to the increased energy of the LUMO which results in an increased the $t_{2g} - {}^3MLCT$ energy gap. On the other hand, an electron withdrawing group results in a red shift in the emission maximum due to the decreased energy of the LUMO, which decreases the $t_{2g} - {}^3MLCT$ energy gap. More recently theoretical calculations have led to a similar conclusion. Yang and co-workers have applied DFT studies to analyse the excited-state properties of $[Re(CO)_3(bpy)Cl]$, $[Re(CO)_3(5,5'$-dibromo-bpy)Cl] and $[Re(CO)_3(4,4'$-dimethyl-bpy)Cl].[48] For these complexes, the excited state responsible for the luminescence was of ${}^3MLCT$ nature. The $t_{2g} - {}^3MLCT$ energy gap increased in the order $[Re(CO)_3(4,4'$-dimethyl-bpy)Cl]) > $[Re(CO)_3(bpy)Cl]$ > $[Re(CO)_3(5,5'$-dibromo-bpy)Cl] i.e. the emission maxima are blue shifted when substituted by an electron donating group and red shifted when substituted by an electron withdrawing group.

Radiative decay from rhenium tricarbonyl complexes provides the first indication of the character of the lowest lying excited state. The factors influencing the rate of non-radiative decay with respect to rhenium(I) tricarbonyl complexes containing polypyridine type ligands will now be discussed. As previously discussed, variations in the structure of the coordinated ligand to the rhenium metal centre have a profound effect on the absorption and emission properties of the metal complexes. Similarly variations in the ligand structure also have an effect on the rate of non-radiative deactivation. A positive linear correlation between S_M and E_0 has been observed for a series of $[Re(CO)_3(4,4'$-X_2-bpy)Cl] complexes (X = NEt_2, NH_2, $NHCOCH_3$, OCH_3, CH_3, H, Cl, Ph, CO_2Et and NO_2) whose ligands are structurally very similar.[47] The lowest energy MLCT transition observed in these complexes involves the filled d_π and the empty π^* orbitals, which are mixed by a back-bonding interaction. When the energy gap between these orbitals is small, there is significant back-bonding between

them, resulting in increased orbital mixing and a reduced amount of charge being exchanged during the MLCT transition i.e. reduced excited state distortion. Hence k_{nr} increases. Alternatively, when the energy gap between the d_π and the π^* orbitals is large, back-bonding and orbital mixing are reduced, thus increasing the amount of charge exchanged during the MLCT. As the amount of charge exchanged increases with the energy gap, E_0, so does the distortion S_M, as the bipyridyl ligand must accept more charge in its π^* orbitals. Consequently k_{nr} decreases. A similar EGL correlation has also been determined for $[Re(CO)_3(4,4'\text{-}X_2\text{-bpy})(4\text{-Et-py})]$ (X = OCH_3, CH_3, $CONEt_2$ and CO_2Et).[56]

Baiano and coworkers have examined the effect of delocalisation and rigidty in the acceptor ligand on MLCT excited state decay in two series of complexes of the type $[Re(CO)_3(BL)(L)]^+$ (BL = 2,3-bis-(2-pyridyl)-pyrazine (dpp) and 2,3-bis-(2-pyridyl)-quinoxaline (dpq); L = *N*-methylimidazole, trimethylphosphine, acetonitrile and substituted pyridines).[19,52] Their results showed that non radiative decay was the dominant mode of excited state relaxation for the two series of complexes. The complexes also obey the energy gap law since a linear relationship was obtained for the ln k_{nr} versus E_{em} plots. The authors concluded that delocalisation of the π^* orbital over a ligand reduces the excited state distortion. This is manifested by a decrease in k_{nr} on going from dpq to dpp. The effect of the delocalisation of the π^* orbital on the MLCT excited state is also reflected on the drop of the S_M value from 1.19 to 0.10 on going from $[Re(CO)_3(dpp)(py)]^+$ to $[Re(CO)_3(dpq)(py)]^+$. To summarise, the structure of the ligand affects the properties of the MLCT state of rhenium(I) tricarbonyl complexes through the energy of the accepting π^* orbital, its delocalisation over the ligand framework and by the extent of its interaction with the rhenium(I) d_π orbitals.

1.4.4.2 Rhenium(I) complexes exhibiting both charge transfer and ligand localised excited states

There are a large number of rhenium(I) tricarbonyl complexes that exhibit ligand localised $^3(\pi\text{-}\pi^*)/^3$IL and ^{3}MLCT excited states. Emission from both ^{3}MLCT and ^{3}IL states was reported by Wrighton and co-workers for the series of complexes $[Re(CO)_3(3\text{-bopy})_2X]$ and $[Re(CO)_3(4\text{-bopy})_2X]$ (3-bopy = 3-benzoylpyridine, 4-bopy = 4-benzoylpyridine; X = Cl, Br or I).[57,58] Emission at room temperature was broad and structureless and was classed as originating from the ^{3}MLCT state. A red shift in the emission maxima of the 4-benzoylpyridine complexes compared to the analogous 3-benzoylpyridine complexes was also observed at room temperature. For example $[Re(CO)_3(3\text{-bopy})_2Cl]$ has a λ_{max} at 546 nm whereas $[Re(CO)_3(4\text{-bopy})_2Cl]$ has a λ_{max} at 600 nm. On lowering the temperature to 77 K, a blue shift in the emission maxima, an increase in emission intensity and longer lifetimes were observed for the 4-benzoylpyridine complexes. At 77 K the authors assigned the emitting level as ^{3}MLCT in character for $[Re(CO)_3(4\text{-bopy})_2Cl]$, $[Re(CO)_3(4\text{-bopy})_2Br]$ and $[Re(CO)_3(4\text{-bopy})_2I]$. For the 3-benzoylpyridine complexes at 77 K, the emission band was structured and was resolved into two components, one with a lifetime of ~ 18 μs and another with a lifetime of ~ 1400 μs. The short-lived component was assigned to a ^{3}MLCT state while the long-lived component was attributed to a ^{3}IL state of the 3-benzoylpyridine.

More recently Busby and coworkers examined the excited state properties of $[Re(CO)_3(4\text{-bopy})_2Cl]$ and $[Re(CO)_3(bpy)(4\text{-bopy})]^+$.[59] The assignment of the lowest excited-state of $[Re(CO)_3(4\text{-bopy})_2Cl]$ as $[Re\rightarrow\pi^*(4\text{-bopy})]$ ^{3}MLCT in character was supported by time-resolved visible absorption (TA) and time-resolved resonance Raman (TR^3) studies. The TA spectrum of $[Re(CO)_3(4\text{-bopy})_2Cl]$ using 393 nm excitation showed a broad absorption with a maximum at 575 nm. This absorption closely resembled the UV-vis spectrum of $[Re^{II}(CO)_3(4\text{-bopy})(4\text{-bopy}^{\bullet-})Cl]$.[60] The

TR[3] spectrum of $[Re(CO)_3(4\text{-bopy})_2Cl]$ was consistent with reduction of one 4-bopy ligand upon excitation. The new bands observed at 1586, 1470, 1330, 1187 and 996 cm^{-1} were attributed to the C-Ph/py stretching and C-H bending modes of the 4-$bopy^{\bullet-}$ radical-anionic ligand.[61]

In contrast, the lowest-lying excited state of $[Re(CO)_3(bpy)(4\text{-bopy})]^+$ was identified as $[Re\rightarrow\pi^*(bpy)]$ ^{3}MLCT in character with no involvement of the 4-bopy ligand. This complex represents an unusual case as the lowest unoccupied redox orbital i.e. π^*(4-bopy) is different from the lowest unoccupied optical orbital i.e. π^*(bpy). $[Re(CO)_3(bpy)(4\text{-bopy})]^+$ was reduced in two reversible one electron steps at $E_{1/2}$ = -1.44 and –1.66 V. These values were close to the first reduction potentials of $[Re(CO)_3(4\text{-bopy})_2Cl]$ (-1.53 V) and $[Re(CO)_3(bpy)(4\text{-Etpy})]^+$ (4-Etpy = 4-ethylpyridine) (-1.56 V). Hence IR spectroelectrochemistry at 223 K of $[Re(CO)_3(bpy)(4\text{-bopy})]^+$ was undertaken in order to decide whether the first reduction is localised on the bpy or the 4-bopy ligand. The shift of the ketone CO band from 1670 cm^{-1} to 1624 cm^{-1} indicated that the first reduction is localised on the 4-benzoylpyridine ligand, yielding $[Re(CO)_3(bpy)(4\text{-bopy}^{\bullet-})]^+$. The TA spectrum of $[Re(CO)_3(bpy)(4\text{-bopy})]^+$ comprises of a broad shoulder between 500 and 600 nm. The TA spectrum of $[Re(CO)_3(bpy)(4\text{-bopy})]^+$ was similar to that of $[Re(CO)_3(bpy)Cl]$. Hence the lowest excited-state was assigned to a $[Re\rightarrow\pi^*(bpy)]$ ^{3}MLCT state. The assignment of the lowest excited-state as ^{3}MLCT(bpy) was also supported by time resolved Infrared spectroscopy as no changes were observed in the region of ketone CO vibrations between 1600 and 1700 cm^{-1}. The authors concluded that the excited electron density is localised on the bpy ligand rather than the 4-bopy ligand.

Phenanthroline type complexes with the generic formula $[Re(CO)_3(s\text{-phen})Cl]$ (*s*-phen represents a 1,10-phenanthroline ligand with methyl groups at various positions on the rings) are another example of emissive rhenium(I) tricarbonyl complexes.[62]

Emission from these complexes at room temperature originates from a ^{3}MLCT state. However in glasses at 77 K, some of these complexes exhibit emission from a single configuration while others show dual luminescence. Where dual luminescemce occurs the two emitting states were very close in energy and show extensive vibrational structure. The relative amount of structure in the spectrum at 77 K depends on the phenanthroline ligand in the complex: 5,6-Me_2phen > Me_4phen > 4,7-Me_2phen. The energy of the first band maximum was found to decrease along the series: 5,6-Me_2phen (464 nm) > Me_4phen (473 nm) > 5,6-Me_2phen (484 nm). The lifetimes for these phenanthroline complexes were double exponential with a short-lived ^{3}MLCT component of around 10 μs and a longlived ^{3}IL component greater than 135 μs. A more recent example of dual luminescence from ^{3}MLCT and ^{3}IL states is from a series of $[Re(CO)_3(L)Cl]$ (L = imidazole derivatives) synthesised by Knör and co-workers.[63]

For rhenium(I) tricarbonyl complexes having substituted bpy and phenanthroline ligands, Demas and Degraff illustrated that subtle variations in the rhenium(I) coordination environment resulted in significant effects on the nature of the emitting excited state.[64] The emission properties of a series of complexes of the form $[Re(CO)_3(L\text{-}L)X]^+$ where L = 2,2'-bipyridine, 1,10-phenanthroline or 5-phenyl-1,10-phenanthroline and X = substituted pyridine or quinoline were studied. All of the complexes were found to exhibit ^{3}MLCT based emission at room temperature. At 77 K, the bpy/pyridine and phenanthroline/pyridine complexes showed broad structureless emission bands with lifetimes between 4.5 and 10.5 μs. These complexes were all classed as ^{3}MLCT emitters. However two complexes $[Re(CO)_3(bpy)(quin)]^+$ and $[Re(CO)_3(5\text{-}Phphen)(py)]^+$ (quin = quinoline, 5-Phphen = 5-phenyl-1,10-phenanthroline and py = pyridine) exhibited highly structured emission bands at 77 K with lifetimes of 1.2 ms and 0.32 ms respectively. The authors concluded the lifetimes were too long for pure ^{3}MLCT emitters. The emission spectrum of $[Re(CO)_3(bpy)(quin)]^+$ was structurally similar to that of

protonated quinoline while the emission spectrum of $[Re(CO)_3(5\text{-Phphen})(py)]^+$ was a good match to that of the protonated ligand 5-phenyl-1,10-phenanthroline. At 77 K, emission from $[Re(CO)_3(5\text{-Phphen})(py)]^+$ was assigned to a $[\pi\text{-}\pi^*(5\text{-Phphen})]$ ^{3}IL state whereas $[Re(CO)_3(bpy)(quin)]^+$ gives rise to $[\pi\text{-}\pi^*(quin)]$ ^{3}IL based emission. Further studies on a number of complexes of the type $[Re(CO)_3(L\text{-}L)(py)]^+$ where L-L is 1,10-phenanthroline, 5,6-dimethyl-1,10-phenanthroline, 4,7-dimethyl-1,10-phenanthroline, 3,4,7,8-tetramethyl-1,10-phenanthroline or 5-phenyl-1,10-phenanthroline indicated the presence of two unequilibrated emitting states, a ^{3}MLCT and a ^{3}IL at 77 K. [65,66,67] Note at room temperature, the complexes displayed broad emission spectra which were all assigned as ^{3}MLCT emitters. At 77 K, the emission spectra showed structure comparable to that of the corresponding free ligands. In the glass formed at 77 K, the solvent dipoles are immobile on the time scale of the excited state and consequently they cannot respond to the change in electronic configuration between the ground and excited state that accompanies an excitation. This results in an increase in the emission energy of the ^{3}MLCT state on going from room temperature to 77 K. Emissions arising from ^{3}IL states are insensitive to solvent and temperature effects, as these transitions involve minimal redistribution of electron density with respect to the solvent sphere. The authors concluded at 77 K, the ^{3}MLCT has been shifted to higher energy so that it lies at similar at similar energy or above the energy of the ^{3}IL state. Hence emission occurs from a state that has substantial ligand-centred character.

The photophysical properties of complexes of the general type $[Re(CO)_3(L\text{-}L)(CNR)]^+$ (L = 2,2'-bipyridine, or substituted phenanthroline; R = *t*-Bu, *n*-alkyl, or 2,6-dimethylphenyl) have also been examined.[68,69,70,71,72] For the series of complexes $[Re(CO)_3(L)(CN\text{-}t\text{-}Bu)]^+$ (L = bpy, 1,10-phenanthroline, 4,7-dimethyl-1,10-phenanthroline or 3,4,7,8-tetramethyl-1,10-phenanthroline) the lowest excited state was controlled by varying L or temperature. At room temperature the emission spectra show a clear progression from broad structureless ^{3}MLCT to highly structured

^{3}IL emission on going from bpy, to 1,10-phenanthroline to 4,7-dimethyl-1,10-phenanthroline to 3,4,7,8-tetramethyl-1,10-phenanthroline.[67,68] The trend in ^{3}IL character revealed in the emission spectra was paralleled by increases in the lifetimes. Lifetimes of 1.97, 10.6, 68.9 and 120.7 μs were obtained for the bpy, 1,10-phenanthroline, 4,7-dimethyl-1,10-phenanthroline and 3,4,7,8-tetramethyl-1,10-phenanthroline complexes respectively. All of the complexes showed increased ^{3}IL character at 77 K as evidenced by the increase in structure of emission spectra. Most notably at 77 K, $[Re(CO)_3(bpy)(CN\text{-}t\text{-}Bu)]^+$ emits from both ^{3}IL and ^{3}MLCT states whereas at room temperature only ^{3}MLCT based emission was observed. Similar trends were also observed for the series of complexes $[Re(CO)_3(s\text{-phen})(CNR)]^+$ where *s*-phen = 1,10-phenanthroline, 4,7-dimethyl-1,10-phenanthroline or 3,4,7,8-tetramethyl-1,10-phenanthroline and CNR = 2,6-dimethylphenylisocynanide.[71] The 1,10-phenanthroline complex was classed as a ^{3}MLCT emitter at room temperature whereas both ^{3}MLCT and ^{3}IL based emission were observed from the 4,7-dimethyl-1,10-phenanthroline and 3,4,7,8-tetramethyl-1,10-phenanthroline complexes at room temperature.

Experimentally, the ^{3}IL character of the emissive excited states of the rhenium(I) complexes discussed in this section are manifested by a sharp, structured, emission band which closely resembles that of the free ligand. However, it should be noted that the observation of a typical broad MLCT emission from a complex with close-lying MLCT and IL states does not necessarily prove that the MLCT is the lowest excited state. This is the case of the complex $[Re(CO)_3(dppz)Cl]$ where dppz is dipyrido[3,2-a:2',3'-c]phenazine (see Figure 1. 14).[73] Note the room temperature emission spectrum is broad and structureless. Excited state resonance Raman spectra of $[Re(CO)_3(dppz)Cl]$ in dichloromethane at room temperature were consistent with a dppz-centred ^{3}IL state. Instead of decaying directly to the ground-state, the ^{3}IL state of $[Re(CO)_3(dppz)Cl]$ is deactivated through a thermally populated higher lying emissive ^{3}MLCT state.

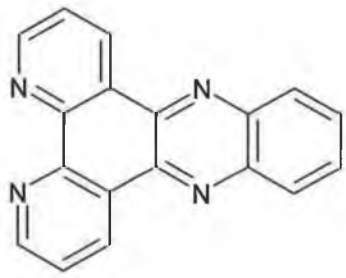

Figure 1. 14 *Structure of the ligand dipyrido[3,2-a:2',3'-c]phenazine (dppz).*

Both the emission and time-resolved Infrared spectra of an analogous complex $[Re(CO)_3(dppz)(PPh_3)]^+$ (PPh_3 = triphenylphosphine) point to an ^{3}IL character of its lowest excited state.[73,74] The emission spectrum has the characteristic, resolved vibronic structure and long lifetime (τ = 42 μs) of a ^{3}IL excited state. Small shifts to lower energy of carbonyl bands were observed in the excited-state IR spectrum when compared to the ground-state spectrum. Each carbonyl band in the excited state is shifted by ~ 8 cm^{-1}. These shifts in the IR spectra indicate that, in the excited-state, rhenium(I) is a better electron donor to the carbonyl ligand than in the ground-state. Hence ^{3}IL(dppz) is a better electron donor to the rhenium(I) metal centre than ground-state dppz. The authors concluded that the ^{3}MLCT state of $[Re(CO)_3(dppz)(PPh_3)]^+$ is too high in energy compared to the ^{3}IL state to provide an efficient deactivation pathway.

The room temperature emission spectrum of $[Re(CO)_3(dppz)(py)]^+$ is structured with two vibronic components at λ_{max} = 556 and 559 nm, with lifetimes of 108 μs and 1.57 μs.[75,76] The photophysical properties of $[Re(CO)_3(dppz)(py)]^+$ (py = pyridine) in acetonitrile were also studied using excited-state IR, transient absorption and resonance Raman spectroscopy on picosecond and nanosecond timescales.[75] The results confirm that the lowest lying emissive state is a ^{3}IL state localised on the dppz

ligand. The studies have also provided detailed information on the dynamics of the complex upon photoexcitation. The dppz ligand was viewed in terms of a phenanthroline (phen) and a phenazine (phz) moiety. The emissive state of $[Re(CO)_3(dppz)(py)]^+$ is more accurately described as an ^{3}IL(phz) state. The picosecond studies show that ^{3}IL(phz) state is formed within 30 ps of excitation from the ^{3}IL(phen) state. In addition, the shift to higher wavenumber of the carbonyl bands in the excited state IR spectrum over a 30 ps timescale is consistent with conversion from ^{3}IL(phen) state to a ^{3}IL(phz) state. Gordon and co workers have investigated the excited states formed upon photoexcitation of Cu(I) and Re(I) complexes of dppz and a number of substituted analogues of this ligand.[77,78] Using a combination of resonance Raman spectroelectrochemistry, transient resonance Raman and excited state absorption techniques, it was shown that the lowest excited state was dppz-centred $^3\pi\pi^*$, except where an electron-withdrawing substituent was present on the dppz.

As previously discussed, the rhenium(I) tricarbonyl complexes of 2,2'-bipyridine or 1,10-phenanthroline have long lived, emissive ^{3}MLCT excited states.[54] Introduction of a NO_2 group to a bipyridine or phenanthroline ligand in a rhenium(I) tricarbonyl complex can strongly influence their photophysical properties. For example, the complexes $[Re(CO)_3(4,4'\text{-}(NO_2)_2\text{-bpy})Cl]$, $[Re(CO)_3(4,4'\text{-}(NO_2)_2\text{-bpy})Etpy]^+$ (Etpy = 4-ethylpyridine) and $[Re(CO)_3(5\text{-}NO_2\text{-phen})Cl]$ are nonemissive at room temperature, compared to the emissive bipyridine and phenanthroline analogues.[21,33,55] The lack of emission was interpreted as evidence for fast nonradiative decay of the ^{3}MLCT state resulting in very short excited state ^{3}MLCT lifetimes. For instance, the ^{3}MLCT lifetimes of $[Re(CO)_3(5\text{-}NO_2\text{-phen})Cl]$ and $[Re(CO)_3(5\text{-}NO_2\text{-phen})Etpy]^+$ are 7.6 ± 1.8 and 170 ± 20 ps respectively.[79] Time-resolved IR spectroscopic (TRIR) studies were conducted by Gabrielsson and coworkers on $[Re(CO)_3(5\text{-}NO_2\text{-phen})Cl]$ in order to ascertain the decay path of the ^{3}MLCT state.[80] The ground-state IR spectrum of $[Re(CO)_3(5\text{-}NO_2\text{-phen})Cl]$ shows three carbonyl bands at 1904, 1921 and 2026 cm^{-1}.

The spectrum recorded at 2ps after excitation shows negative bands at 1904, 1921 and 2026 cm^{-1} and transient bands at 1972, 2010 and 2095 cm^{-1}. These bands were attributed to formation of a ^{3}MLCT excited-state. The ^{3}MLCT spectral features decay with a lifetime of 10.4 ± 0.4 ps. Decay of the ^{3}MLCT spectral features is accompanied by a growth of two bands at 1886 and 2015 cm^{-1}. These bands decay with a lifetime of 30.5 ± 2 ps. This secondary transient in the TRIR spectra was assigned to a ^{3}IL state of an nπ* origin. Note, the proposed ^{3}nπ* intraligand character of the secondary transient is consistent with the a downward shift of the carbonyl bands as observed for other rhenium(I) tricarbonyl complexes.[81,82] The presence of the ^{3}nπ* state provides a deactivation pathway for the ^{3}MLCT excited-state in $[Re(CO)_3(5\text{-}NO_2\text{-}phen)Cl]$. Conversion to the ^{3}nπ* state is much faster than the usual decay to the ground state of ^{3}MLCT. Hence the ^{3}MLCT lifetime is shorter than the analogous phenanthroline complex that does not contain a nitro group.

The nature and dynamics of the lowest excited states of $[Re(CO)_3(5\text{-}NO_2\text{-}phen)L]^+$ (where L = 4-ethylpyridine (4-Etpy), imidazole (imH)) were investigated using picosecond visible and IR transient absorption spectroscopy.[79] The transient absorption spectra of $[Re(CO)_3(5\text{-}NO_2\text{-}phen)(4\text{-}Etpy)]^+$ and $[Re(CO)_3(5\text{-}NO_2\text{-}phen)(imH)]^+$ show bands at ~ 460 nm and 600 nm that closely resemble spectra of reduced nitro-aromatic radical anions. In addition, the carbonyl bands observed in the picosecond TRIR spectra of $[Re(CO)_3(5\text{-}NO_2\text{-}phen)(4\text{-}Etpy)]^+$ and $[Re(CO)_3(5\text{-}NO_2\text{-}phen)(imH)]^+$ are shifted to higher wavenumbers. These features are characteristic of a ^{3}MLCT $[Re^{II}(CO)_3(5\text{-}NO_2\text{-}phen^{\bullet-})(L)]^+$ state. For $[Re(CO)_3(5\text{-}NO_2\text{-}phen)(L)]^+$, the ^{3}MLCT state undergoes deactivation through the same ^{3}IL nπ* state as proposed for $[Re(CO)_3(5\text{-}NO_2\text{-}phen)Cl]$.[80] The ^{3}MLCT state of $[Re^{II}(CO)_3(5\text{-}NO_2\text{-}phen^{\bullet-})(Him)]^+$ also undergoes imidazole→Re(II) electron transfer. Imidazole→Re(II) electron transfer leads to the formation of a ^{3}LLCT excited state formulated as $[Re(CO)_3(5\text{-}NO_2\text{-}phen^{\bullet-})(Him^{\bullet+})]^+$. The nonemissive ^{3}LLCT state decays to the ground state with a lifetime of 19 ps in D_2O and 50 ps in methanol.

1.4.4.3 Photoinduced electron transfer in rhenium(I) carbonyl complexes

As previously discussed in Section 1.1, transition metal chemistry is focused towards the design of suitable supramolecular systems for potential use in artificial photosynthesis. Rhenium(I) complexes have been extensively studied because of their potential application in photochemically driven molecular devices.[8,55,83] In most of the systems that have been previously synthesised, an organic spacer separates the metal donor/acceptor units.[3,4,5] The mononuclear rhenium complexes that will be discussed in this section represent an interesting case where charge separation is achieved in two organic units linked by a rhenium metal centre.

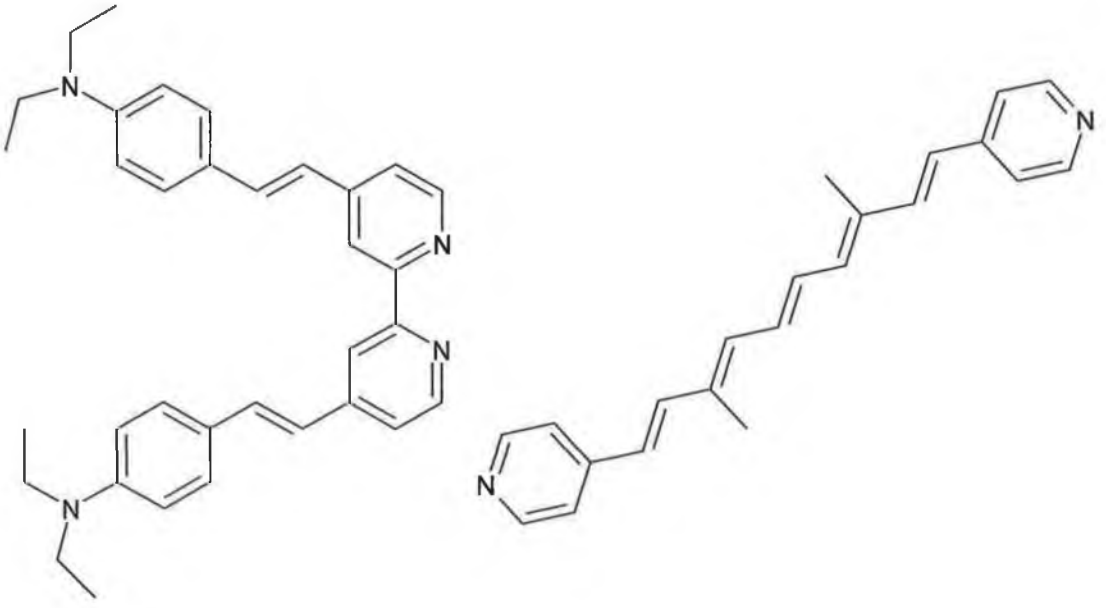

DEAS-bpy BPP

Figure 1. 15 *Structures of the ligands 4,4'-bis[p-(diethyl-amino)-α-styryl]-2,2'-bipyridine (DEAS-bpy) and 1,10-bis(4-pyridyl)-3,8-dimethyl-1,3,5,7,9-decapentaene (BPP).*

Long-lived charge separation in the mononuclear complex [(DEAS-bpy)Re(CO)$_3$(BPP)]$^+$ (where DEAS-bpy = 4,4'-bis[*p*-(diethyl-amino)-α-styryl]-2,2'-bipyridine, BPP =1,10-bis(4-pyridyl)-3,8-dimethyl-1,3,5,7,9-decapentaene; see Figure 1. 15) at room temperature has been observed by Ziessel and coworkers.[84,85] Weak ligand-centred emission at 298 K was initially observed in the tricarbonyl complex [Re(CO)$_3$(DEAS-bpy)Cl].[55] Replacement of the chloride with BPP was found to quench the emission at 298 K. Following detailed ground and excited-state absorption studies, it was proposed that optical excitation of [Re(CO)$_3$(DEAS-bpy)(BPP)]$^+$ produces a charge-separated [Re(CO)$_3$(DEAS-bpy$^{\bullet+}$)(BPP$^{\bullet-}$)]$^+$ state which has a lifetime of 4.3 μs. This process is formally viewed as a ligand-ligand charge transfer (LLCT) excited state.

Another case of interesting intramolecular photoreactivity occurs in [Re(CO)$_3$(dmb)(MQ$^+$)]$^{2+}$ (dmb = 4,4'-Me$_2$-2,2'-bipyridyl; MQ$^+$ = *N*-Me-4,4'-bipyridinium) complex.[86] Absorption of light in the corresponding [Re(CO)$_3$(dmb)Cl] complex results in the population of a Re→dmb ^{3}MLCT which decays with a lifetime of 10 ns.[87] Optical excitation (355 or 400 nm) of [Re(CO)$_3$(dmb)(MQ$^+$)]$^{2+}$ populates a Re→dmb ^{3}MLCT excited state. The Re→dmb ^{3}MLCT excited state [Re^{II}(CO)$_3$(dmb$^{\bullet-}$)(MQ$^+$)]$^{2+}$ undergoes an ultrafast intramolecular electron transfer dmb$^{\bullet-}$→ MQ$^+$ with a lifetime of 8 ps in acetonitrile or 14 ps in ethylene glycol.[88,89,] This process is summarised in Figure 1. 16. Picosecond time-resolved resonance Raman and IR studies have revealed that intramolecular electron transfer is accompanied by structural reorganisation of the MQ$^+$ and rhenium(I) tricarbonyl units.[90] The MQ ligand in the [Re^{II}(CO)$_3$(dmb)(MQ$^{\bullet}$)]$^{2+}$ excited state has a planar quinoidal structure. Positive shifts of the carbonyl bands in the TRIR spectra indicate shortening of the carbonyl bands due to a decrease of electron density on the rhenium(I) metal centre upon electron transfer.

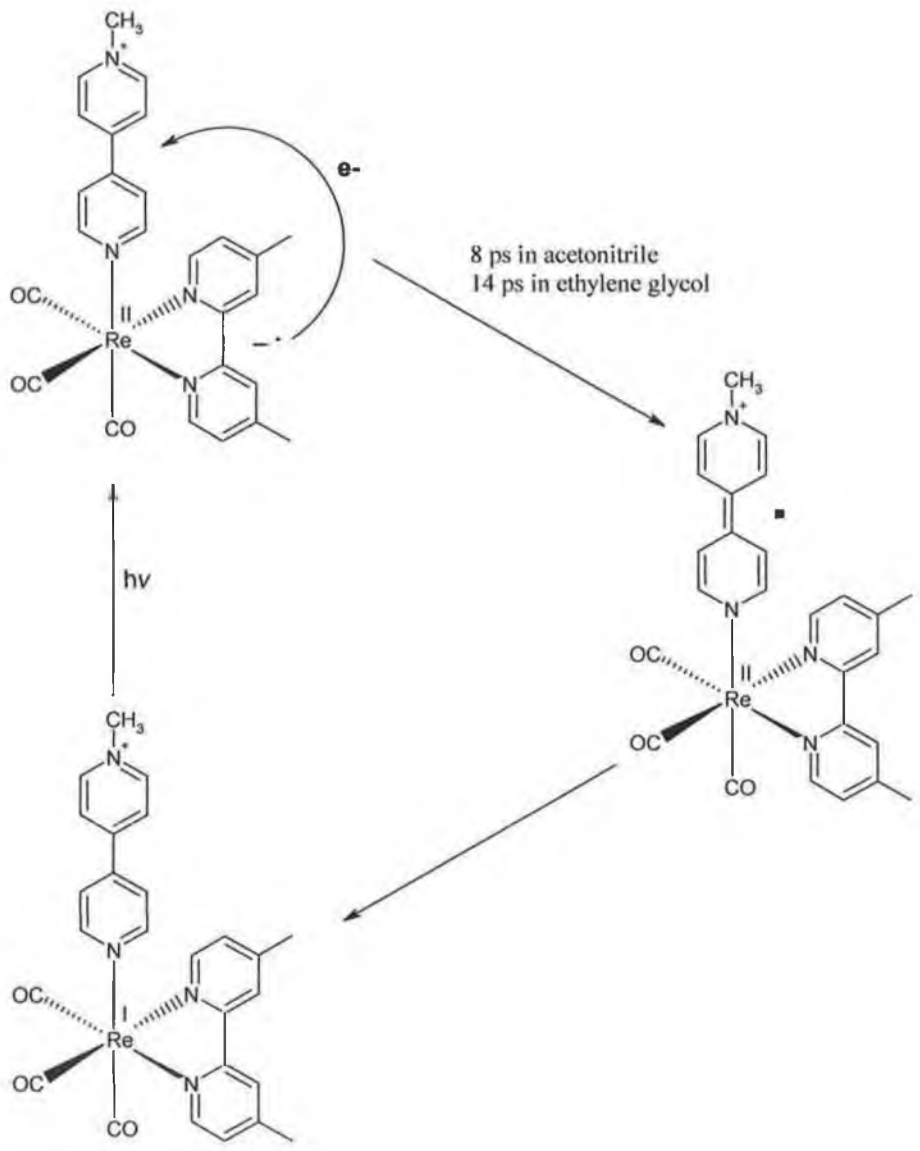

Figure 1. 16 *Inter-ligand electron transfer from the Re→dmb MLCT excited state of* $[Re(CO)_3(dmb)(MQ^+)]^{2+}$.[88]

Further studies into solvent-dependent dynamics of excited-state electron transfer in $[Re(CO)_3(dmb)(MQ^+)]^{2+}$ were also carried out.[91] $MQ^{\bullet}\rightarrow Re^{II}$ back electron transfer

was found to be moderately dependent on the molecular nature of the solvent. The observed solvent dependence on the electron transfer rate was explained by interactions between the positively charged MQ^+ and solvent molecules in the electron-transfer product $[Re(CO)_3(dmb)(MQ^+)]^{2+}$. Slower rates were observed for axial ligands in which the acceptor group is separated from the coordinating pyridine fragment by a spacer.[92]

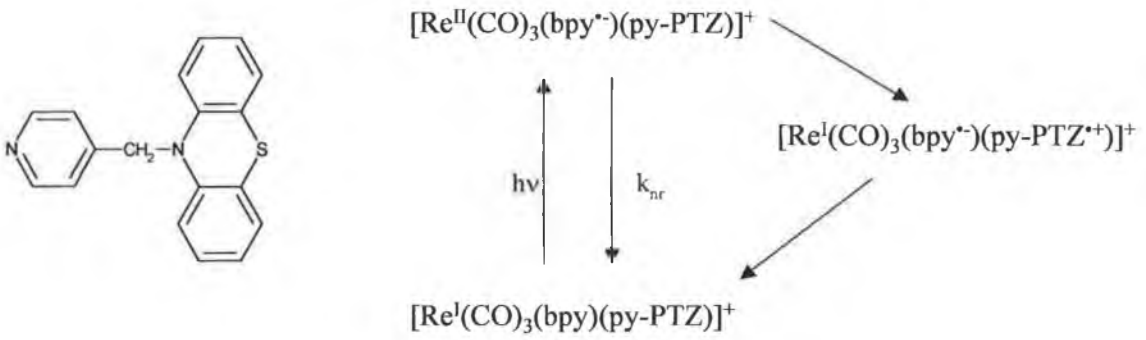

Figure 1. 17 *Structure of the py-PTZ ligand and the mechanism for the population of the py-PTZ→bpy LLCT state for* $[Re(py\text{-}PTZ)(CO)_3(bpy)]^+$.

The ligand py-PTZ (pyridine-phenothiazine) is an oxidisable ligand. This property of the py-PTZ ligand plays an interesting role in the excited-state dynamics of $[Re(CO)_3(bpy)(py\text{-}PTZ)]^+$.[93,94] Excitation of $[Re(CO)_3(bpy)(py\text{-}PTZ)]^+$ results in the formation of $[Re^{II}(CO)_3(bpy^{\bullet-})(py\text{-}PTZ)]^+$. An electron is transferred from py-PTZ to Re(II) (< 10 ns) forming $[Re^{I}(CO)_3(bpy^{\bullet-})(py\text{-}PTZ^{\bullet+})]^+$. This is viewed as a py-PTZ→bpy ligand to ligand charge transfer, LLCT, excited state. The LLCT excited state decays to the ground-state by intramolecular charge-transfer, $bpy^{\bullet-}\rightarrow py\text{-}PTZ^{\bullet+}$. Figure 1. 17 summarises this process. Note the quenching of the $[Re^{II}(CO)_3(bpy^{\bullet-})(py\text{-}PTZ)]^+$ excited state by py-PTZ is inhibited in rigid media as the required folding of the py-PTZ to reach a conformation suitable for electron transfer is prevented.[93]

1.4.4.4 Photoreactivity

Rhenium(I) polypyridine tricarbonyl complexes with a chloride or a nitrogen donor in the axial position do not undergo any ligand photodissociation under visible irradiation. Photodissociation of a CO ligand has been observed in rhenium(I) tricarbonyl complexes with a phosphorus ligand in the axial position.[95] Rhenium tricarbonyl complexes of the type $[Re(CO)_3(X_2\text{-bpy})(PR_3)]^+$ (X_2-bpy = 4,4'-X_2-2,2'-bipyridine) were photoactive at ambient temperature. Excitation of these complexes in acetonitrile solution gave the biscarbonyl complexes *cis,trans*-$[Re(CO)_2(X_2\text{-bpy})(PR_3)(CH_3CN)]^+$. These reactions were the first reported examples of photochemical ligand substitution reactions of rhenium diimine tricarbonyl complexes via their ^{3}LF excited states. Koike and coworkers have since looked at the photostability of complexes of the form $[Re(CO)_3(X_2\text{-bpy})Cl]$ and $[Re(CO)_3(X_2\text{-bpy})(py)]^+$ (py = pyridine) compared to their equivalent phosphorous containing complexes $[Re(CO)_3(X_2\text{-bpy})(PR_3)]^+$.[96] The following theories were used to explain the photoreactivity of the phosphorous complexes compared to the chloride and pyridine derivatives:

i) ^{3}LF excited states of rhenium diimine tricarbonyl complexes with a phosphorous ligand can be populated from the ^{3}MLCT states at ambient temperature.

ii) Large band gaps between the ^{3}LF and ^{3}MLCT states in the chloride and pyridine complexes.

iii) The strong π-acidity of PR_3 compared to the π-base Cl^- and the weaker π-acid pyridine causes a much weaker Re-C bond between the metal and the CO ligand trans to the phosphorous ligand compared to the Re-C bonds of the chloride and pyridine complexes.

When population of the ^{3}LF state occurs, the bonds between the rhenium and the ligands are weakened. The weakest bonds, i.e. Re-CO (axial) bonds of the phosphorous containing complexes are broken while the Re-CO bonds in the chloro and pyridine complexes are not weak enough to be broken.

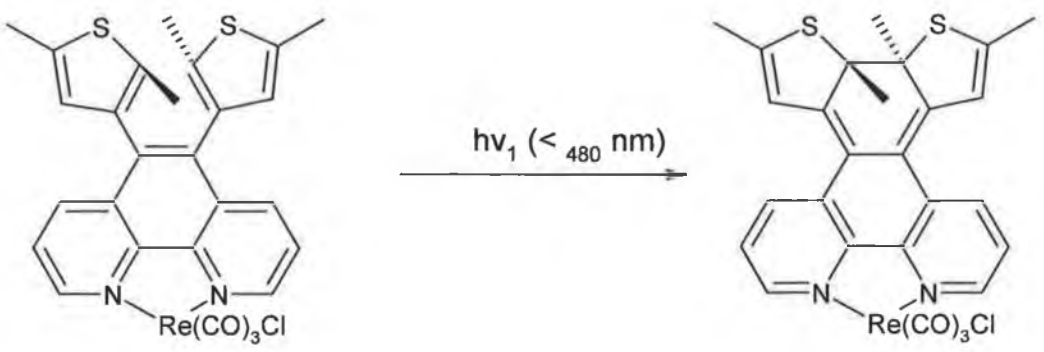

Figure 1. 18 *Photoinduced cyclisation of diarylethene-1,10-phenanthroline.*[97]

There are a few examples of photochemistry originating from ligands coordinated to a rhenium tricarbonyl. Wing-Wah Yam and co-workers recently reported photochemically induced cyclisation of a diarylethene-containing 1,10-phenanthroline ligand coordinated to a $[Re(CO)_3Cl]$ metal fragment (see Figure 1. 18).[97] Upon UV excitation of the complex at $\lambda = 313$ nm, three new absorption bands at 390 nm, 546 nm and 580 nm were observed in the absorption spectrum. By comparison with the photocyclised form of the free ligand, these new absorptions were attributed to absorptions of the closed form, generated by photocyclisation of the open form. The nature of the excited state involved the photocyclisation is not yet fully understood.

Wrighton and coworkers have studied the photochemical properties of $[Re(CO)_3$(*trans*-4-styrylpyridine)$_2Cl]$.[98] Absorption studies showed the lowest lying transition at 366 nm is a spin allowed singlet IL (π-π^*) transition. Irradiation of

$[Re(CO)_3(trans\text{-}4\text{-}styrylpyridine)_2Cl]$ leads to efficient *trans* → *cis* isomerisation of the styrlpyridine ligands (Figure 1. 19).

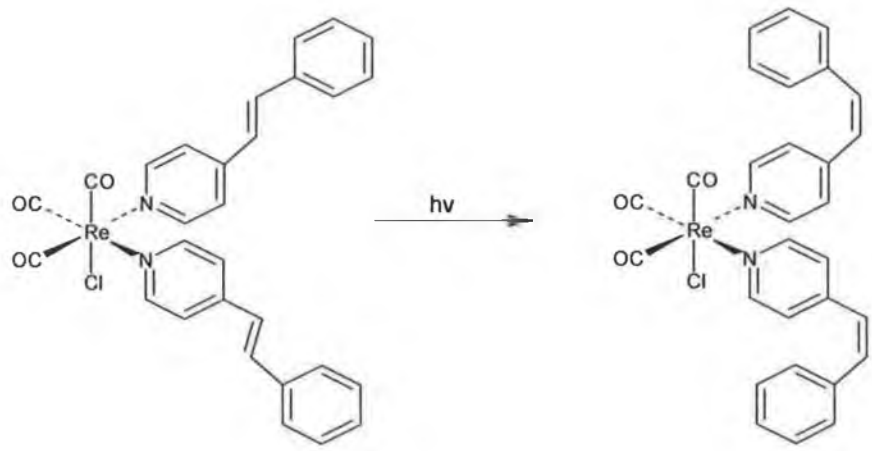

Figure 1. 19 *Photoinduced trans/cis isomerisation of* $[Re(CO)_3(trans\text{-}4\text{-}styrylpyridine)_2Cl]$.

The similarity between the isomerisation of $[Re(CO)_3(trans\text{-}4\text{-}styrylpyridine)_2Cl]$ and the free styrylpyridine ligand led the authors to propose that the isomerisation occurs form a ^{3}IL state. Femtosecond and picosecond time-resolved visible absorption, resonance Raman and IR studies of $[Re(CO)_3(trans\text{-}4\text{-}styrylpyridine)_2Cl]$ have concluded that ligand photoisomerisation occurs from a *trans*-4-styrylpyridine localised ^{3}IL state of $^3\pi\pi$ character.[99] TRIR spectra measured 2 ps after 400 nm excitation of $[Re(CO)_3(trans\text{-}4\text{-}styrylpyridine)_2Cl]$, show the A'(1) carbonyl band of the ^{3}IL state shifts to lower energy by ~10 cm^{-1} compared to the corresponding band in the ground state IR spectrum. This ^{3}IL state then undergoes a 12 ps conversion to another ^{3}IL state. Note the the A'(1) carbonyl band of this ^{3}IL state is downshifted by ~ 5 cm^{-1}. This switching of ^{3}IL states was interpreted as rotation of the C=C bond. Isomerisation to the *cis* form and return to the ground state follows.

Photoisomerisation also occurs in the bipyridyl complex $[Re(CO)_3(bpy)(trans\text{-}4\text{-}styrylpyridine)]^+$ via a Re→bpy MLCT state.[100,101,102] Optical excitation (400 nm) of $[Re(CO)_3(bpy)(trans\text{-}4\text{-}styrylpyridine)]^+$ populates a Re→bpy ^{1}MLCT excited state. This rapidly (~0.23 ps) undergoes ^{1}MLCT→^{3}MLCT intersystem crossing. The ground-state IR spectrum of $[Re(CO)_3(bpy)(trans\text{-}4\text{-}styrylpyridine)]^+$ shows two carbonyl bands at 1932 and 2034 cm^{-1}. The TRIR spectrum recorded measured at 1ps after excitation shows the ground state bleach bands at 1932 and 2034 cm^{-1} and transient bands at 1963, 1995 and 2061 cm^{-1}. These bands were attributed to formation of a Re→bpy ^{3}MLCT excited-state. The Re→bpy ^{3}MLCT spectral features disappear after 10 ps. The decay of the ^{3}MLCT bands is accompanied by growth of a band at 2027 cm^{-1} and a broad band between 1910 and 1960 cm^{-1}. This transient resembled the TRIR spectral pattern observed for $[Re(CO)_3(trans\text{-}4\text{-}styrylpyridine)_2Cl]$. Consequently it was attributed to a *trans*-4-styrylpyridine localised ^{3}IL state. The 2027 cm^{-1} band decays after 12 ps while another band grows at 2031 cm^{-1}. This band was attributed to rotation of the C=C bond resulting in perpendicular orientation of the phenyl and pyridine rings of the styrylpyridine ligand. This band then decays with isomerisation to the *cis* form and a return to the ground state.

1.5 Dinuclear systems containing rhenium(I)

1.5.1 Electronic and structural properties of bridging ligands

Polypyridine type ligands have been extensively used to build binuclear systems. In such systems the metal units are linked by bridging ligands. Ligands capable of linking two metal centres are termed bridging ligands. The choice of suitable bridging ligands is crucial in determining the properties of bimetallic complexes, because:

i) Their coordinating sites influence the spectroscopic and redox properties of the metal centres.

ii) Their structure and orientation of their coordinating sites determine the architecture of the complex.

iii) Their chemical nature controls electronic communication between the metal centres.

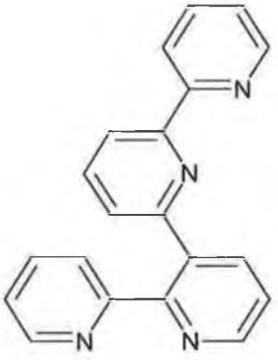

2,2':3',2":6",2"'-quaterpyridine[103,104]
(qpy)

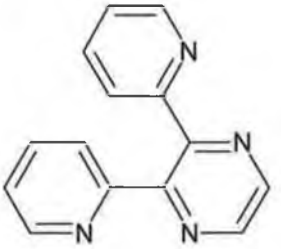

2,3-bis-(2-pyridyl)-pyrazine[105,106]
(2,3-dpp)

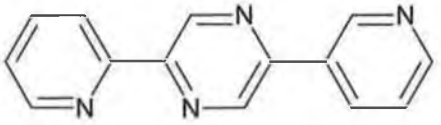

2,5-bis-(2-pyridyl)-pyrazine[107]
(2,5-dpp)

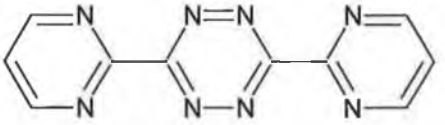

3,6-bis-(2-pyridyl)-1,2,4,5-tetrazine[108]
(bmtz)

Figure 1. 20 *Examples of π-accepting bridging ligands.*

Bridging ligands are generally classed in terms of their σ-donating and π-accepting abilities. The π-accepting ligands form the majority of bridging ligands. There is a wide range of bidentate-bridging ligands available but the most widely studied are

those based on neutral derivatives of pyridine and pyrazine. Some examples are shown in Figure 1. 20. Such ligands mediate intermetallic communication via low-lying π* orbital. Due to the low-lying π*-orbitals of these bridging ligands, the lowest MLCT transition is usually bridged based. When luminescence is observed, it originates from the bridging ligand. Likewise the first reduction wave of these complexes is found on the bridging ligand. Upon coordination of a second metal centre to a mononuclear complex with a π-accepting bridging ligand, the following trends are observed:

i) The bridging ligand reduction potential becomes much less negative.
ii) The first metal-centred oxidation potential becomes slightly more positive.
iii) The absorption and emission maxima shift to lower energy.

The above trends are attributed to further stabilisation of the π*-levels of the bridging ligand upon coordination of a second metal centre.

Examples of σ-donating ligands are shown in Figure 1. 21. The strong σ-donating abilities of these ligands arise from the formation of their anionic analogues when complexed to a metal centre. Bimolecular systems containing σ-donor bridging ligands have very different properties to complexes containing strong π-acceptor bridging ligands. These properties are best illustrated using $[M(bpy)_2(bpt)]^+$ where M = Ru(II) or Os(II).[109,110] The lowest π* level of bpt^- is at higher energy than the π* levels of the bpy ligands. Hence the lowest energy absorption and emission bands are bpy-based.

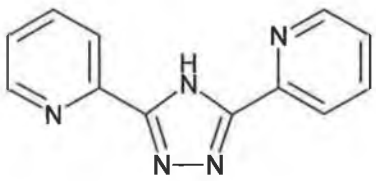

3,5-bis-(pyridin-2-yl)-1,2,4-triazole[109,110]
(Hbpt)

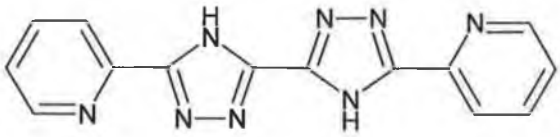

5,5'-bis-(pyridin-2"-yl)-3,3'-bis(1H-1,2,4-triazole)[111]

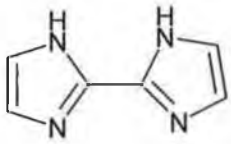

2,2-biimidazole[112]
(H_2bii)

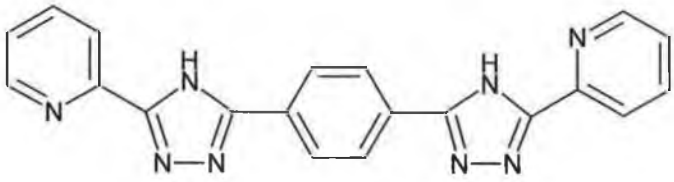

1,4-bis(5-(2-pyridyl)-1H-1,2,4-triazole-3-yl)benzene[113]

Figure 1. 21 *Examples of σ-donating bridging ligands.*

Furthermore, the absorption and emission bands of the dinuclear complexes are observed at higher energy than those of the mononuclear compounds. The negative charge of the bpt^- anion is shared upon coordination of a second metal centre. This effect causes a decrease in electron density on the metal centres. The energy of the d_π metal orbital is stabilised, thus increasing the energy separation between the d_π level and the bpy-based π^* orbital. This is reflected in the blue shift of the absorption and emission bands. This is in sharp contrast to the previously described π-accepting bridges.

1.5.2 Previous complexes of ruthenium(II) and rhenium(I)

There has been considerable interest in the study of photoinduced electron and energy transfer between components in supramolecular systems due to the potential development of devices capable of performing light-induced functions.[4,13,114] Interest has focused on the low spin d^6 metal complexes $[Ru(bpy)_3]^{2+}$, $[Os(bpy)_3]^{2+}$ and $[Re(CO)_3(bpy)Cl]$ due to their favourable redox excited-state properties. Studies on various Ru(II)/Os(II) polypyridine systems have shown that excitation of the Ru(II) centre results in emission from the Os(II) centre following intercomponent energy transfer.[115,116,117] Previous examples of Ru(II)/Re(I) systems, which are less common are discussed in this section.

Shown in Figure 1. 22 are examples of previously studied heteronuclear Ru(II)/Re(I) complexes. In each complex, the bridging ligand is a conjugated system with a relatively small intermetallic distance between the metal centres. The photophysical and electrochemical properties of the heteronuclear complexes shown in Figure 1. 22 have been studied.[118,119,120] For each of these complexes, intercomponent energy transfer occurs from the rhenium centre to the ruthenium centre, i.e. only ruthenium emission is observed when the complex is excited at the wavelength of the ruthenium or rhenium absorption maximum.

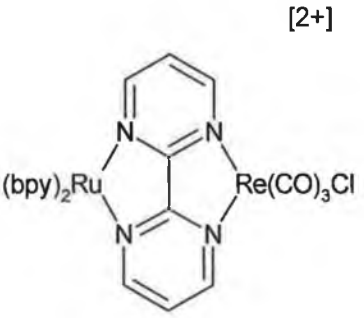

$[Ru(bpy)_2(bpym)Re(CO)_3Cl]^{2+}$ [118]
bpym = 2,2'-bipyrimidine

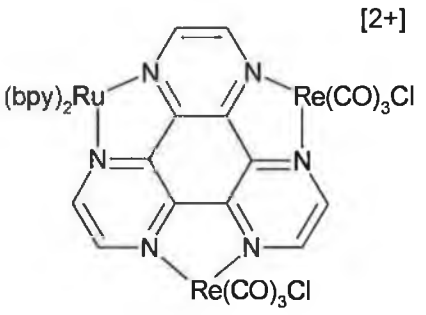

$[Ru(bpy)_2(HAT)\{Re(CO)_3Cl\}_2]^{2+}$ [119]
HAT = benzo[1,2-b:3,4-b':5,6-b"]tripyrazine

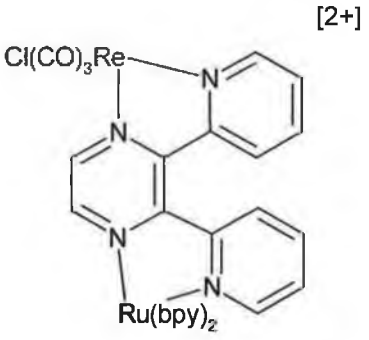

$[Ru(bpy)_2(2,3\text{-}dpp)Re(CO)_3Cl]^{2+}$ [120],
2,3-dpp = 2,3-bis-(2-pyridyl)-pyrazine

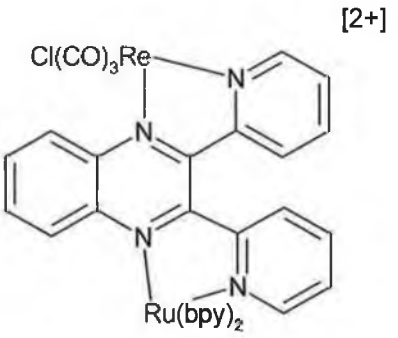

$[Ru(bpy)_2(2,3\text{-}dpq)Re(CO)_3Cl]^{2+}$ [120]
2,3-dpq = 2,3-bis-(2-pyridyl)-quinoxaline

Figure 1. 22 *Examples of Ru(II)/Re(I) heteronuclear complexes.*

Ward and coworkers have synthesised a number of Ru(II)/Re(I) complexes containing the asymmetric ligand 2,2':3',2":6",2'"-quaterpyridine (AB).[121] This quaterpyridine ligand is a binucleating ligand with two bpy-type binding sites, A and B. The interesting feature of this ligand is that these sites, A and B, are both sterically and electronically inequivalent. Chelating site B is more sterically hindered when compared to site A. The structures of two of the complexes synthesised by Ward are shown in Figure 1. 23. In both cases the first metal in the formula is

coordinated to the sterically less hindered site (labelled A). Interestingly, when one equivalent of the metal was reacted with the ligand, the metal only binded to site A. Only under more extreme conditions does the second metal co-ordinate at site B.

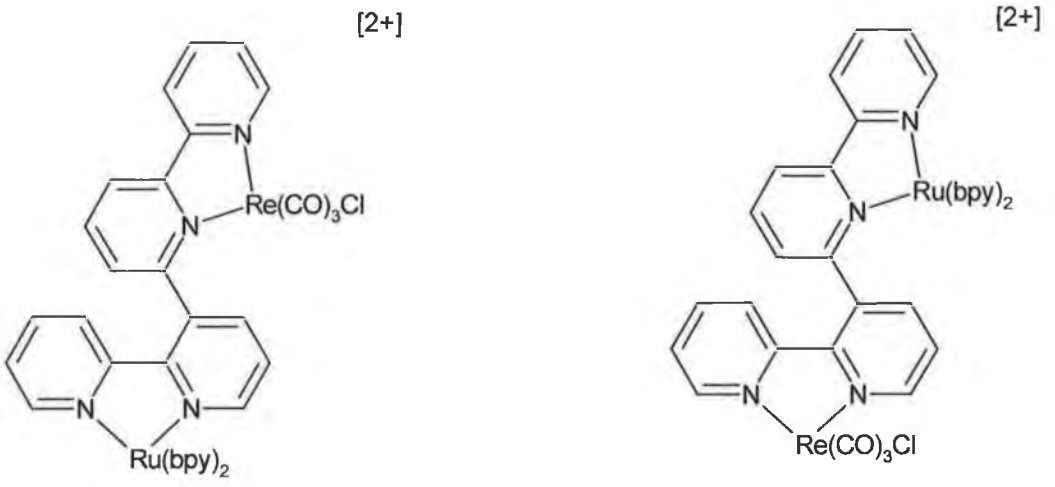

Ru-AB-Re Re-AB-Ru

Figure 1. 23 *Heterodinuclear Ru(II)/Re(I) complexes of the asymmetric quaterpyridine ligand, AB.*

In both Ru-AB-Re and Re-AB-Ru, the metal fragments are photochemically and redox active. Both complexes exhibit site-dependent absorption, luminescence and electrochemical properties. The positional isomers Ru-AB-Re and Re-AB-Ru exhibit either Ru-based or Re-based emission, depending on the coordination sites of the metal. This was attributed to the direction of energy transfer. The luminescence state of the Ru-AB-Re complex is centred on the Ru-based moiety i.e. Re → Ru energy transfer. In the Re-AB-Ru complex, luminescence is centred on the Re moiety Ru → Re energy transfer. This is in contrast to other Ru(II)/Re(II) polypyridyl complexes in which the direction of energy transfer was always Re → Ru (Figure 1. 22).

Figure 1. 24 shows the mixed-metal complex $[Ru(bpy)_2(bpyen)Re(CO)_3(py)]^{3+}$. When excited at 355 nm in dichloromethane, the complex was found to emit at both 610 nm (Ru) and 540 nm (Re).[122] The emissions were assigned as ^{3}MLCT in origin, and were based on each of the metal centres. Communication via the bridging ligand bpyen was poor, but was sufficient to allow Ru → Re energy transfer between the metal centres. The dual emission observed in $[Ru(bpy)_2(bpyen)Re(CO)_3(py)]^{3+}$ is different to the other examples of heteronuclear Ru(II)/Re(I) complexes shown in Figure 1. 22 and Figure 1. 23, as these complexes all exhibited emission originating from a single metal centre.

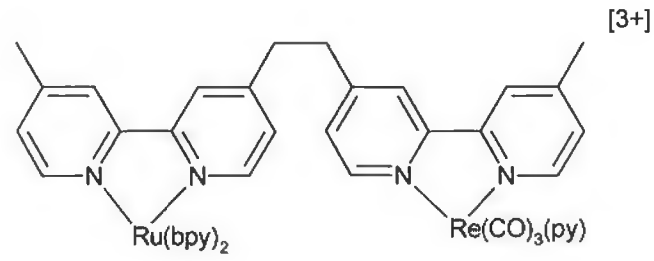

Figure 1. 24 *The mixed-metal complex* $[Ru(bpy)_2(bpyen)Re(CO)_3(py)]^{3+}$ *where bpyen = 1,2-bis(4'-methyl-2,2'-bipyridyl-4-yl)ethane.*

Encinas and coworkers have reported dual emission from the Ru(II)/Re(I) complex, $[Ru(bpy)_2(dstyb)Re(CO)_3Cl]^{2+}$ (see Figure 1. 25).[123] The luminescence spectrum of $[Ru(bpy)_2(dstyb)Re(CO)_3Cl]^{2+}$ at room temperature showed two distinct emission features at 621 nm and 695 nm. The band maximum at 621 nm was attributed to emission from the ^{3}Ru → dstyb CT excited state, while the band at 695 nm assigned to an intra-ligand transition (^{3}IL) from the bridging ligand dstyb.

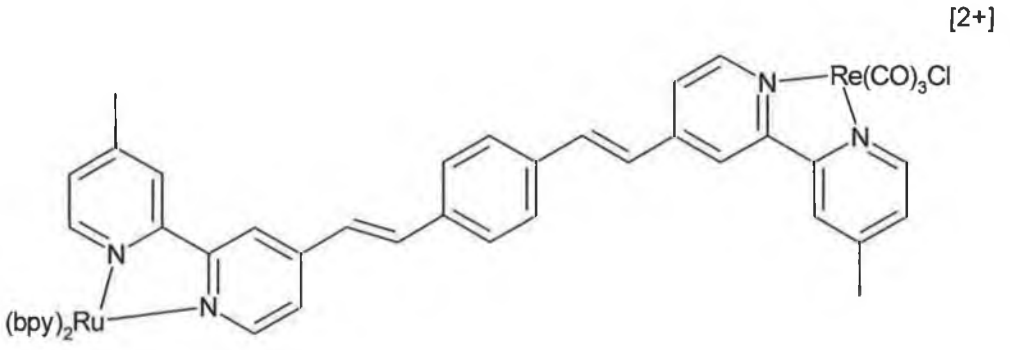

Figure 1. 25 *The heteronuclear Ru(II)/Re(I) complex* $[Ru(bpy)_2(dstyb)Re(CO)_3Cl]^{2+}$*, where dstyb is the bridging ligand 1,4-bis[2-(4'-methyl-2,2'-bipyridyl-4-yl)ethenyl]benzene.*

By comparing the excitation spectrum of $[Ru(bpy)_2(dstyb)Re(CO)_3Cl]^{2+}$ with the absorption spectra of $[Ru(bpy)_2(dstyb)Re(CO)_3Cl]^{2+}$ and the mononuclear ruthenium complex $[Ru(bpy)_2(dstyb)]^{2+}$, the authors established the relaxation pathways for the excitation energy in the heteronuclear complex. These results indicated that emission from the ^{3}IL(dstyb) state is sensitised by the rhenium based absorption, whereas the ^{3}Ru $\rightarrow$ dstyb CT emission is not directly sensitised by the rhenium based absorption. They also concluded that some of the light absorbed by the rhenium based chromophore of $[Ru(bpy)_2(dstyb)Re(CO)_3Cl]^{2+}$ is firstly transferred to the bridging ligand and then redistributed between the ^{3}IL(dstyb) and ^{3}Ru $\rightarrow$ dstyb CT levels (Figure 1. 26).

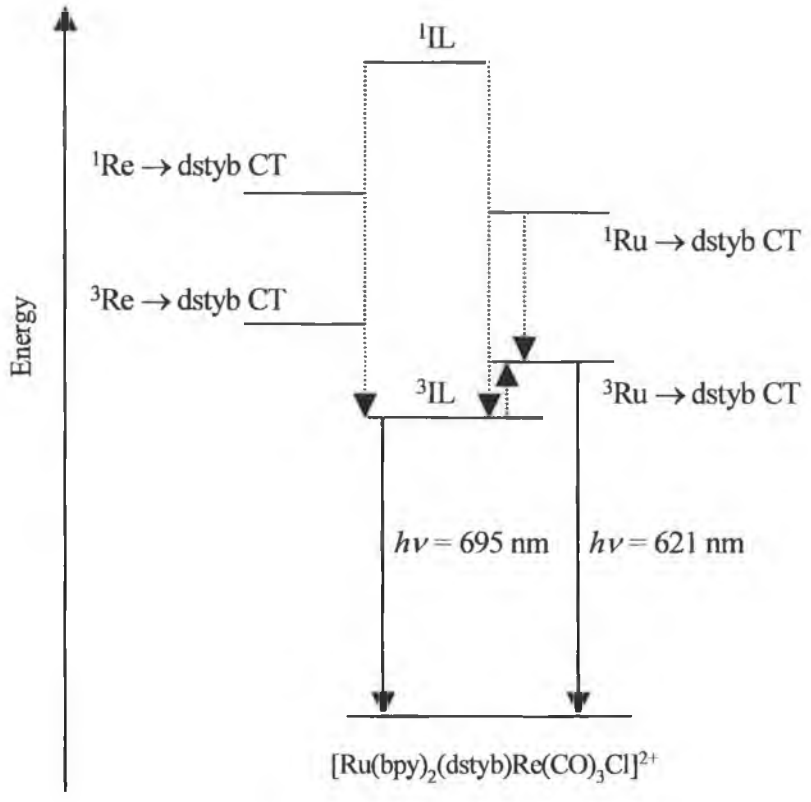

Figure 1. 26 *Schematic energy level diagram for* $[Ru(bpy)_2(dstyb)Re(CO)_3Cl]^{2+}$.

The overall excitation process of $[Ru(bpy)_2(dstyb)Re(CO)_3Cl]^{2+}$ involves an indirect Re → Ru energy transfer process mediated by the bridging ligand. This is in contrast to the other Ru(II)/Re(I) complexes illustrated in Figure 1. 22, where Re → Ru energy transfer is mediated by direct excitation of the Re-based chromophore.

1.6 Scope of thesis

Chapter 2 describes the synthesis, purification and characterisation of a series of mononuclear rhenium(I) tricarbonyl complexes containing substituted 3-(pyridin-2-yl)-1,2,4-triazole ligands. The electronic properties of the pyridyl-triazole complexes

are compared to $[Re(CO)_3(bpy)Cl]$, where bpy is 2,2'-bipyridyl. The substitution of groups on the triazole ligand and the effect of these substituents on the ground-state and excited-state properties of the complexes is also examined. Chapter 3 introduces a series of 3-(pyrazin-2-yl)-1,2,4-triazole ligands and the corresponding rhenium(I) tricarbonyl complexes of these ligands. The pyrazyl-triazole ligands are analogous to those prepared in Chapter 2. The pyrazyl-triazole complexes have also been prepared and studied in the same systematic method as their pyridyl-triazole analogues.

Chapter 4 deals with the ligand 3,5-bis(pyridin-2-yl)-1,2,4-triazole (Hbpt). Unlike the triazole ligands discussed in Chapters 2 and 3, the Hbpt ligand provides the opportunity to coordinate two metal centres. Chapter 4 will firstly discuss the synthesis and characterisation of the rhenium(I) and ruthenium(II) complexes containing the Hbpt ligand. The mononuclear complexes discussed will include $[Re(CO)_3(Hbpt)Cl]$, $[Ru(bpy)_2(bpt)]^+$ and $[Ru(d_8\text{-}bpy)_2(bpt)]^+$. The synthesis and characterisation of the dinuclear complexes $[\{Re(CO)_3Cl\}_2(Hbpt)]$, $[Ru(bpy)_2(bpt)Re(CO)_3Cl]^+$ and $[Ru(d_8\text{-}bpy)_2(bpt)Re(CO)_3Cl]^+$ are also discussed in Chapter 4. The photophysical and electrochemical properties of both the mononuclear and dinuclear complexes will also be examined. The deuteriated complex $[Ru(d_8\text{-}bpy)_2(bpt)Re(CO)_3Cl]^+$, whereby the bipyridine rings are deuteriated aids the elucidation of the ^1H NMR spectra. Particular attention will also be paid to the photophysics of $[Ru(bpy)_2(bpt)Re(CO)_3Cl]^+$ and its deuteriated analogue $[Ru(d_8\text{-}bpy)_2(bpt)Re(CO)_3Cl]^+$ with the use of partial deuteriation as a probe in the location of the excited state.

Chapter 5 discusses the methylation of the ruthenium(II) bipyridyl complex containing the pyrazyl-triazole ligand 3-(pyrazin-2-yl)-5-phenyl-1,2,4-triazole. In addition selective deuteration of the bipyridyl ligands and the triazole ligand is also employed. A comparison of the ^1H NMR spectra of the deuteriated and undeuteriated complexes aids structural characterisation of the complexes. The photophysical and electrochemical properties of all complexes are also examined. Wavelength

dependent ground-state resonance Raman measurements are also discussed in order to elucidate the electronic transitions in the absorption spectra of the methylated complexes.

In Chapter 6 the instrumentation and techniques used to characterise the compounds are listed and the use of each will be described in the course of the work. Some final remarks on the work and suggestions for future work will be considered in chapter 7. Finally two appendices are supplemented to the thesis. The first discusses the attempted synthesis of a heteronuclear complex $[Ru(bpy)_2LM(CO)_4]^{2+}$ (where L = 2,3-bis-(2-pyridyl)-pyrazine; M = Cr, Mo or W). The second appendix refers to the poster presentations made during the course of this research.

1.7 Bibliography

1 D.A. Gust, T.A. Moore, *Science*, 1989, 244, 35.

2 J.R. Norris, P. Gast, *J. Photochem.*, 1985, 29, 185.

3 J.M. Lehn, *Angew. Chem. Int Ed. Engl.*, **1988**, 27, 89.

4 J.M. Lehn, *Supramolecular Chemistry: Concepts and Perspectives*, VCH, Weinheim, **1995**.

5 J.P. Sauvage, J.P. Collin, J.C. Chambron, S. Guillerez, C. Coudet, V. Balzani, F. Barigelletti, L. De Cola, L. Flamigni, *Chem. Rev.*, **1994**, 94, 993

6 F. Scandola, C.A. Bignozzi, C. Chiorboli, M.T. Indelli, M.A. Rampi, *Photoprocesses in Trans. Metal Complexes, Biosystems and other Molecules,* E. Kochanski (Ed.), Series C, Vol. 376, Kluwer, Dordrecht, **1991**, 234

7 V. Balzani, L. Moggi, *Coord. Chem. Rev.*, **1990**, 97, 313

8 V. Balzani, F. Scandola, *Supramolecular Photochemistry" Ellis Horwood, Chichester*, **1991**.

9 T. Förster, *Discuss. Faraday Soc.*, **1959**, 27,7

10 D.L. Dexter, *J. Chem. Phys.*, **1953**, 21, 836

11 R.F. Ziessel, *J. Chem. Ed.*, **1997**, 74, 673.

12 A. Gilbert, J. Baggott, *Essentials of Molecular Photochemistry,* Blackwell Science, London, **1991**.

13 V. Balzani, A. Juris, M. Venturi, S. Campagna and S. Serroni, *Chem. Rev.* **1996**, 96, 759.

14 D.J. Stufkens, A. Vlček, *Inorg. Chem.,* **1996**, 35, 2902.

15 F. Scandola, V. Balzani, *J. Chem. Ed.*, **1983**, 60, 814

16 J. N. Demas, *J. Chem. Ed.*, **1983**, 60, 807.

17 J.V. Caspar, T.D. Westmoreland, G.H. Allen, P.G. Bradley, T.J. Meyer, W.H. Woodruff, *J. Am. Chem. Soc.,* **1984**, 106, 3492.

18 A.A. Martí, G. Mezei, L. Maldonado, G. Paralitici, R.C. Raptis, J.L. Colón, *Eur. J. Inorg. Chem.,* **2005**, 118.

19 J.A. Baiano, W. Rorer Murphy, *Inorg. Chem.,* **1991**, 30, 4594.

20 N.H. Damrauer, T.R. Boussie, M. Devenney, J.K. McCusker, *J. Am. Chem. Soc.,* **1997**, 119, 8253.

21 M. Wrighton, D. L. Morse, *J. Am. Chem. Soc.,* **1974**, 96, 998

22 J.C. Luong, L. Nadjo, M.S. Wrighton, *J. Am. Chem. Soc.*, **1978**, 100, 5790.

23 D.L. Morse, M.S. Wrighton, *J. Am. Chem. Soc.*, **1976**, 98, 3931.

24 K.K.-W. Lo, W.-K. Hui, C.-K. Chung, K.H.-K. Tsang, D.C.-M. Ng, N. Zhu, K.-K. Cheung, *Coord. Chem. Rev.,* **2005,** 249, 1434.

25 V.W.-W. Yam, K.M.-C. Wong, V.W.-M. Lee, K.K.-W. Lo, K. -K. Cheung, *Organometallics,* **1995**, 14, 4034.

26 D.I. Yoon, C.A. Berg-Brennan, H. Lu, J.T. Hupp, *Inorg. Chem.,* **1992**, 31, 3192.

27 C.A. Berg-Brennan, D.I. Yoon, R.V. Slone, A.P. Kazala, J.T. Hupp, *Inorg. Chem.,* **1996**, 35, 2032.

28 K.K.-W. Lo, W.-K. Hui, D.C.-M. Ng, K.-K. Cheung, *Inorg. Chem.,* **2002**, 41, 40.

29 B.P. Sullivan, T.J. Meyer, J. Chem. Soc. *Chem. Commun.*, **1984**, 1244.

30 F.P.A. Johnson, M.W. George, F. Hartl, J.J. Turner, *Organometallics*, **1996**, 15, 3374.

31 H.A. Goodwin, F. Lions, *J. Am. Chem. Soc.*, **1959**, 81, 6415

32 R. Sahai, D.P. Rillema, R. Shaver, S. Van Wallendael, D.C.Jackman, M. Boldaji, *Inorg. Chem.*, **1989**, 25, 1022

33 J.K. Hino, L. Della Ciana, W.J. Dressick, B.P. Sullivan, *Inorg. Chem.*, **1992**, 31, 1072

34 W.M. Xue, N. Goswami, D.M. Eichhorn, P.L. Orizondo, D.P. Rillema, *Inorg. Chem.*, **2000**, 39, 4467.

35 R. Argazzi, E. Bertolasi, C. Chiorboli, C.A. Bignozzi, M.K. Itokazu, N.Y. Murakami Iha, *Inorg. Chem.*, **2001**, 40, 6885

36 L.W. Houk, G.R. Dobson, *Inorg. Chem.*, **1966**, 5, 2119.

37 D.R. Gamelin, M.W. George, P. Glyn, F.W. Grevels, F.P.A. Johnson, W. Klotzbücher, S.L. Morrison, G. Russell, K. Schaffner, J.J. Turner, *Inorg. Chem.*, **1994**, 33, 3246.

38 G.J. Stor, S.L. Morrison, D.J. Stufkens, A. Oskam, *Organometallics,* **1994**, 13, 2641

39 D.M. Dattelbaum, K.M. Onberg, P.J. Hay, N.L. Gebhart, R.L. Martin, J.R. Schoonover, T.J. Meyer, *J. Phys. Chem. A,* **2004**, 108, 3527.

40 A. Klein, C. Vogler, W. Kaim, , *Organometallics,* **1996**, 15, 236

41 S. Van Wallendael, R.J. Shaverm D.P. Rillema, B.J. Yoblinski, M. Stathis, T.F. Guarr, *Inorg. Chem.*, **1990**, 29, 1761

42 W. Kaim, H.E.A. Kramer, C. Volger, J. Rieker, *J. Organomet. Chem.*, **1989**, 367, 107

43 H. Hartmann, T. Scheiring, J. Fiedler, W. Kaim, *J. Organomet. Chem,*. **2000**, 604, 267.

44 S. Frantz, J. Fiedler, I. Hartenbach, T. Schleid, W. Kaim, *J. Organomet. Chem,*. **2002**, 689, 3049

45 G. Knör, M. Leirer, A. Vogler, *J. Organomet. Chem.*, **2000**, 610, 16.

46 K.A. Walters, Y.J. Kim, J.T. Hupp, *Inorg. Chem.,* **2002**, 41, 2909.

47 L.A.Worl, R. Duesing, P. Chen, L. D. Ciana, T.J. Meyer, *J. Chem. Soc. Dalton Trans.,* **1991**, 849.

48 L. Yang, A. Ren, J. Feng, X. Liu, Y. Ma, M. Zhang, X. Liu, J. Shen, H. Zhang, *J. Phys. Chem. A,* **2004**, 108, 6797

49 L. Yang, A. Ren, J. Feng, X. Liu, Y. Ma, H. Zhang, *Inorg. Chem.,* **2004**, 43, 5961.

50 B.D. Rossendaar, D.J. Stufkens, A. Vlček Jr., *Inorg. Chem.,* **1996**, 35, 2902.

51 H.A. Nieuwenhuis, D.J. Stufkens, R.A. McNicholl, A.H.R. Al-Obaidi, C.G. Coates, S.E.J. Bell, J.J. McGarvey, J. Westwell, M.W. George, J.J. Turner, *J. Am. Chem. Soc.,* **1995**, 117, 5579.

52 J.A. Baiano, R.J. Kessler, R.S. Lumpkin, M.J. Munley, W. Rorer Murphy, *J Phys. Chem.,* **1995**, 99, 17680.

53 J.V. Caspar, T.J. Meyer, *J. Phys. Chem.,* **1983**, 87, 952.

54 D.J. Stufkens, A. Vlček Jr., *Coord. Chem. Rev.,* **1998**, 177, 127.

55 A. Juris, S. Campagna, I. Bidd, J.M. Lehn, R. Ziessel, *Inorg. Chem.* **1988**, 27, 4007.

56 P. Chen, R. Duesing, D.K. Graff, T.J. Meyer *J. Phys. Chem.,* **1991**, 95, 5850.

57 S.M. Fredericks, J.C. Luong, M.S. Wrighton, *J. Am. Chem., Soc.,* **1979**, 101, 7415.

58 P.J. Giordano, S.M. Fredericks, M.S. Wrighton, D.L. Morse, *J. Am. Chem., Soc.,* **1978**, 100, 2257.

59 M. Busby, P. Matousek, M. Towrie, I.P. Clark, M. Motevalli, F. Hartl, A. Vlček, Jr., *Inorg. Chem.,* **2004**,43,4523.

60 C.-F. Shu, M.S. Wrighton, *Inorg. Chem.*, **1988**, 27, 4326.

61 T. Tahara, H. Hamaguchi, M. Tasumi, *J. Phys. Chem.,* **1987**, 91, 5875.

62 D.R. Striplin, G.A. Crosby, *Coord. Chem. Rev.*, **2001** 211, 163.

63 M. Leirer, G. Knör, A. Vogler, *Inorg. Chim. Acta.*, **1999**, 288, 150.

64 L. Sacksteder, A. Zipp, E. Brown, J. Streich, J.N. Demas, B. DeGraff, *Inorg.*

Chem., **1990**, 29, 4335.

65 L. Wallace, D.P. Rimella, *Inorg. Chem.,* **1993**, 32, 3836.

66 L. Wallace, D.C. Jackman, D.P. Rillema, J.W. Merkert, , *Inorg. Chem.*, **1995**, 34, 5210.

67 A.P. Zipp, L. Sacksteder, J. Streich, A. Cook, J.N. Demas, B.A. DeGraff, *Inorg. Chem.*, **1993**, 32, 5629.

68 R.M. Leasure, L. Sacksteder, D. Nesselrodt, G.A. Reitz, J.N. Demas, B.A. DeGraff, *Inorg. Chem.,* **1991**,30, 3722.

69 L. Sacksteder, M. Lee, J.N. Demas, B.A. DeGraff, *J. Am. Chem., Soc.,* **1993**, 115, 8230.

70 S.R. Stoyanov, J.M. Villegas, A.J. Cruz, L.L. Lockyear, J.H. Reibenspies, D.P. Rillema, *J. Chem. Theory Comput.,* **2005**, 1, 95.

71 J.M. Villegas, S.R. Stoyanov, W. Huang, D.P. Rillema, *J. Chem. Soc. Dalton Trans.,* **2005**, 1042.

72 J.M. Villegas, S.R. Stoyanov, W. Huang, D.P. Rillema, *Inorg. Chem.,* **2005**, 44, 2297

73 J.R. Schoonover, W.D. Bates, T.J. Meyer, *Inorg. Chem.,* **1995**, 34, 6421.

74 J.R. Schoonover, G.F. Strousse, R.B. Dyer, W.D. Bates, P. Chen, T.J. Meyer, *Inorg. Chem.,* **1996**, 35, 273.

75 J. Dyer, W.J. Blau, C.G. Coates, C.M. Creely, J.D. Gavey, M.W. George, D.C. Grills, S. Hudson, J.M. Kelly, P. Matousek, J.J. McGarvey, J. McMaster, A.W. Parker, M. Towrie, J.A. Weinstein, *Photochem. Photobiol. Sci.,* **2003**, 2, 542.

76 R. Diaz, A. Francois, A.M. Leia, B. Loeb, E. Norambuena, M. Yanez, *Helvetica Chimica Acta,***2006,** 89, 1220.

77 N.J. Lundin, P.J. Walsh, S.L. Howell, J.J. McGarvey, A.G. Blackman, K.C. Gordon, *Inorg. Chem.,* **2005**, 44, 3551.

78 P.J. Walsh, K.C. Gordon, N.J. Lundin, A.G. Blackman, *J. Phys. Chem. A,* **2005**, 109, 5933.

79 M. Busby, A. Gabrielsson, P. Matousek, M. Towrie, A.J. Di Bilio, H.B. Gray, A. Vlček, Jr., *Inorg. Chem.,* **2004**, 43, 4994.

80 A. Gabrielsson, P. Matousek, M. Towrie, F. Hartl, S. Záliš, A. Vlček, Jr., *J. Phys. Chem. A,* **2005**, 109, 6147

81 D.M. Dattelbaum K.M. Omberg, P. Jeffry Hay, N.L. Gebhart, R.L. Martin, J.R. Schoonover, T.J. Myer, *J. Phys. Chem. A,* **2004**, 108, 3527.

82 M.K. Kuimova, W.Z. Alsindi, J. Dyer, D.C. Grills, O.S. Jina, P. Matousek, A.W. Parker, P. Portius, X. Zhong Sun, M. Towrie, C. Wilson, J. Yang, M.W. George, *J. Chem. Soc. Dalton Trans.,* **2003**, 3996.

83 V. Balzani, A. Credi, M. Venturi, *Molecular Devices and Machines; A journey into the nanoworld*, VCH, Weinheim **2003**.

84 R. Ziessel, A. Juris, M. Venturi, *Chemm. Commun*, **1997**, 1593

85 R. Ziessel, A. Juris, M. Venturi, *Inorg. Chem.,* **1998**, 37, 5061.

86 A. Vlček, Jr., M. Busby, *Coord. Chem. Rev.,* **2006**, 250, 1755.

87 J.V. Caspar, T.J. Meyer, *J. Phys. Chem.,* **1983**, 87, 952.

88 J.R. Schoonover, P. Chen, W.D. Bates, R.B. Dyer, T.J. Meyer, *Inorg. Chem.,* **1994**, 33, 793

89 D.J. Liard, A. Vlček, Jr., *Inorg. Chem.,* **2000**, 39, 485.

90 D.J. Liard, M. Busby, I.R. Farrell, P. Matousek, M. Towrie, A. Vlček, Jr., *J. Phys. Chem. A,* **2004**, 108, 556.

91 D.J. Liard, C.J. Kleverlaan, A. Vlček, Jr., *Inorg. Chem.,* **2003**, 42, 7995

92 N.E. Katz, S.L. Mecklenburg, T.J. Meyer, *Inorg. Chem.,* **1995,** 34 1282

93 P. Chen, T.D. Westmoreland, E. Danielson, K.S. Schanze, D. Anthon, P.E. Neveux, T.J. Meyer, *Inorg. Chem.,* **1987**, 26, 1116.

94 P.Chen, R. Deusing, G. Tapolsky, T.J. Meyer, *J. Am. Chem. Soc.,* **1989**, 111, 8305.

95 K. Koike, J. Tanabe, S. Toyama, H. Tsubaki, K. Sakamoto, J.R. Westell, F.P.A. Johnson, H. Hori, H. Saitoh, O. Ishitani, *Inorg. Chem.,* **2000**, 39, 2777.

96 K. Koike, N. Okoshi, H. Hori, K. Takeuchi, O. Ishitani, H. Tsubaki, I.P.

Clark, M.W. George, F.P.A. Johnson, J.J. Turner, *J. Am. Chem. Soc.*, **2002**, 124, 11448.

97 V. W. –W. Yam, C. Ko, N. Zhu, *J. Am. Chem. Soc.*, **2004**, 126, 12734.

98 M.S. Wrighton, D.L. Morse, L. Pdungsap, *J. Am. Chem. Soc.*, **1975**, 97, 2073.

99 M. Busby, P Matousek, M. Towrie, A. Vlček, Jr., *J. Phys. Chem. A*, **2004**, 109, 3000.

100 O.S. Wenger, L.M. Henling, M.W. Day, J.R. Winkler, H.B. Gray, *Inorg. Chem.*, **2003**, 43, 2043.

101 V. W. –W. Yam, V. C. –Y. Lau, L.X. Wu, *J. Chem. Soc. Dalton Trans.*, **1998**, 1461.

102 A. Sarto Polo, M. Kayoko Itokazu, K. Morelli Frin, A. Otávio de Toledo, N.Y. Murakami Iha, *Coord. Chem. Rev.*, **2006**, 250, 1669.

103 M.D. Ward, *J. Chem. Soc. Dalton Trans.*, **1993**, 1321.

104 V. Balzani, D.A. Bardwell, F. Barigelletti, F.L. Cleary, M. Guardigli, J.C. Jeffery, T. Sovrani, M.D. Ward, *J. Chem. Soc. Dalton Trans.*, **1995**, 3601.

105 K. Kalyanasundaram, M.K. Nazeeruddin, *Inorg. Chem.*, **1990**, 29, 1888.

106 G. Denti, S. Serroni, S. Campagna, V. Ricevuto, V. Balzani, *Coord. Chem. Rev.*, **1991**, 111, 227.

107 V. Balzani, P. Ceroni, A. Juris, M. Venturi, S. Campagna, F. Puntotiero, S. Serroni, *Coord. Chem. Rev.*, **2001**, 219, 545.

108 W. Kaim, *Coord. Chem. Rev.*, **2002**, 230, 127.

109 R. Hage, A.H.J. Dijkhuis, J.G. Haasnoot, R. Prins, J. Reedijk, B.E. Buchanan, J.G. Vos, *Inorg. Chem.*, **1988**, 27, 2185.

110 R. Hage, J.G. Haasnoot, D.J. Stufkens, T.L. Snoeck, J.G. Vos, J. Reedijk, *Inorg. Chem.*, **1989**, 28, 1413

111 C. Di Pietro, S. Serroni, S. Campagna, M.T. Gandolfi, R. Ballardini, S. Fanni, W.R. Browne, J.G. Vos, *Inorg. Chem.*, **2002**, 41, 2871.

112 S. Baitalik, U.Flörke, K. Nag, *Inorg. Chem.*, **1999**, 38, 3296.

113 F. Weldon, L. Hammarström, E. Mukhtar, R. Hage, E. Gunneweg, J.G.

Haasnoot, J. Reeijk, W.R. Browne, A.L. Guckian, J.G. Vos, *Inorg. Chem.,* **2004**, 43, 4471.

114 F. Barigelletti, L. Flamingi, *Chem. Soc. Rev.,* **2000**, 29, 1.

115 X. Wang, A. Del Guerzo, R.H. Schmehl, *J. Photochem and. Photobiol C: Photochem. Rev.,* **2004**, 5, 55.

116 W.R. Browne, F. Weldon, A. Guckian, J.G. Vos, *Collect. Czech. Chem. Commun.,* **2003**, 68. 1467.

117 W.R. Browne, R. Hage, J.G. Vos, *Coord. Chem. Rev.,* **2006**, 250, 1653.

118 A. Vogler, J. Kisslinger, *Inorg. Chim. Acta.,* **1986**, 115, 193.

119 R. Sahai, D.P. Rillema, R. Shaver, S. Van Wallendael, D.C. Jackman, M. Boldaji, *Inorg. Chem.,* **1989**, 28, 1022.

120 K. Kalyanasundaram, M.K. Nazeeruddin, *J. Chem. Soc. Dalton Trans.,* **1990**, 1657.

121 D.A. Bardwell, F. Bargelletti, R.L. Cleary, L. Flamigni, M. Guardigli, J.C. Jeffery, M.D. Ward, *Inorg. Chem.,* **1995**, 34, 2438.

122 S. van Wallendael, D.P. Rillema, *J. Chem. Soc., Chem. Commun.,* **1990**, 1081.

123 S. Encias, A.M. Barthram, M.D. Ward, F. Barigelletti, S. Campagna, *Chem. Commun.,* **2001**, 277.

Chapter 2

Rhenium(I) complexes containing substituted pyridyl-triazole ligands.

Chapter 2 introduces a series of pyridyl-triazole ligands and the corresponding rhenium(I) tricarbonyl complexes of these ligands. All the complexes were characterised and examined for their photophysical and electrochemical properties. The introduction and the discussion of the properties of the complexes in Chapter 2 are relevant also for the pyrazyl-triazole complexes discussed in Chapter 3 and the dinuclear complexes discussed in Chapter 4.

2.1 Introduction

Polypyridyl complexes with d^6 metal centres have generated widespread interest in recent years due to their photophysical and photochemical properties.[1] These complexes have the ability to play the role of light absorption and/or light emission sensitisers in systems that mimic energy or electron transfer processes in naturally occurring photosynthetic systems.[2] Complexes with d^6 metal centres such as Ru(II), Os(II) and Rh(III) have been extensively studied whilst complexes containing Re(I) have been researched to a lesser degree.[3,4] The properties of these complexes can be controlled by the σ-donor and π-acceptor properties of the ligands in the coordination sphere. Strong π-acceptor ligands such as 2,2'-bipyrazine, 2,2'-biquinoline and 2,2'-bipyridine stabilise the filled metal orbitals causing higher oxidation and lower reduction potentials.[5,6] Strong σ-donor ligands (pyrazoles and imidazoles)[7,8] donate electron density to the metal centre giving rise to lower oxidation potentials and more negative reduction potentials. By changing the nature of the ligands, not only are the redox potentials altered, but also the energies of the absorption and emission bands. Hence the σ-donor and π-acceptor properties of a ligand enable the fine tuning of the ground and excited-state properties of a complex.

1,2,4-triazole ligands are an interesting category of ligand as they are strong σ-donors and weak π-acceptors. Since the first report of a ruthenium complex containing a 1,2,4-triazole in 1983,[9] complexes containing 1,2,4-triazoles and their derivatives have generated a significant amount of interest.[10,11] These asymmetric bidentate ligands combine a σ-donor triazole fragment with a π-acceptor unit (see Figure 2. 1). Previous work on a number of metal complexes containing 1,2,4-triazole ligands has revealed that coordination is possible via N_2 or N_4 (Figure 2. 1). Furthermore it has been widely accepted that the N_2 coordination site is a better σ-donor than the N_4 site.[12] Another interesting property of these ligands that cannot be overlooked is the presence of a proton on the 1,2,4-triazole. This proton can be removed under basic conditions resulting in

a negative charge which resides on the triazole. The presence of this negative charge on the triazole has given rise to ruthenium(II) complexes with unusual photophysical properties.[13,14]

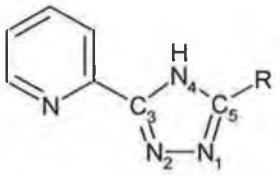

pyridyl-triazole

Figure 2. 1 *General structure of a substituted 3-(pyridin-2-yl)-1,2,4-triazole.*

In this chapter the synthesis and properties of a series of new mononuclear rhenium tricarbonyl complexes containing various 3-(pyridin-2-yl)-1,2,4-triazole ligands are described. The structure of the complexes has been determined using NMR and infra-red (IR) spectroscopy. The electronic properties of the pyridyl-triazole complexes are compared to $[Re(CO)_3(bpy)Cl]$ (bpy = 2,2'-bipyridyl). The substitution of groups on the triazole ligand and the effect of these substituents on the ground-state and excited-state properties of the complexes is also examined. Previous studies have shown that ruthenium bipyridyl complexes containing a 1,2,4-triazole ligand exhibit interesting acid-base properties.[13,15] Thus, the effect of deprotonation of the ligand on the physical properties of the complexes has also been investigated. The structures and abbreviations for the ligands cited in this chapter are shown in Figure 2. 2.

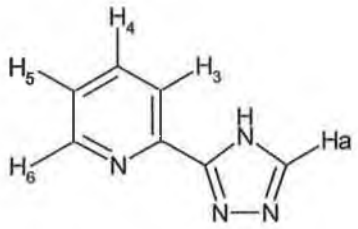

3-(pyridin-2-yl)-1,2,4-triazole
(Hpytr)

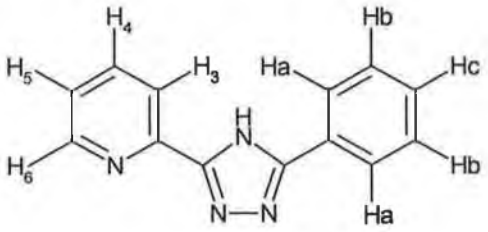

3-(pyridin-2-yl)-5-phenyl-1,2,4-triazole
(Hphpytr)

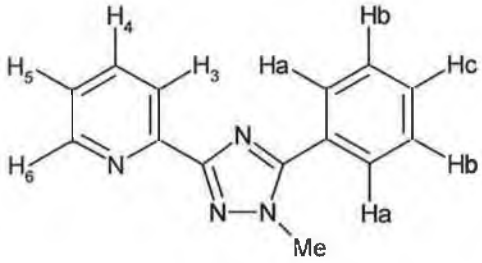

1-methyl-3-(pyridin-2-yl)-5-phenyl-
1,2,4-triazole
(Mephpytr)

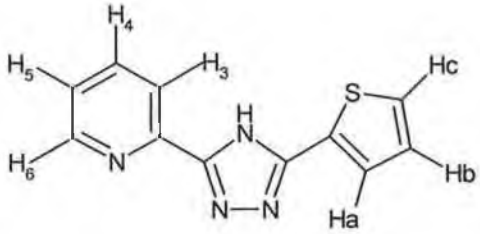

3-(pyridin-2-yl)-5-(thiophen-2-yl)-
1,2,4-triazole
(Hthpytr)

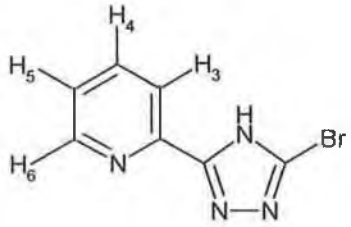

3-(pyridin-2-yl)-5-bromo-1,2,4-triazole
(HBrpytr)

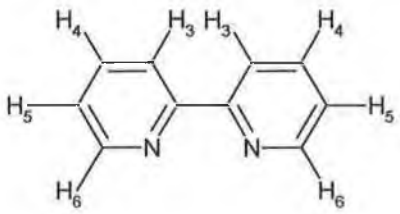

2,2'-bipyridyl
(bpy)

Figure 2. 2 *Structures of the ligands and their abbreviations as cited throughout this chapter.*

2.2 Results and discussion

2.2.1 Syntheses

The syntheses of the 1,2,4-triazole ligands were carried out following literature methods. Procedures for the synthesis of 1,2,4-triazole ligands are well understood, hence other synthetic routes were not explored. The general synthetic route used in the preparation of the 1,2,4-triazole is outlined in Scheme 2. 1. The appropriate acid chloride was used in order to obtain the desired substituent in the "5" position.

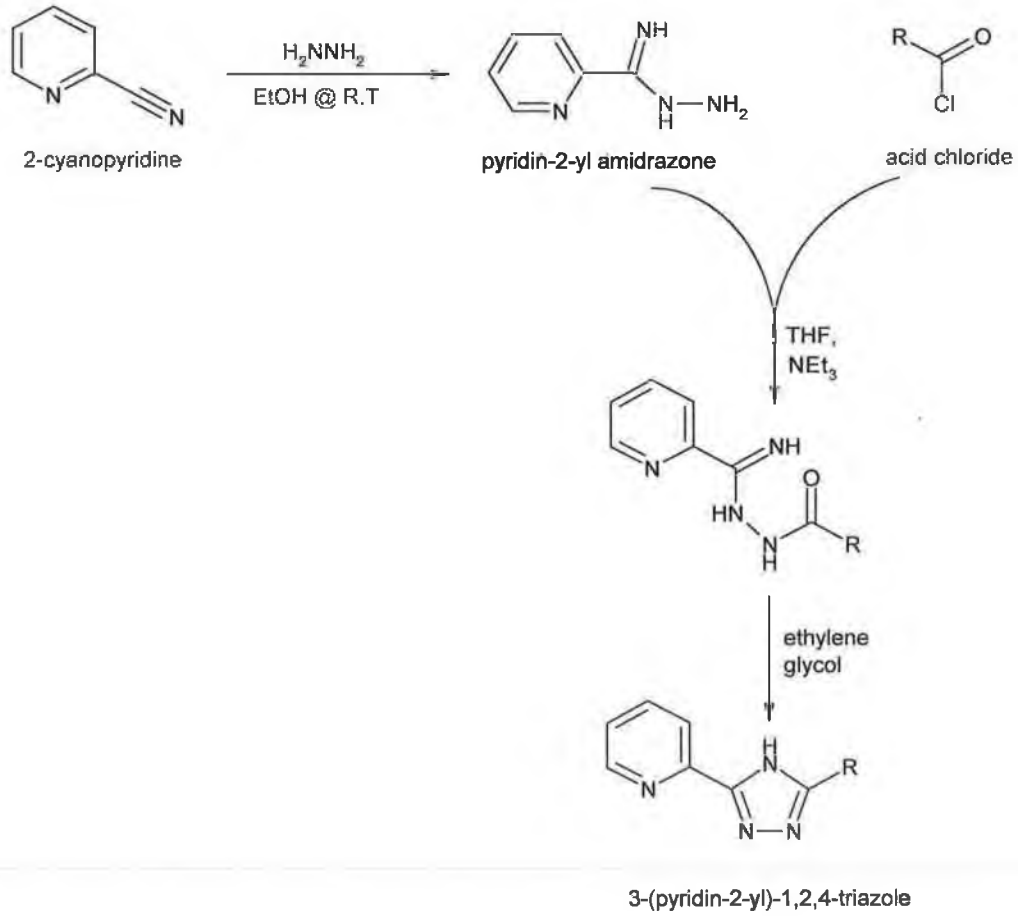

Scheme 2. 1 Synthetic scheme employed in the preparation of the ligands.

The Mephpytr has a methyl group on the N_1 in the 1,2,4 triazole. This was achieved by using methyl hydrazine instead of hydrazine. HBrpytr was synthesised by bromination of Hpytr according to a previously published procedure.[15]

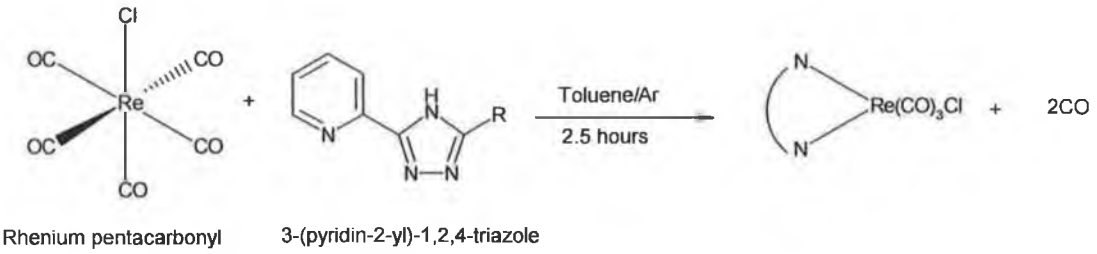

Rhenium pentacarbonyl 3-(pyridin-2-yl)-1,2,4-triazole

Scheme 2. 2 *Reaction of rhenium pentacarbonyl with a substituted 3-(pyridin-2-yl)-1,2,4-triazole ligand.*

The complexes were prepared from the free ligands and $Re(CO)_5Cl$ via a thermal substitution reaction (Scheme 2. 1). The triazole ligand was dissolved in toluene. In the past coordination of a ruthenium metal centre to a triazole ligand has resulted in the formation of a negatively charged triazole ligand.[16,17] However, the added precaution of addition of a few drops of trifluoroacetic acid was taken to ensure that the protonated rhenium triazole complexes were isolated. $Re(CO)_5Cl$ in toluene was slowly added to the acidified toluene solution. This solution was refluxed under an argon atmosphere. The reactions were monitored using infra-red spectroscopy. The reaction was completed when there was no evidence of any $Re(CO)_5Cl$ in the IR spectrum. The complexes were isolated as yellow solids.

2.2.2 Elemental analysis

As previously discussed, 1,2,4-triazoles contain a proton on the triazole unit. The theoretical CHN percentages were calculated with the assumption that the proton remains on the triazole on complexation to the rhenium tricarbonyl fragment. The

CHN analysis confirms the presence of a proton on the triazole ring as the theoretical percentages are within a similar range to the actual CHN percentages found. If there were a negative charge residing on the triazole in the complexes, the measured CHN percentages would be hugely different from the theoretical percentages as a counter ion would be required to isolate the complexes. Although the CHN percentages of the complexes were confirmed by CHN analysis, no information regarding the coordination mode of the triazole may by obtained using this technique.

2.2.3 Infra red spectroscopy

IR spectra of all the complexes were recorded in the CO sretching region (2200 – 1700 cm^{-1}) of the IR spectrum. The IR spectral data of the complexes in THF is presented in Table 2. 1. All complexes have spectra which are dominated by three metal-carbonyl bands.

Complex	$\nu_{(CO)}$ cm^{-1}		
$[Re(CO)_3(Hpytr)Cl]$	2020	1915	1890
$[Re(CO)_3(pytr)Cl]^-$	2014	1906	1881
$[Re(CO)_3(Hphpytr)Cl]$	2023	1921	1895
$[Re(CO)_3(phpytr)Cl]^-$	2016	1908	1891
$[Re(CO)_3(Mephpytr)Cl]$	2023	1918	1890
$[Re(CO)_3(Hthpytr)Cl]$	2023	1922	1895
$[Re(CO)_3(thpytr)Cl]^-$	2015	1906	1893
$[Re(CO)_3(HBrpytr)Cl]$	2025	1921	1895
$[Re(CO)_3(Brpytr)Cl]^-$	2018	1910	1882
$[Re(CO)_3(bpy)Cl]$	2018	1917	1892

Table 2. 1 *IR spectral data for rhenium (I) complexes in THF solution in the carbonyl region. Complexes were deprotonated using triethylamine.*

The IR spectrum of $[Re(CO)_3(bpy)Cl]$ is well understood.[18,19] $[Re(CO)_3(bpy)Cl]$ possess C_s symmetry with three IR active modes [A'(1) + A'(2) + A'']. $[Re(CO)_3(bpy)Cl]$ exists in a facial isomeric form with two carbonyls *trans* to the 2,2'-bipyridyl and one CO *trans* to the chloride.[20] The CO bands are observed at 2018, 1917 and 1892 cm^{-1} for $[Re(CO)_3(bpy)Cl]$ (Table 2. 1 and Figure 2. 3).

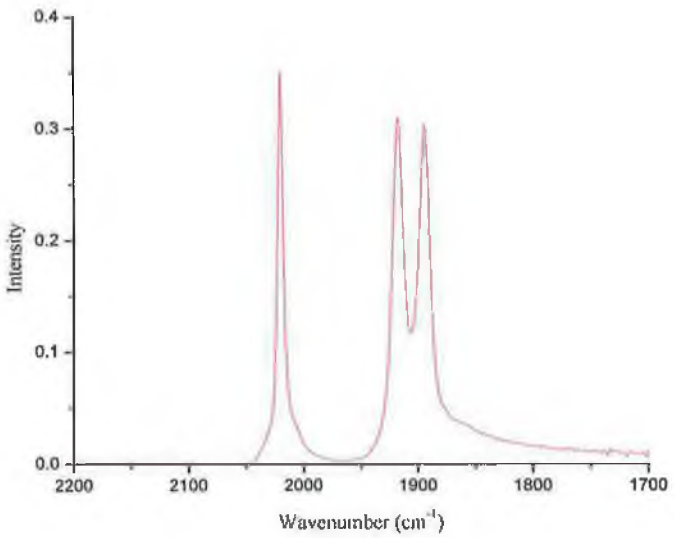

Figure 2. 3 *IR (CO-stretching region) of $[Re(CO)_3(bpy)Cl]$ in THF at 298 K.*

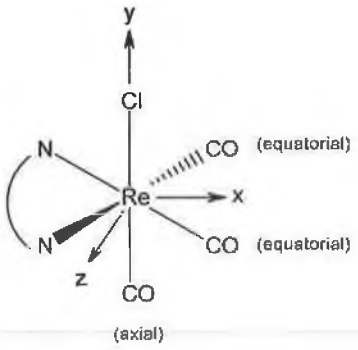

Figure 2. 4 *Coordination environment for the facial structure of a rhenium tricarbonyl complex.*

Figure 2. 5 shows the IR spectra of $[Re(CO)_3(Hphpytr)Cl]$ and $[Re(CO)_3(phpytr)Cl]^-$. The CO bands in these spectra are typical of the pyridyl-triazole complexes synthesised in this chapter. By comparison with the spectrum of $[Re(CO)_3(bpy)Cl]$, this pattern corresponds to 3 CO ligands in a facial isomer arrangement (Figure 2. 4). As a point of interest the corresponding meridional isomers would give rise to a very weak signal of the highest frequency carbonyl vibration.[21]

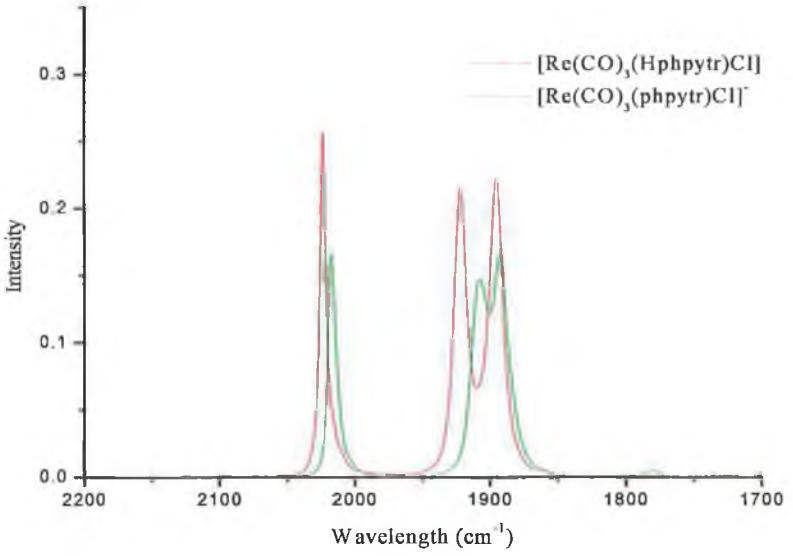

Figure 2. 5 *IR specta (CO-stretching region) of $[Re(CO)_3(Hphpytr)Cl]$ and $[Re(CO)_3(phpytr)Cl]^-$ in THF at 298 K.*

As previously discussed, the elemental analysis of the $[Re(CO)_3(triazole)Cl]$ complexes indicates the presence of a proton on the triazole fragment of the ligands. IR spectra were recorded in triethylamine so as to observe the spectral shifts on deprotonation of the triazole (Table 2. 1 and Figure 2. 5). No spectral changes were observed for $[Re(CO)_3(bpy)Cl]$ and $[Re(CO)_3(Mephpytr)Cl]$ in the presence of triethylamine. The CO bands were generally found to shift to lower frequency on deprotonation.

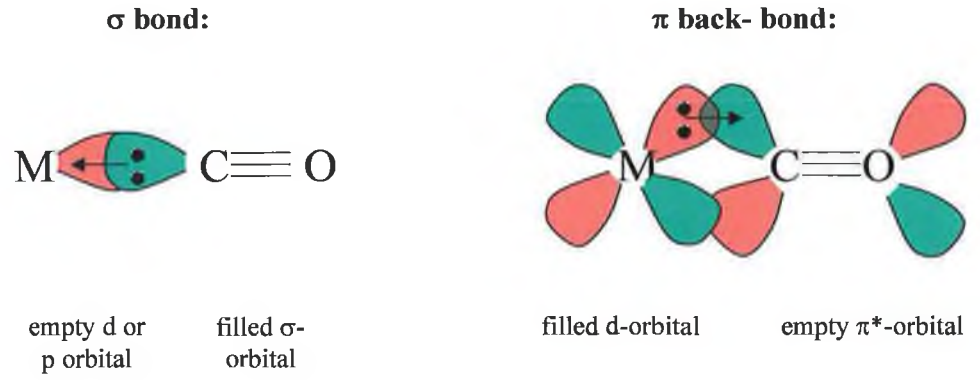

Figure 2. 6 *Bonding interaction of the CO ligand with the rhenium(I) metal centre.*

The shift of the metal-carbonyl absorptions to lower frequency for the deprotonated triazole complexes compared to their protonated analogues is most likely due to competition by the pyridyl-triazole and carbonyl ligands for π-electron density from the d_π orbitals of the rhenium(I). Figure 2. 6 illustrates this bonding interaction which is known as back-bonding. The presence of a negative charge on the triazole increases the σ-donor ability of the triazole ligand. This increases the electron density on the rhenium, which enhances the back bonding between the rhenium d_π orbitals and the CO π* orbitals. With increased back-bonding, metal-carbonyl stretches shift to lower frequency in the IR spectum. Hence the metal-carbonyl stretches for the deprotonated complexes were observed at lower frequency compared to the analogous protonated complexes. Similar trends were observed in the IR spectra of protonated/deprotonated derivatives of $[Mo(CO)_4(bpz)]$ where bpz is 2,2'-bipyrazine.[22]

2.2.4 ^{1}H NMR spectroscopy

The rhenium(I) complexes are diamagnetic low spin d^6 species. NMR spectroscopy has been widely used for the structural characterisation of rhenium tricarbonyl complexes.[23,24] The numbering system employed in the assignment of ^{1}H NMR peaks is shown in Figure 2. 7. The relevant ^{1}H-NMR data of all the protonated complexes are presented in Table 2. 2. The coordination-induced shifts (c.i.s. = $\delta_{complex}$-δ_{ligand}) are in parentheses. Data for $[Re(CO)_3(bpy)Cl]$ is also shown for comparative purposes.

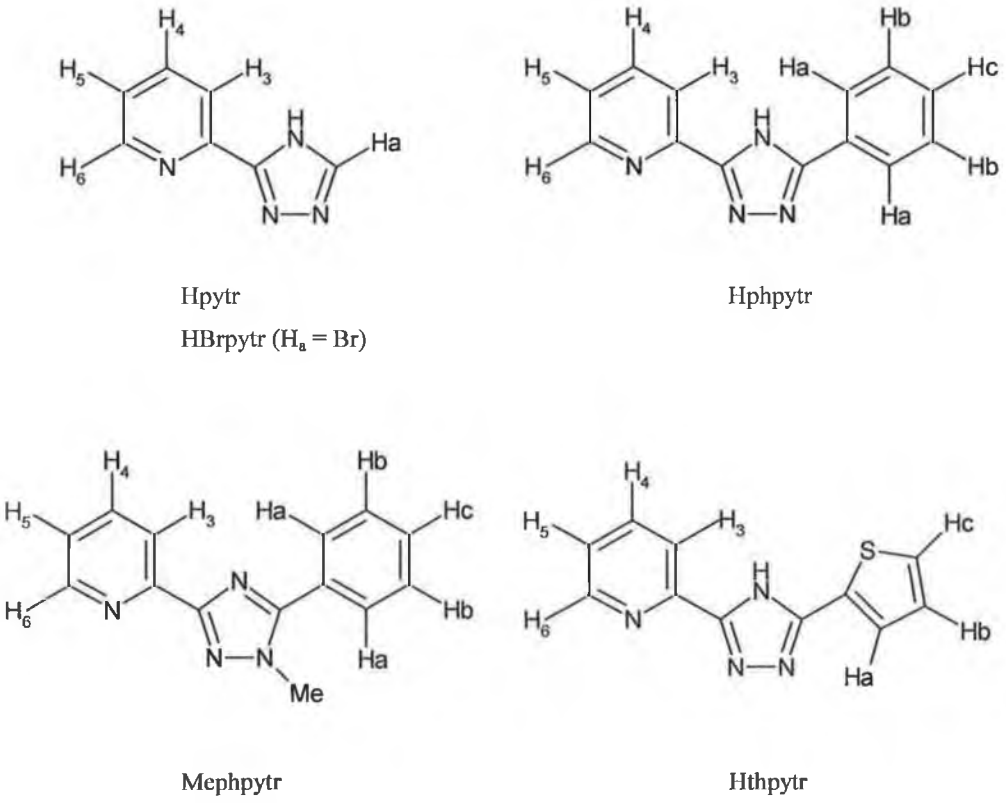

Figure 2. 7 *Structures of the 1,2,4-triazole ligands discussed in this section. The numbers on the protons describe the numbering system employed in the assignment of the ^{1}H NMR peaks.*

Complex	ppm						
	H_3	H_4	H_5	H_6	H_a	H_b	H_c
$[Re(CO)_3(Hpytr)Cl]$	8.37	8.34	7.79	9.07	9.45	—	—
	(0.20)	(0.37)	(0.31)	(0.40)	(1.35)	—	—
$[Re(CO)_3(Hphpytr)Cl]$	8.45	8.39	7.81	9.09	8.39	7.51	7.51
	(0.22)	(0.37)	(0.30)	(0.39)	(0.13)	(0.11)	(0.11)
$[Re(CO)_3(Mephpytr)Cl]$	8.38	8.36	7.80	9.06	7.94	7.73	7.73
	(0.20)	(0.37)	(0.31)	(0.40)	(0.05)	(0.05)	(0.14)
$[Re(CO)_3(Hthpytr)Cl]$	8.36	8.34	7.78	9.07	7.77	7.28	7.88
	(0.15)	(0.33)	(0.26)	(0.38)	(0.22)	(0.10)	(0.13)
$[Re(CO)_3(HBrpytr)Cl]$	8.38	8.37	7.83	9.09	—	—	—
	(0.27)	(0.35)	(0.29)	(0.41)	—	—	—
$[Re(CO)_3(bpy)Cl]$	8.72	8.37	7.82	9.12	—	—	—
	(0.21)	(0.38)	(0.45)	(0.41)	—	—	—

Table 2. 2 *^1H NMR data for the rhenium(I) tricarbonyl complexes. All spectra were obtained in d_6-acetone. Values in parenthesis are the coordinated induced shifts relative to the free ligands in d_6-acetone.*

The asymmetric 1,2,4-triazole ligands complexed to the rhenium tricarbonyl fragment display signals between 7.0 and 9.15 ppm. $[Re(CO)_3(Mephpytr)Cl]$ is the only complex that displays a signal below 7.0 ppm. The singlet resonance with an intergration of 3 observed at 4.15 ppm is assigned to the methyl group present on the 1,2,4-triazole. Assignment of proton resonances were made by comparison with the model $[Re(CO)_3(bpy)Cl]$ complex and with the aid of two dimensional (COSY) spectra. A sample COSY spectrum of the aromatic region of $[Re(CO)_3(Mephpytr)Cl]$ in d_6-acetone is displayed in Figure 2. 8. Figure 2. 9 shows sample ^{1}H-NMR spectra of $[Re(CO)_3(Hpytr)Cl]$, $[Re(CO)_3(Hphpytr)Cl]$ and $[Re(CO)_3(bpy)Cl]$ obtained in d_6-acetone.

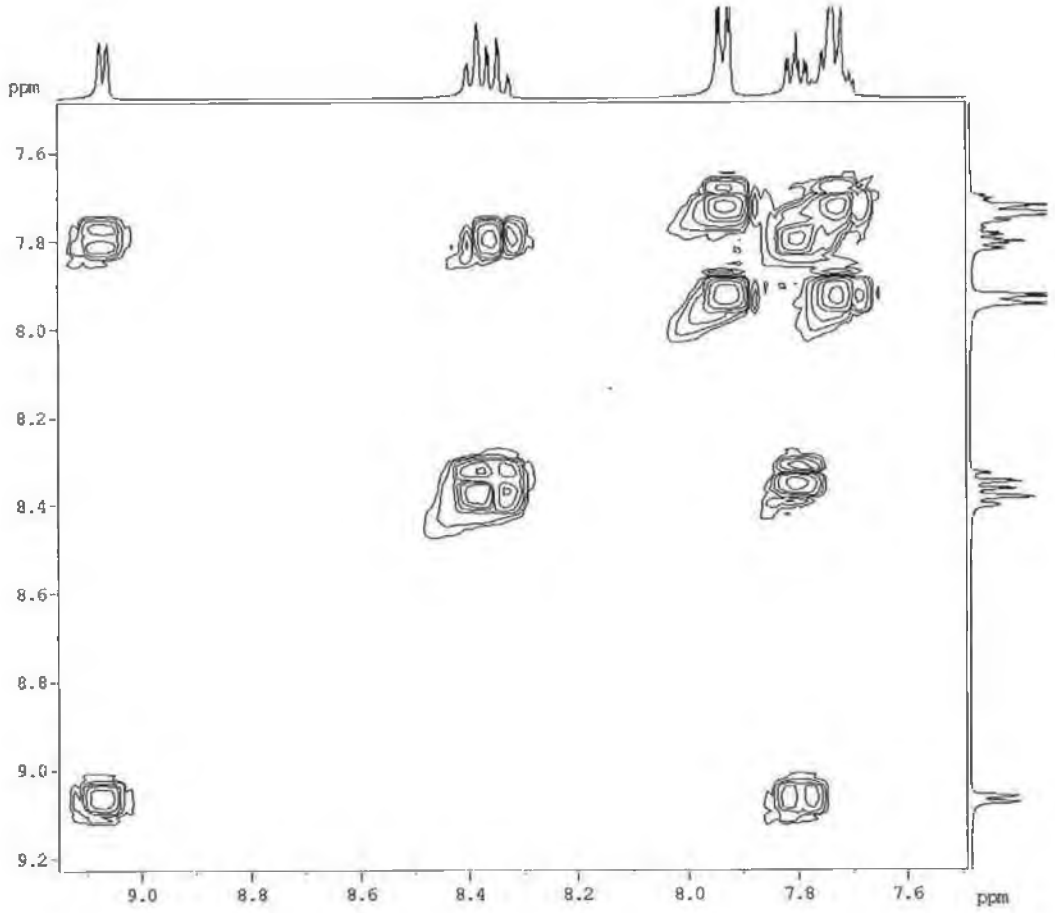

Figure 2. 8 *COSY NMR spectrum of [Re(CO)$_3$(Mephpytr)Cl] in d_6-acetone.*

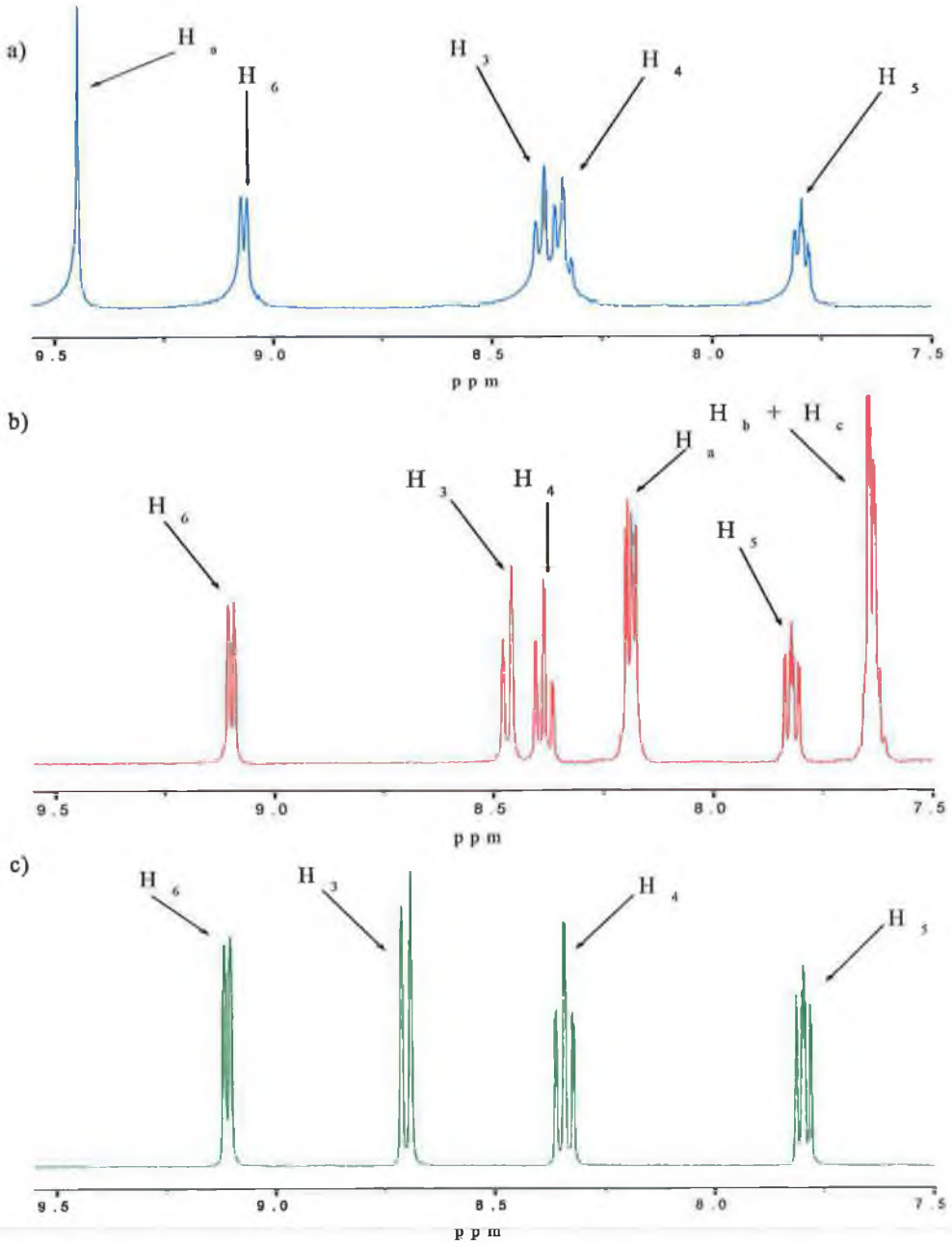

Figure 2. 9 *^1H NMR spectra of $[Re(CO)_3(Hpytr)Cl]$ (a), $[Re(CO)_3(Hphpytr)Cl]$ (b) and $[Re(CO)_3(bpy)Cl]$ (c) in d_6-acetone.*

Previous publications of bipyridine complexes place the resonance of the H_6 proton adjacent to the coordinated nitrogen fartherest downfield.[24,25,26] Hence the peak positions of the coordinated pyridine ring were identified as follows: the H_6 (doublet) and H_5 (multiplet) protons were located in the range of 9.06 and 7.80 ppm. The H_3 and H_4 protons were generally found to overlap at around 8.35 ppm. The chemical shifts of the H_4, H_5 and H_6 protons are in the same range as the equivalent protons in $[Re(CO)_3(bpy)Cl]$. The H_3 proton in the pyridyl-triazole complexes was generally found slightly upfield relative to the corresponding proton in $[Re(CO)_3(bpy)Cl]$ (Figure 2. 9 and Table 2. 2). In the past there have been reports of electron delocalisation from the triazole to an adjacent pyrazine or pyridine ring.[17] There may be a similar interaction occurring in these pyridyl-triazole complexes. Hence the H_3 proton experiences an increase in electron density and is found upfield relative to the H_3 proton in $[Re(CO)_3(bpy)Cl]$. The introduction of the various substituents onto the triazole ring induces only small changes in the shifts of the pyridine protons.

The c.i.s values of the pyridyl-triazole complexes listed in Table 2. 2 are all positive. In the past positive c.i.s values have been attributed to ligand-to-metal σ-donation when a ligand coordinates to a metal centre.[7,27,] Clearly, the influence of the rhenium(I) metal shifts the proton resonances of the coordinated pyridine but leaves the proton resonances of the uncoordinated triazole substituents relatively unaffected. The only exceptions to this trend were H_a in $[Re(CO)_3(Hpytr)Cl]$ which experienced a c.i.s. shift of 1.35. This is possibly due to a reduction in electron density caused by σ-donation to the rhenium and electron delocalisation between the triazole and the pyridine. Note H_a in $[Re(CO)_3(Hpytr)Cl]$ is located on the 1,2,4-triazole while the protons in the other substituents are a greater distance from the triazole. Hence these protons do not experience coordination induced shifts to the same extent as H_a in $[Re(CO)_3(Hpytr)Cl]$.

The ^1H NMR spectra of $[Re(CO)_3(Hpytr)Cl]$, $[Re(CO)_3(Hphpytr)Cl]$ and $[Re(CO)_3(bpy)Cl]$ are shown Figure 2. 9. The ^1H-NMR spectra indicate the

formation of only one isomer. Coordination of a metal centre to the Hpytr ligand may occur at either of the two non-equivalent nitrogens on the triazole ring (Figure 2. 10).[16] These coordination isomers are referred to as the "N_2" isomer and the "N_4" isomer. The N_2 isomer and N_4 isomer in Ru(II) complexes incorporating 1,2,4-triazole ligands have exhibited different redox potentials and absorption and emission maxima.[12,13] Hence identification of the coordination mode in the rhenium tricarbonyl complexes is particularly important.

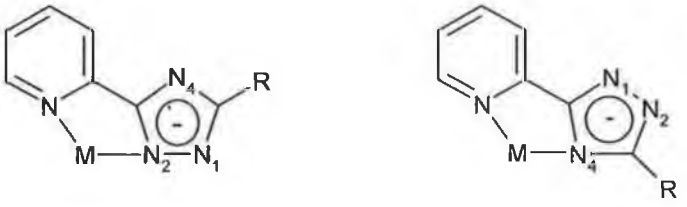

N_2 Isomer N_4 Isomer

Figure 2. 10 *The two possible modes of coordination of a metal centre to a substituted 3-(pyridin-2-yl)-1,2,4-triazole.*

The extent of N_2/N_4 coordination in Ru(II) complexes is governed by the size of the substituents on the triazole ring.[28] Bulky triazole substituents such as a phenyl or a thiol group favour the formation of the N_2 isomer in Ru(II) complexes.[29,30] Both $[Re(CO)_3(Hphpytr)Cl]$ and $[Re(CO)_3(Hthpytr)Cl]$ contain a bulky phenyl or thiol substituent. Therefore from a steric viewpoint, formation of the N_2 isomer is favoured. Previous studies have found that Ru(II) complexes containing the Hpytr ligand formed both N_2 and N_4 isomers in a 1:1 ratio.[16] Therefore the formation of both linkage isomers is anticipated in $[Re(CO)_3(Hpytr)Cl]$, however evidence for the formation of only a single isomer was observed in the ^1H NMR spectrum. The resonances of the pyridine rings in $[Re(CO)_3(Hpytr)Cl]$ are similar to those in $[Re(CO)_3(Hphpytr)Cl]$ where N_2 coordination is proposed. Formation of only the N_2 isomer in $[Ru(CO)_2(Hpytr)Cl_2]$ and $[Rh(L)_2(Hpytr)]^{3+}$ (L = 2,2'-

bipyridine/1,10-phenanthroline) has been observed.[31,32] In the complex $[Re(CO)_3(NH_2bpt)Cl]$ (NH_2bpt = 4-amino-3,5-bis(pyridin-2-yl)-1,2,4-triazole) the authors proposed the large radius of rhenium(I) leads to the formation of just the N_2 coordination isomer.[33] Therefore it is not unreasonable to deduce that the N_2 isomer was also formed in $[Re(CO)_3(Hpytr)Cl]$. No crystals suitable for X-ray analysis were obtained. In the absence of such crystals, the coordination mode of the ligands cannot be determined with certainty, however as discussed above coordination via the N_2 position seems most likely.

Complex	ppm						
	H_3	H_4	H_5	H_6	H_a	H_b	H_c
$[Re(CO)_3(pytr)Cl]^-$	8.28	8.15	7.51	8.94	8.32	—	—
	(-0.09)	(-0.15)	(-0.28)	(-0.13)	(-1.13)	—	—
$[Re(CO)_3(phpytr)Cl]^-$	8.11	8.11	7.45	8.87	8.22	7.38	7.27
	(-0.34)	(-0.28)	(-0.36)	(-0.22)	(-0.17)	(-0.13)	(-0.24)
$[Re(CO)_3(thpytr)Cl]^-$	8.12	8.11	7.47	8.88	7.35	7.07	7.61
	(-0.24)	(-0.23)	(-0.31)	(-0.19)	(-0.42)	(-0.21)	(-0.27)
$[Re(CO)_3(Brpytr)Cl]^-$	8.12	8.15	7.52	8.87	—	—	—
	(-0.31)	(-0.26)	(-0.35)	(-0.22)	—	—	—

Table 2. 3 *^1H NMR data for the deprotonated rhenium tricarbonyl complexes. All spectra were obtained in d_6-acetone. The complexes were deprotonated by addition of triethylamine. Values in parenthesis are the coordination induced shifts relative to the free ligands.*

Spectra were also recorded in basic solution resulting in deprotonation of the triazole unit. A basic solution was obtained by addition of triethylamine to the ^1H NMR sample in d_6-acetone. The spectral data of the pyridyl-triazole complexes obtained in basic solution is summarised in Table 2. 3. The coordination induced shifts ($\delta_{complex}$ - δ_{ligand}) are also shown in parentheses. The deprotonated

complexes were found upfield relative to the corresponding protonated complexes. No spectral shifts were observed for $[Re(CO)_3(bpy)Cl]$ or $[Re(CO)_3(Mephpytr)Cl]$ in basic solution. Figure 2. 11 shows the spectral shifts due to deprotonation of the triazole ring for the $[Re(CO)_3(Hpytr)]$ complex. Deprotonation of the coordinated 1,2,4-triazole has a strong influence on the resonance frequency of the H_a triazole proton of $[Re(CO)_3(Hpytr)]$.

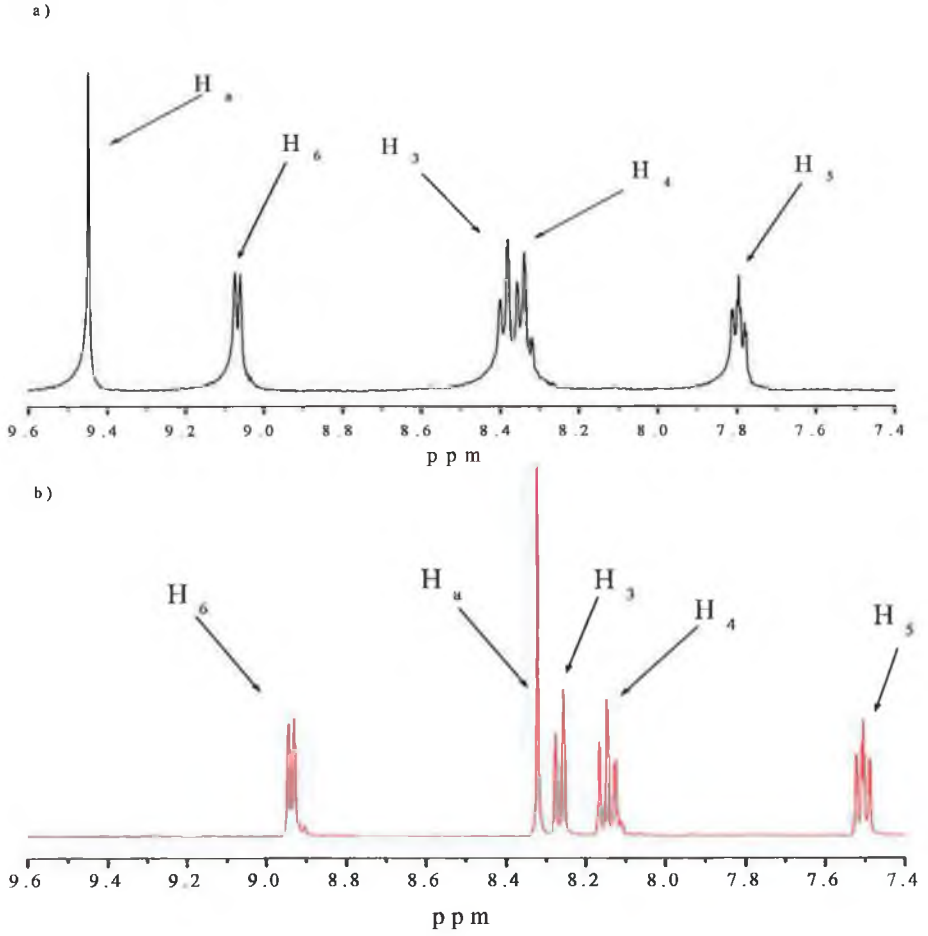

Figure 2. 11 *^1H NMR spectra of (a) $[Re(CO)_3(Hpytr)Cl]$ and (b) $[Re(CO)_3(pytr)Cl]^-$. All spectra were obtained in d_6-acetone. The complexes were deprotonated by addition of triethylamine.*

The shift in the resonance positions of the pyridyl-triazole protons can be explained by the increased electron density in the triazole ring, which probably also affects the electron density in the pyridyl ring and the triazole substituents. Similar shifts were also observed on deprotonation of the triazole ligand in $[Ru(bpy)_2(Hpytr)](PF_6)_2$.[28]

2.2.5 Absorption and emission properties

The UV-vis absorption spectra of all complexes synthesised in this chapter were recorded in dichloromethane at room temperature. Figure 2. 12 shows the absorption spectra of $[Re(CO)_3(Hpytr)Cl]$, $[Re(CO)_3(pytr)Cl]^-$ and $[Re(CO)_3(bpy)Cl]$ at room temperature. These spectra illustrate the considerable effect that protonation/deprotonation of the triazole ligand has on the spectral properties of the complexes compared to $[Re(CO)_3(bpy)Cl]$. An understanding of the absorption spectrum of $[Re(CO)_3(bpy)Cl]$ is essential before interpretation of the absorption spectra of the pyridyl-triazole complexes. $[Re(CO)_3(bpy)Cl]$ has an absorption band at 390 nm which is assigned to an MLCT $[Re\rightarrow\pi^*(bpy)]$ transition.[34] The intense band at 292 nm is of intraligand $[\pi\rightarrow\pi^*(bpy)]$ origin. $[Re\rightarrow\pi^*(CO)]$ transitions have been reported for $[Re(CO)_5Cl]$ at 280 nm.[35] Such transitions in $[Re(CO)_3(bpy)Cl]$ are weak in intensity and are masked by the intense $\pi\rightarrow\pi^*$ transitions associated with the bipyridyl ligand.

The absorption spectra of the pyridyl-triazole complexes are similar to that of $[Re(CO)_3(bpy)Cl]$. Hence the absorption bands between 290 and 400 nm are classed as MLCT transitions i.e. $[Re\rightarrow L\pi^*]$ where L is a pyridyl-triazole ligand. A summary of the MLCT transitions is presented in Table 2. 4. Note, the absorption maxima of the pyridyl-triazole complexes are blue shifted relative to $[Re(CO)_3(bpy)Cl]$. For example the absorption maximum of $[Re(CO)_3(Hphpytr)Cl]$ is observed at 350 nm, while the absorption maximum of $[Re(CO)_3(bpy)Cl]$ is observed at 390 nm. More intense bands (not listed in Table 2. 4) of ligand based $[\pi\rightarrow\pi^*(L)]$ origin occur at higher energy in the UV region of the absorption spectra. The positions the MLCT bands are governed by the σ-

donor and π-acceptor properties of the triazole ligands. Pyridyl-triazole ligands are better σ-donor's relative to 2,2'-bipyridyl.[13] As a result the π* level of the triazole ligand is at higher energy compared to 2,2'-bipyridyl. This increases the energy gap between the HOMO and the LUMO, causing a blue shift in the MLCT of the pyridyl-triazole complexes compared to $[Re(CO)_3(bpy)Cl]$.

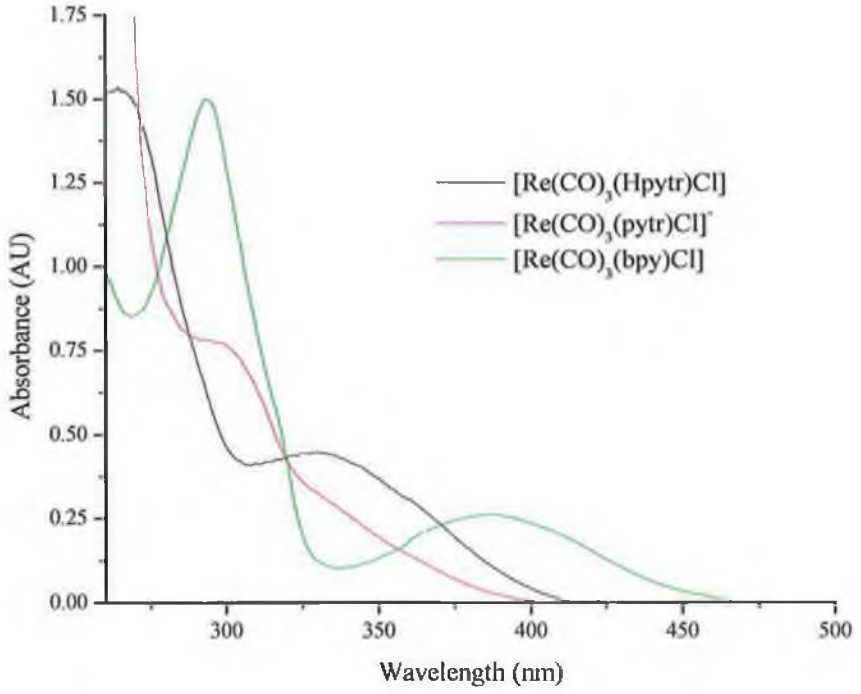

Figure 2. 12 *Absorption spectra of $[Re(CO)_3(Hpytr)Cl]$, $[Re(CO)_3(pytr)Cl]^-$ and $[Re(CO)_3(bpy)Cl]$ in dichloromethane at room temperature. $[Re(CO)_3(Hpytr)Cl]$ was deprotonated using triethylamine.*

Complex	298 K			77 K
	λ_{abs} (nm)[a]/ ($\varepsilon \times 10^3$)	λ_{em} (nm)[a]/ τ(ns)[b]	ϕ [b]	λ_{em}(nm)[b]/ τ(μs)[b]
[Re(CO)$_3$(Hpytr)Cl]	330 (3.4)	580 (51)	0.0032	493 (8.97)
[Re(CO)$_3$(pytr)Cl]$^-$	300 (2.8)	530 (65)	0.0060	484 (9.35)
[Re(CO)$_3$(Hphpytr)Cl]	350 (3.5)	552 (101)	0.0034	497 (5.25)
[Re(CO)$_3$(phpytr)Cl]$^-$	305 (2.6)	516 (159)	0.0081	492 (7.78)
[Re(CO)$_3$(Mephpytr)Cl]	338 (3.6)	537 (735)	0.0117	489 (16.17)
[Re(CO)$_3$(Hthpytr)Cl]	350 (3.4)	542 (274)	0.0049	473 (7.06)
	—	—	—	505 (72.31)
[Re(CO)$_3$(thpytr)Cl]$^-$	310 (2.9)	518 (315)	0.0089	475 (10.32)
	—	—	—	505 (43.91)
[Re(CO)$_3$(HBrpytr)Cl]	330 (3.1)	550 (55)	0.0085	482 (5.42)
[Re(CO)$_3$(Brpytr)Cl]$^-$	295 (2.4)	528 (78)	0.0087	478 (5.75)
[Re(CO)$_3$(bpy)Cl]	390 (3.7)	600 (54)	0.0058	530 (3.60)

Table 2. 4 *Absorption maxima and luminescence properties of the rhenium(I) pyridyl-triazole complexes. τ refers to the emission lifetime while ϕ denotes the radiative quantum yield.* [a] *Data in dichloromethane,* [b] *in deoxygenated dichloromethane, and* [c] *in ethanol/methanol (4:1).*

The rhenium(I) complex [Re(CO)$_3$(bpyCOOH)Cl] where bpyCOOH is 2,2'-bipyridine-5-carboxylic acid, has a [Re→π*(bpyCOOH)] MLCT absorption maximum at 390 nm.[36] At pH 8, the carboxylate derivative [Re(CO)$_3$(bpyCOO)Cl]$^-$ is formed. This deprotonated complex has an [Re→π*(bpyCOO$^-$)] absorption maximum at 375 nm. This blue shift in the absorption maximum was attributed to an increase in the energy necessary to transfer an electron from the rhenium(I) metal centre to the bpy ligand when a negative charge resides on the latter fragment. This behaviour is clearly observed

for the presently reported rhenium(I) complexes (see Figure 2. 12 and Table 2. 4). For example $[Re(CO)_3(Hpytr)Cl]$ has an absorption maximum at 330 nm, whereas the deprotonated complex $[Re(CO)_3(pytr)Cl]^-$ exhibits an absorption maximum at 300 nm. Deprotonation of the pyridyl-triazole complexes generates a negatively charged triazole ligand, which is a much better σ-donor. This increases the energy necessary to transfer an electron from the Re(I) metal centre to the pyridyl-triazole ligand when a negative charge resides on the triazole. This results in a blue shift in the absorption maxima of the deprotonated complexes compared to their protonated derivatives.

All the pyridyl-triazole complexes emit at 298 K (Table 2. 4). The emission spectra were broad and featureless. Figure 2. 13 displays the emission spectra for $[Re(CO)_3(Hphpytr)Cl]$, $[Re(CO)_3(phpytr)Cl]^-$ and $[Re(CO)_3(bpy)Cl]$ in dichloromethane. The emission maxima of the pyridyl-triazole complexes were generally found at higher energy relative to $[Re(CO)_3(bpy)Cl]$. The λ_{max} of the deprotonated complexes are blue shifted when compared to the protonated complexes. The emssion spectra are broad and structureless at 77 K except for $[Re(CO)_3(Hthpytr)Cl]$. The structured spectra of $[Re(CO)_3(Hthpytr)Cl]$ and $[Re(CO)_3(thpytr)Cl]^-$ at 77 K are shown in Figure 2. 15.

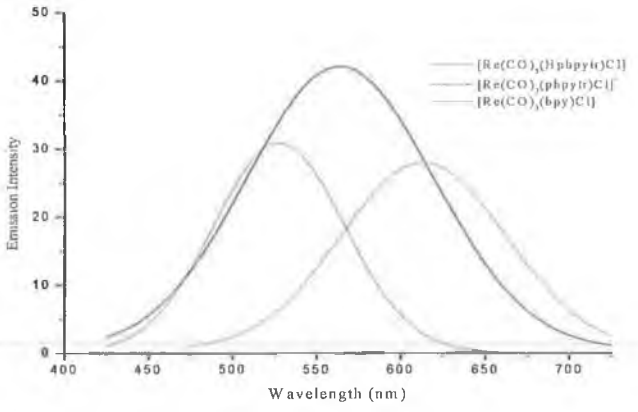

Figure 2. 13 *Emission spectra of $[Re(CO)_3(Hphpytr)Cl]$, $[Re(CO)_3(phpytr)Cl]^-$ and $[Re(CO)_3(bpy)Cl]$ in dichloromethane at 298 K.*

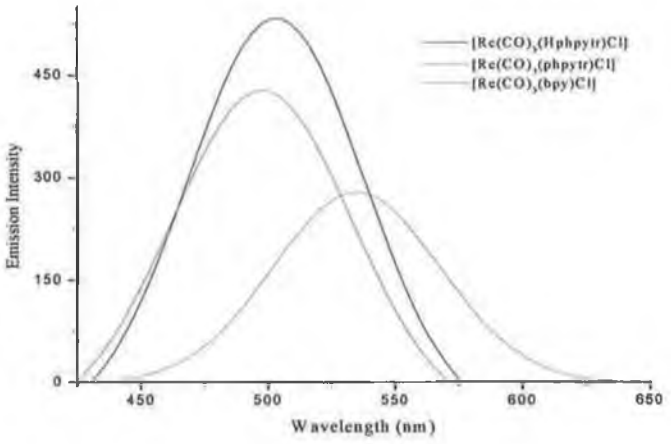

Figure 2. 14 *Emission spectra of [Re(CO)$_3$(Hphpytr)Cl], [Re(CO)$_3$(phpytr)Cl]$^-$ and [Re(CO)$_3$(bpy)Cl] in ethanol:methanol (4:1) at 77 K. The emission spectrum of [Re(CO)$_3$(phpytr)Cl]$^-$ was recorded in the presence of triethylamine.*

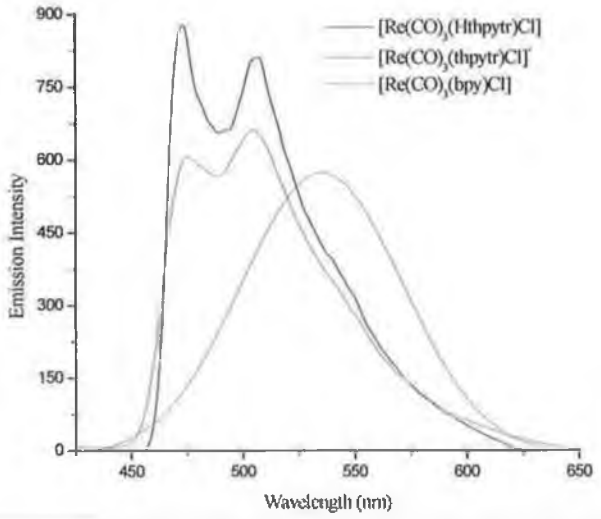

Figure 2. 15 *Emission spectra of [Re(CO)$_3$(Hthpytr)Cl] and [Re(CO)$_3$(thpytr)Cl]$^-$ at 77 K in ethanol:methanol (4:1). The spectrum of [Re(CO)$_3$(bpy)Cl] is also shown for comparative purposes.*

The emission properties of the free ligand Hthpytr compared to the complex $[Re(CO)_3(Hthpytr)Cl]$ were also examined at 77 K. Upon excitation at 325 nm the ligand Hthpytr emits with an emission maximum of 425 nm at 77 K (see Figure 2. 16). The emission maximum of Hthpytr is blue shifted by approximately 50 nm compared to the high energy band in the emission spectrum of the complex $[Re(CO)_3(Hthpytr)Cl]$ at 77 K.

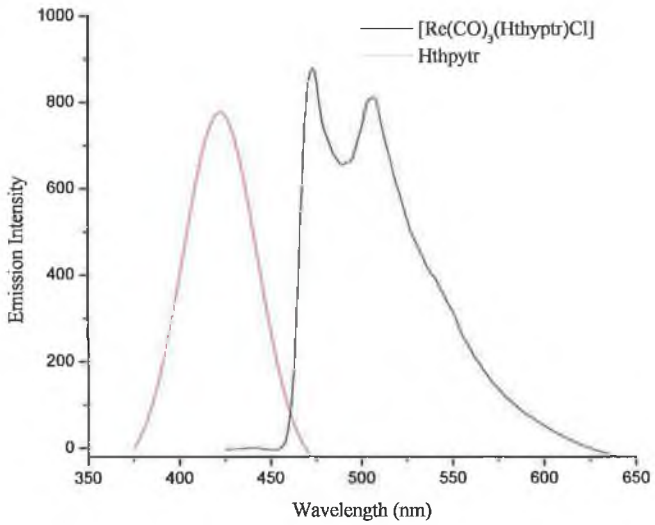

Figure 2. 16 *Emission spectra at 77 K in ethanol:methanol (4:1) of* $[Re(CO)_3(Hthpytr)Cl]$ *and Hthpytr.*

Excited state lifetimes of the pyridyl-triazole complexes were measured at room temperature (298 K) and 77 K. The data are presented in Table 2. 4. In addition, the radiative quantum yields obtained in deoxygenated dichloromethane at 298 K are also presented in Table 2. 4. The lifetimes at 298 K and 77 K along with the radiative quantum yield were also determined for $[Re(CO)_3(bpy)Cl]$. The lifetime of 54 ns and the quantum yield of 0.005 obtained for $[Re(CO)_3(bpy)Cl]$ at 298 K in deoxygenated dichloromethane are comparable with the previous values of 51 ns and 0.005 obtained by Caspar and Meyer.[37] Lifetimes in the range of 51 to 274

ns were obtained for $[Re(CO)_3(Hpytr)Cl]$, $[Re(CO)_3(Hphpytr)Cl]$, $[Re(CO)_3(Hthpytr)Cl]$ and $[Re(CO)_3(HBrpytr)Cl]$ at 298 K (see Table 2. 4). $[Re(CO)_3(Mephpytr)Cl]$ was found to have a particularly long lifetime of 735 ns at 298 K compared to the other complexes. Deprotonation of the triazole ligand was found to increase the lifetime and quantum yield compared to the corresponding protonated complex. For example a lifetime of 101 ns and a quantum yield of 0.0034 was obtained for $[Re(CO)_3(Hphpytr)Cl]$ compared to the lifetime of 159 ns and quantum yield of 0.0081 observed for $[Re(CO)_3(phpytr)Cl]^-$. No clear pattern can be seen regarding the influence of the triazole substituent on the lifetime of the excited state.

For all of the emitting complexes listed in Table 2. 4 with the exception of $[Re(CO)_3(Hthpytr)Cl]$ at 77 K, the emitting level can be labelled as MLCT in character according to the following considerations:

(i) The position and shape of the emission band is consistent with that previously reported for similar complexes assigned as MLCT emitters.[38,39,40]

(ii) There is a blue shift in the emission band on cooling from 298 K to 77 K.[41]

(iii) The time range (microseconds) of the 77 K emission is typical of MLCT states.[42, 43,44]

The position of the emission is blue shifted with respect to $[Re(CO)_3(bpy)Cl]$ (600 nm) when the pyridyl-triazole ligand is both protonated and deprotonated (i.e. 580 nm vs. 530 nm in the case of $[Re(CO)_3(Hpytr)Cl]$ compared to $[Re(CO)_3(pytr)Cl]^-$). Yang and co-workers used Denisty Functional Theory (DFT) to analyse the ground and excited state properties of $[Re(CO)_3(bpy)Cl]$, $[Re(CO)_3(5,5'$-dibromo-bpy)Cl] and $[Re(CO)_3(4,4'$-dimethyl-bpy)Cl].[45] For these complexes, the excited state responsible for the luminescence was of ^{3}MLCT in nature. The emission maxima (compared to $[Re(CO)_3(bpy)Cl]$) were blue shifted when substituted by an electron donating group (CH_3) and were red shifted when substituted by an

electron withdrawing group (Br). The authors concluded the electron donating CH_3 group leads to blue shifts in the emission maxima due to the increased energy of the LUMO which results in an increase in energy between the emissive and ground electronic states. On the other hand, the electron withdrawing Br group causes a red shift in the emission maximum due to the decreased energy of the LUMO, which leads to a reduction in the energy gap between ground and the ^{3}MLCT states. Hence the blue shift in the emission maxima of the pyridyl-triazole complexes compared to $[Re(CO)_3(bpy)Cl]$ most likely arises from the increased energy of the LUMO of the electron donating pyridyl-triazole ligand compared to 2,2-bipyridyl which leads to an increased energy gap between the ground and the ^{3}MLCT states. Deprotonation of the triazole enchances the electron donating ability of the ligand.[10,11] Hence the energy gap between ground and the ^{3}MLCT states increases. Consequently the emission maxima of the deprotonated complexes are blue shifted relative to their protonated analogues and $[Re(CO)_3(bpy)Cl]$.

A decrease in luminescence lifetimes from 142 ns to 2 ns upon protonation of the pyridyl-triazole ligand in $[Ru(bpy)_2(pytr)]^+$ has been attributed to population of a non-radiative ^{3}MC decay path arising from the decrease in the MLCT/MC gap on protonation.[46] It is possible the protonated pyridyl-triazole complexes decay via a ^{3}MC excited state while the deprotonated complexes do not efficiently populate this state at 298 or 77 K. Therefore the deprotonated complexes exhibit longer lifetimes and higher quantum yields compared to their protonated analogues.

$[Re(CO)_3(Hthpytr)Cl]$ has luminescence properties that are not understandable within the simple scheme of MLCT emission outlined above. The 77 K emission properties of rhenium tricarbonyl complexes can usually grouped into two main classes:

i) The emission band is featureless and has a lifetime in the range 1-50 μs; In this instance, the luminescence is considered to have "pure" MLCT character.[45, 47]

ii) The emission band is structured but can be resolved into two components, one with a lifetime of about 10 μs (^{3}MLCT) and another long-lived lifetime between 50-1000 μs ($^3\pi\pi^*$).[48,49]

As previously discussed all of the complexes discussed above with the exception of [Re(CO)$_3$(Hthpytr)Cl] fall into class (i). The structured emission of [Re(CO)$_3$(Hthpytr)Cl] at 77 K, with one short-lived component of 7.06 μs and a long lived component of 76.31 μs indicates that the emitting level has MLCT and LC character i.e. class (ii). Usually the energy of the LC emission in rhenium tricarbonyl polypyridine complexes occurs at similar energy to the free ligand. It is somewhat puzzling that the energy of the LC phosphorescence in the free ligand at 77 K is about 50 nm higher in energy than the proposed LC emission in [Re(CO)$_3$(Hthpytr)Cl]. The SPC and laser systems used in the lifetime measurements have excitation wavelengths of 337 and 355 nm respectively. Unfortunately the Hthpytr ligand does not absorb at either of these wavelengths, hence the phosphorescence lifetime of the free ligand could not be measured. The lifetime and structure of the emission band of [Re(CO)$_3$(Hthpytr)Cl] at 298 K indicates this complex is an MLCT emitter in fluid solution. This is not surprising as the position of MLCT states are subject to medium rigidity, so that with an increase in temperature the MLCT states are shifted to lower energy and become the lowest emitting levels.

Previous photophysical investigations of [Re(CO)$_3$(*s*-phen)Cl] type complexes (where *s*-phen = 1,10-phenanthroline, 4,7-dimethyl-1,10-phenanthroline, 5,6-dimethyl-1,10-phenanthroline, 3,4,7,8-tetramethyl-1,10-phenanthroline) have revealed the ^{3}MLCT manifold is relatively constant in all of the complexes and lies at ~ 475 nm (21,000 cm^{-1}) with a lifetime of ~ 12 μs at 77 K.[50] The methyl substituted complexes also displayed $^3\pi\pi^*$ emission. Various temperature dependent studies led to the following conclusions: (i) When the ^{3}MLCT and $^3\pi\pi^*$ states are separated by more than 1,000 cm^{-1}, only the lowest triplet state is emissive at 77 K. (ii) A separation of less than 1,000 cm^{-1} between the ^{3}MLCT

and $^3\pi\pi^*$ states results in dual emission. Like the phenanthroline type complexes, it is possible there is a very small energy separation between the ^{3}MLCT and $^3\pi\pi^*$ states in $[Re(CO)_3(Hthyptr)Cl]$ and $[Re(CO)_3(thyptr)Cl]^-$ compared to the other pyridyl-triazole complexes. Hence emission is detected from both the ^{3}MLCT and $^3\pi\pi^*$ states. When the asymmetric Hthpytr ligand is coordinated to the rhenium metal centre, it is possible electron density is delocalised in varying degrees throughout the coordinated ligand. As a result, location of the $^3\pi\pi^*$ state in the coordinated ligand is different to that of the free ligand. Consequently emission from the free ligand is not observed at the same energy as the complex. Temperature dependent studies should be carried out in order to confirm the exact nature of the dual emission observed in $[Re(CO)_3(Hthyptr)Cl]$ and $[Re(CO)_3(thyptr^-)Cl]$.

2.2.6 Ground-state and excited-state pK_a measurements

As observed in Section 2.2.5, the absorption and emission spectra of the rhenium complexes synthesised in this chapter are pH dependent. The possibility of protonation of the coordinated triazole opens up the whole area of acid-base photochemistry. By measurement of the ground and excited state pK_a's of the triazole one can confirm if the excited state is located on the pyridyl-triazole ligand.[51] If the excited state is located on the triazole ligand, it will become more basic in the excited state due to the excited electron. This will reduce its ability to deprotonate, resulting in a higher pK_a in the excited state (i.e. a higher pK_a* value than that of the pK_a).[52,53] Conversely location of the excited state electron on any other ligand in the complex would cause a higher acidity in the triazole unit when the complex is excited. This would result in a lower pK_a* compared to the pK_a.[46,51] The pH dependence of the absorption and emission spectra were monitored in Britton-Robinson buffer. pH adjustments were made by adding 75 μl of 2 M NaOH or 2 M H_2SO_4 to a 100 cm^3 volume of the dissolved complex. The complexes $[Re(CO)_3(Hphpytr)Cl]$ and $[Re(CO)_3(Hthpytr)Cl]$ were found to be insoluble in Britton-Robinson buffer. Hence no acid-base data is available for these complexes.

The ground-state acid-base chemistry of the complexes was investigated using UV/Vis absorption spectroscopy. At pH 1.00 in Britton-Robinson buffer $[Re(CO)_3(Hpytr)Cl]$ exhibits a λ_{max} at 315 nm. This gradually blue shifts on increasing pH. The effect of pH on the absorption spectrum of $[Re(CO)_3(Hpytr)Cl]$ is shown in Figure 2. 17. All pH changes were reversible and were found to be independent of the direction of pH change. A plot of change in absorbance (monitored at 315 nm) against pH results in a curve with only one inflection point (Figure 2. 17). The pH inflection point (pH_i) is also the pK_a of the complex. Similar spectral changes were observed for $[Re(CO)_3(Hpytr)Cl]$. The pK_a values of $[Re(CO)_3(Hpytr)Cl]$ and $[Re(CO)_3(HBrpytr)Cl]$ are summarised in Table 2. 5.

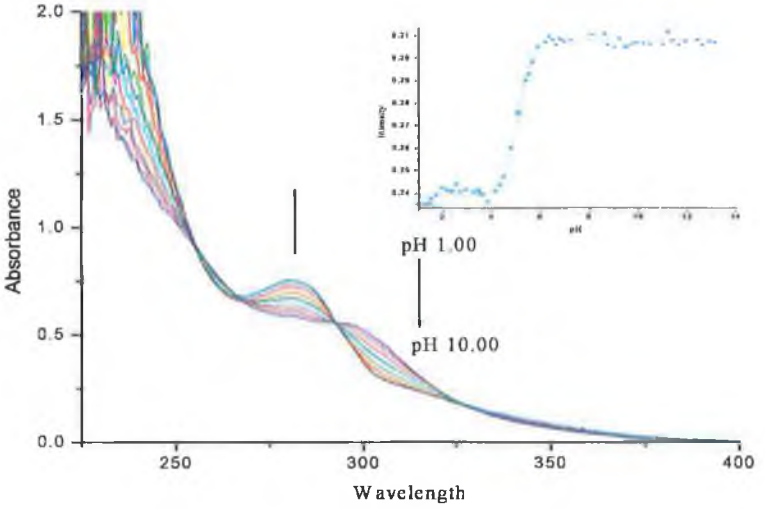

Figure 2. 17 *Ground state pK_a titration (pH 1 —pH 10) of $[Re(CO)_3(Hpytr)Cl]$ in Britton Robinson buffer. Inset shows a plot of absorbance at 315 nm versus increasing pH, with fitted curve.*

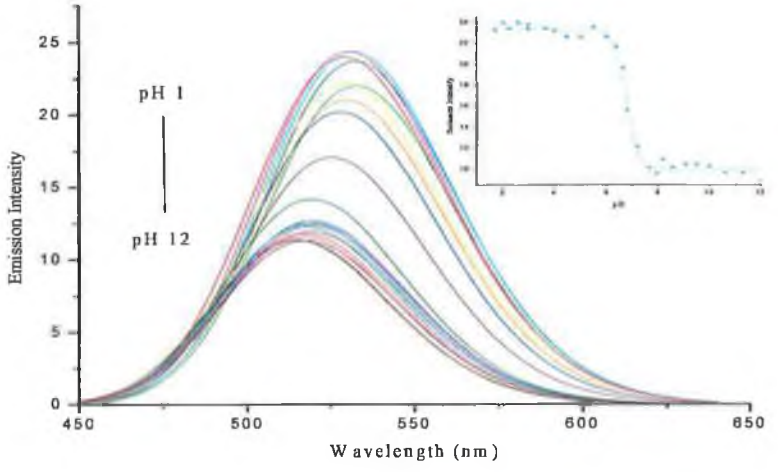

Figure 2. 18 *Excited state pK_a titration (pH 1 —pH 12) of $[Re(CO)_3(Hpytr)Cl]$ in Britton Robinson buffer, excited at 293 nm. Inset, a plot of intensity versus increasing pH, with fitted curve*

Figure 2. 18 shows the pH dependence of the emission spectra of $[Re(CO)_3(Hpytr)Cl]$. The spectra were obtained by exciting the complex at 293 nm, which is an isobestic point in the ground state pK_a titration (see Figure 2. 17). Exciting the complex at an isobestic point ensures that, both $[Re(CO)_3(Hpytr)Cl]$ and $[Re(CO)_3(pytr)Cl]^-$ absorb light to the same extent. Thus, any difference in luminescence behaviour is determined solely by the pH of the solution. At pH 1, the λ_{max} is at 532 nm. The λ_{max} shifts to 518 nm with increasing pH while the emission intensity was found to decrease with increasing pH. A plot of emission (monitored at 532 nm) against pH results in a curve (inset Figure 2. 18) which allows the pH_i^* to be determined. Unlike the ground-state titrations, pH_i^* does not equal pK_a^*. This is due to the protonated and deprotonated species having different luminescence lifetimes. The pK_a^* can be calculated from pH_i^* and the lifetimes of the protonated (τ_a) and deprotonated (τ_b) species using Equation 2.1.

$$pK_a^* = pH_i^* + \log(\tau_a/\tau_b) \qquad \textbf{2. 1}$$

Another method of calculating pK_a^* is with Försters equation, as given in Equation 2.2. Försters equation relates pK_a^* to the ground-state pK_a and the emission maxima (in wavenumbers) of the protonated (ν_a) and deprotonated (ν_b) species for a given temperature, T.

$$pK_a^* = pK_a + \{0.625(\nu_b-\nu_a)/T\} \qquad \textbf{2. 2}$$

The values of pK_a and pK_a^* are presented in Table 2. 5. Similar pK_a^* values were obtained using Equation 2.1 and Equation 2.2.

Complex	pK_a	pH_i*	pK_a* (1)	pK_a* (2)
$[Re(CO)_3(Hpytr)Cl]$	5.1	6.8	6.8	6.4
$[Re(CO)_3(HBrpytr)Cl]$	2.5	3.7	3.7	3.9

Table 2. 5 *Ground-state and excited-state pK_a, values for the rhenium tricarbonyl complexes. The pK_a* (1) values were obtained using Equation 2.1 and the pK_a* (2) values were calculated using Equation 2.2.*

There are few literature reports of acid-base studies of rhenium(I) tricarbonyl complexes. Costa and coworkers synthesised a series of ester and carboxylic acid-derivatives of the form $[Re(CO)_3(2,2'$-bipyridine$)Cl]$ and $[Re(CO)_3(2,2'$-bipyridine$)($pyridine$)]CF_3SO_3$, in which the carboxylic acid or ester function resided on the bipyridyl or pyridine fragment.[54] The following conclusions were reached regarding this series of complexes: if the ligand that contains the protonated/deprotonated site participates in the MLCT transition, the absorption and emission spectra were pH dependent. For example the complex $[Re(CO)_3(bpy\text{-}COOCH_3)(py\text{-}COOH)]CF_3SO_3$ showed no changes in the absorption spectra in the pH range 2-10. In this case deprotonation of the pyridine fragment was possible. Therefore it was concluded that the MLCT transition is $Re \rightarrow \pi^*bpy\text{-}COOCH_3$ based. Since both $[Re(CO)_3(Hpytr)Cl]$ and $[Re(CO)_3(HBrpytr)Cl]$ exhibited spectral changes in the pH range 1-12, it is reasonable to conclude that absorption and emission in the triazole complexes involves the pyridyl-triazole ligand. Kunkely and coworkers deduced, when the low energy absorption band is IL based in a rhenium tricarbonyl complex, the absorption maximum red shifts on deprotonation of the coordinated ligand, while a blue shift in the absorption maximum is observed when the absorption band is MLCT based.[55] The absorption maxima of $[Re(CO)_3(Hpytr)Cl]$ and $[Re(CO)_3(HBrpytr)Cl]$ are blue shifted on deprotonation of the coordinated pyridyl-triazole ligand, thus confirming the absorption process is MLCT based.

The acidity of a coordinated triazole ring is strongly dependent on the nature of the substituent in the C_5 position of the triazole. For example, pK_a values of 4.1 and 1.3 were obtained for the ruthenium(II) complexes $[Ru(bpy)_2(Hpytr)]^{2+}$ and $[Ru(bpy)_2(HBrpytr)]^{2+}$.[12,15,56] This is caused by the electron withdrawing bromine group lowering the electron density on the triazole ring and therefore causing the triazole ring to become more acidic. A similar trend was observed for the rhenium(I) complexes $[Re(CO)_3(Hpytr)Cl]$ and $[Re(CO)_3(HBrpytr)Cl]$. pK_a values of 5.1 and 2.5 were obtained for $[Re(CO)_3(Hpytr)Cl]$ and $[Re(CO)_3(HBrpytr)Cl]$ respectively. The electron withdrawing properties of the bromine atom result in an electron deficient triazole ligand and therefore a lower pK_a value is observed for $[Re(CO)_3(HBrpytr)Cl]$ compared to $[Re(CO)_3(Hpytr)Cl]$.

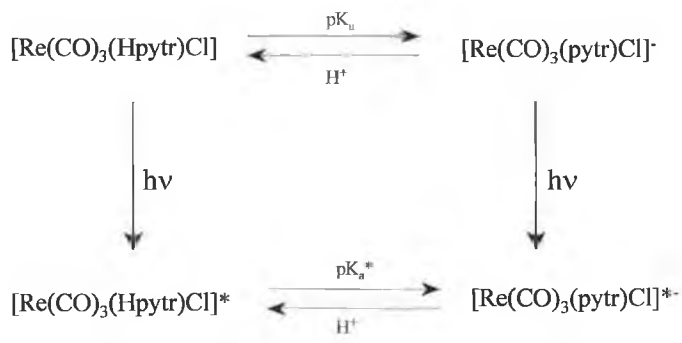

Scheme 2. 3 *Acid-base process for the complex $[Re(CO)_3(Hpytr)Cl]$.*

The results obtained show the co-ordinated pyridyl-triazole is more acidic in the excited state than in the ground state i.e. both complexes have a higher pK_a* compared to the pK_a (Table 2. 5). This is an important observation; since it shows the triazole ligands actively participate in the emission processes i.e. the electron resides in the pyridyl-triazole after excitation of the complex. After excitation, the electron rich pyridine ring can bind a proton much easier than in the ground state. This behaviour is quite different to the analogous ruthenium(II) complexes $[Ru(bpy)_2(Hpytr)]^{2+}$ and $[Ru(bpy)_2(HBrpytr)]^{2+}$ where the excited-state pK_a values

are lower than the ground-state pK_a values.[12,15] For example $[Ru(bpy)_2(Hpytr)]^{2+}$ has a pK_a value of 4.1 compared to a pK_a* value of 2.1. The authors concluded that the observed difference between the pK_a and pK_a* values was a result of the pyridyl-triazole ligands acting as "spectator" ligands not actively participating in the emission process. After excitation from the ruthenium(II) metal centre to the bipyridyl ligand, the ruthenium ion has a charge of 3+. This increase in charge is offset by an increase in donation from the triazole ligand to the ruthenium metal centre. This effect causes a higher acidity of the pyridyl-triazole ligand when the complex is excited. The ability to deprotonate the coordinated pyridyl-triazole ring results in the rhenium(I) complexes exhibiting acid-base photochemistry. Scheme 2. 3 outlines the acid-base processes in the triazole complexes synthesised in this chapter. Note the above scheme also represents the acid base process for $[Re(CO)_3(HBrpytr)Cl]$.

2.2.7 Electrochemistry

Electrochemistry is another important technique which may be employed in the study of the electronic properties of these complexes. Triazoles are σ-donors, so they increase electron density on a metal centre. Therefore, complexes containing triazoles should have lower metal based oxidation potentials than those of the corresponding bipyridine based complexes. Pyridine and related compounds are strong π-acceptors, so they reduce the electron density on a metal centre and thus result in increased oxidation potentials compared to halide based complexes. The effect of combining a σ-donor triazole fragment with a π-accepting pyridine unit on the oxidation potentials of a rhenium metal centre compared to $[Re(CO)_3(bpy)Cl]$ are explored in this section.

Cyclic voltammetry was carried out in dry acetonitrile with 0.1 M tetrabutylammonium tetrafluoroborate ($TBABF_4$). The measurements are all reported versus the Fc/Fc^+ couple. Rhenium pyridyl-triazole complexes have an interesting acid base chemistry, as already shown by the pK_a titrations. Under normal conditions, the triazole is protonated. However, upon deprotonation of the

triazole with one drop of 0.1M triethylamine in acetonitrile, poor quality voltammograms were obtained. Hence only the electrochemistry of the protonated complexes will be discussed. An understanding of the electrochemical processes of $[Re(CO)_3(bpy)Cl]$ is essential before interpretation of the cyclic voltammetry of the pyridyl-triazole complexes. Electrochemical studies of $[Re(CO)_3(bpy)Cl]$ have been previously carried out in acetonitrile with 0.1 M tetra-*n*-butylammonium hexafluorophosphate (TBAH) as electrolyte.[57] The electrochemical processes are summarised in Scheme 2. 4.

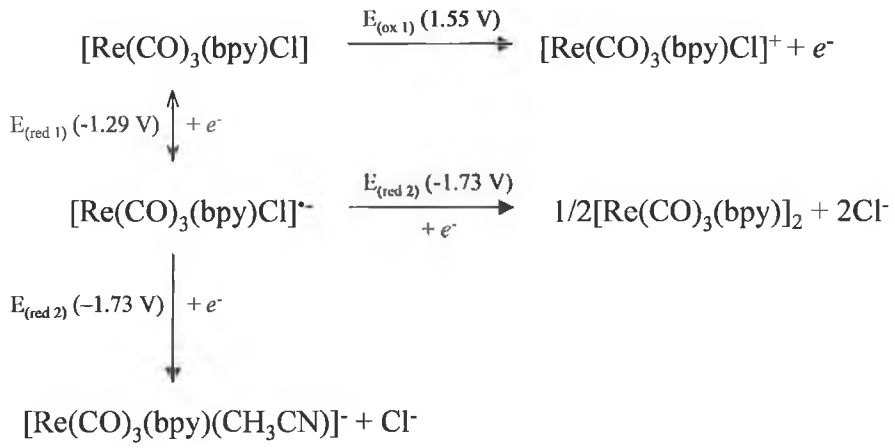

Scheme 2. 4 *Scheme of redox processes for $[Re(CO)_3(bpy)Cl]$.*

The one electron oxidation of $[Re(CO)_3(bpy)Cl]$ is followed by rapid loss of the chlorine to form $[Re(CO)_3(bpy)(CH_3CN)]^+$. Hence an irreversible oxidation is observed. In the case of reduction of $[Re(CO)_3(bpy)Cl]$, the one-electron bipyridyl based reduction ($E_{(red\ 1)}$) is reversible. The second (irreversible) reduction at much more negative potential is assigned to an electrochemical process involving chloride dissociation. This is followed either by solvation or dimerisation. Similar trends were observed when voltammograms of $[Re(CO)_3(bpy)Cl]$ were recorded in acetonitrile and 0.1 M ($TBABF_4$) (Figure 2. 19). An irreversible oxidation was observed at 1.51 V which can be attributed to the formation of $[Re(CO)_3(bpy)(CH_3CN)]^+$. The reversible bipyridyl based

reduction is observed at -1.29 V. The irreversible reduction at –1.73 V is a result of chlorine loss.

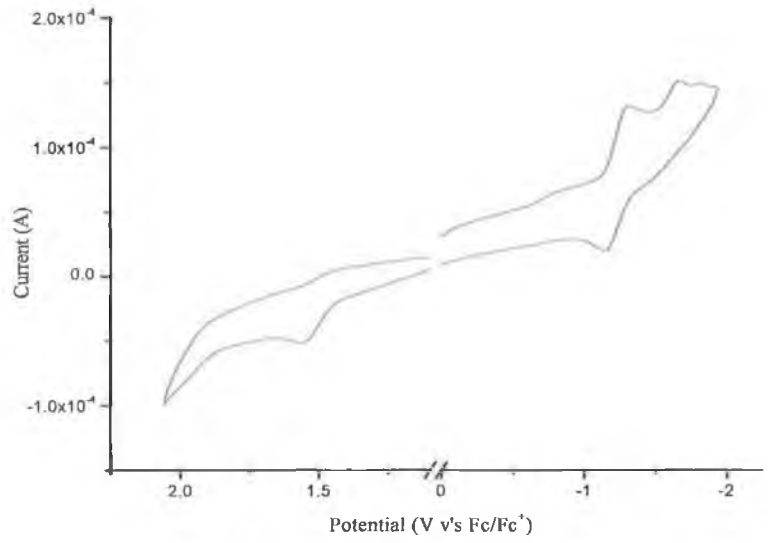

Figure 2. 19 *Cyclic voltammogram of the oxidation of [Re(CO)$_3$(bpy)Cl] in 0.1M TBABF$_4$ in acetonitrile with a scan rate of 100 mV/s.*

Complex	E (V)		
	Re (I)/(II)	Reduction	
[Re(CO)$_3$(Hpytr)Cl]	1.44[a]	—	-2.07[b]
[Re(CO)$_3$(Hphpytr)Cl]	1.45[a]	—	-1.87[b]
[Re(CO)$_3$(Mephpytr)Cl]	1.48[a]	—	-1.81[b]
[Re(CO)$_3$(Hthpytr)Cl]	1.43[a]	—	-1.92[b]
[Re(CO)$_3$(HBrpytr)Cl]	1.40[a]	—	-1.99[b]
[Re(CO)$_3$(bpy)Cl]	1.55[a]	-1.29	-1.73[b]

Table 2. 6 *CV electrochemical results (v's Fc/Fc$^+$) in acetonitrile with 0.1 M TBABF$_4$.* [a]*Anodic peak potential corresponding to an irreversible step.* [b]*Cathodic peak potential corresponding to an irreversible step.*

Table 2. 6 summarises the redox data for the pyridyl-triazole complexes. All values have been corrected using the redox potential of ferrocene under the same experimental conditions as a secondary reference. Figure 2. 20 shows a CV of $[Re(CO)_3(Hphpytr)Cl]$. The CV of $[Re(CO)_3(Hphpytr)Cl]$ is typical of the pyridyl-triazole complexes. By comparison with $[Re(CO)_3(bpy)Cl]$ and other rhenium(I) complexes, the redox processes are relatively straightforward to assign.[58,59] An electrochemically irreversible oxidation was observed near 1.40 V for the pyridyl-triazole complexes. This has been assigned to oxidation of the rhenium(I) centre. The similar potentials for oxidation of the triazole complexes suggest that the d_π energy levels remain relatively constant in these complexes. The oxidation potential of the rhenium(I) metal is sensitive to the ligands in the coordination sphere. Triazole ligands are better σ-donors compared to 2,2'-bipyridyl,[12] therefore the rhenium(I) metal centre is easier to oxidise when coordinatined to a pyridyl-triazole. Hence the oxidation potentials of the triazole complexes are observed at lower potential when compared to $[Re(CO)_3(bpy)Cl]$ (Table 2. 6).

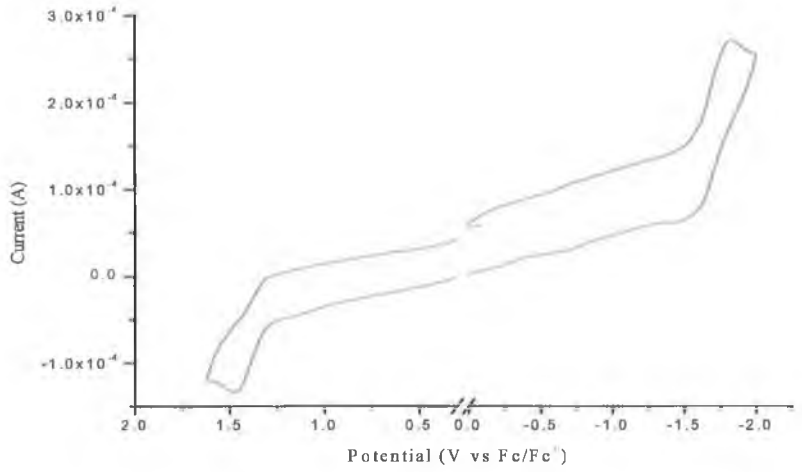

Figure 2. 20 *Cyclic voltammogram of $[Re(CO)_3(Hphpytr)Cl]$ in acetonitrile with 0.1M $TBABF_4$.*

An irreversible reduction is observed at ~ -1.90 V (*Table 2. 6*). This is assigned to reduction of the coordinated pyridyl-triazole ligand (Equation 2.3).

$$[Re(CO)_3(\text{pyridyl-triazole})Cl] + e^- \rightarrow [Re(CO)_3(\text{pyridyl-triazole}^{\bullet-})Cl] \qquad \mathbf{2.3}$$

The reduction potential of the pyridyl-triazole ligands are much more negative than the reduction potential of the 2,2'-bipyridyl ligand measured for $[Re(CO)_3(bpy)Cl]$. This also indicates the triazole ligands are weaker π acceptors than 2,2'-bipyridyl. Reduction of the coordinated triazole ligand in the ruthenium complex $[Ru(bpy)_2(Hpytr)]^{2+}$ was also observed at a very negative potential (-2.25 V) compared to reduction of the two bipyridyl ligands (-1.49 V, -1.73 V).[12] It is highly unlikely the irreversible reduction observed for the pyridyl-triazole complexes is due to the electrochemical process involving chloride dissociation as observed for $[Re(CO)_3(bpy)Cl]$ and other rhenium polypyridine type complexes (see Scheme 2. 4).[60,61] Note this process only occurs following reduction of the coordinated ligand.

2.3 Conclusions

A range of pyridyl-triazole ligands have been prepared and characterised. These ligands were subsequently reacted with $Re(CO)_5Cl$. The mononuclear complexes thus formed were characterised by IR spectroscopy, ^1H NMR spectroscopy and elemental analysis. The elemental analysis confirms the presence of a proton on the triazole. The formation of a single coordination isomer was observed for each pyridyl-triazole complex. The exact coordination mode of the rhenium metal centre to the triazole ligand is still unclear. Crystal structures of the complexes should be obtained in order to confirm the coordination mode.

Spectroscopic studies show that the σ-donor nature of the triazole results in a blue shift of both the absorption and emission spectra when compared to $[Re(CO)_3(bpy)Cl]$. This has been explained as being due to the increased electron density on the rhenium metal centre, which in turn increases the energy of the

MLCT transition. The oxidation potential of the rhenium centre in each of the complexes has been reduced significantly with respect to $[Re(CO)_3(bpy)Cl]$. This is again due to the σ-donor properties of the triazole ligands. Luminescent lifetimes, pK_a titrations and electrochemical studies all point towards the fact that the excited state of the complexes lies on the pyridyl-triazole ligand at room temperature. All of the pyridyl-triazole complexes with the exception of $[Re(CO)_3(Hthpytr)Cl]$ may also be considered to have "pure" MLCT character at 77 K. The structured emission of $[Re(CO)_3(Hthpytr)Cl]$ at 77 K, with one short-lived lifetime component and a long lived lifetime component indicates that there are two different emitting levels i.e. ^{3}MLCT and $^3\pi\pi^*$. Temperature dependent studies are necessary in aprotic and protic media in order to confirm the nature of the emissive states for $[Re(CO)_3(Hthpytr)Cl]$ at 77 K. These complexes may be seen as model complexes, which should aid in the synthesis, purification and characterisation of the pyrazine type complexes in Chapter 3.

2.4 Experimental

2.4.1 Synthesis of the Ligands

3-(pyridin-2-yl)-1,2,4-triazole (Hpytr)[12]

Hydrazine hydrate (4.80 g, 0.150 mol) was slowly added to a solution of 2-cyanopyridine (10.00 g, 0.111 mol) in 100 cm^3 of ethanol. The reaction mixture was gently heated to 40°C. After the formation of a pale yellow solution the heat was turned off and the reaction was left stirring overnight. The yellow precipitate (2-pyridylamidrazone) was filtered and washed with cold ethanol. The amidrazone was slowly added to 50 cm^3 of formic acid at 0 °C. After stirring for 3 hours, the excess formic acid was removed. The remaining oil was refluxed in 30 cm^3 of ethylene glycol for 1 hour. The triazole precipitated on cooling of the ethylene glycol and was collected under vacuum. The triazole was recrystallised twice from acetone to yield a fine white powder. Yield: 5.95 g, 0.041 mol, 43 %.

^{1}H NMR (d_6-acetone), δ in ppm : H_3: 8.09 (d); H_4: 7.98 (t); H_5: 7.51 (t); H_6: 8.70 (d); H_a: 8.27 (s).

3-(pyridin-2-yl)-5-phenyl-1,2,4-triazole (Hphpytr) [29]

Hydrazine hydrate (1.92g, 0.060 mol) was slowly added to a solution of 2-cyanopyridine (5.00 g, 0.056 mol) in 20 cm^3 of ethanol. The reaction mixture was gently heated to 40 °C . After the formation of a yellow solution the heat was turned off and the reaction was left stirring overnight. The 2-pyridyl amidrazone (yellow precipitate) was filtered under vacuum and washed with ethanol. Benzoyl chloride (6.60g, 47 mmol) was added dropwise to a stirred solution of 4 cm^3 of triethylamine and 2-pyridyl amidrazone in 20 cm^3 of dry THF. The yellow suspension was stirred for three hours at room temperature. The yellow crystals were filtered under vacuum and left drying overnight. The crystals were dissolved in ethylene glycol and refluxed for three hours. The ethylene glycol solution was allowed cool to room temperature. 10 cm^3 of cold water was added to the solution to aid precipitation. The white triazole ligand precipitated overnight and was collected under vacuum. The triazole was recrystallised twice from ethanol to yield a fine white powder. Yield: 5.92 g, (56 %, 0.027 mol). ^{1}H NMR (d_6-acetone), δ in ppm: H_3: 8.28 (d); H_4: 8.02 (t); H_5: 7.48 (m); H_6: 8.70 (d); H_a: 8.22 (d); H_b: 7.51 (m); H_c: 7.51 (m).

1-methyl-3-(pyridin-2-yl)-5-phenyl-1,2,4-triazole (Mephpytr)

This ligand was prepared in a similar manner to that described previously for Hphpytr, only in this case methylhydrazine was used instead of hydrazine to react with 2-cyanopyridine. Yield 5.66 g, 0.024 mol, 43 %. Elemental analysis for $C_{14}H_{12}N_4$: Calculated C, 71.19; H, 5.08; N, 23.73. Found C, 71.75; H, 5.19; N, 22.61. ^{1}H NMR (d_6-Acetone), δ in ppm: H_3: 8.18 (d); H_4: 7.89 (m); H_5: 7.42 (m); H_6: 8.68 (d); H_a: 7.89 (m); H_b: 7.58 (m); H_c: 7.58 (m); Me: 3.58 (s).

3-(pyridin-2-yl)-5-(thiophen-2-yl)-1,2,4-triazole (Hthpytr) [29]

3.63 g (0.027 mol) of 2-pyridyl amidrazone was dissolved in 50 cm^3 of dry THF and 5 cm^3 of triethylamine. 4 cm^3 (0.037 mol) of 2-thiophene-acid chloride was slowly added to this solution. The yellow suspension was stirred for 2 hours at room temperature. The yellow precipitate that formed was collected under vacuum. The precipitate was refluxed in ethylene glycol for 1 hour. The triazole ligand precipitated and was collected under vacuum. The ligand was recrystallised in ethanol, yielding a white compound. Yield 2.83 g, 0.012 mol, 44 %. ^{1}H NMR (d_6-acetone), δ in ppm: H_3: 8.21 (d); H_4: 8.01 (m); H_5: 7.52 (m); H_6: 8.69 (d), H_a: 7.55 (m); H_b: 7.18 (m); H_c: 7.75 (d).

3-(pyridin-2-yl)-5-Bromo-1,2,4-triazole (HBrpytr)[15]

0.840 g (0.006 mol) of 3-(pyridin-2-yl)-1,2,4-triazole (Hpytr) was added to 15 cm^3 of water. The ligand was fully dissolved by slow addition of 10 M NaOH (pH 12). 0.6 cm^3 of Br_2 (99 %, d = 3.199 g/cm^3) was slowly added while maintaining a pH of 12 by addition of concentrated NaOH. The solution was stirred for 3 hours. The solution was acidified to pH 3 with concentrated HCl. The brominated ligand precipitated and was collected by vacuum filtration. Yield 1.03 g, 4.6 mmol, 77 %. ^{1}H NMR (d_6-acetone), δ in ppm: H_3: 8.28 (d); H_4: 8.02 (t); H_5: 7.48 (m); H_6: 8.70 (d).

2.4.2 Preparation of the rhenium(I) complexes

[$Re(CO)_5Cl$] (100 mg) and an equimolar amount of the appropriate ligand were refluxed in toluene (50 cm^3) under an argon atmosphere for 2.5 hours to give a dark yellow solution. The reaction mixture was refrigerated overnight. The resulting yellow precipitate was collected by filtration yielding the desired product.

[$Re(CO)_3$(Hpytr)Cl]

Yield 0.086 g, 0.19 mmol, 72 %. Elemental analysis for $ReC_{10}H_6N_4O_3Cl$: Calculated C, 26.58; H, 1.34; N, 12.40; Found C, 26.70; H, 1.02; N, 11.82; ^1H NMR (d_6-acetone), δ in ppm: H_3: 8.37 (m); H_4: 8.34 (m); H_5: 7.79 (m); H_6: 9.07 (d); H_a: 9.45(s). ν_{CO} (cm^{-1}) in THF: 2020, 1915, 1890.

[$Re(CO)_3$(Hphpytr)Cl]

Yield 0.123 g, 0.23 mmol, 83 %. Elemental analysis for $ReC_{16}H_{10}N_4O_3Cl$: Calculated C, 36.40; H, 1.90; N, 10.61; Found C, 36.99; H, 2.17; N, 10.29; ^1H NMR (d_6-acetone), δ in ppm: H_3: 8.45 (d); H_4: 8.39 (m); H_5: 7.81 (m); H_6: 9.06 (d); H_a: 8.39 (m); H_b: 7.51 (m); H_c: 7.51 (m). ν_{CO} (cm^{-1}) in THF: 2023, 1921, 1895.

[$Re(CO)_3$(Mephpytr)Cl]

Yield 0.115 g, 0.21 mmol, 79 %. Elemental analysis for $ReC_{17}H_{12}N_4O_3Cl$: Calculated C, 37.68; H, 2.23; N, 10.34; Found C, 37.44; H, 2.23; N, 10.34; ^1H NMR (d_6-acetone), δ in ppm: H_3: 8.38 (m); H_4: 8.36 (m); H_5: 7.80 (m); H_6: 9.06 (d); H_a: 7.94 (m); H_b: 7.73 (m); H_c: 7.73 (m); Me: 4.15 (s). ν_{CO} (cm^{-1}) in THF: 2023, 1918, 1890.

[$Re(CO)_3$(Hthpytr)Cl]

Yield 0.098 g, 0.18 mmol, 68 %. Elemental analysis for $ReC_{14}H_8N_4O_3ClS$: Calculated C, 31.49; H, 1.51; N, 10.49; Found C, 31.90; H, 1.42; N, 10.09; ^1H NMR (d_6-Acetone), δ in ppm: H_3: 8.36 (d); H_4: 8.34 (m); H_5: 7.78 (m); H_6: 9.07 (d); H_a: 7.88 (d); H_b: 7.28 (m); H_c: 7.77 (m). ν_{CO} (cm^{-1}) in THF: 2023, 1922, 1895.

[$Re(CO)_3$(HBrpytr)Cl]

Yield 0.117 g, 0.22 mmol, 80 %. Elemental analysis for $ReC_{10}H_5N_4O_3ClBr$: Calculated C, 22.60; H, 1.51; N, 10.55; Found C, 22.35; H, 1.13; N, 10.23; ^1H NMR (d_6-Acetone), δ in ppm: H_3: 8.38 (m); H_4: 8.37 (m); H_5: 7.83 (m); H_6: 9.09 (d). ν_{CO} (cm^{-1}) in THF: 2025, 1921, 1895.

[$Re(CO)_3$(bpy)Cl]

Yield 0.111 g, 0.24 mmol, 91 %. ^1H NMR (d_6-Acetone), δ in ppm: H_3: 8.72 (d); H_4: 8.37 (m); H_5: 7.82 (m); H_6: 9.12 (d). ν_{CO} (cm^{-1}) in THF: 2018, 1917, 1892.

2.5 Bibliography

1 V. Balzani, A. Juris, M. Venturi, S. Campagna, *Chem. Rev.* **1996**, 96, 759.

2 V. Balzani, A. Credi, M. Venturi, *Molecular Devices and Machines; A journey into the nanoworld*, VCH, Weinheim **2003.**

3 (a) A. Juris, V. Balzani, F. Barigelletti, S. Campagna, P. Besler, A. von Zelewsky, *Coord. Chem. Rev.* **1988**, 84, 85. (b) F.R. Keene, *Coord. Chem. Rev.* **1997**, 121, 159.

4 (a) K.E. Splan, M.H. Keefe, A.M. Massari, K.A. Walters, J.T. Hupp, *Inorg. Chem.* **2002**, 41, 619. (b) E.C. Constable, E. Schofield, *Chem. Commun*, **1998**, 403, (c) M. Fujita, *Chem. Soc. Rev.* **1998**, 27, 417.

5 S.D. Ernst, W. Kaim, *Inorg. Chem.*, **1989**, 28, 1520.

6 F. Barigelletti, A. Juris, V. Balzani, P. Belser, *Inorg. Chem.*, **1983**, 22, 3335.

7 P.J. Steel, E.C. Constable, *J. Chem. Soc., Dalton Trans.*, **1990**, 1389

8 P.J. Steel, F. Llahousse, C. Marzin, *Inorg. Chem.*, **1983**, 22, 1488.

9 J.G. Vos, J.G. Haasnoot, *Inorg. Chim. Acta.*, **1983**, 71, 155.

10 M.H. Klingele, S. Brooker, *Coord. Chem. Rev.*, **2003**, 241, 119.

11 J.G. Haasnoot, , *Coord. Chem. Rev.,* **2000**, 200, 131.

12 R. Hage, PhD. Thesis, **1991,** Leiden University, The Netherlands.

13 S. Fanni, T.E. Keyes, C.M. O'Connor, H. Hughes, R. Wang, J.G. Vos, *Coord. Chem. Rev.,* **2000**, 208, 77.

14 F. Barigelletti, L DeCola, V. Balzani, R. Hage, J.G. Haasnoot, J. Reedijk, J.G. Vos, *Inorg. Chem,* **1989**, 28, 4344.

15 C. Di Pietro, S. Serroni, S. Campagna, M.T. Gandolfi, R. Ballardini, S. Fanni, W.R. Browne, J.G. Vos, *Inorg. Chem,* **2002**, 41, 2871.

16 B.E. Buchanan, R.Wang, J.G. Vos, R. Hage, J.G. Haasnoot, J. Reedijk, *Inorg. Chem,* **1990**, 29, 3263.

17 H.A. Nieuwenhuis, J.G. Haasnoot, R. Hage, J. Reedijk, T.L. Snoeck, D.J. Stufkens, J.G. Vos, *Inorg. Chem.,* **1991**, 30, 48.

18 M.W. George, F.P.A. Johnson, J.R. Westwell, P.M. Hodges, J.J. Turner, *J. Chem. Soc., Dalton Trans.,* **1993**, 2977.

19 R.W. Balk, D.J. Stufkens, A. Oskam, *J. Chem. Soc., Dalton Trans.,* **1981**, 1124.

20 D.J. Stufkens, A. Vlček Jr., *Coord. Chem. Rev.,* **1998**, 177, 127

21 G.J. Stor, S.L. Morrison, D.J. Stufkens, A. Oskam, *Organometallics*, **1994**, 13, 2641.

22 E.S. Dodsworth, A.B.P Lever, G. Eryavec, R.J. Crutchley, *Inorg. Chem.,* **1985**, 24, 1906.

23 E.C. Constable, K.R. Seddon, *J. Chem. Soc., Chem. Commun.,* **1982**, 34

24 A. Llobet, P. Doppelt, T.J. Meyer, *Inorg. Chem.,* **1988**, 27, 514.

25 S. Van Wallendael, R.J. Shaver, D.P. Rillema, B.J. Yoblinski, M. Stathis, T.F. Guarr, *Inorg. Chem.,* **1990**, 29, 1761

26 M.R. Waterland, T.J. Simpson, K.C. Gordon, A.K. Burrell, *J. Chem. Soc., Dalton Trans.,* **1998**, 185

27 G. Orellana, C.A. Ibarra, J. Santoro, *Inorg. Chem.,* **1988**, 27, 1025

28 R. Hage, R. Prins, J.G. Haasnoot, J. Reedijk, J.G. Vos, *J. Chem. Soc., Dalton Trans,* **1987**, 1389

29 W.R. Browne, PhD. Thesis, **2002**, Dublin City University.

30 W.R. Browne, F. Weldon, A. Guckian, J.G. Vos, *Collect. Czech. Chem. Commun.*, **2003**, 68, 1467.

31 D. Mulhern, PhD. Thesis, **2003**, Dublin City University.

32 H.M. Burke, J.F. Gallagher, M.T. Indelli, J.G. Vos, *Inorg. Chim. Acta.*, **2004**, 357, 2989.

33 A.L. Rheingold, P. Saisuwan, N.C. Thomas, *Inorg. Chim. Acta.*, **1993**, 214, 41.

34 M. Wrighton, D.L. Morse, *J. Am. Chem. Soc.*, **1974**, 96, 998.

35 G.L. Geoffroy, M.S. Wrighton, *Organometallic Photochemistry*, Academic Press: New York, **1979**.

36 I. Costa, M. Montali, P. Pallavicine, A. Perotti, L. Prodi, N. Zaccheroni, *J. Organomet. Chem.*, **2000**, 593, 267

37 J.V. Caspar T.J. Meyer, *J. Phys. Chem.*, **1983**, 87, 952.

38 L. Yang, A. Ren, J. Feng, Y. Ma, H. Zhang, *Inorg. Chem.*, **2004**, 43, 5961.

39 N.M. Shavaleev, Z.R. Bell, T.L. Easun, R. Rutkaite, L. Swanson, M.D. Ward, *J. Chem. Soc. Dalton Trans.*, **2004**, 3678.

40 J.M. Villegas, S.R. Stoyanov, W. Heung, D.P. Rillema, *J. Chem. Soc. Dalton Trans.*, **2005**, 1042.

41 N.H. Damrauer, J.K. McCusker, *Inorg. Chem.*, **1999**, 38, 4268.

42 A.A. Marti, G. Mezei, L. Maldonado, G. Paralitici, R. G. Raptis, J.L. Colon, *Eur. J. Inorg. Chem.*, **2005**, 118.

43 A. Juris, S. Campagna, I. Bidd, J.M. Lehn, R. Ziessel, *Inorg. Chem.*, **1988**, 27, 2438.

44 A. Vlček, *Coord. Chem. Rev.*, **2000**, 200-202, 933.

45 L. Yang, A. Ren, J. Feng, X. Liu, Y. Ma, M. Zhang, X. Liu, J. Shen, H. Zhang, *J. Phys. Chem. A*, **2004**, 108, 6797

46 R. Wang, J.G. Vos, R.H. Schmehl, R. Hage, *J. Am. Chem. Soc.*, **1992**, 114, 1964.

47 L.A. Worl, R. Duesing, P. Chen, L.D. Ciana, T.J. Meyer, *J. Chem. Soc. Dalton Trans.*, **1991**, 849.

48 S.M. Fredericks, J.C. Luong, M.S. Wrighton, *J. Am. Chem. Soc.*, **1979**,

101, 7415.

49 L. Sacksteder, M. Lee, J.N. Demas, B.A. Degraff, *J. Am. Chem. Soc.*, **1993**, 115, 8230.

50 D.R. Striplen, G.A. Crosby, *Coord. Chem. Rev.*, **2001**, 211, 163.

51 B.E. Buchanan, J.G. Vos, M. Kaneko, W.J.M. van der Putten, J.M. Kelly, R. Hage, R.A.G. de Graff, R.Prins, J.G. Haasnoot, J. Reedijk, *J. Chem. Soc. Dalton Trans.*, **1990**, 2425.

52 R.J. Crutchley, N. Kress, A.B.P. Lever, *J. Am. Chem. Soc.*, **1983**, 105, 1170.

53 J.G. Vos, *Polyhedron*, **1992**, 11, 2285.

54 I. Costa, M. Montali, P. Pallavicine, A. Perotti, L. Prodi, N. Zaccheroni, *J. Organomet. Chem.*, **2000**, 593, 267

55 H. Kunkely, A. Volger, *Inorg. Chim. Acta*, **2003**, 343, 357.

56 S. Fanni, C. Di Pietro, S. Serroni, S. Campagna, J.G. Vos, *Inorg. Chem.*, **2000**, 3, 42.

57 B.P. Sullivan, T.J. Meyer, C.M. Bolinger, D. Conrad, W.J. Vining, *J. Chem. Soc., Chem. Commun.*, **1985**, 1414

58 J.C. Luong, L. Nadgo, M.S. Wrighton, *J. Am. Chem. Soc.*, **1978**, 100, 5790.

59 S. Frantz, W. Kaim, J. Fiedler, C. Duboc, *Inorg. Chim. Acta*, **2004**, 357, 3657.

60 W. Kaim, H.E.A. Kramer, C. Volger, J. Rieker, *J. Organomet. Chem.*, **1989**, 367, 107

61 A. Klein, C. Vogler, W. Kaim, *Organometallics*, **1996**, 15, 236.

Chapter 3

Rhenium(I) complexes containing substituted pyrazyl-triazole ligands.

Chapter 3 introduces a series of pyrazyl-triazole ligands and the corresponding rhenium(I) complexes of these ligands. This chapter begins with the structural characterisation of the complexes using IR and NMR spectroscopy. An investigation of the photophysical and electrochemical properties of the complexes with respect to $[Re(CO)_3(bpy)Cl]$ *is also presented in this chapter. In these complexes, the photophysical properties were found to be strongly dependent upon the protonation state of the pyrazyl-triazole ligand.*

3.1 Introduction

The ground state and excited state properties of rhenium complexes can be tuned by changing the ligand coordinated to the metal centre. So far, two types of ligands have been employed. The first class of ligands have stronger π-acceptor and weaker σ-donor properties than 2,2'-bipyridine (bpy), causing low reduction potentials and high oxidation potentials for their rhenium complexes. The absorption and emission maxima of such complexes are red shifted compared to $[Re(CO)_3(bpy)Cl]$. Examples of these rhenium(I) complexes include those containing the following ligands: 2,2'-bipyrazine, 2,2'-bipyrimidine, 2,3-bis-(2-pyridyl)-pyrazine and pyridine-2-carbaldehyde-*N*-isopropylimine.[1,2,3,4] Ligands of the second class have stronger σ-donor and weaker π-acceptor properties than 2,2-bipyridine. The oxidation potential of the complexes are now lower than that of $[Re(CO)_3(bpy)Cl]$, while the absorption and emission maxima are blue shifted. Examples are rhenium complexes with imidazole derivatives as ligands.[5] It is worth noting, there are few example of rhenium complexes with strong σ-donor ligands.

As discussed in Chapter 2, a range of pyridyl-triazole ligands and their corresponding rhenium(I) complexes have been prepared and characterised. During the characterisation of these complexes it was noted that the oxidation potential of these complexes were lower than $[Re(CO)_3(bpy)Cl]$, while the absorption and emission maxima were blue shifted relative to $[Re(CO)_3(bpy)Cl]$. Due to their advantageous properties, it was decided to retain the strong σ-donor triazole unit and to replace the pyridine of the pyridyl-triazole with pyrazine, a well-known strong π-acceptor. It is hoped that by studying the effect of the stronger π-accepting pyrazine ring on the photophysical properties, this might yield a better understanding of the influence of 1,2,4-triazole ligand systems on the properties of rhenium complexes. In Figure 3. 1, the structures of the pyrazyl-triazole ligands prepared are given. These are analogous to those prepared in

Chapter 2. As before, their rhenium(I) complexes have also been prepared and studied in the same systematic method as their pyridyl-triazole analogues.

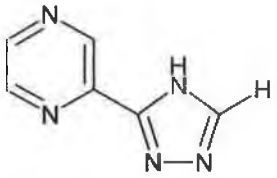

3-(pyrazin-2-yl)-1,2,4-triazole
(Hpztr)

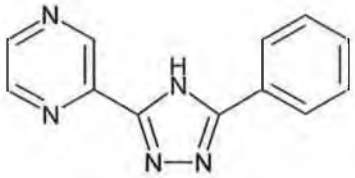

3-(pyrazin-2-yl)-5-phenyl-1,2,4-triazole
(Hphpztr)

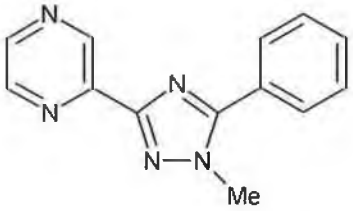

1-methyl-3-(pyrazin-2-yl)-5-phenyl
1,2,4-triazole
(Mephpztr)

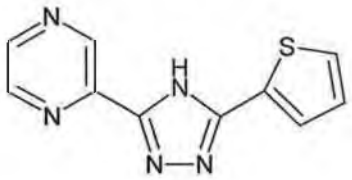

3-(pyrazin-2-yl)-5-(thiophen-2-yl)-
-1,2,4-triazole
(Hthpztr)

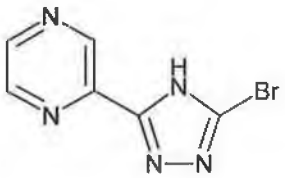

3-(pyrazin-2-yl)-5-bromo-1,2,4-triazole
(HBrpztr)

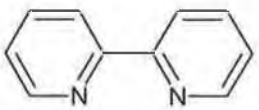

2,2'-bipyridyl
(bpy)

Figure 3. 1 *Structures of the ligands and their abbreviations as cited throughout this chapter.*

3.2 Results and discussion

3.2.1 Synthesis

The synthesis of the pyrazyl-triazole ligands were carried out by the same method as was used for the synthesis of the analogous pyridyl-triazole ligands (see Chapter 3, Scheme 1), starting from cyanopyrazine instead of cyanopyridine. The rhenium complexes of the pyrazyl-triazole ligands were prepared in a similar manner to the complexes of the corresponding pyridyl-triazole ligands. The synthesis of the pyrazyl-triazole complexes were carried out in acidified-toluene. The pyrazyl-triazole ligand was firstly dissolved in toluene. As has been observed for ruthenium complexes containing pyrazyl-triazole ligands, the ligands deprotonate upon coordination of the metal centre.[6,7] However the added precaution of addition of a few drops of trifluoroacetic acid was taken to ensure that the protonated complexes were isolated. The $[Re(CO)_5Cl]$ in toluene was slowly added to the acidified toluene solution. Again, the standard procedure of heating this soloution at reflux under nitrogen was undertaken. As the reactions proceeded, the colour changed from an off white colour to a dark orange solution upon complexation. Reaction times were typically in the order of 3 hours. By following the reactions with infra-red spectroscopy, as before, it was possible to monitor the progress of the complexation. As previously explained (Section 2.4.4), the formation of coordination isomers comes about due to the different binding sites at N_2 and N_4 of the triazole. For the complexes prepared in this section, the formation of only one isomer was observed (see Section 3.2.3). Like the analogous pyridyl-triazole complexes, CHN analysis of the pyrazyl-triazole complexes confirms the complexes were isolated with a protonated 1,2,4-triazole unit.

3.2.2 Infra-red spectroscopy

A comparison of the carbonyl stretching frequencies of the pyrazyl-triazole complexes with literature data can be used to confirm their geometry as well as to provide an insight into the electronic properties of the ligands. The infra-red (IR) spectra of the complexes in THF show three strong absorptions in the carbonyl stretching region (2200–1700 cm^{-1}, Table 3. 1). Figure 3. 2 shows the IR spectra of $[Re(CO)_3(Hthpztr)Cl]$ and $[Re(CO)_3(thpztr)Cl]^-$, which are typical of the complexes discussed in this section. In the protonated complexes one band is centred at ~2025 cm^{-1} with two resolved bands between 1925 cm^{-1} and 1895 cm^{-1}. Three strong carbonyl absorption bands were also observed for the deprotonated complexes (Table 3. 1 and Figure 3. 2). The three carbonyl bands of the deprotonated complexes were all observed at lower frequency compared to their protonated analogues.

Complex	$\nu_{(CO)}$ **cm^{-1}**		
$[Re(CO)_3(Hpztr)Cl]$	2027	1925	1897
$[Re(CO)_3(pztr)Cl]^-$	2018	1914	1889
$[Re(CO)_3(Hphpztr)Cl]$	2026	1927	1901
$[Re(CO)_3(phpztr)Cl]^-$	2017	1916	1890
$[Re(CO)_3(Mephpztr)Cl]$	2028	1926	1894
$[Re(CO)_3(Hthpztr)Cl]$	2027	1926	1897
$[Re(CO)_3(thpztr)Cl]^-$	2018	1917	1886
$[Re(CO)_3(HBrpztr)Cl]$	2025	1928	1899
$[ReCO)_3(Brpztr)Cl]^-$	2016	1915	1887
$[Re(CO)_3(bpy)Cl]$	2018	1917	1892

Table 3. 1 *IR data for the carbonyl stretching of the rhenium(I) tricarbonyl complexes. All measurements are in THF and complexes were deprotonated using triethylamine.*

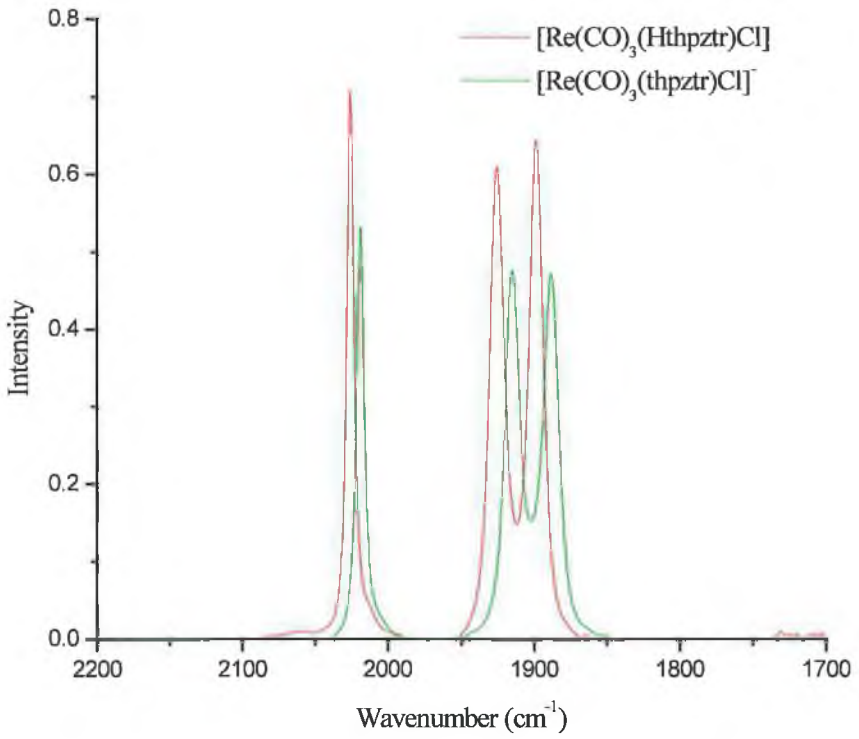

Figure 3. 2 *IR spectra (CO-stretching region) of [Re(CO)$_3$(Hthpztr)Cl] and [Re(CO)$_3$(thpztr$^-$)Cl] in THF at 298 K.*

Like the IR spectrum of [Re(CO)$_3$(bpy)Cl], the CO pattern of the pyrazyl-triazole complexes also corresponds to three CO ligands in a facial isomer arrangement.[8,9] Pyrazine type ligands have lower π^* energy levels than 2,2'-bipyridine.[1,2] This leads to a more favourable back-bonding interaction between the d_π orbitals of rhenium(I) and the pyrazyl-triazole π^* orbitals compared to [Re(CO)$_3$(bpy)Cl]. This interaction leaves less electron density available for back-bonding between the rhenium d_π orbitals and the CO π^* orbitals. As a result the carbonyl bonds in the pyrazyl-triazole complexes are shorter than the carbonyl bonds in

$[Re(CO)_3(bpy)Cl]$. This explains the observed increase in CO stretching frequencies for the pyrazyl-triazole complexes (see Table 3. 1).

The three CO bands of the deprotonated pyrazyl-triazole complexes were all observed at lower frequency compared to their protonated analogues. For example the CO bands of $[Re(CO)_3(Hthpztr)Cl]$ were observed at 2027, 1926 and 1897 cm^{-1} while the CO bands of $[Re(CO)_3(thpztr)Cl]^-$ shifted to 2018, 1917, and 1886 cm^{-1} (see Table 3. 1 and Figure 3. 2). Deprotonation of a triazole ligand enhances the σ-donor abilities of the ligand.[10] The presence of this negative charge increases the electron density on the rhenium metal centre. This enhances the back-bonding interaction between the rhenium d_π orbitals and the CO π^* orbitals, while reducing the back-bonding between the rhenium d_π orbitals and the pyrazyl-triazole π^* orbitals. The CO bond lengthens, and as a result the CO vibrations occur at lower wavenumber when compared to the analogous protonated complexes. These trends were previously observed in the IR spectra of protonated/deprotonated bipyrazine molybdenum and tungsten tetracarbonyl complexes.[11]

Both the pyridyl- and the pyrazyl-triazole complexes show three CO bands in the CO stretching region (2200 – 1700 cm^{-1}) of the IR spectrum. In the case of the pyrazyl-triazole complexes the CO bands are observed at higher frequency compared to the corresponding pyridyl-triazole complexes. For example the CO bands of the pyridyl-triazole complex $[Re(CO)_3(Hpytr)Cl]$ were observed at 2020, 1915 and 1890 cm^{-1} while the CO bands of the pyrazyl-triazole complex $[Re(CO)_3(Hpztr)Cl]$ shifted to 2027, 1925 and 1897 cm^{-1} (see Tables 2.1 and 3.1). Pyrazyl-triazole ligands have lower π^* energy levels than pyridyl-triazole ligands.[10,12] This leads to a more favourable back-bonding interaction between the d_π orbitals of the rhenium(I) and the pyrazyl-triazole π^* orbitals compared to the pyridyl-triazole complexes. This interaction leaves less electron density available for back-bonding between the rhenium d_π orbitals and the CO π^* orbitals. As a result the carbonyl bonds of the pyrazyl-triazole complexes are

shorter than the carbonyl bonds of the pyridyl-triazole. This explains the observed increase in CO stretching frequencies for the pyrazyl-triazole complexes

3.2.3 NMR spectroscopy

NMR spectroscopy has been used for the structural characterisation of rhenium tricarbonyl complexes.[3,13,14] The numbering system employed in the assignment of ^{1}H NMR peaks is shown in Figure 3. 3

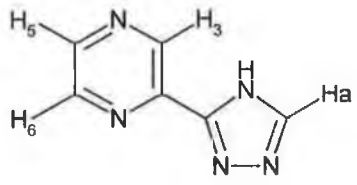

Hpztr

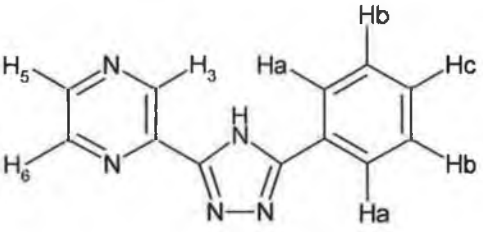

Hphpztr

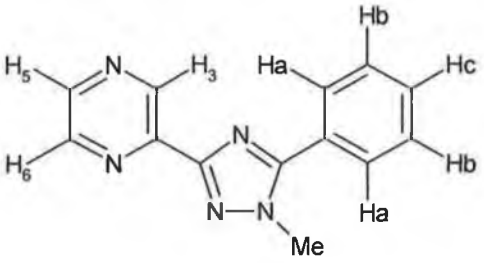

Mephpztr

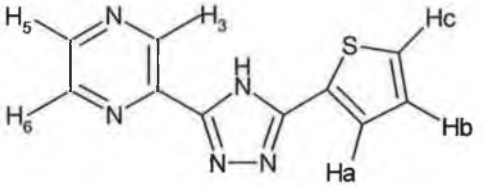

Hthpztr

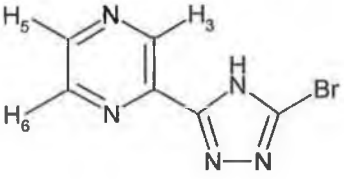

HBrpztr

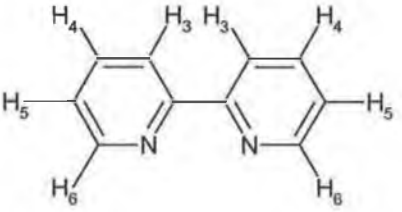

2,2'-bipyridyl

Figure 3. 3 *Structures of ligands discussed in this section. The numbers on the protons describe the numbering system employed in the assignment of ^{1}H NMR peaks.*

Having previously synthesised the series of pyridyl-triazole ligands and complexes discussed in Chapter 2, the synthesis and characterisation of the pyrazine analogues was not expected to provide any major complications. In fact, the spectra of the pyrazyl-triazole compounds were actually more straightforward to assign since they have one proton less. The relevant ^{1}H-NMR data of all the protonated complexes are presented in Table 3. 2. The coordination-induced shifts (c.i.s. = $\delta_{complex}$-δ_{ligand}) are in parentheses. It is seen that the shift upon coordination is similar in all complexes i.e. positive c.i.s. values. Assignments were made with the aid of two dimensional (COSY) spectra. Data for $[Re(CO)_3(bpy)Cl]$ is also included for comparative purposes. A sample COSY spectrum of $[Re(CO)_3(Hthpztr)Cl]$ in d_6-acetone is displayed in Figure 3. 4.

Complex	H_3	H_4	H_5	H_6	H_a	H_b	H_c
$[Re(CO)_3(Hpztr)Cl]$	9.59	—	9.16	9.05	9.53	—	—
	(0.27)	—	(0.45)	(0.35)	(1.03)	—	—
$[Re(CO)_3(Hphpztr)Cl]$	9.65	—	9.16	9.05	8.23	7.66	7.66
		—					
$[Re(CO)_3(Mephpztr)Cl]$	9.60	—	9.11	9.02	7.94	7.75	7.75
	(0.28)	—	(0.45)	(1.12)	(0.05)	(0.06)	(0.06)
$[Re(CO)_3(Hthpztr)Cl]$	9.63	—	9.15	9.01	8.07	8.00	7.43
	(0.26)	—	(0.40)	(0.26)	(0.29)	(0.40)	(0.22)
$[Re(CO)_3(HBrpztr)Cl]$	9.60	—	9.14	9.04	—	—	—
	(0.27)	—	(0.31)	(0.36)	—	—	—
$[Re(CO)_3(bpy)Cl]$	8.72	8.37	7.82	9.12	—	—	—
					—	—	—

Table 3. 2 *^{1}H NMR data for the rhenium tricarbonyl complexes. All data was obtained in d_6-acetone. Values in parenthesis are the coordinated induced shifts relative to the free ligands.*

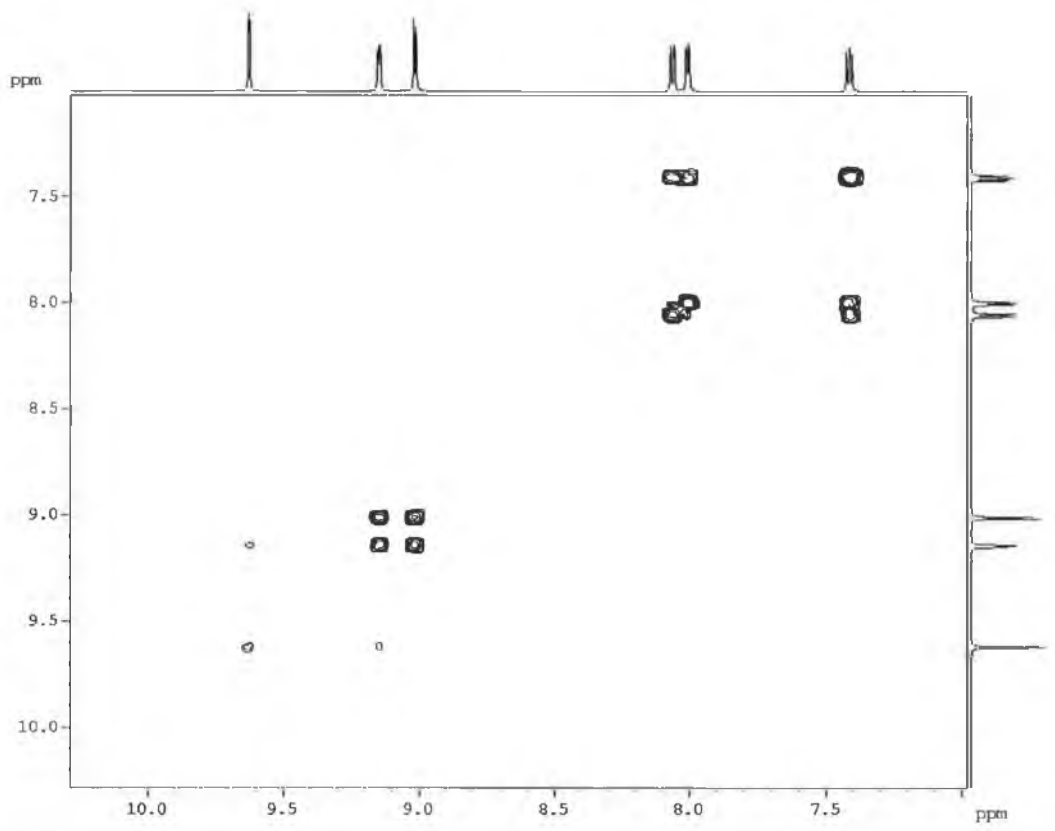

Figure 3. 4 *COSY NMR spectrum of [Re(CO)$_3$(Hthpztr)Cl] in d_6-acetone.*

Figure 3. 5 displays the ^{1}H NMR spectra of the pyrazyl-triazole complexes [Re(CO)$_3$(HBrpztr)Cl] and [Re(CO)$_3$(Hthpztr)Cl]. The spectrum of [Re(CO)$_3$(bpy)Cl] is also included in Figure 3. 5 for comparative purposes. The formation of only one isomer was observed for all of the triazole complexes. The assignment of the pyrazyl-triazole protons was relatively straightforward, as the chemical shifts and coupling constants were compared to those of other pyrazine type complexes.[10,15] The H_3 of the pyrazine ring is weakly coupled to the H_5 proton (J = 1.6 Hz) and is observed at very low field (9.60 — 9.65 ppm). The H_6 proton is more strongly coupled to the H_5 proton (J = 3.2 Hz) and is observed in the range of 9.01 – 9.05 ppm. The splitting pattern of the H_5 is more complicated, as it is coupled with the H_6 proton (J = 3.2 Hz) and with the H_3 proton (J = 1.6

Hz). The H_3, H_5 and H_6 protons are highlighted in Figure 3. 5. Note the absence of a H_4 proton in the pyrazyltriazole complexes compared to $[Re(CO)_3(bpy)Cl]$.

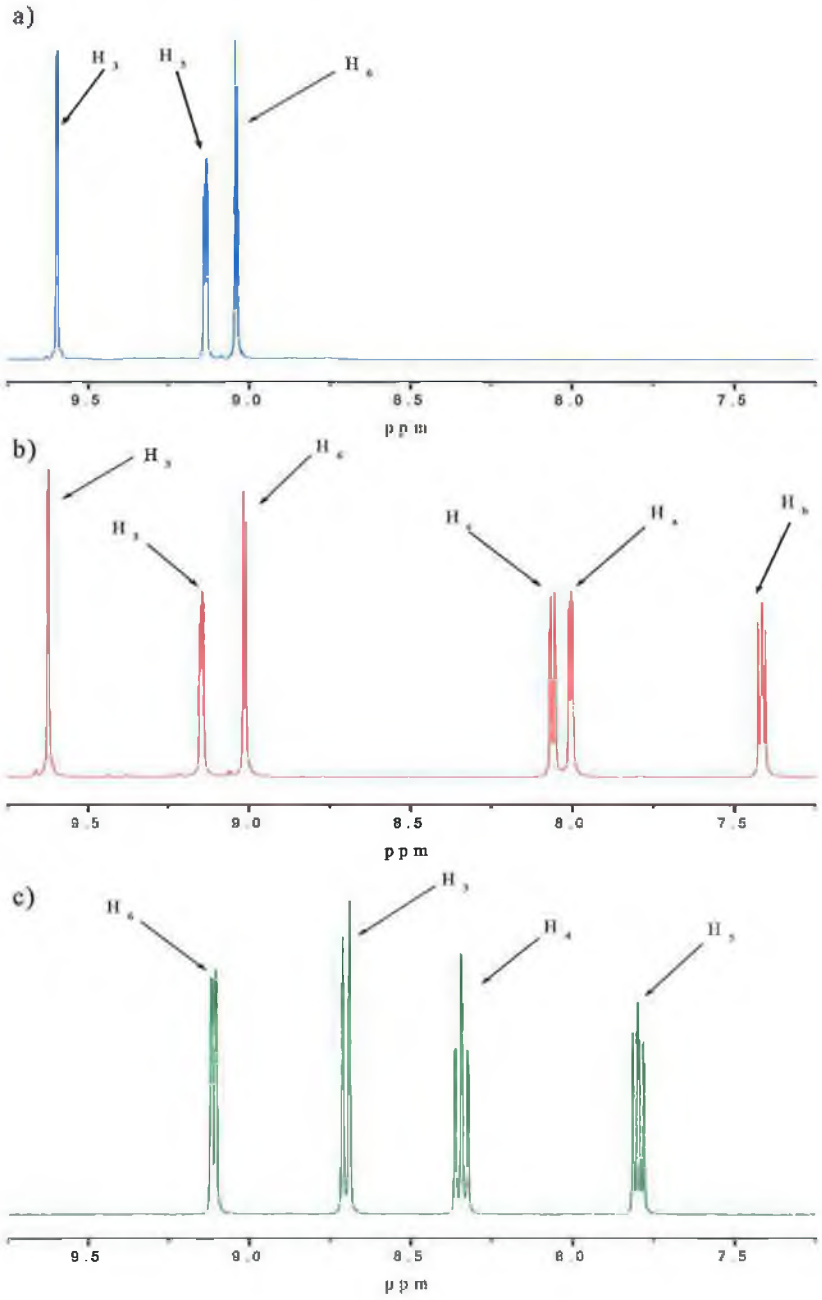

Figure 3. 5 *^1H NMR spectra of $[Re(CO)_3(HBrpztr)Cl]$ (a), $[Re(CO)_3(Hthpztr)Cl]$ (b) and $[Re(CO)_3(bpy)Cl]$ in d_6-acetone.*

The second nitrogen atom in the pyrazine ring clearly influences the resonances of the H_5 and H_3 protons in the pyrazyl-triazole complexes compared to $[Re(CO)_3(bpy)Cl]$ (Figure 3. 5). This nitrogen deshields the H_3 and H_5 protons, hence these protons are shifted downfield relative to $[Re(CO)_3(bpy)Cl]$. This deshielding effect is not experienced as much by H_6. This is a possible explanation for the H_6 protons in the pyrazyl-triazole complexes occurring at similar chemical shift to the H_6 proton in $[Re(CO)_3(bpy)Cl]$.

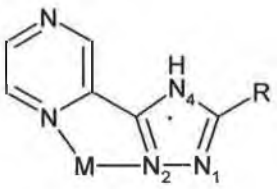

N_2 Isomer

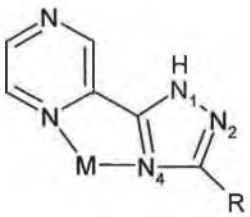

N_4 Isomer

Figure 3. 6 *The two possible modes of coordination of a metal centre to HRpztr.*

Ruthenium polypyridyl complexes coordinated to pyrazyl-triazole ligands can form both N_2 and N_4 coordination isomers (Figure 3. 6).[10,16]. Like the rhenium(I) complexes containing a pyridyl-triazole ligand (Chapter 2), the formation of only one isomer was observed for the pyrazyl-triazole complexes. No suitable crystals were obtained for X-ray structure determination. Unfortunately it is impossible to deduce the exact coordination mode using just ^{1}H-NMR studies. As outlined for the pyridyl-triazole complexes, it seems most likely coordination of the rhenium tricarbonyl unit occurs via the N_2 in the analogous pyrazyl-triazole complexes.

Complex	H_3	H_4	H_5	H_6	H_a	H_b	H_c
$[Re(CO)_3(pztr)Cl]^-$	9.41	—	8.90	8.73	8.34	—	—
	(0.09)	—	(0.19)	(0.03)	(-0.16)	—	—
$[Re(CO)_3(phpztr)Cl]^-$	9.29	—	8.86	8.66	8.23	7.41	7.30
	(-0.06)	—	(-0.06)	(-0.11)	(0.12)	(-0.13)	(-0.19)
$[Re(CO)_3(thpztr)Cl]^-$	9.46	—	8.69	8.90	7.56	7.21	7.67
	(0.09)	—	(-0.06)	(0.15)	(-0.22)	(-0.39)	(+0.46)
$[Re(CO)_3(Brpztr)Cl]^-$	9.33	—	8.84	8.68	—	—	—
	(0.27)	—	(0.01)	(0.00)	—	—	—

Table 3. 3 *^1H NMR data for the deprotonated rhenium tricarbonyl complexes. All spectra were obtained in d_6-Acetone. The complexes were deprotonated by addition of triethylamine. Values in parenthesis are the coordinated induced shifts relative to the free ligands.*

Spectra were also recorded in basic solution, resulting in deprotonation of the triazole unit. A basic solution was obtained by addition of triethylamine to the ^1H NMR sample in d_6-acetone. The spectral data of the pyrazyl-triazole unit obtained in basic solution are summarised in Table 3. 3. No spectral shifts were observed for $[Re(CO)_3(bpy)Cl]$ or $[Re(CO)_3(Mephpztr)Cl]$ in basic solution. Figure 3. 7 shows the ^1H NMR spectrum of $[Re(CO)_3(Hphpztr)]$ compared to $[Re(CO)_3(phpztr)]^-$. The deprotonated complexes were generally found upfield relative to the corresponding protonated complexes.

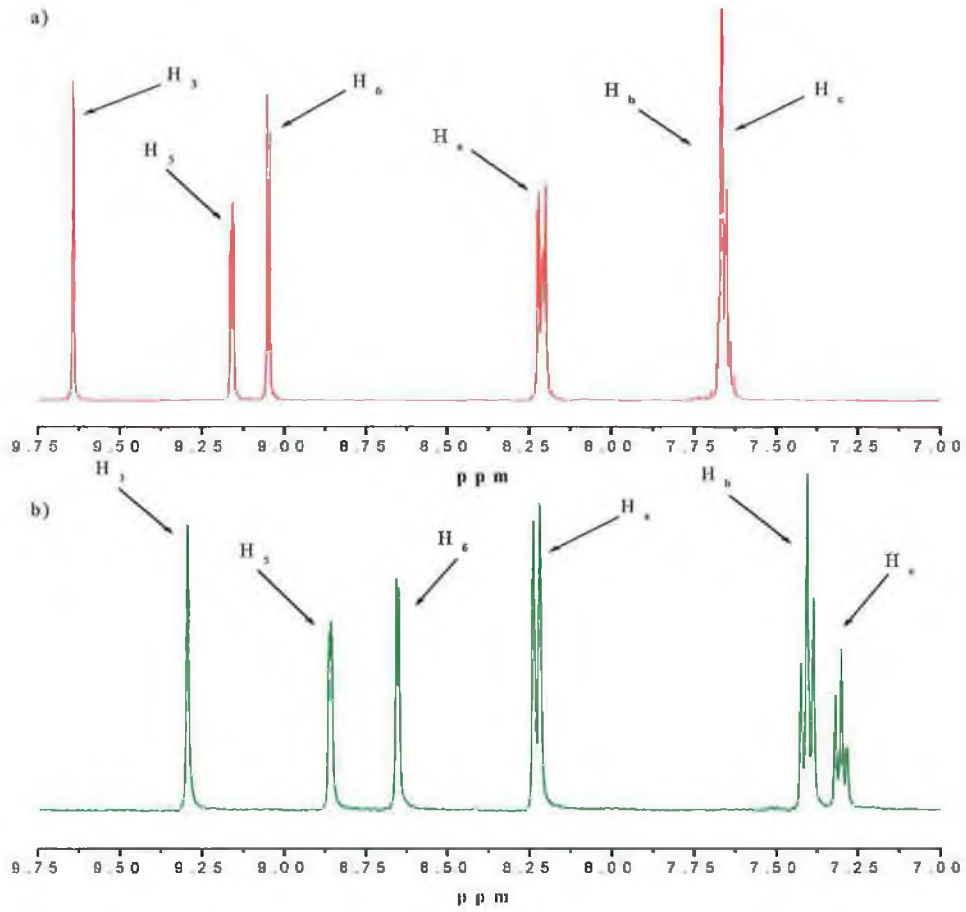

Figure 3. 7 *^1H NMR spectra of (a) $[Re(CO)_3(Hphpztr)Cl]$ and (b) $[Re(CO)_3(phpztr)Cl]^-$.*

In this case the upfield shift in the resonance positions of the pyrazyl-triazole protons (Table 3. 3 and Figure 3. 7) is most likely a consequence of deprotonation of the triazole and resulting transfer of electron density from the negatively charged triazole ring to the π-accepting pyrazine ring. Similar trends were also observed on deprotonation of the triazole ligand in the ruthenium complex $[Ru(bpy)_2(Hpztr)](PF_6)_2$.[7]

3.2.4 Absorption and emission properties

The absorption spectra of the complexes synthesised in this chapter were recorded in dichloromethane at room temperature. Absorption spectra of $[Re(CO)_3(Hphpztr)Cl]$ and $[Re(CO)_3(phpztr)Cl]^-$ compared to $[Re(CO)_3(bpy)Cl]$ are shown in Figure 3. 8. The absorption spectra of $[Re(CO)_3(Hphpztr)Cl]$ and $[Re(CO)_3(phpztr)Cl]^-$ are typical of the pyrazyl-triazole complexes discussed in this section. The absorption maxima are summarised in (Table 3. 4). The low energy absorption bands of the protonated complexes are similar in position and shape to that of $[Re(CO)_3(bpy)Cl]$ (Figure 3. 8) and other rhenium(I) tricarbonyl complexes.[1,17,18,19,20] Hence the low energy absorption bands between 390 and 410 nm can be assigned to metal to ligand charge transfer (MLCT) transitions from the rhenium (d^6) metal orbitals to the unoccupied (π^*) orbitals of the pyrazyl-triazole.

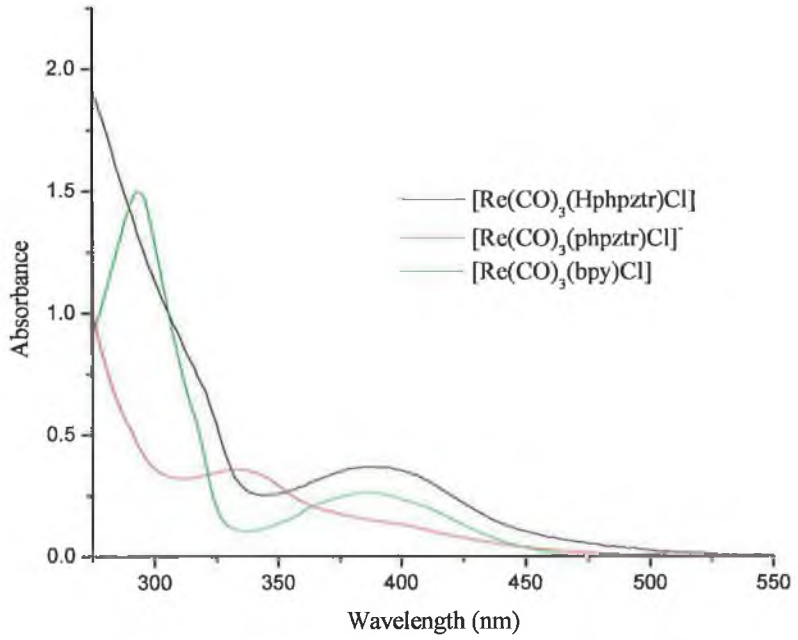

Figure 3. 8 *Absorption spectra of $[Re(CO)_3(Hphpztr)Cl]$, $[Re(CO)_3(phpztr)Cl]^-$ and $[Re(CO)_3(bpy)Cl]$ in dichloromethane at 298 K.*

The rhenium(I) complex $[Re(CO)_3(bpz)Cl]$ (bpz = 2,2'-bipyrazine) has an absorption maximum at 450 nm.[1] As the pyrazyl-triazole ligand contain a pyrazine unit, the absorption maxima of the pyrazyl-triazole complexes are anticipated to occur at similar wavelength to that of $[Re(CO)_3(bpz)Cl]$. This is not the case as the complexes $[Re(CO)_3(Hpztr)Cl]$, $[Re(CO)_3(Hphpztr)Cl]$, $[Re(CO)_3(Hthpztr)Cl]$, $[Re(CO)_3(Mephpztr)Cl]$, and $[Re(CO)_3(HBrpztr)Cl]$ have absorption maxima at 395 nm, 390 nm, 400 nm, 390 nm and 410 nm respectively i.e. the absorption maxima are blue shifted relative to $[Re(CO)_3(bpz)Cl]$. The position of MLCT transitions are governed by both the σ-donor and π-acceptor properties of the ligands coordinated to the metal centre. In the case of the pyrazyl-triazole comples, the strong σ-donor properties of the triazole unit most likely increase the ligand field separation. This results in an increased energy separation between the HOMO and the LUMO of the pyrazyl-triazole complexes compared to $[Re(CO)_3(bpz)Cl]$. Hence the absorption maxima of the pyrazyl-triazole complexes are blue shifted relative to $[Re(CO)_3(bpz)Cl]$.

The MLCT absorption maxima of the deprotonated pyrazyl-triazole complexes are blue shifted compared to $[Re(CO)_3(bpy)Cl]$ and their protonated analogues. For example $[Re(CO)_3(phpztr)Cl]^-$ has an absorption maximum at 337 nm whereas the absorption maxima of $[Re(CO)_3(Hphpztr)Cl]$ and $[Re(CO)_3(bpy)Cl]$ are both observed at 390 nm (see Figure 3. 8). The presence of a negative charge on the triazole raises the energy of the π* (LUMO) level of the pyrazyl-triazole ligand. Therefore the gap between the HOMO and the LUMO increases, thus resulting in a blue shift of the MLCT band compared to the protonated complex. A similar shift in the absorption maxima was observed with protonation/deprotonation of the uncoordinated nitrogen in $[Re(CO)_3(4,4'\text{-bpy})_2Cl]$ (4,4'-bpy = 4,4'-bipyridyl).[21] The MLCT absorption maxima of the protonated/deprotonated complexes are summarised in Table 3. 4. Note there was no change in the absorption spectrum of $[Re(CO)_3(Mephpztr)Cl]$ in basic solution, as an unlabile methyl group rather than a proton is present on the triazole.

Complex	298 K			77 K
	λ_{abs} (nm)[a]/ ($\varepsilon \times 10^3$)	λ_{em} (nm)[a]/ τ(ns)[b]	ϕ [b]	λ_{em}(nm)[b]/ τ(μs)[b]
$[Re(CO)_3(Hpztr)Cl]$	395 (4.1)	—	—	535 (6.93)
$[Re(CO)_3(pztr)Cl]^-$	330 (3.5)	612 (44)	0.0009	535 (8.25)
$[Re(CO)_3(Hphpztr)Cl]$	390 (4.0)	630 (50)	0.0003	545 (4.85)
$[Re(CO)_3(phpztr)Cl]^-$	337 (3.3)	565 (76)	0.0013	550 (5.91)
$[Re(CO)_3(Mephpztr)Cl]$	390 (4.2)	625 (89)	0.0015	540 (9.74)
$[Re(CO)_3(Hthpztr)Cl]$	400 (3.9)	—	—	535 (6.03)
$[Re(CO)_3(thpztr)Cl]^-$	350 (3.1)	610 (69)	0.0016	535 (8.83)
$[Re(CO)_3(HBrpztr)Cl]$	410 (4.4)	—	—	540 (6.30)
$[Re(CO)_3(Brpztr)Cl]^-$	330 (3.4)	610 (71)	0.0006	535 (6.66)
$[Re(CO)_3(bpy)Cl]$	390 (3.7)	600 (54)	0.0058	530 (3.60)

Table 3. 4 *Absorption maxima and luminescence properties of the rhenium complexes. τ refers to the emission lifetime while ϕ denotes the radiative quantum yield. [a]Data in dichloromethane, [b]in deoxygenated dichloromethane, [c]in ethanol/methanol (4:1).*

The absorption maxima of the pyrazyl-triazole complexes (see Table 3. 4) are red shifted relative to the analogous pyridyl-triazole complexes (see Table 2. 4). For instance, $[Re(CO)_3(Hpztr)Cl]$ has an MLCT band maximum at 395 nm whereas $[Re(CO)_3(Hpytr)Cl]$ has an MLCT band maximum at 330 nm. This difference in wavelength is due to the weak π-acceptor properties of the pyridyl-triazole ligands compared to the pyrazyl-triazole ligands. Hence the π^* levels of the pyridyl-triazole complexes are higher in energy compared to the analogous pyrazyl-triazole complexes. This is a factor in the red shift of the MLCT bands of the pyrazyl-triazole complexes compared to the analogous pyridyl-triazole complexes.

$[Re(CO)_3(Hphpztr)Cl]$ was the only protonated complex which emitted in dichloromethane at room temperature. However, upon addition of triethylamine to a dichloromethane solution of the complexes, all of the complexes were found to emit (see Table 3. 4). Note the complex $[Re(CO)_3(Mephpztr)Cl]$ which contains an unlabile methyl group was also found to emit at room temperature. Figure 3. 9 shows the emission spectra of $[Re(CO)_3(Hphpztr)Cl]$, $[Re(CO)_3(phpztr)Cl]^-$ and $[Re(CO)_3(bpy)Cl]$ in dichloromethane at room temperature. Like the absorption spectra of the complexes, protonation/deprotonation of the triazole has a significant effect on the emission properties of the complexes (Figure 3. 9 and Table 3. 4). The emission maximum of $[Re(CO)_3(phpztr)Cl]^-$ was blue shifted compared to $[Re(CO)_3(Hphpztr)Cl]$. There were no changes in the emission spectra of $[Re(CO)_3(Mephpztr)Cl]$ and $[Re(CO)_3(bpy)Cl]$ in the presence of triethylamine.

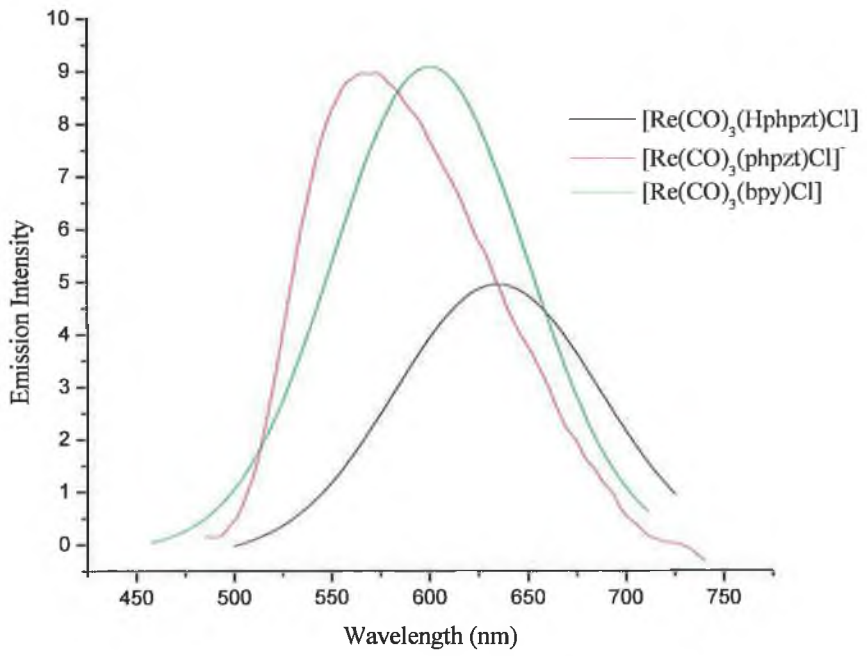

Figure 3. 9 *Emission spectra of $[Re(CO)_3(Hphpztr)Cl]$, $[Re(CO)_3(phpztr)Cl^-]$ and $[Re(CO)_3(bpy)Cl]$ in dichloromethane at 298 K.*

The emission spectra observed for the pyrazyl-triazole complexes were found to be temperature dependent (Table 3. 4). All of the complexes emitted at 77 K yielding broad, structureless emission spectra. As the temperature was lowered from 298 K to 77 K, a significant blue shift of the spectrum was observed. This is associated with a phenomenon known as "rigidochromism". In the alcoholic glass formed at 77 K, the solvent dipoles are immobile on the time scale of the excited state and consequently they cannot respond to the change in electronic configuration between the ground and excited state that accompanies an excitation. The result is an increase in the emission energy, which is confirmed by a blue shift in the emission spectra. Another observation at low temperature is the increase in emission intensity and a longer lifetime of the excited state of the complex i.e. lifetimes in the μs range. At 77 K, the complex and its environment are rigid, making it less susceptible to vibronic coupling to low frequency, high amplitude Re-N vibrations, which contribute to radiationless decay.[22] Solvent interactions, which may contribute to radiationless decay are also considerably reduced in the frozen matrix. The emission spectra of $[Re(CO)_3(Hphpztr)Cl]$, $[Re(CO)_3(phpztr)Cl]^-$ and $[Re(CO)_3(bpy)Cl]$ at 77 K are shown in Figure 3. 10. Emission maxima of the deprotonated complexes were found to blue shift by ~ 5 nm compared to their protonated derivatives. The emission spectra of both the protonated and deprotonated complexes show a red shift in the emission maxima compared to $[Re(CO)_3(bpy)Cl]$ at 77 K.

For all of the emitting complexes listed in Table 3. 4, the emitting level can be labelled as ^{3}MLCT in character according to the following considerations:

i) The position and shape of the emission band is consistent with that previously reported for similar complexes assigned as ^{3}MLCT emitters.[5,,23]

ii) There is a blue shift in the emission band on cooling from 298 K to 77 K.[24]

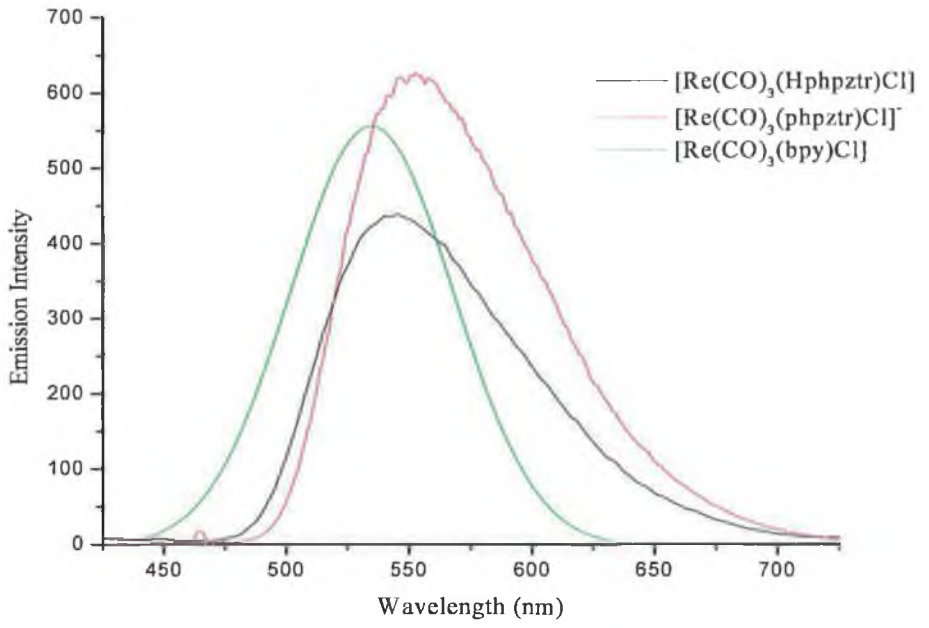

Figure 3. 10 *Emission spectra of [Re(CO)$_3$(Hphpztr)Cl], [Re(CO)$_3$(phpztr)Cl]$^-$ and [Re(CO)$_3$(bpy)Cl] are in ethanol:methanol (4:1) at 77 K. The emission spectrum of [Re(CO)$_3$(phpztr)Cl]$^-$ was recorded in the presence of triethylamine.*

Lifetimes and quantum yields were also obtained at 298 K in deoxygenated dichloromethane. The results are collated in Table 3. 4. The lifetime of 54 ns and the quantum yield of 0.005 obtained at 298 K for [Re(CO)$_3$(bpy)Cl] is comparable with the previous values of 51 ns and 0.005 obtained by Caspar and Meyer.[23] The lifetimes of the emissive pyrazyl-triazole complexes are similar to that of [Re(CO)$_3$(bpy)Cl] at 298 K (see Table 3. 4). In addition, lower quantum yield values were obtained for the pyrazyl-triazole complexes compared to [Re(CO)$_3$(bpy)Cl], indicating that the emission efficiencies of these complexes are less than that of [Re(CO)$_3$(bpy)Cl]. The lifetime of MLCT excited states of rhenium(I) polypyridyl complexes in fluid solution are expected to be dominated by non-radiative processes.[25,26,27] The energy gap law predicts that the non-

radiative decay rate for rhenium(I) polypyridyl complexes should decay exponentially with the increasing difference in energy between the emitting and ground-state levels.[23,28,29] The energy gap law may be applied to explain the low quantum yields and short lifetimes of the pyrazyl-triazole complexes.

No emission was detected from $[Re(CO)_3(Hpztr)Cl]$, $[Re(CO)_3(Hthpztr)Cl]$ and $[Re(CO)_3(HBrpztr)Cl]$ at 298 K, whereas the deprotonated derivatives of these complexes were found to emit. The lack of emission from $[Re(CO)_3(Hpztr)Cl]$, $[Re(CO)_3(Hthpztr)Cl]$ and $[Re(CO)_3(HBrpztr)Cl]$ at 298 K is most likely a result of population of non-radiative decay paths. Previous studies by Worl and coworkers for a series of $[Re(CO)_3(4,4'\text{-}X_2\text{-}bpy)Cl]$ complexes (X = NEt_2, NH_2, $NHCOCH_3$, OCH_3, CH_3, H, Cl, Ph, CO_2Et, and NO_2) found the lowest energy MLCT transition for these complexes involves the filled d_π orbitals and the empty bpy π^* orbitals, which are mixed by a back-bonding interaction.[30] When the energy gap between these orbitals was small, there was significant back-bonding between them, resulting in enhanced orbital mixing and increased non-radiative decay paths i.e. longer non-radiative decay constants. The IR spectra of the protonated pyrazyl-triazole complexes (see Section 3.2.2) indicated a stronger back-bonding interaction between the d_π orbitals of rhenium and the pyrazyl-triazole π^* orbitals compared to $[Re(CO)_3(bpy)Cl]$. This enhanced coupling between the d_π and π^* orbitals most likely increases the non-radiative decay paths of the protonated pyrazyl-triazole complexes compared to $[Re(CO)_3(bpy)Cl]$. Hence $[Re(CO)_3(Hphpztr)Cl]$ and $[Re(CO)_3(Mephpztr)Cl]$ are weakly emissive while no emission was detected from $[Re(CO)_3(Hpztr)Cl]$, $[Re(CO)_3(Hthpztr)Cl]$ or $[Re(CO)_3(HBrpztr)Cl]$. On the other hand, deprotonation of the triazole ligand was found to reduce the back-bonding interaction between the rhenium metal centre and the triazole ligand (Section 3.2.2). This reduction in the $Re\rightarrow\pi^*$ back bonding most likely reduces the electronic coupling between the excited and ground states, thus reducing the non-radiative decay paths. Hence emission was detected from all of the deprotonated complexes. This reduced coupling between the excited and ground-state can also explain the longer lifetime observed for $[Re(CO)_3(phpztr)Cl]^-$ compared to $[Re(CO)_3(Hphpztr)Cl]$.

At 77 K, the lifetimes of all of the pyrazyl-triazole complexes were longer compared to $[Re(CO)_3(bpy)Cl]$. For example lifetimes of 4.85 μs, 5.91 μs and 3.60 μs were obtained for $[Re(CO)_3(Hphpztr)Cl]$, $[Re(CO)_3(phpztr)Cl]^-$ and $[Re(CO)_3(bpy)Cl]$ at 77 K. Since the emission maxima of the pyrazyl-triazole complexes are red shifted compared to $[Re(CO)_3(bpy)Cl]$, the rate of non radiative decay for the pyrazyl-triazole is expected to increase according to the energy gap law i.e. shorter lifetimes compared to $[Re(CO)_3(bpy)Cl]$ are anticipated.

Differences were observed in the emission properties of the pyrazyl-triazole complexes (see Table 3. 4) compared to the corresponding pyridyl-triazole complexes (see Table 2. 4). For example $[Re(CO)_3(Hphpztr)Cl]$ was the only emissive protonated pyrazyl-triazole complex at room temperature, whereas emission was detected from all of the protonated pyridyl-triazole complexes at room temperature. The room temperature emission spectra showed a red shift from 552 nm for $[Re(CO)_3(Hphpytr)Cl]$ to 625 nm for $[Re(CO)_3(Hphpztr)Cl]$. A decrease in the emission lifetimes from 101 ns in $[Re(CO)_3(Hphpytr)Cl]$ to 50 ns in $[Re(CO)_3(Hphpztr)Cl]$ was also observed. In addition the emission maximum of $[Re(CO)_3(Mephpztr)Cl]$ is red shifted by 88 nm relative to $[Re(CO)_3(Mephpytr)Cl]$. The red shift in the emission maximum of $[Re(CO)_3(Mephpztr)Cl]$ compared to $[Re(CO)_3(Mephpytr)Cl]$ is also accompanied by a decrease in the emission lifetimes from 735 ns to 89 ns. A red shift in the emission maxima of the deprotonated pyrazyl-triazole complexes compared to the analogous deprotonated pyridyl-triazole complexes was also observed. For instance, the pyridyl-triazole complex $[Re(CO)_3(pytr)Cl]^-$ has an emission maximum at 516 nm whereas the pyrazyl-triazole complex $[Re(CO)_3(pztr)Cl]^-$ has an emission maximum at 612 nm. A decrease in the emission lifetimes of the deprotonated pyrazyl-triazole complexes compared to the corresponding pyridyl-triazole complexes was also observed. For example a decrease in the emission lifetime from 159 ns to 76 ns was observed for $[Re(CO)_3(phpytr)Cl]^-$ compared to $[Re(CO)_3(phpztr)Cl]^-$. At 77 K, emission was detected from all of the pyrazyl- and pyridyl-triazole complexes. Similarly at 77 K, a red shift in the emission maximum along with a decrease in the emission

lifetime was observed for the pyrazyl-triazole complexes compared to the corresponding pyridyl-triazole complexes. At 77 K, $[Re(CO)_3(Hpztr)Cl]$ has a emission maximum of 535 nm and decays with a lifetime of 6.93 μs while the pyridyl-triazole complex $[Re(CO)_3(Hpytr)Cl]$ has an emission maximum of 493 nm and a lifetime of 8.97 μs.

The red shift in the emission maxima of both the protonated and deprotonated pyrazyl-triazole complexes relative to the analogous pyridyl-triazole complexes can be attributed to the strong π-acceptor properties of pyrazine relative to pyridine. As a consequence the energy gap between the ^{3}MLCT and ground electronic state of the pyrazyl-triazole complexes is smaller compared to the pyridyl-triazole complexes. Hence the emission maxima of the pyrazyl-triazole complexes are red shifted relative to the analogous pyridyl-triazole complexes. A similar red shift in the emission maximum was observed for $[Re(CO)_3(bpz)Cl]$ compared to $[Re(CO)_3(bpy)Cl]$.[1] Note, $[Re(CO)_3(bpy)Cl]$ has an emission maximum of 600 nm while $[Re(CO)_3(bpz)Cl]$ has an emission maximum of 750 nm. The red shift in the emission maximum of $[Re(CO)_3(bpz)Cl]$ compared to $[Re(CO)_3(bpy)Cl]$ was attributed to the stronger π acceptor properties of 2,2'-bipyrazine compared to 2,2'-bipyridine which subsequently results in a smaller energy gap between the ^{3}MLCT state and the ground electronic state.

As previously discussed, the lifetimes of ^{3}MLCT states are dependent on the "energy gap law" and the energy gap between the ^{3}MLCT and ^{3}MC states. The red shift in the emission maxima of pyrazyl-triazole compared to the corresponding pyridyl-triazole complexes indicates that there is a smaller energy gap between the ground and the emissive electronic states. This decrease in the energy gap may result in increased coupling between the ground- and the excited-state levels of the pyrazyl-triazole complexes i.e. increasing the nonradiative decay pathways. In addition, pyrazyl-triazole ligands are weaker σ-donors than pyridyl-triazole ligands. The effect of a weaker σ-donor ligand is to reduce the ligand field splitting in a metal complex; this results in a decrease in the energy gap between the ^{3}MLCT and ^{3}MC states. Hence the ^{3}MC states are populated

more efficiently i.e. a decrease in the luminescence lifetime is observed for the pyrazyl-triazole complexes. Decreases in the energy gap between ^{3}MLCT and ^{3}MC states have accounted for shorter lifetimes in ruthenium(II) terpyridine complexes. Duati and co-workers postulated that the increase in the luminescence lifetime of [Ru(tpy)(L1N$_2$N$_2$)] (where tpy = 2,2';6',2''-terpyridine and L1N$_2$N$_2$ = 2,6-bis([1,2,4]triazol-3-yl)pyridine) compared to $[Ru(tpy)_2]^{2+}$ is rationalised by an increase in the ^{3}MLCT-^{3}MC gap and a subsequent decrease in the nonradiative relaxation rate due to the enhanced σ-donor properties of 2,2';6',2''-terpyridine compared to 2,6-bis([1,2,4]triazol-3-yl)pyridine.[31] As previously discussed, the lack of emission from [Re(CO)$_3$(Hpztr)Cl], [Re(CO)$_3$(Hthpztr)Cl] and [Re(CO)$_3$(HBrpztr)Cl] at 298 K is most likely a result of population of non-radiative decay paths. The red shift in the emission maxima of the pyrazyl-triazole complexes relative to the corresponding pyridyl-triazole complexes at 77 K indicates that the ground and the emissive electronic states energy gap is smaller for the pyrazyl-triazole complexes. The smaller energy gap increases the non-radiative decay paths. Pyrazyl-triazole ligands are considered weaker σ-donor ligands than pyridyl-triazole ligands. Hence the ^{3}MLCT-^{3}MC gap is smaller for the pyrazyl-triazole complexes i.e. the ^{3}MC non-radiative decay states are populated more efficiently. The smaller energy gap between the ground and the emissive electronic states along with the reduced ^{3}MLCT — ^{3}MC energy gaps enhance the non-radiative decay paths in [Re(CO)$_3$(Hpztr)Cl], [Re(CO)$_3$(Hthpztr)Cl] and [Re(CO)$_3$(HBrpztr)Cl] compared to the corresponding pyridyl-triazole complexes. Hence no emission was detected from [Re(CO)$_3$(Hpztr)Cl], [Re(CO)$_3$(Hthpztr)Cl] and [Re(CO)$_3$(HBrpztr)Cl] at 298 K.

3.2.5 Ground-state and excited state pK_a measurements

The protonation and deprotonation of the pyrazyl-triazole ligand alters its σ donor and π acceptor properties. This is evident from the absorption and emission maxima (see Table 3. 4). By investigating the acid-base behaviour of this type of rhenium(I) complex, important information about its electronic state properties can be obtained. The ground state behaviour tends to be a measure of the amount of electron donation from the ligand to the metal, while the excited state measurements can give information about the nature of the emitting state. Upon coordination to the rhenium metal centre, the acidity of the triazole proton in the ground state increases considerably, which is generally explained by σ donation from the ligand to the metal centre.

Figure 3. 11 is a typical example of the acid-base chemistry of the rhenium(I) complexes containing a pyrazyl-triazole ligand. All the spectroscopic changes of the complexes are reversible in the pH range 1-10. The absorption titrations are performed by adjusting the pH of a solution of the complex in Britton Robinson buffer. pH adjustments were made by adding 75 μl of 2 M NaOH or 2 M H_2SO_4 to a 100 ml volume of the dissolved complex. By monitoring the spectral changes, at a wavelength where there is considerable change as a function of pH, a graphical analysis was carried out by plotting absorbance against pH. The pK_a was determined from the point of inflection of the curve. The pK_a obtained represents the pK_a of the triazole ring. In all titrations there is a blue shift of the MLCT band as the pH is increased due to the resultant increase in the HOMO-LUMO gap

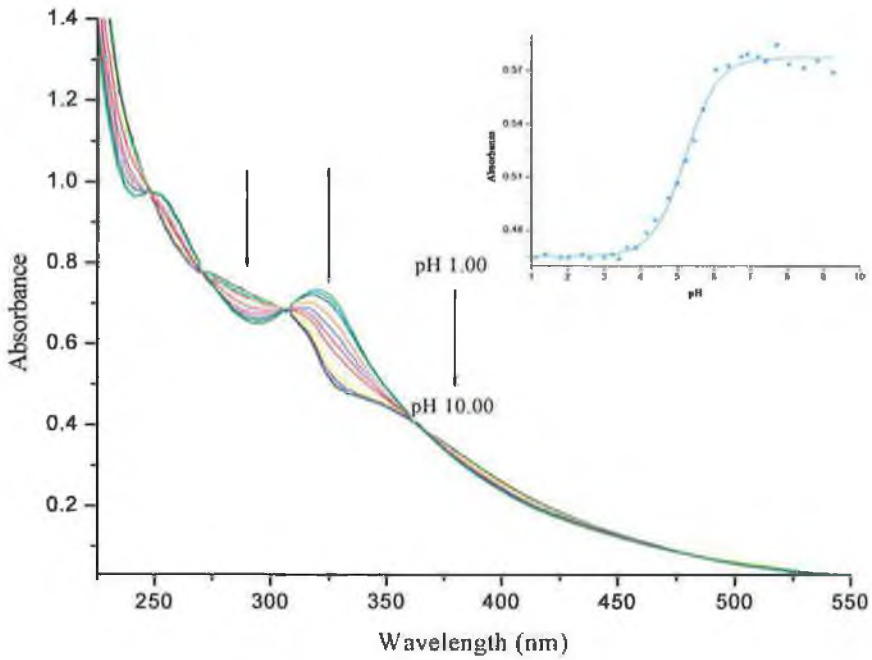

Figure 3. 11 *pH dependence of the absorption spectra of [Re(CO)$_3$(Hpztr)Cl] in Britton-Robinson buffer. Inset, shows a plot of absorbance at 350 nm versus increasing pH.*

Complex	pK_a	pH_i*	pK_a* (1)	pK_a* (2)
[Re(CO)$_3$(Hpztr)Cl]	5.2	—	—	—
[Re(CO)$_3$(Hphpztr)Cl]	5.2	5.8	5.7	5.9
[Re(CO)$_3$(Hthpztr)Cl]	4.1	7.8	7.6	—
[Re(CO)$_3$(HBrpztr)Cl]	2.4	4.3	4.3	3.5

Table 3. 5 *Ground-state and excited-state pK_a values for the rhenium tricarbonyl complexes. The pK_a* (1) values were obtained using Equation 3. 2 and the pK_a* (2) values were calculated using Equation 3. 3.*

The pK_a values for the complexes are summarised in *Table 3. 5*. In every case the acid/base behaviour observed can be explained by protonation/deprotonation of the triazole moiety as indicated in Equation 3.1.

$$[Re(CO)_3(Htr)Cl] \leftrightarrow [Re(CO)_3(tr)Cl]^- + H^+ \qquad \textbf{3. 1}$$

By examination of Table 3. 5, it can be seen that the acidity of the coordinated triazole ring is strongly dependent on the nature of the non-coordinated substituent in the C_5 position of the 1,2,4-triazole. The effect of the introduction of an electron withdrawing bromine group or thiophene ring is particularly relevant. A comparison of the pK_a value of $[Re(CO)_3(Hpztr)Cl]$ with those of $[Re(CO)_3(HBrpztr)Cl]$ and $[Re(CO)_3(Hthpztr)Cl]$ shows that the pK_a value of the triazole ring increases by 1.1 pH units in the presence of a thiophene ring, while an increase of 2.8 pH units is observed with a bromine substituent. This observed increase in acidity in the presence of a thiophene or bromine substituent can be attributed to a reduction in the electron density on the 1,2,4-triazole in the presence of an electron withdrawing substituent. A pK_a value of 3.7 was obtained for $[Ru(bpy)_2(Hpztr)]^{2+}$, while a pK_a value of 1.4 was obtained for $[Ru(bpy)_2(HBrpztr)]^{2+}$.[10,32] The observed difference in pK_a values for these ruthenium(II) bipyridyl complexes was also attributed to a reduction in electron density on the triazole ring in the presence of an electron withdrawing bromine substituent. Analysis of the pK_a values observed for $[Re(CO)_3(Hpztr)Cl]$ and $[Re(CO)_3(Hphpztr)Cl]$, shows that the effect of the introduction of a phenyl ring is far less dramatic and does not result in any change in the pK_a value.

The emission of the pyrazyl-triazole complexes was weak in aqueous solution. $[Re(CO)_3(Hpztr)Cl]$ did not emit in neutral, acidic or basic conditions while $[Re(CO)_3(Hthpztr)Cl]$ only emitted when deprotonated. Figure 3. 12 shows the pH dependence of the emission spectra of $[Re(CO)_3(HBrpztr)Cl]$, which is a typical example of the the rhenium(I) complexes containing a pyrazyl-triazole ligand.. The spectra were obtained by exciting the complex at 325 nm, which is an isosbestic point in the pH dependent absorbance spectrum. At pH 1, λ_{max} is at

642 nm. The λ_{max} shifts to 623 nm with increasing pH while the emission intensity was found to increase with increasing pH. A plot of emission (monitored at 642 nm) against pH results in a curve (inset of Figure 3. 12) which allows pH_i^* to be determined. The excited-state pK_a values (pH_i^*) obtained from the emission titration plots are not reliable, as they need to be corrected for the liftimes of the protonated and deprotonated species using Equation 3. 2:

$$pK_a^* = pH_i^* + \log(\tau_a/\tau_b) \qquad \textbf{3. 2}$$

The pK_a^* values for $[Re(CO)_3(Hphpztr)Cl]$ and $[Re(CO)_3(HBrpztr)]$ were also calculated using Försters equation, as given in Equation 3. 3:

$$pK_a^* = pK_a + \{0.625(\nu_b-\nu_a)/T\} \qquad \textbf{3. 3}$$

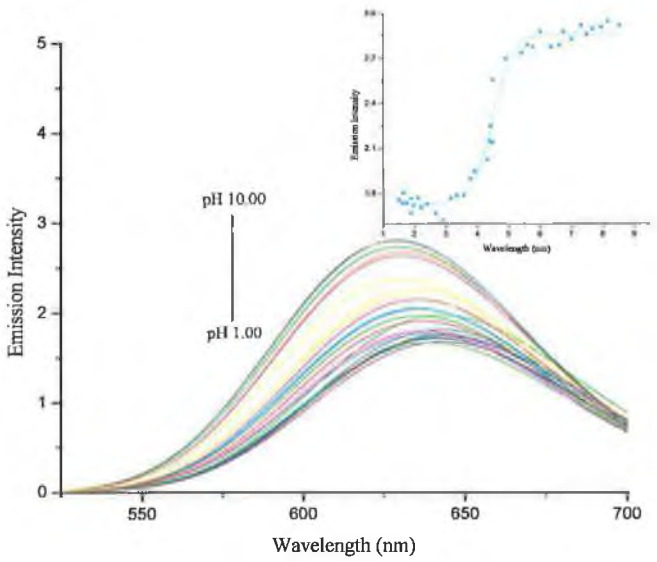

Figure 3. 12 *Excited state pK_a titration (pH1 – pH10) of $[Re(CO)_3(HBrpztr)Cl]$ in Britton Robinson buffer. Inset – Plot of emission intensity at 642 nm versus increasing pH.*

The pKa* values are presented in Table 3. 5. Although there are differences between the calculated excited-state pK_a values of the complexes using Equation 3. 2 and Equation 3. 3, the general trend for the coordinated pyrazyl-triazole complexes is that they are more basic in the excited state than in the ground-state (i.e. $pK_a^* > pK_a$). This is an interesting result as it shows the electron resides on the pyrazyl-triazole ligand after excitation of the complex. After excitation, the electron-rich pyrazyl-triazole (i.e an electron resides on the pyrazine) can bind a proton much easier than in the ground-state, and is therefore more basic. Similar trends have been observed for ruthenium bipyridyl complexes containing pyrazyl-triazole ligands.[10,33]

3.2.6 Electrochemistry

Cyclic voltammetry was used to study the redox properties of the rhenium complexes. Just as the change from a pyridine to a pyrazine was evident from spectroscopic studies, so too were the effects of the pyrazine visible from electrochemical studies on the series of complexes presented here. The cyclic voltammetry of the complexes in acetonitrile presents one oxidation and two reduction processes, which are all irreversible. *Table 3. 6* summarises the redox potentials for the pyrazyl-triazole complexes. All values have been corrected using the redox potential of ferrocene under the same experimental conditions as a secondary reference. *Figure 3. 13* shows a CV of $[Re(CO)_3(Hphpztr)Cl]$. The CV of $[Re(CO)_3(Hphpztr)Cl]$ is typical of the pyrazyl-triazole complexes.

Complex	E (V)		
	Re (I)/(II)	Reduction	
$[Re(CO)_3(Hpztr)Cl]$	1.64[a]	-0.87[b]	-1.28[b]
$[Re(CO)_3(Hphpztr)Cl]$	1.60[a]	-1.05[b]	-1.42[b]
$[Re(CO)_3(Mephpztr)Cl]$	1.60[a]	-0.96[b]	-1.46[b]
$[Re(CO)_3(Hthpztr)Cl]$	1.70[a]	-0.83[b]	-1.33[b]
$[Re(CO)_3(HBrpztr)Cl]$	1.69[a]	-0.72[b]	-1.26[b]
$[Re(CO)_3(bpy)Cl]$	1.55[a]	-1.29[b]	-1.73[b]

Table 3. 6 *Electrochemical data (v's Fc/Fc^+) in acetonitrile with 0.1 M $TBABF_4$ at 100 mV/s scan rate. [a]Anodic peak potential corresponding to an irreversible step. [b]Cathodic peak potential corresponding to an irreversible step.*

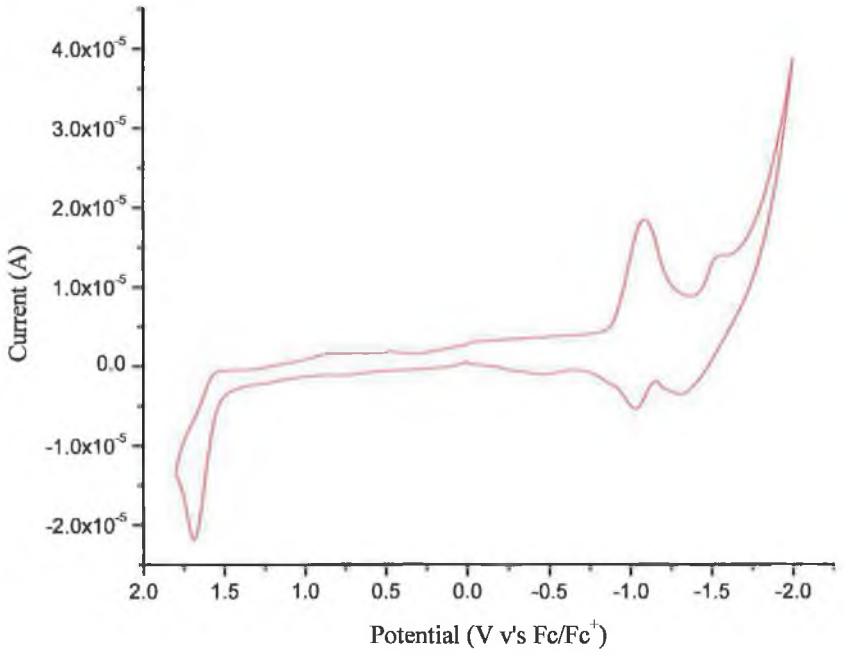

Figure 3. 13 *Cyclic voltammogram of the oxidation of [Re(CO)$_3$(Hphpztr)Cl] in 0.1 M TBABF$_4$ in acetonitrile with a scan rate of 100 mV/s.*

An electrochemically ireversible oxidation was observed near 1.65 V for the pyrazyl-triazole complexes. This has been assigned to oxidation of the rhenium(I) centre. Typically an increase of approximately 100-150mV in the oxidation potential is observed on going from [Re(CO)$_3$(bpy)Cl] to the pyrazyl-triazole complexes. The higher oxidation potentials are an indication that the metal ion has less electron density, which is most likely caused by the strong π-accepting pyrazyl-triazole ligands. The pyrazyl-triazole ligands exhibit a more positive Re(I)/(II) oxidation potential than their pyridine analogues (see Table 2. 6). For example, oxidation of the rhenium(I) metal centre is observed at 1.44 V for [Re(CO)$_3$(Hpytr)Cl] whereas oxidation of the rhenium(I) metal centre is observed at 1.64 V for [Re(CO)$_3$(Hpztr)Cl]. This is due mainly to the weaker σ-

donor/stronger π-acceptor properties of the pyrazine over the pyridine ligand, which reduces the relative electron density on the rhenium(I) metal centre.[34] A similar trend was observed for ruthenium bipyridyl complexes containing triazole ligands.[7,10,35] For example, oxidation of the ruthenium metal centre in $[Ru(bpy)_2(Hpztr)]^{2+}$ was observed at 1.30 V compared to $[Ru(bpy)_2(Hpytr)]^{2+}$ where oxidation of the ruthenium metal centre was observed at 1.20 V.

The first reduction of the pyrazyl-triazole complexes is irreversible with $i_c/i_a > 1$. The reduction is assigned to the coordinated pyrazyl-triazole ligand (Equation 3. 4) and is comparable with $[Ru(bpy)_2(Hpztr)]^{2+}$ and other ruthenium complexes containing pyrazyl-triazole ligands.[7,10] The reduction potentials of the pyrazyl-triazole ligands are observed at less negative potential than that of 2,2-bipyridyl (see Table 3. 6). For example reduction of $[Re(CO)_3(Hpztr)Cl]$ at –0.87 V compared to reduction of $[Re(CO)_3(bpy)Cl]$ at –1.29 V is consistent with the stronger π-accepting ability of the pyrazyl-triazole ligands compared to 2,2'-bipyridyl.

$$[Re(CO)_3(\text{pyrazyl-triazole})Cl] + e^- \rightarrow [Re(CO)_3(\text{pyrazyl-triazole}^{\bullet-})Cl] \qquad \textbf{3. 4}$$

The second reduction at more negative potential is also irreversible. It is assigned to an electrochemical process involving chloride dissociation and follows the trends observed for other rhenium(I) polypyridyl complexes.[36,37]

3.3 Conclusions

A range of pyrazyl-triazole ligands and their rhenium complexes have been successfully prepared and characterised. Yields were comparable to those obtained for the pyridyl-triazole analogues. The complexes were characterised by a variety of means: elemental analysis, IR spectroscopy and ^1H NMR spectroscopy. ^1H NMR spectroscopy again illustrated the change in chemical shift caused by complexation with the metal. Typical pyrazine signals were obtained, with long range coupling evident.

UV/Vis spectra displayed all the typical elements of rhenium polypyridyl complexes. MLCT bands in the region of 400 nm are observed in the spectra. These are red shifted with respect to the pyridine complexes due to the increase in the π-acceptor nature of the pyrazine. This was also apparent in the emission spectra of the complexes. As before, deprotonation of the triazole resulted in these values shifting as a direct consequence of the increase in the triazole's σ-donor nature. Ground and excited state pK_a measurements indicated that the excited state is based on the pyrazine ligand in all cases.

The lack of emission detected from $[Re(CO)_3(Hpztr)Cl]$, $[Re(CO)_3(Hthpztr)Cl]$ and $[Re(CO)_3(HBrpztr)Cl]$ at 298 K was most likely a result of population of non-radiative decay paths due to the strong back bonding interaction between the d_π orbitals of rhenium and the pyrazyl-triazole π* orbitals. The observed emission from the deprotonated derivatives of the pyrazyl-triazole complexes was explained in terms of the reduction in the Re→π* back bonding which most likely reduces the electronic coupling between the excited and ground states, thus reducing the non-radiative decay paths. At 77 K, the deprotonated complexes showed longer lifetimes for the ^{3}MLCT when compared to $[Re(CO)_3(bpy)Cl]$ and their protonated analogues.

As for the electrochemical behaviour of the complexes, it is important to emphasise the following points:

(i) The metal centred oxidation potential increased moving from bpy to the pyrazyl-triazole ligand, which is expected because pyrazine is a better π acceptor than bpy.

(ii) The pyrazyl-triazole ligands exhibit a more positive Re(I)/(II) oxidation potential than their pyridine analogues which is due mainly to the weaker σ-donor/stronger π-acceptor properties of pyrazine over pyridine.

(iii) The first reduction potentials of the complexes correlate well with the first of $[Ru(bpy)_2pztr]^{2+}$ and they can be assigned to reduction of coordinated pyrazyl-triazole ligands.

A more complete discussion of the electrochemical properties of the pyrazyl-triazole ligands cannot be done because the reduction waves are irreversible under the experimental conditions.

3.4 Experimental

The ligands were prepared according to literature methods.[10,38,39]

3.4.1 Preparation of the Ligands

3-(pyrazin-2-yl)-1,2,4-triazole (Hpztr)[10]

20 cm^3 of ethanol was added to a mixture of (5.0 g; 48 mmol) of molten 2-cyanopyrazine and an equimolar amount of hydrazine hydrate (2.40 g, 48 mmol). The solution was stirred at room temperature for 1 hour. Yellow crystals of 2-pyrazylamidrazone were collected by filtration. The pyrazylamidrazone (14 g; 100 mmol) was dissolved in a 10 fold excess of cold formic acid at temperatures below 10 ^{0}C. The mixture was stirred for 3 hours at room temperature. After subsequent heating to dryness at 120 ^{0}C the ligand precipitated. The ligand was recrystallised from hot ethanol. Yield: 3.38 g, 43 mmol, 48 %. ^{1}H NMR (d_6-DMSO), δ in ppm: H_3: 9.46 ppm (d); H_5: 8.70 ppm (dd; H_6: 8.66 ppm (d); H_a: 8.25 ppm (s).

3-(pyrazin-2-yl)-5-phenyl-1,2,4-triazole (Hphpztr) [39]

Hydrazine hydrate (2.37g, 47 mmol) was slowly added to a solution of 2-cyanopyrazine (5 g, 47 mmol) in 20 cm^3 of ethanol. The reaction mixture was gently heated to 40 °C . After the formation of a yellow solution the heat was turned off and the reaction was left stirring overnight. The pyrazylamidrazone (yellow precipitate) was filtered under vacuum and washed with ethanol. Benzoyl chloride (6.60g, 47 mmol) was added dropwise to a stirred solution of 4 cm^3 of triethylamine and an equimolar amount of the pyrazylamidrazone in 20 cm^3 of dry THF. The yellow suspension was stirred for three hours at room temperature. The yellow crystals were filtered under vacuum and left to dry overnight. The crystals were dissolved in ethylene glycol and refluxed for three hours. The ethylene glycol solution was allowed cool to room temperature. 10 cm^3 of cold water was added to the solution to aid precipitation. The white triazole ligand precipitated overnight and was collected under vacuum. The product was recrystallised ethanol to yield a fine white powder. Yield: 7.14 g, (68 %, 32 mmol). ^{1}H NMR (d_6-Acetone), δ in ppm: H_3: 9.35 (d); H_5: 8.80 (dd); H_6: 8.77 (d); H_a: 8.11 (d); H_b: 7.51 (dd); H_c: 7.49 (dd).

1-methyl-3-(pyrazin-2-yl)-5-phenyl-1,2,4-triazole (Mephpztr)

This ligand was prepared in a similar manner to that described previously for Hphpztr, only in this case methylhydrazine was used instead of hydrazine to react with 2-cyanopyrazine. Yield 4.74 g, 20 mmol, 31 %. Elemental analysis for $C_{14}H_{12}N_4$: Calculated C, 71.19; H, 5.08; N, 23.73. Found C, 71.48; H, 4.99; N, 23.55. ^{1}H NMR (d_6-acetone), δ in ppm: H_3: 8.18 (d); H_5: 7.42 (m); H_6: 8.68 (d); H_a: 7.89 (d); H_b: 7.58 (dd); H_c: 7.58 (dd) Me: 3.58 (s).

3-(pyrazin-2-yl)-5-thiophen-2-yl-1,2,4-triazole (Hthpztr)

As for Hphpztr except: 6.89 g (47 mmol) of 2-thiophene-acid chloride was used in place of the benzoyl chloride. Yield 6.67 g (29 mmol, 62 %). ^{1}H NMR (d_6-DMSO), δ in ppm: H_3: 9.29 (d); H_5: 8.77 (m); H_6: 8.76 (dd,); H_a: 7.74 (d); H_b: 7.69 (d); H_c: 7.21 (dd).

3-(pyrazin-2-yl)-5-Bromo-1,2,4-triazole (HBrpztr)[32]

0.84 g (6 mmol) of 3-(pyrazin-2-yl)-1,2,4-triazole (Hpztr) was added to 15 cm^3 of water. The ligand was fully dissolved by slow addition of 10 M NaOH (pH 12). 0.6 ml of Br_2 (99 %, d = 3.199 g/cm^3) was slowly added while maintaining a pH of 12 by addition of concentrated NaOH. The solution was stirred for 3 hours. The solution was acidified to pH 3 with concentrated HCl. The brominated ligand precipitated and was collected by vacuum filtration. Yield 1.65 g, 4.98 mmol, 83 %. ^1H NMR (d_6-DMSO), δ in ppm: H_3: 9.40 (s); H_5: 8.72 (d); H_6: 8.65 (d).

3.4.2 Preparation of the Complexes

0.277 mmol of the appropriate ligand was dissolved in 50 cm^3 of toluene. A few drops of trifluroacetic acid were added to this solution. $[Re(CO)_5Cl]$ (100 mg, 0.277 mmol) was added to the acidified toluene solution. This solution was refluxed under an argon atmosphere for 4 hours yielding an orange coloured solution. The reaction mixture was refrigerated overnight. The resulting orange precipitate was collected under vacuum filtration yielding the desired product.

$[Re(CO)_3(Hpztr)Cl]$

Yield 0.104 g, 0.231 mmol, 82 %. Elemental analysis for $ReC_9H_5N_5O_3Cl$: Calculated C, 23.87; H, 1.10; N, 15.47; Found C, 24.05; H, 1.05; N, 15.82; ^1H NMR (d_6-Acetone), δ in ppm: H_3: 9.59 (d); H_5: 9.16 (dd); H_6: 9.05 (d); H_a: 9.53(s). ν_{CO} (cm^{-1}) in THF: 2027, 1925, 1897.

$[Re(CO)_3(Hphpztr)Cl]$

Yield 0.113 g, 0.213 mmol, 77 %. Elemental analysis for $ReC_{15}H_9N_5O_3Cl$: Calculated C, 34.06; H, 1.70; N, 13.24; Found C, 34.77; H, 1.65; N, 13.82; ^1H NMR (d_6-acetone), δ in ppm: H_3: 9.65 (d); H_5: 9.16 (dd); H_6: 9.05 (d); H_a: 8.23 (d); H_b: 7.66 (s); H_c: 9.66 (dd); ν_{CO} (cm^{-1}) in THF: 2026, 1927, 1901.

[Re(CO)$_3$(Mephpztr)Cl]

Yield 0.110 g, 0.202 mmol, 73 %. Elemental analysis for $ReC_{16}H_{11}N_5O_3Cl$: Calculated C, 35.39; H, 2.03; N, 12.90; Found C, 35.99; H, 2.08; N, 12.75; ^1H NMR (d_6-acetone), δ in ppm: H_3: 9.60 (d); H_5: 9.11 (dd); H_6: 9.02 (d); H_a: 7.94 (d); H_b: 7.75 (m); H_c: 7.75 (m); Me 4.23. ν_{CO} (cm^{-1}) in THF: 2028, 1926, 1894.

[Re(CO)$_3$(Hthpztr)Cl]

Yield 0.113 g, 0.216 mmol, 78 %. Elemental analysis for $ReC_{13}H_7N_5O_3SCl$: Calculated C, 29.18; H, 1.32; N, 13.09; Found C, 29.13; H, 1.09; N, 12.70; ^1H NMR (d_6-acetone), δ in ppm: H_3: 9.63 (d); H_5: 9.15 (dd); H_6: 9.01 (d); H_a: 8.23 (d); H_b: 7.66 (m); H_c: 9.66 (d). ν_{CO} (cm^{-1}) in THF: 2027, 1926, 1897.

[Re(CO)$_3$(HBrpztr)Cl]

Yield 0.118 g, 0.222 mmol, 80 %. Elemental analysis for $ReC_9H_4N_5O_3BrCl$: Calculated C, 20.33; H, 0.76; N, 13.17; Found C, 20.40; H, 0.74; N, 12.85; ^1H NMR (d_6-acetone), δ in ppm: H_3: 9.60 (d); H_5: 9.14 (dd); H_6: 9.04 (d). ν_{CO} (cm^{-1}) in THF: 2025, 1928, 1899.

3.5 Bibliography

1 W. Kaim, H.E.A. Kramer, C. Vogler, J. Rieker, *J. Organomet. Chem.,* **1989**, 367, 107

2 A. Klein, C. Vogler, W. Kaim, *Organometallics,* **1996**, 15, 236.

3 S. Van Wallendael, R.J. Shaver, D.P. Rillema, B.J. Yoblinski, M. Stathis, T.F. Guarr, *Inorg. Chem.,* **1990**, 29, 1761.

4 D.J. Stufkens, *Coord. Chem. Rev.,* **1990**, 104, 39.

5 M. Leirer, G. Knor, A. Vogler, *Inorg. Chim. Acta,* **1999**, 288, 150.

6 B.E. Buchanan, R.Wang, J.G. Vos, R. Hage, J.G. Haasnoot, J. Reedijk, *Inorg. Chem,* **1990**, 29, 3263.

7 H.A. Nieuwenhuis, J.G. Haasnoot, R. Hage, J. Reedijk, T.L. Snoeck, D.J. Stufkens, J.G. Vos, *Inorg. Chem.,* **1991**, 30, 48.

8 G.J. Stor, S.L. Morrison, D.J. Stufkens, A. Oskam, *Organometallics*, **1994**, 13, 2641.

9 K. Yang, S.G. Bott, M.G. Richmond, *Organometallics,* **1995**, 14, 2387.

10 R. Hage, Ph. D. Thesis, Leiden University, **1991**.

11 E.S. Dodsworth, A.B.P Lever, G. Eryavec, R.J. Crutchley, *Inorg. Chem.,* **1985**, 24, 1906.

12 S. Fanni, T.E. Keyes, C.M. O'Connor, H. Hughes, R. Wang, J.G. Vos, *Coord. Chem. Rev.,* **2000**, 208, 77.

13 M.R. Waterland, T.J. Simpson, K.C. Gordon, A.K. Burrell, *J. Chem. Soc., Dalton Trans.,* **1998**, 185

14 A. Llobet, P. Dopplet, T.J. Meyer, *Inorg. Chem.,* **1988**, 27, 514.

15 R.J. Crutchley, A.B.P. Lever, *Inorg. Chem.,* **1982**, 21, 2276.

16 B.E. Buchanan, E. McGovern, P. Harkin, J.G. Vos, *Inorg. Chim. Acta.,* **1998**, 154, 1.

17 M. Wrighton, D.L. Morse, *J. Am. Chem. Soc.,* **1974**, 96, 998.

18 M.R. Waterland, T.J. Simpson, K.C. Gordon, A.K. Burrell, *J. Chem. Soc. Dalton Trans.,* **1998**, 185.

19 G.Knor, M. Leirer, A. Volger, *J. Organomet. Chem.,* **2000**, 610, 16.

20 N.M. Shavaleev, A. Barbieri, Z.R. Bell, M.D. Ward, *New. J. Chem.,* **2004**, 28, 398.

21 P.J. Giordano, M.S. Wrighton, *J. Am. Chem. Soc.*, **1979**, 96, 998.

22 D.J. Stufkens, A. Vlček Jr., *Coord. Chem. Rev.*, **1998**, 127.

23 J.V. Caspar T.J. Meyer, *J. Phys. Chem.*, **1983**, 87, 952.

24 N.H. Damrauer, J.K. McCusker, *Inorg. Chem.*, **1999**, 38, 4268.

25 T.J. Neyer, *Pure Appl. Chem.* **1986**, 58, 1193.

26 L. Sacksteder, A.P. Zipp, E.A. Brown, J. Streich, J.N. Demas, B.N. DeGraff, *Inorg. Chem.*, **1990**, 29, 4335.

27 E.M. Kober, J.L. Marshall, W.J. Dressick, B.P. Sullivan, J.V. Caspar, T.J. Meyer, *Inorg. Chem.*, **1985**, 24, 2755.

28 E.M. Kober, J.V. Caspar, R.S. Lumpkin, T.J. Meyer, *J. Phys. Chem.*, **1986**, 90, 3722.

29 L.D. Ciana, W.J. Dressick, D. Sandrini, M. Maestri, M. Ciano, *Inorg. Chem.*, **1990**, 29, 2792..

30 L.A. Worl, R. Duesing, P. Chen, L. Della Ciana, T.J. Meyer, *J. Chem. Soc. Dalton Trans.*, **1991**, 849.

31 M. Duati, S. Tasca, F.C. Lynch, H. Bohlen, J.G. Vos, S. Stagni, M.D. Ward, *Inorg. Chem.*, **2003**, *42, 8377*

32 (a) S. Fanni, C. Di Pietro, S. Serroni, S. Campagna and J. G. Vos, *Inorg. Chem. Commun.*, **2000**, *3*, 42 and (b) C. Di Pietro, S. Serroni, S. Campagna, M. T. Gandolfi, R. Ballardini, S. Fanni, W. R. Browne and J.G. Vos, *Inorg. Chem.*, **2002**, 41, 2871

33 J.G. Vos, *Polyhedron,* **1992**, 11, 2285.

34 (a) E.S. Dodsworth, A.B.P. Lever, *Chem. Phys. Letts.*, **1986**, 124, 152. (b) D.P. Rillema, G. Allen, T.J. Meyer, D. Conrad, *Inorg. Chem.*, **1983**, 22, 1617.

35 R. Hage, R. Prins, J.G. Haasnoot, J. Reedijk, J.G. Vos, *J. Chem. Soc. Dalton Trans.*, **1987**, 1389.

36 S. Frantz, W. Kaim, J. Fiedler, C. Duboc, *Inorg. Chim. Acta.*, **2004**, 357, 3657.

37 H. Hartmann, T. Scheiring, J. Fiedler, W. Kaim, *J. Organomet. Chem.*, **2000**, 604, 267.

38 H.P. Hughes, Ph. D. Thesis, Dublin City University, **1993**.

39 W.R. Browne, Ph. D. Thesis, Dublin City University, **2001.**

Chapter 4

Rhenium(I) and ruthenium(II) complexes with 3,5-bis(pyridin-2-yl)-1,2,4-triazole.

Chapter 4 introduces the ligand 3,5-bis(pyridin-2-yl)-1,2,4-triazole (Hbpt). Unlike the other triazole ligands discussed in Chapters 2 and 3, the Hbpt ligand provides the opportunity to coordinate two metal centres. The synthesis of the rhenium(I) monomer, the homo-nuclear rhenium(I) dinuclear complex and the hetero-nuclear ruthenium(II)-rhenium(I) dinuclear complex bridged by the Hbpt ligand are described in this chapter. The complexes have been characterised by IR spectroscopy, ^{1}H NMR spectroscopy and elemental analysis. The photophysical and electrochemical properties of all complexes have also been examined. In addition selective deuteriation together with spectroscopic measurements was used to probe the energy transfer process in the dinuclear ruthenium(II)-rhenium(I) complex.

4.1 Introduction

The design and synthesis of polynuclear metal complexes containing electroactive and photoactive units are topics of great interest because of the potential of such complexes to serve as building blocks for supramolecular assembles and molecular devices. For instance, it is possible to develop photochemical molecular devices (PMDs) that can perform light energy collection, charge separation and electronic energy transfer.[1] Considerable research has focused on rhenium(I), ruthenium(II) and osmium(II) polypyridyl complexes as building blocks in the synthesis of supramolecular assembles.[2,3] These assemblies incorporating photoactive units of rhenium(I), ruthenium(II) or osmium(II) have been constructed on the basis of the attractive electrochemical and excited state properties of these metal centres.[4]

Particular attention has been paid to metal-metal interactions in dinuclear metal complexes. Metal-metal interactions alter the photophysical properties of dinuclear systems and the rate of energy and/or electron transfer between two metal centres. The degree of metal-metal interaction permits the distinction between a supramolecular species (made of weakly interacting components which keep their characteristic properties in an assembly) and a large molecule (made of strongly interacting components which lose their characteristic properties in an assembly). Over the last number of years, many dinuclear ruthenium and heteronuclear ruthenium-osmium systems have exhibited communication between the two metal centres.[1] More recently, research has centred on heteronuclear rhenium-ruthenium systems. It is interesting to study whether enhanced communication is observed for these rhenium-ruthenium complexes compared to the analogous ruthenium-ruthenium or ruthenium-osmium systems. The important role played by the bridging ligand in determining the metal-metal communication is well recognised. The bridging ligand separating the metal units has two major functions within a supramolecular structure:

i) A structural role in controlling metal-metal distances and angles

ii) Control of electronic communication between the metal components

The two main types of bridging ligands that have been employed to synthesise dinuclear systems are strong π-acceptors and strong σ-donors. In the case of π-accepting bridging ligands, the bridging ligand is directly involved in the electrochemical reduction and emission processes associated with the binuclear system. Examples of π-accepting bridging ligands are 2,2'-bipyrimidine (bpm), benzo[1,2-b:3,4-b'5,6-b'']tripyrazine (HAT), 2,3-bis(2-pyridyl)pyrazine (2,3-dpp), 2,3-bis(2-pyridyl)quinoxaline (bpq) and 3,6-bis(2-pyridyl)-1,2,4,5-tetrazine (bptz).[5,6,7] In the case of strong σ-donor bridging ligands, the bridging ligand functions as a building block for the synthesis of the dinuclear system. Strong σ-donor bridging ligands have less influence on the emission properties compared to π-accepting bridging ligands. Examples of such systems are $Ru(bpy)_2$ dimers with the strong σ-donor ligands 2,2'-bisimidazolate, 5,5'-bis-(pyridin-2"-yl)-3,3'-bis(1H-1,2,4-triazole) and 1,4-bis(5-(2-pyridyl)-1H-1,2,4-triazole-3-yl)benzene.[8,9,10,11] Note in these cases, emission is bpy based rather than centred on the bridging ligand. For a list of the most common bridging ligands and their electronic and redox properties see reference 12.

In almost all studies of polypyridyl bimetallic rhenium(I) complexes, the bridging ligands have been symmetrical, placing the metal centres in equivalent environments. In order to direct energy or electron transfer in the excited state of a complex, it is necessary to confer asymmetry on the system. This has normally been accomplished by using different metals or metals with different spectator ligands.[13,14] However, it is possible to develop asymmetry on a ligand-bridged polypyridyl complex by introducing asymmetry into the bridging ligand. This has two major effects:

i) It creates inequivalence in the redox properties of the metal sites

ii) Such ligands should provide a method of conferring directed energy/electron-transfer properties to a complex in which the metal sites are equivalent i.e. both metals are $Re(CO)_3Cl$.

The synthesis and characterisation of mononuclear and dinuclear rhenium tricarbonyl complexes incorporating the asymmetric bridging ligand 3,5-bis(pyridin-2-yl)-1,2,4-triazole (Hbpt) will be discussed in this chapter. This chapter also reports the photophysical and electrochemical properties of the mononuclear and bimetallic rhenium tricarbonyl complexes. Previous work on a number of ruthenium complexes containing 1,2,4-triazole ligands has revealed that coordination is possible via N_2 and N_4 of the 1,2,4-triazole ligand. Another interesting point is that the N_2 and N_4 atoms have different σ-donor capacities.[15,16] The influence of the inequivalent N_2 and N_4 coordination modes on the dinuclear rhenium(I) complex will also be studied.

The anion of 3,5-bis(pyridin-2-yl)-1,2,4-triazole (bpt^-), is a particularly interesting bridging ligand. The photophysical and photochemical properties of its ruthenium and osmium homo- and heterometallic complexes have been extensively studied.[17,18] The interaction between metal centres in the dinuclear complexes is very efficient, thus supporting the conclusion that this ligand is a suitable bridge for binuclear complexes that can exhibit photoinduced electron or energy transfer. As a consequence, this chapter also reports the synthesis and chatacterisation of a heterometallic rhenium-ruthenium complex incorporating the bpt^- anion as a bridging ligand. The synthesis and characterisation of a deuteriated analogue of the ruthenium-bpt-rhenium complex is also reported. Selective deuteriation of ligands in heteroleptic Ru(II) polypyridyl complexes simplifies complicated ^1H NMR spectra.[19] Hence deuteriation of the bipyridyl ligands in this heteronuclear complex will aid the interpretation of the ^1H NMR spectra.

In Chapter 2 it was concluded that in mononuclear rhenium tricarbonyl complexes containing a pyridyl-triazole ligand, the excited-state is localised on the pyridyl-triazole ligand. It is now of interest to investigate whether the 3,5-bis(pyridin-2-

yl)-1,2,4-triazole ligand acts as an energy transfer trap or is simply a spectator ligand in the emission process of the heteronuclear rhenium-ruthenium complex. Hence the photophysical and electrochemical properties of the rhenium-ruthenium complex will be studied. Deuteriation of one of the ligands in a mixed ligand complex will only increase the emission lifetime if the emitting state is located on that ligand.[20,21] In addition, selective deuteriation together with spectroscopic measurements will be used to probe the energy transfer process in the dinuclear complex. The structures and abbreviations for the ligands cited in this chapter are shown in Figure 4. 1.

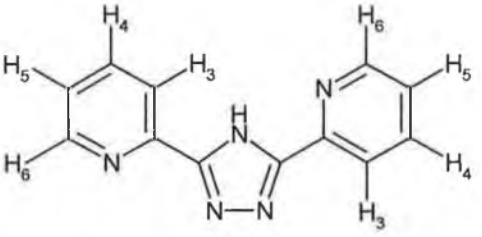

3,5-bis(pyridin-2-yl)-1,2,4-triazole
(Hbpt)

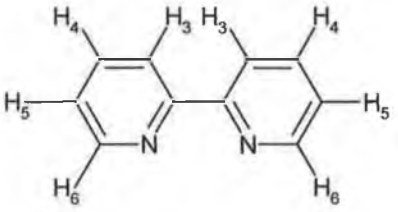

2,2'-bipyridyl
(bpy)

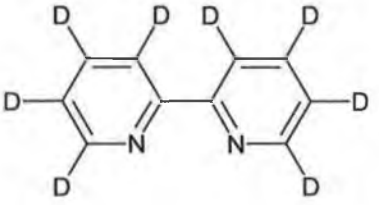

d_8-bpy

Figure 4. 1 *Srructures of the ligands and their abbreviations as cited throughout this chapter.*

4.2 Results and Discussion

4.2.1 Syntheses

The Hbpt ligand was synthesised as previously reported.[22] The synthetic route employed in the synthesis is described in Figure 4. 2.

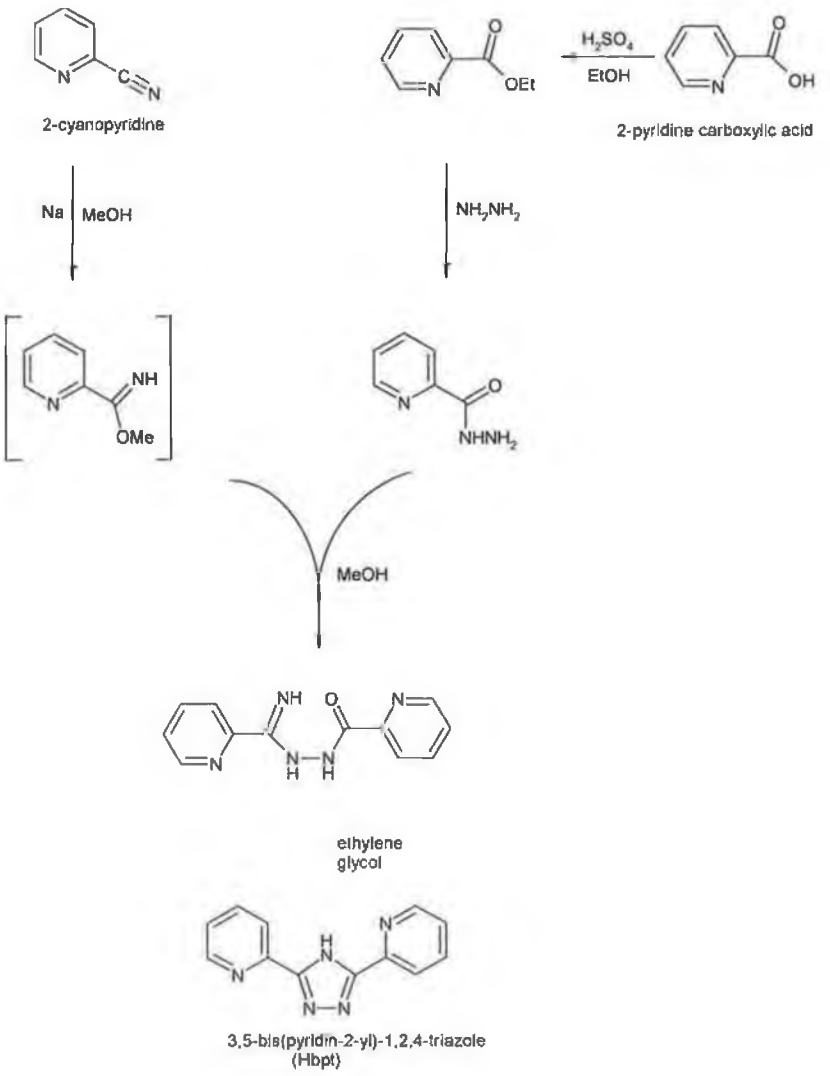

Figure 4. 2 *Synthetic route used to synthesise 3,5-bis(pyridin-2-yl)-1,2,4-triazole*

Synthesis of the rhenium complexes was readily achieved by control of the metal:ligand ratio. The synthesis of the mononuclear rhenium complex $[Re(CO)_3(Hbpt)Cl]$ was carried out in acidified-toluene. The Hbpt ligand (in excess) was firstly dissolved in toluene. As has been observed for ruthenium complexes containing pyridyl-triazole ligands, the ligands deprotonate upon coordination of the metal centre.[15,23,24] However, the added precaution of addition of a few drops of trifluoroacetic acid was taken to ensure that the protonated complexes were isolated. The $Re(CO)_5Cl$ in toluene was slowly added to the acidified toluene solution. This reaction mixture was refluxed for 4 hours. Note it is important when synthesising mononuclear complexes to ensure complete dissolution of the ligand before adding the $Re(CO)_5Cl$ so as to minimise the amount of dinuclear complex formed. Previous studies have found that Ru(II) complexes incorporating pyridyl-triazole ligands give rise to the formation of both N_2 and N_4 isomers (Figure 4. 3).[25] ^1H NMR studies (see Section 4.2.2) show the formation of one $[Re(CO)_3(Hbpt)Cl]$ coordination isomer. The dinuclear rhenium complex $[\{Re(CO)_3Cl\}_2Hbpt]$ was synthesised by reaction of $Re(CO)_5Cl$:Hbpt in a 2:1 ratio for 6 hours in an acidified toluene solution.[26,27]

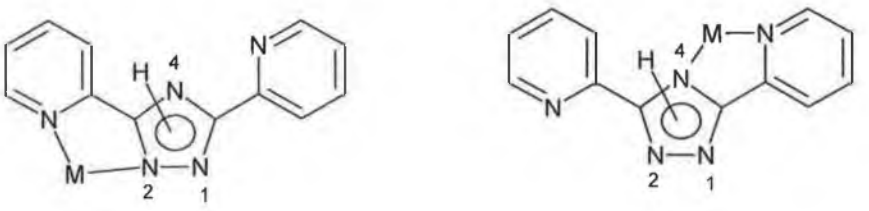

N_2 Isomer N_4 Isomer

Figure 4. 3 *The two possible modes of coordination of a metal centre to the Hbpt ligand.*

The mononuclear precursor $[Ru(bpy)_2bpt]^+$ was prepared following literature procedures.[15] Purification was carried with a neutral alumina column. The N_2 isomer was eluted first with acetonitrile followed by elution of the N_4 isomer with

methanol. The N_2 isomer was subsequently recrystallised from water/acetone (1/1). 2 M NaOH was added to the solution to ensure the triazole was fully deprotonated. This product was then collected and vacuum dried. [Ru(d_8-bpy)$_2$bpt](PF$_6$) was synthesised and purified as for [Ru(bpy)$_2$bpt](PF$_6$) with one change, [Ru(d_8-bpy)$_2$Cl$_2$] was used instead of [Ru(bpy)$_2$Cl$_2$]. The heteronuclear [Ru(bpy)$_2$(bpt)Re(CO)Cl]$^+$ complex was prepared by refluxing molar equivalents of [Ru(bpy)$_2$bpt](PF$_6$) and Re(CO)$_5$Cl in methanol under an argon atmosphere. The reaction was monitored using IR spectroscopy. The reaction was complete when there was no evidence of any Re(CO)$_5$Cl in the IR spectrum. [Ru(d_8-bpy)$_2$(bpt)Re(CO)Cl]$^+$ was synthesised using the same procedure as that used to synthesise [Ru(bpy)$_2$(bpt)Re(CO)Cl]$^+$. [Ru(d_8-bpy)$_2$bpt](PF$_6$) was the ruthenium precursor used to synthesise [Ru(d_8-bpy)$_2$(bpt)Re(CO)Cl]$^+$. Reaction times were typically in the order of 6 hours. The complexity of the ^{1}H NMR spectrum of [Ru(bpy)$_2$(bpt)Re(CO)Cl]$^+$ (see Figure 4. 8, Section 4.2.2.2) indicates the formation of isomers. The ^{1}H NMR spectrum of the deuterated complex [Ru(d_8-bpy)$_2$(bpt)Re(CO)Cl]$^+$ is shown in Figure 4. 9. It is immediately clear, that by the partial deuteration of the complex, it becomes possible to distinguish the bpt protons from those of the bipyridyl ligand. The ^{1}H NMR spectrum of [Ru(d_8-bpy)$_2$(bpt)Re(CO)Cl]$^+$ shows the formation of two isomers in a 2:1 ratio. The predominant isomer is termed Isomer I whilst the minor isomer is termed Isomer II. Attempts to isolate the structural isomers of [Ru(bpy)$_2$(bpt)Re(CO)Cl]$^+$ were unsuccessful. Careful recrystallisation of [Ru(d_8-bpy)$_2$(bpt)Re(CO)Cl]$^+$ from acetone/ethanol (2/1 v/v) yielded three fractions. Fraction one contained Isomer I; fraction two contained Isomer II while fraction three contained a mixture of both isomers.

4.2.2 NMR spectroscopy

As ruthenium(II) and rhenium(I) complexes are diamagnetic low-spin d^6 species, NMR spectroscopy has been used in the elucidation of the structure of these complexes.[28,2930,31] Two coordination sites are present on the Hbpt ligand (N_2 and

N_4), it is hoped the binding mode of the triazole ligands can be determined using NMR spectroscopy.

4.2.2.1 Mononuclear complexes

The structure and ^1H NMR spectrum of $[Ru(bpy)_2bpt]^+$ is well understood. This will be briefly summarised, as both of these properties are important in the interpretation of the NMR spectra of the dinuclear complex $[Ru(bpy)_2(bpt)Re(CO)Cl]^+$. Table 4. 1 lists the chemical shifts of the bpt^- protons of the ruthenium and rhenium mononuclear complexes. The chemical shifts of the bpy ligands in $[Ru(bpy)_2bpt]^+$ have not been presented in detail as they fall in the normal range expected for these protons. Figure 4. 5 shows the ^1H NMR spectra of $[Re(CO)_3(Hbpt)Cl]$, $[Ru(d_8\text{-}bpy)_2bpt]^+$ and $[Ru(bpy)_2bpt]^+$ in d_3-acetonitrile.

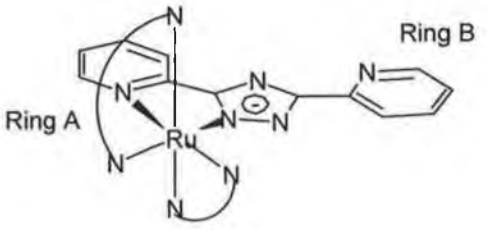

Figure 4. 4 *Structure of $[Ru((bpy)_2bpt]^+$.*

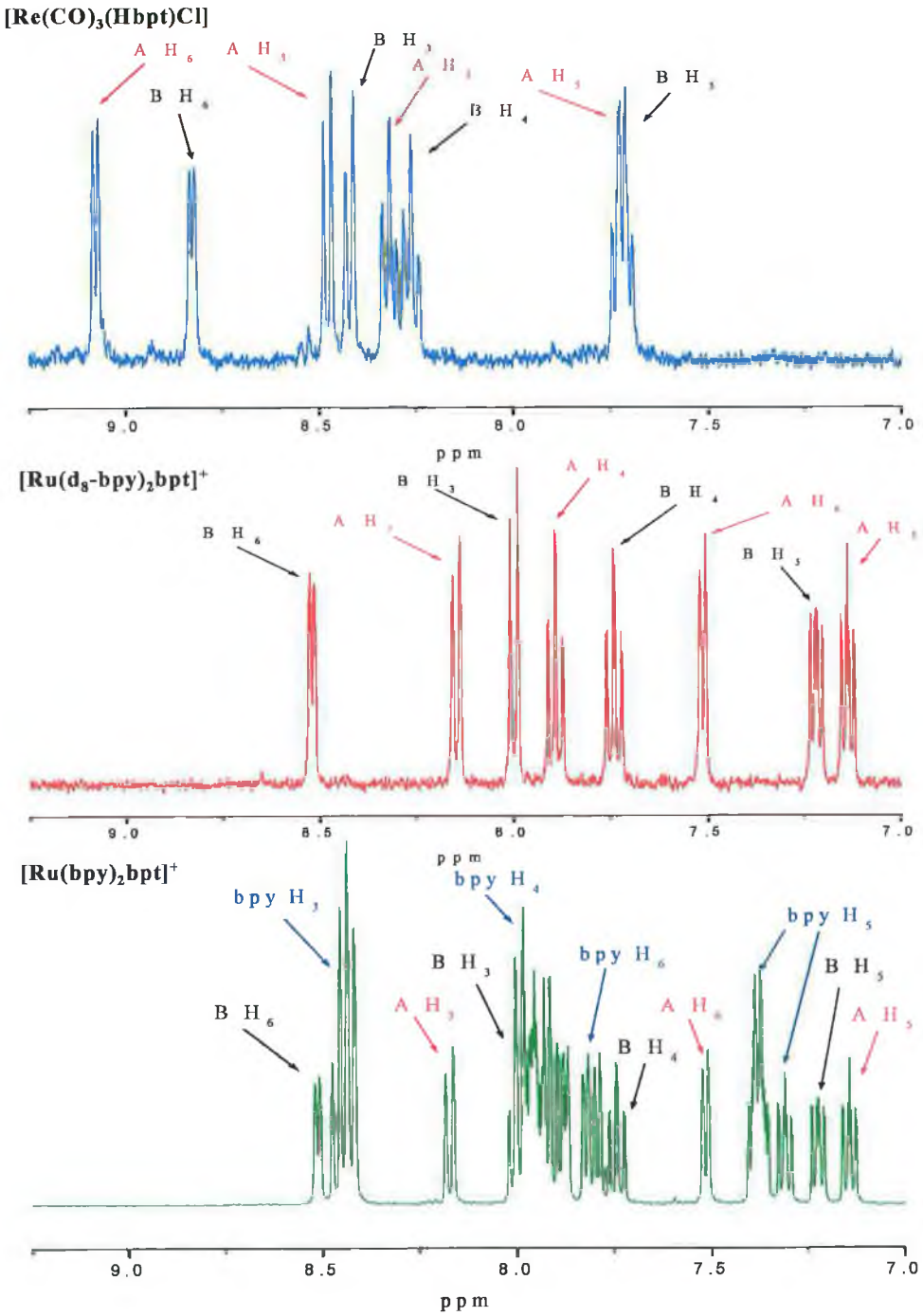

Figure 4. 5 *^1H NMR spectra of $[Re(CO)_3(Hbpt)Cl]$, $[Ru(d_8\text{-bpy})_2bpt]^+$ and $[Ru(bpy)_2bpt]^+$ in d_3-acetonitrile. A refers to ring A and B refers to ring B as depicted in Figure 4. 4.*

	ppm			
Ring A	H_3	H_4	H_5	H_6
$[Ru(bpy)_2bpt]^+$	8.15	7.90	7.15	7.52
	(- 0.07)	(- 0.06)	(- 0.33)	(- 1.18)
bpy resonances	8.41-8.60	7.94-8.00	7.30-7.40	7.78-7.87
$[Ru(d_8\text{-}bpy)_2bpt]^+$	8.15	7.90	7.15	7.52
	(- 0.07)	(- 0.06)	(- 0.33)	(- 1.18)
$[Re(CO)_3(Hbpt)Cl]$	8.41	8.32	7.70	9.07
	(+ 0.19)	(+ 0.36)	(+ 0.22)	(+ 0.36)
Ring B	H_3	H_4	H_5	H_6
$[Ru(bpy)_2bpt]^{2+}$	8.00	7.75	7.22	8.53
	(- 0.23)	(- 0.21)	(- 0.26)	(- 0.17)
$[Ru(d_8\text{-}bpy)_2bpt]^{2+}$	8.00	7.75	7.22	8.53
	(- 0.23)	(- 0.21)	(- 0.26)	(- 0.17)
$[Re(CO)_3(Hbpt)Cl]$	8.46	8.25	7.70	8.82
	(+ 0.23)	(+ 0.29)	(+ 0.22)	(+ 0.11)

Table 4. 1 *^1H NMR data for the metal complexes. All spectra were obtained in d_3-acetonitrile. Values in parenthesis are the coordinated induced shifts relative to the free ligand.*

The X-ray structure of $[Ru(bpy)_2bpt]^+$ shows one pyridine ring is bound to the $Ru(bpy)_2$ moiety (Ring A) and the other ring (Ring B) is free (Figure 4. 4).[32] This gives rise to the two distinct sets of pyridine protons in the ^1H NMR spectra of $[Ru(bpy)_2bpt]^+$ and $[Ru(d_8\text{-}bpy)_2bpt]^+$ (Figure 4. 5). The ^1H NMR spectrum of $[Ru(bpy)_2bpt]^+$ is extremely complex, with a total of 24 aromatic protons. However, the ^1H NMR spectrum of $[Ru(d_8\text{-}bpy)_2bpt]^+$ aids structural characterisation. With all of the 2,2'-bipyridine signals gone, it is possible to easily identify all of the bpt^- ligand signals. Both Table 4. 1 and Figure 4. 5 show

the H_6 proton of ring A is present at 7.52 ppm, whilst the H_6 proton of ring B is observed at 8.53 ppm. The H_6 proton of ring A is directed just above a pyridine ring of an adjacent bpy ligand. This diamagnetic anisotropic effect explains the large differences between ring A and ring B for the H_6 resonances. Note since the $Ru(bpy)_2$ is bound to the bpt^- ligand via the N_2, ring B is projected away from any bpy ligand. Hence there is a smaller shift in the bpt^- protons of ring B upon coordination to the $Ru(bpy)_2$ moiety.

The ^1H NMR spectrum of the free Hbpt ligand displays four sets of resonances in the aromatic region. Coordination of the $Re(CO)_3Cl$ unit lowers the symmetry of the Hbpt moiety and splits the degeneracy of each pair of protons. All peaks are shifted downfield upon metal attachment i.e. postitive coordination induced shifts (c.i.s). The ^1H NMR data and the c.i.s values of $[Re(CO)_3(Hbpt)Cl]$ are summarised in Table 4. 1. The ^1H NMR spectra of $[Re(CO)_3(Hbpt)Cl]$, $[Ru(bpy)_2bpt]^+$ and $[Ru(d_8\text{-}bpy)_2bpt]^+$ are shown in Figure 4. 5. Assignment of proton resonances in the $[Re(CO)_3(Hbpt)Cl]$ complex were made by comparison with the pyridyl-triazole complexes synthesised in Chapter 2 and with the aid of two dimensional (COSY) techniques. Previous publications of bipyridine complexes place the resonance of the H_6 proton adjacent to the coordinated nitrogen fartherest downfield.[31,33,34] Hence the peak positions of the coordinated pyridine ring (ring A) were identified as follows: the H_6 (doublet) and H_5 (multiplet) protons were located at 9.07 and 7.77 ppm. The doublet (8.41 ppm) and multiplet (8.32 ppm) are assigned to H_3 and H_4 respectively. Assignment of the ring B protons is now straightforward (Table 4. 1).

It is possible for 1,2,4-triazole complexes to form N_1 and N_2 linkage isomers (Figure 4. 3), however the formation of only a single $[Re(CO)_3(Hbpt)Cl]$ isomer was observed. In the complex $[Re(CO)_3(NH_2bpt)Cl]$ (NH_2bpt = 4-amino-3,5-bis(pyridin-2-yl)-1,2,4-triazole) the authors proposed the large radius of rhenium(I) leads to the formation of just the N_2 coordination isomer.[35] The extent of N_2/N_4 coordination in Ru(II) complexes is governed by the size of the substituents on the triazole ring.[36] Bulky triazole substituents such as a phenyl or

a pyridine group favour the formation of the N_2 isomer in Ru(II) complexes.[37] In addition, the formation of a single isomer was also reported for a series of ruthenium carbonyl complexes of the form $[Ru(L)(CO)_2Cl_2]$, where L = 3-(pyrazin-2-yl)-1,2,4-triazole or 3-(pyrazin-2-yl)-5-phenyl-1,2,4-triazole.[38] The crystal structures of these complexes showed that the ligand was coordinated to the ruthenium metal centre via the N_2 of the triazole ring. Therefore it is not unreasonable to deduce that the N_2 isomer was also formed in $[Re(CO)_3(Hbpt)Cl]$. No crystals suitable for X-ray analysis were obtained. In the absence of such crystals, the coordination mode of the ligands cannot be determined with certainty, however coordination via the N_2 position seems most likely.

4.2.2.2 Dinuclear Complexes

The following dinuclear complexes were synthesied: $[\{Re(CO)_3Cl\}_2Hbpt]$, $[Ru(bpy)_2(bpt)Re(CO)_3Cl]^+$ and $[Ru(d_8\text{-}bpy)_2(bpt)Re(CO)_3Cl]^+$. Table 4. 2 lists the chemical shifts of the bpt protons of the dinuclear complexes $[\{Re(CO)_3Cl\}_2Hbpt]$, $[Ru(bpy)_2(bpt)Re(CO)_3Cl]^+$ and $[Ru(d_8\text{-}bpy)_2(bpt)Re(CO)_3Cl]^+$.

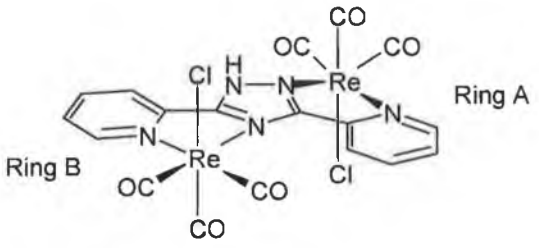

Figure 4. 6 *Proposed structure of $[\{Re(CO)_3Cl\}_2Hbpt]$.*

	ppm			
	H_3	H_4	H_5	H_6
$[\{Re(CO)_3Cl\}_2(Hbpt)]$				
Ring A	8.23	8.23	7.60	9.03
	(0.01)	(0.27)	(0.11)	(0.33)
Ring B	8.23	8.23	7.60	9.03
	(0.01)	(0.27)	(0.11)	(0.33)
$[Ru(bpy)_2(bpt)Re(CO)_3Cl]^+$				
Isomer I: Ring A	8.69	8.10	7.38	7.82
	(0.47)	(0.14)	(- 0.11)	(- 0.88)
Ring B	7.93	8.02	7.49	8.95
	(- 0.29)	(0.06)	(0.00)	(0.25)
Isomer II: Ring A	8.32	8.03	7.27	7.39
	(0.10)	(0.07)	(- 0.22)	(- 1.31)
Ring B	8.11	8.11	7.44	8.80
	(- 0.11)	(0.15)	(-0.05)	(0.10)
$[Ru(d_8\text{-}bpy)_2(bpt)Re(CO)_3Cl]^+$				
Isomer I: Ring A	8.69	8.10	7.38	7.82
	(0.47)	(0.14)	(- 0.11)	(- 0.88)
Ring B	7.93	8.02	7.49	8.95
	(- 0.29)	(0.06)	(0.00)	(0.25)
Isomer II: Ring A	8.32	8.03	7.27	7.39
	(0.10)	(0.07)	(- 0.22)	(- 1.31)
Ring B	8.11	8.11	7.44	8.80
	(- 0.11)	(0.15)	(-0.05)	(0.10)

Table 4. 2 *Chemical shifts (ppm) of the protons of the bis(pyridyl)triazole ligand for $[\{Re(CO)_3Cl\}_2(Hbpt)]$ and the two isomers of the heteronuclear complexes $[Ru(bpy)_2(bpt)Re(CO)_3Cl]^+$ and $[Ru(d_8\text{-}bpy)_2(bpt)Re(CO)_3Cl]^+$ in d_3-acetonitrile. Values in parenthesis are the coordinated induced shifts relative to the free ligands.*

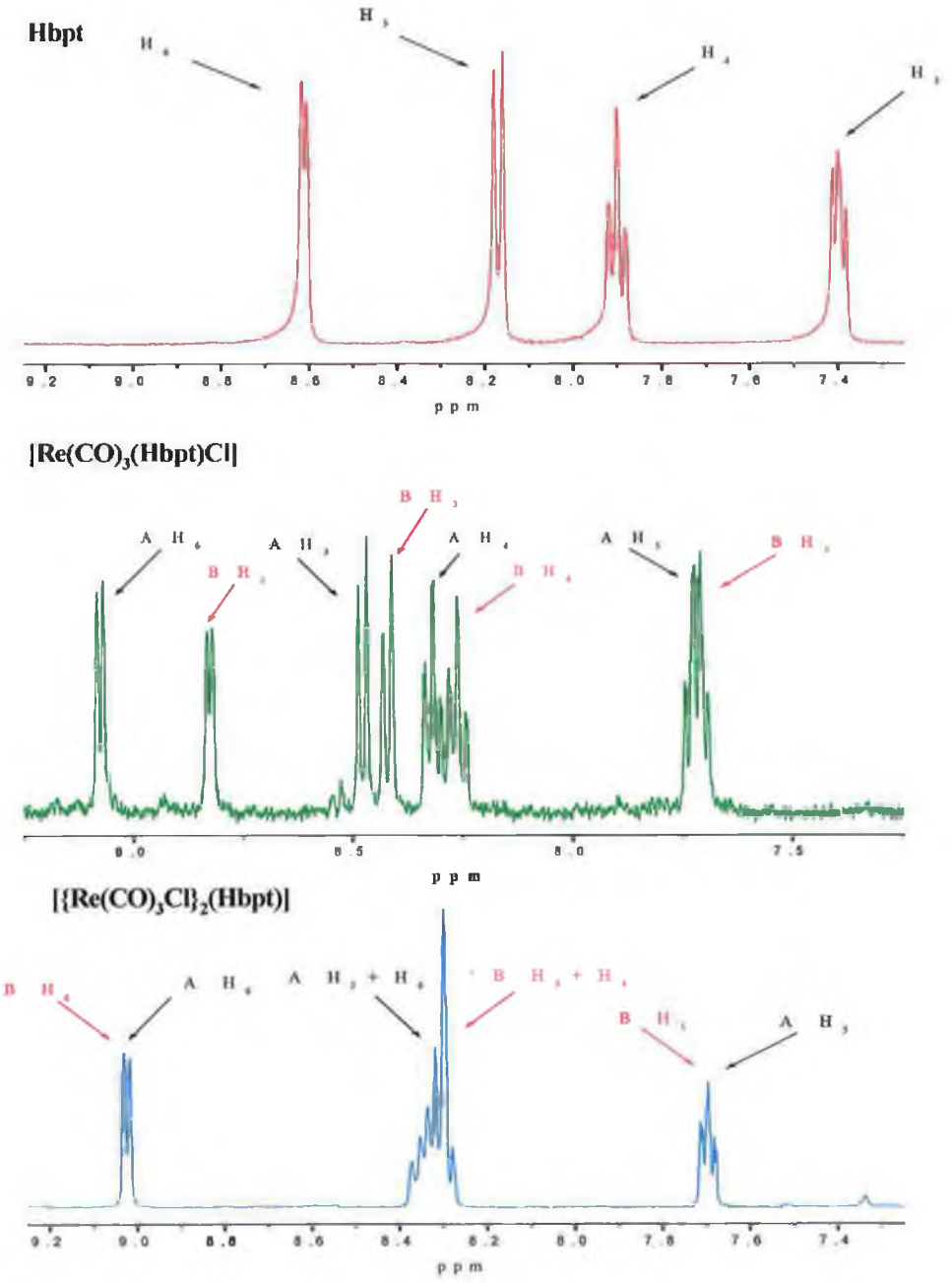

Figure 4. 7 *^{1}H NMR spectra of [Re(CO)$_3$(Hbpt)Cl] and [{Re(CO)$_3$Cl}$_2$Hbpt] and Hbpt in d_3-acetonitrile. A refers to ring A and B refers to ring B as depicted in Figure 4. 6.*

The ^{1}H NMR spectrum of the dinuclear complex [{Re(CO)$_3$Cl}$_2$Hbpt] will be discussed first. ^{1}H NMR spectra of Hbpt, [Re(CO)$_3$(Hbpt)Cl] and [{Re(CO)$_3$Cl}$_2$Hbpt] are presented in Figure 4. 7. Attachment of a second rhenium tricarbonyl fragment to [Re(CO)$_3$(Hbpt)Cl] results in a down field shift of the ring B protons. Note the resonances of both rings are found to overlap. The ^{1}H NMR spectra of [Re(CO)$_3$(Hbpt)Cl] and the pyridyl-triazole complexes synthesised in Chapter 2 place the resonance of the H_6 proton adjacent to the coordinated nitrogen fartherest downfield. Hence the peak positions were identified as follows: the H_6 (doublet) and H_5 (multiplet) protons were located at 9.03 and 7.60 ppm. The multiplet at 8.32 ppm is assigned to the H_3 and H_4 protons. A structure similar to that shown in Figure 4. 6, where the rhenium tricarbonyl fragments are bound via N_2 and N_4 of the triazole unit is proposed for the binuclear complex [{Re(CO)$_3$Cl}$_2$Hbpt]. Dinuclear rhenium(I) complexes can exhibit *cis/trans* isomerisation of the chloride ligand. However, no evidence for isomeric mixtures were detected in the ^{1}H NMR spectrum of [{Re(CO)$_3$Cl}$_2$Hbpt]. The *trans* isomer is favoured by analogy to structurally characterised dinuclear rhenium(I) complexes.[39] Note attempts by Kaim and coworkers to synthesise the tetranuclear complex [{Re(CO)$_3$Cl}$_4$(bmtz)] (bmtz = 3,6-bis(2-pyrimidyl)-1,2,4,5-tetrazine) were unsuccessful.[40] The authors concluded steric interference inhibited the formation of the tetranuclear complex. Hence it is unlikely the metal centres are coordinated through N_1 and N_2 of the triazole.

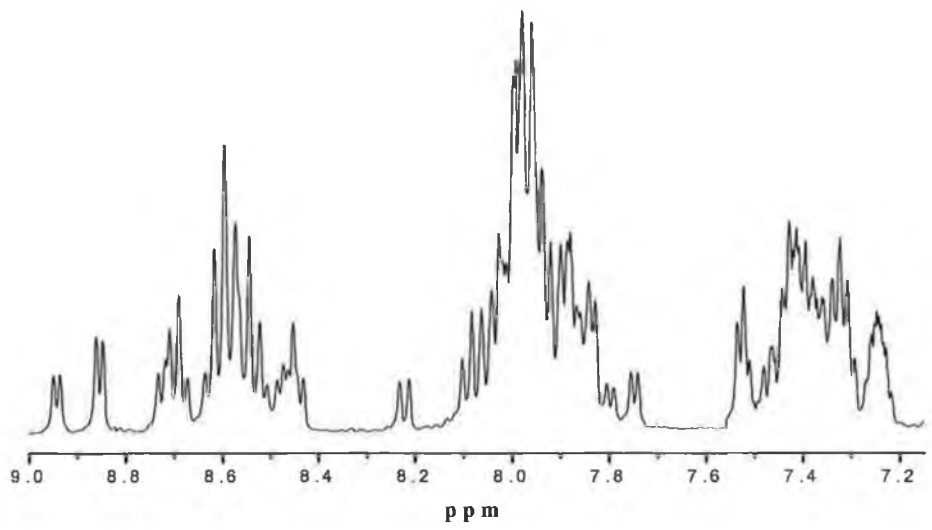

Figure 4. 8 *^{1}H NMR spectrum of [Ru(bpy)$_2$(bpt)Re(CO)$_3$Cl]$^+$ in d_6-acetone.*

The ^{1}H NMR spectrum of [Ru(bpy)$_2$(bpt)Re(CO)$_3$Cl]$^+$ is presented in Figure 4. 8. The complexity of the ^{1}H NMR spectrum of [Ru(bpy)$_2$(bpt)Re(CO)$_3$Cl]$^+$ illustrates the formation of isomers. Hence the spectrum is extremely difficult to interpret. The ^{1}H NMR spectrum of the deuterated complex [Ru(d_8-bpy)$_2$(bpt)Re(CO)Cl]$^+$ is shown in Figure 4. 9. It is immediately clear, that by the partial deuteration of the complex, it becomes possible to distinguish the bpt$^-$ protons from those of the bipyridyl ligand. The ^{1}H NMR spectrum of [Ru(d_8-bpy)$_2$(bpt)Re(CO)Cl]$^+$ shows the formation of two isomers in a 2:1 ratio. The predominant isomer is termed Isomer I whilst the minor isomer is termed Isomer II. The dinuclear complex [{Ru(bpy)$_2$}$_2$(bpt)]$^{3+}$ may also exist as two geometrical isomers depending on the relative orientation of the 2,2'-bipyridine ligands (see Figure 4. 10).[15,41] Furthermore, for each geometrical isomer, an optical isomer is present.

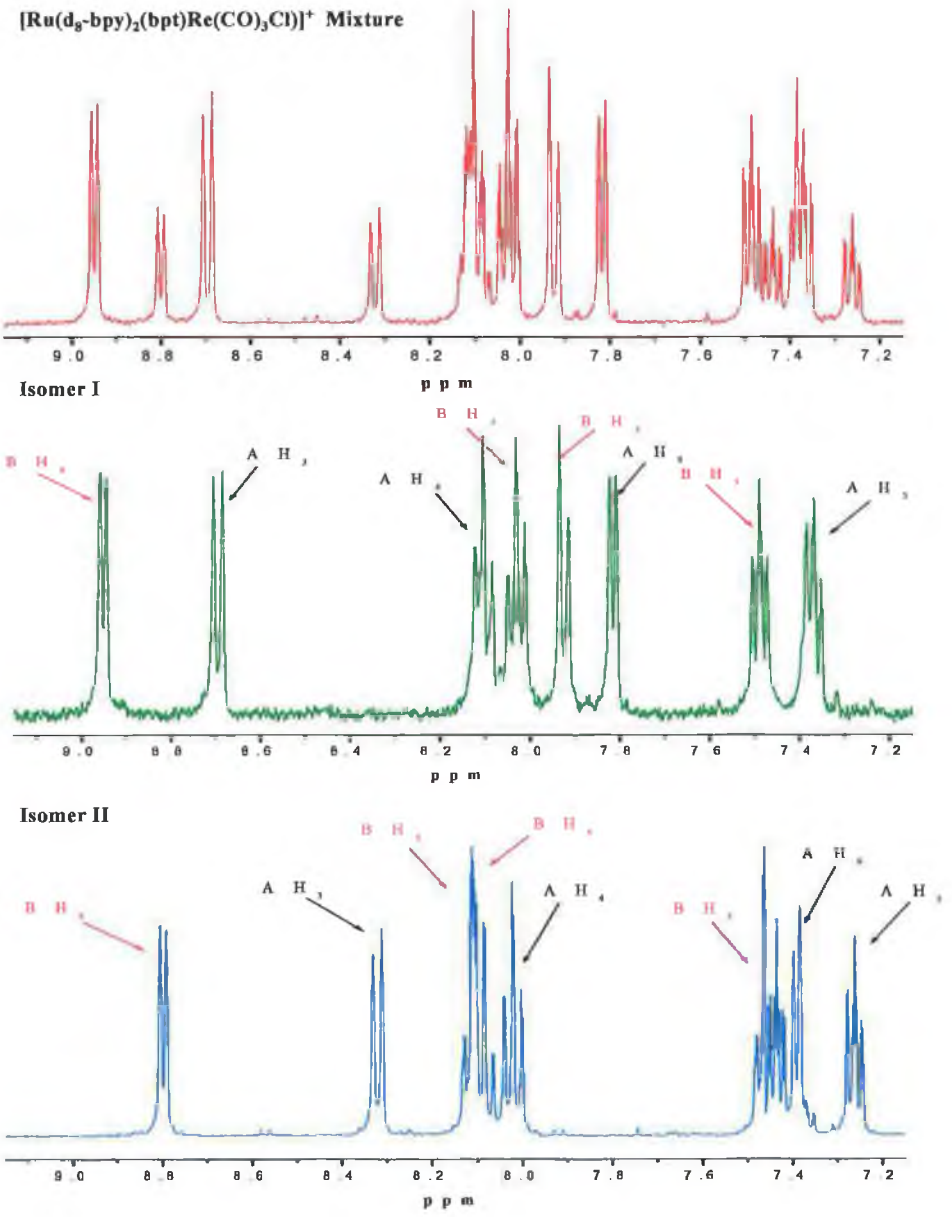

Figure 4. 9 *^1H NMR spectra of [Ru(d8-bpy)2(bpt)Re(CO)3Cl]: Isomer I and IsomerII. A refers to ring A and B refers to ring B as depicted in Figure 4. 11.*

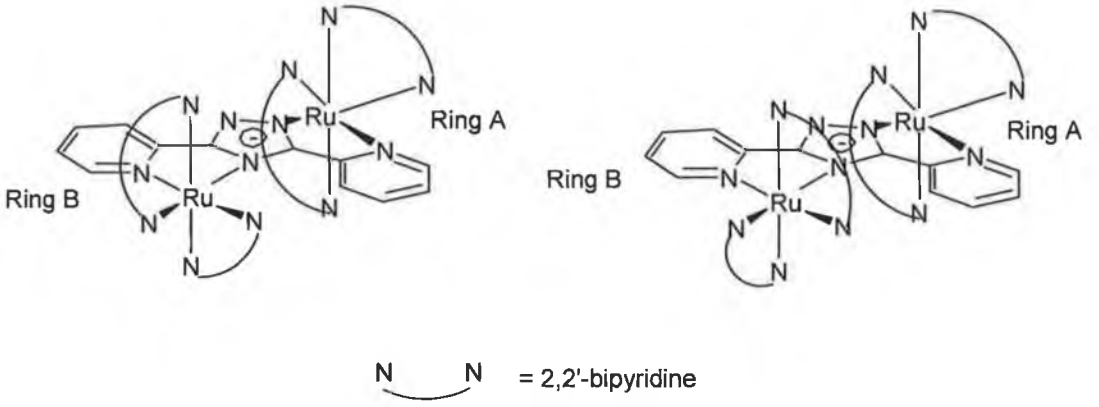

Figure 4. 10 *Geometrical isomers of* $[\{Ru(bpy)_2\}_2(bpt)]^{3+}$. *Note ion charges have been omitted for clarity.*

The formation of structural isomers has also been observed in heteronuclear bimetallic complexes containing a $Re(CO)_3Cl$ moiety. Previous reports of the heterodinuclear complex $[(\eta^5\text{-}C_5Me_5)ClRh(\mu\text{-bptz})Re(CO)_3Cl](PF_6)$ (bptz = 3,6-bis-(2-pyridyl)-1,2,4,5-tetrazine) showed structural isomerism.[42] ^1H NMR spectroscopy showed two isomers present in a 2:1 ratio. It was proposed isomers arose from two different orientations of the chloride ligand bound to the rhodium metal centre. Considering the reasons for isomer formation in $[(\eta^5\text{-}C_5Me_5)ClRh(\mu\text{-bptz})Re(CO)_3Cl](PF_6)$ and the dinuclear complex $[\{Ru(bpy)_2\}_2(bpt)]^{3+}$, the observation of two isomers in the ^1H NMR spectra of $[Ru(bpy)_2(bpt)Re(CO)_3Cl]^+$ and $[Ru(d_8\text{-}bpy)_2(bpt)Re(CO)_3Cl]^+$ may also be due to the different orientation of the bipyridyl ligands. The possible structurual isomers of $[Ru(bpy)_2(bpt)Re(CO)_3Cl]^+$ and $[Ru(d_8\text{-}bpy)_2(bpt)Re(CO)_3Cl]^+$, are shown in Figure 4. 11. Steric interactions between the $Ru(bpy)_2$ and the $Re(CO)_3Cl$ moieties prevents a configuration in which the two metal centres are coordinated via N_1 and N_2 of the triazole.

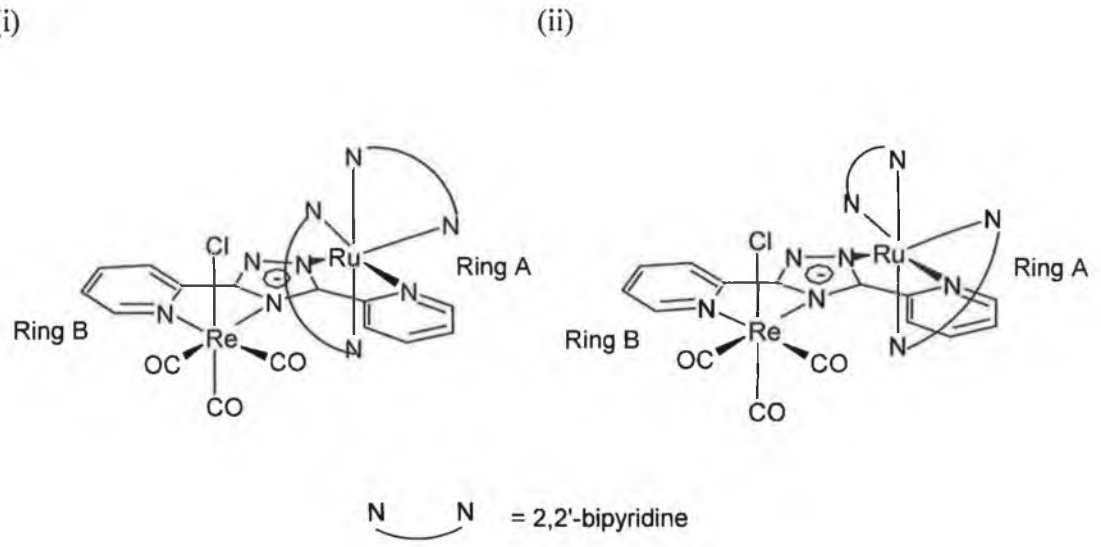

Figure 4. 11 *The possible structural isomers of* $[Ru(bpy)_2(bpt)Re(CO)_3Cl]^+$ *and* $[Ru(d_8\text{-}bpy)_2(bpt)Re(CO)_3Cl]^+$. *Note ion charges have been omitted for clarity.*

The protons of the pyridine fragment coordinated to $Re(CO)_3Cl$ were easily identified by comparison with the resonances of coordinated pyridines in $[Re(CO)_3(Hbpt)Cl]$ and $[\{Re(CO)_3Cl\}_2(Hbpt)]$. It is noted that in general the resonances of the rhenium(I) bound pyridines (ring B) are found at higher field than those of the ruthenium bound pyridine (ring A). This difference in chemical shift is most likely due to the relatively strong $Re(d_\pi)\rightarrow\pi^*(CO)$ back donation compared to $Ru(d_\pi)\rightarrow\pi^*(bpy)$.[43] The ^1H NMR spectra of $[Re(CO)_3(Hbpt)Cl]$ and the pyridyl-triazole complexes synthesised in Chapter 2 place the resonance of the H_6 proton adjacent to the nitrogen coordinated to the rhenium metal centre. furtherest downfield. Hence the peak positions of Ring B of Isomer I were identified as follows: the H_6 (doublet) and H_5 (multiplet) protons were located at 8.95 and 7.49 ppm. The doublet at 7.93 ppm and the multiplet at 8.02 ppm are assigned to H_3 and H_4. The assignment of ring A protons is now relatively straightforward. The doublet at 8.69 ppm and the multiplet at 8.10 ppm are assigned to H_3 and H_4. The H_6 (doublet) and H_5 (multiplet) protons were observed at 7.82 and 7.38 ppm. There is a considerable difference between the

resonances of H_3 (Ring A) in the mononuclear complex $[Ru(bpy)_2bpt]^+$ and the heteronuclear complexes $[Ru(bpy)_2(bpt)Re(CO)_3Cl]^+$ and $[Ru(d_8\text{-}bpy)_2(bpt)Re(CO)_3Cl]^+$ (see Table 4. 1 and Table 4. 2). The H_3 proton of $[Ru(bpy)_2bpt]^+$ is observed at 8.15 ppm. Coordination of a $Re(CO)_3Cl$ unit to ring B shifts the resonance of the H_3 proton to 8.69 ppm. The observed shift in the resonance of the H_3 proton must be the result of close contact between the H_3 proton and one of the equatorial carbonyl groups coordinated to the rhenium(I) metal centre (see Figure 4. 12). This equatorial carbonyl deshields the H_3 (Ring A,) hence this proton is shifted downfield relative to $[Ru(bpy)_2bpt]^+$. A similar interaction explained the observed differences between the chemical shifts of the H_3 proton in $[Mo(CO)_4abpy]$ and $[\{Mo(CO)_4\}_2abpy]$ (abpy = 2,2'-azopyridine).[44] The H_3 protons of $[Mo(CO)_4abpy]$ and $[\{Mo(CO)_4\}_2abpy]$ were observed at 8.50 and 9.17 ppm.

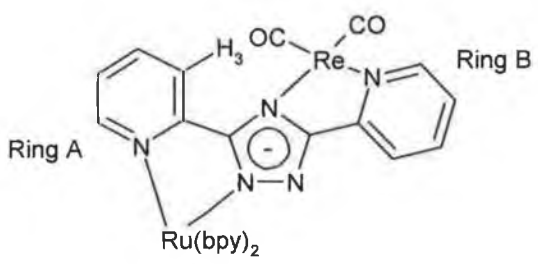

Figure 4. 12 *Interaction between H_3 (ring A) and the equatorial carbonyl in the heteronuclear complexes $[Ru(bpy)_2(bpt)Re(CO)_3Cl]^+$ and $[Ru(d_8\text{-}bpy)_2(bpt)Re(CO)_3Cl]^+$. Note ion charges have been omitted for clarity.*

The ^1H NMR spectrum of the second isomer is similar to that of the first isomer and the same explanations for the observed chemical shifts as given for the spectrum of Isomer I are valid. Large differences exist between the resonances of the H_6 protons of Ring A for Isomer I and Isomer II (see Table 4. 2). The geometrical isomers (i) and (ii) in Figure 4. 11 account for the observed differences in the ^1H NMR spectra. The H_6 proton (Ring A) of the geometrical isomer (ii) in Figure 4. 11 is directed towards a bpy ligand, whereas no bpy ligand

is in the vicinity of the H_6 proton (Ring A) of the geometrical isomer (i). It is possible the different orientations of the bipyridyl ligands with respect to the H_6 proton give rise to two different resonances (7.82 ppm Isomer I and 7.39 ppm Isomer II). The H_6 proton (ring A) of Isomer II is directed just above a pyridine ring of an adjacent bpy ligand whereas whereas no bpy ligand is in the vicinity of the H_6 proton of Isomer I. This diamagnetic anisotropic effect results in an upfield shift in the resonances of the H_6 proton of Isomer II relative Isomer I. The different orientations of the 2,2'-bipyridyl ligands in the dinuclear complex $[\{Ru(bpy)_2\}_2(bpt)]^{3+}$ accounted for the observed differences in chemical shifts between the two geometrical isomers.[15] Villani and coworkers have successfully separated the stereoisomers of the dinuclear complex $[\{Ru(bpy)_2\}_2(bpt)]^{3+}$ using semipreparative chromatography. The use of a similar chromatographic system to separate the isomers of $[Ru(d_8\text{-}bpy)_2(bpt)Re(CO)_3Cl]^+$ and $[Ru(bpy)_2(bpt)Re(CO)_3Cl]^+$ should be explored.

4.2.3 Infra red spectroscopy

IR spectra of the complexes were recorded in the CO stretching region (2200 – 1700 cm^{-1}) of the IR spectrum. All of the complexes have spectra, which are dominated by three metal carbonyl bands. The carbonyl stretching frequencies in THF are summarised in Table 4. 3. Data for $[Re(CO)_3(bpy)Cl]$ is also included for comparative purposes. A comparison of the stretching frequencies of the mono and dinuclear complexes to those of $[Re(CO)_3(bpy)Cl]$,[45,46] reveals that the CO ligands are in a facial isomer arrangement around the rhenium(I) metal centre. Figure 4. 13 shows the IR spectra of $[Re(CO)_3(bpt)Cl]^-$ and $[Ru(bpy)_2(bpt)Re(CO)3Cl]^+$.

Complex	ν_{CO} (cm^{-1})		
$[Re(CO)_3(bpy)Cl]$	2018	1917	1892
$[Re(CO)_3(Hbpt)Cl]$	2022	1913	1889
$[Re(CO)_3(bpt)Cl]^-$	2012	1904	1879
$[\{Re(CO)_3Cl\}_2(Hbpt)]$	2029	1917	1897
$[Ru(bpy)_2(bpt)Re(CO)_3Cl]^+$	2021	1912	1889
$[Ru(d_8\text{-}bpy)_2(bpt)Re(CO)_3Cl]^+$	2021	1912	1889

Table 4. 3 *IR data for the carbonyl stretching of the metal complexes. All measurements are in THF. The spectrum of $[Re(CO)_3(bpt)Cl]^-$ was recorded in the presence of triethylamine.*

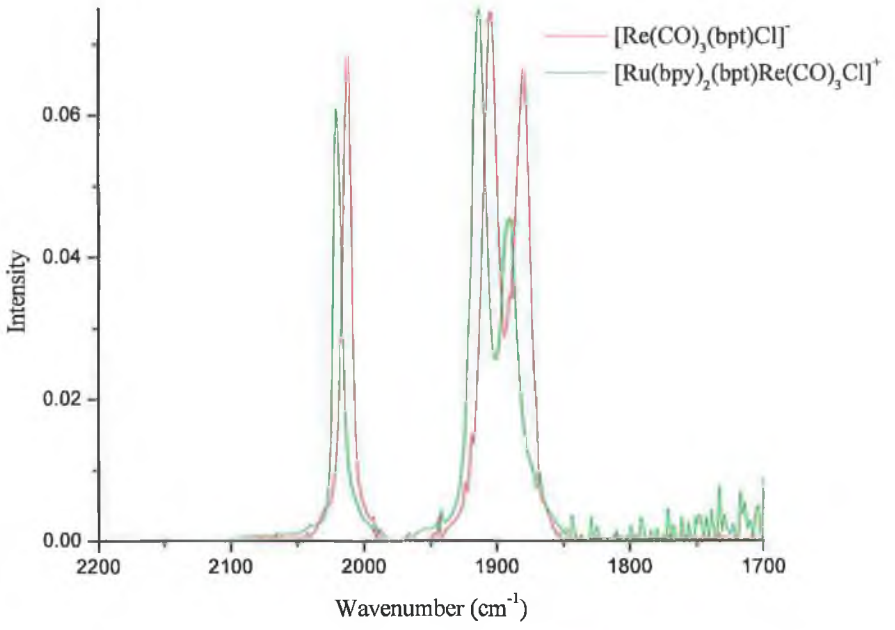

Figure 4. 13 *IR spectra (CO-stretching region) of $[Re(CO)_3(bpt)Cl]^-$ and $[Ru(bpy)_2(bpt)Re(CO)_3Cl]^+$ in THF at 298 K. Note the spectrum of $[Re(CO)_3(bpt)Cl]^-$ was recorded in the presence of triethylamine.*

The carbonyl stretching frequencies can be used to provide an insight into the electronic properties of the bridging ligands in dinuclear rhenium tricarbonyl complexes. Previous work suggests both the σ-donating and π-accepting abilities of the bridging ligand must be considered.[47,48] Therefore the IR spectra of the mononuclear complexes will be discussed first. The metal carbonyl stretching frequencies of $[Re(CO)_3(Hbpt)Cl]$ in THF are similar to those of $[Re(CO)_3(bpy)Cl]$ (Table 4. 3). Deprotonation of $[Re(CO)_3(Hbpt)Cl]$ yields $[Re(CO)_3(bpt)Cl]^-$, which has a negative charge present on the triazole. The presence of the negative charge on the triazole increases the σ-donor ability of the triazole ligand. The increased σ-donor ability of the triazole ligand increases the electron density on the rhenium metal centre, thus enhancing the back-bonding interaction between the rhenium d_π orbitals and the CO π* orbitals. As a result the CO bond lengthens and the CO vibrations of $[Re(CO)_3(bpt)Cl]^-$ are observed at lower frequency compared to $[Re(CO)_3(Hbpt)Cl]$ and $[Re(CO)_3(bpy)Cl]$. Similar trends were observed in the IR spectra of rhenium tricarbonyl chelates of azopyrimidine and azoimidazole on formation of the corresponding anion radicals.[49]

Coordination of a second $Re(CO)_3Cl$ moiety to $[Re(CO)_3(Hbpt)Cl]$ results in only minor IR spectral changes. Three CO bands are observed in the IR spectrum of $[\{Re(CO)_3Cl\}_2(Hbpt)]$, although the CO bands are observed at higher frequency compared to the mononuclear complex $[Re(CO)_3(Hbpt)Cl]$. This observation can be explained by a reduction in the electron density on the Hbpt bridging ligand on coordination of a second $Re(CO)_3Cl$ fragment. This reduces the electron density available for back-bonding between the rhenium d_π and the CO π* orbitals, resulting in the observed increase in CO stretching frequencies of $[\{Re(CO)_3Cl\}_2(Hbpt)]$ compared to $[Re(CO)_3(Hbpt)Cl]$.

The IR spectra of the dinuclear complexes $[Ru(bpy)_2(bpt)Re(CO)_3Cl]^+$ and $[Ru(d_8\text{-}bpy)_2(bpt)Re(CO)_3Cl]^+$ exhibit three CO bands at similar frequency (Table 4. 3). As expected, deuteriation of the 2,2'-bipyridyl ligands in $[Ru(d_8\text{-}bpy)_2(bpt)Re(CO)_3Cl]^+$ has no effect on the CO stretching frequencies (see Table

4. 3). $[Ru(bpy)_2(bpt)Re(CO)_3Cl]^+$ and $[Ru(d_8\text{-}bpy)_2(bpt)Re(CO)_3Cl]^+$ both contain the deprotonated bpt ligand. Surprisingly the CO vibrations of these complexes are observed at higher frequency compared to $[Re(CO)_3(bpt)Cl]^-$. It is possible the presence of the $Ru(bpy)_2$ fragment reduces the electron density on the bpt^- ligand. Hence the back-bonding interaction between the rhenium metal centre and the carbonyl ligands is reduced. This results in the shift to higher frequency for the CO vibrations in $[Ru(bpy)_2(bpt)Re(CO)_3Cl]^+$ and $[Ru(d_8\text{-}bpy)_2(bpt)Re(CO)_3Cl]^+$ compared to $[Re(CO)_3(bpt)Cl]^-$. $[Ru(d_8\text{-}bpy)_2(bpt)Re(CO)_3Cl]^+$ was isolated as two isomers, Isomer I and Isomer II. No differences were observed in the IR spectra of the two isomers. This is not surprising as both Isomer I and Isomer II have similar bonding properties toward the rhenium(I) metal centre thus keeping the local symmetry close to C_s. Hence three similar bands are observed in the IR spectra of each fraction. The ^1H NMR spectrum of the heterodinuclear complex $[(\eta^5\text{-}C_5Me_5)ClRh(\mu\text{-}bptz)Re(CO)_3Cl](PF_6)$ (bptz = 3,6-bis-(2-pyridyl)-1,2,4,5-tetrazine) showed the formation of two isomers.[42] Note, only one isomer was detected in the IR spectrum.

4.2.4 Absorption and emission studies

Absorption and emission data for all complexes discussed in this chapter are presented in Table 4. 4. The table also contains data for $[Re(CO)_3(bpy)Cl]$ and $[Ru(bpy)_3]^{2+}$ and $[\{Ru(bpy)_2\}_2(bpt)]^{3+}$.

Complex	298 K			77 K
	λ_{abs} (nm)[a]/ $\varepsilon \times 10^3$ ($M^{-1}cm^{-1}$)	λ_{em} (nm)[a]/ τ (ns)[b]	ϕ[b]	λ_{em}(nm)[b] /τ (μs)[b]
$[Re(CO)_3(bpy)Cl]$	390 (3.7)	600 (54)	0.0058	530 (2.68)
$[Re(CO)_3(Hbpt)Cl]$	360 (3.6)	540 (< 20)	0.0023	480 (5.80)
$[Re(CO)_3(bpt)Cl]^-$	300 (2.1)	520 (48)	0.0028	480 (6.17)
$[\{Re(CO)_3Cl\}_2(Hbpt)]$	319 (8.0)	533 (45)	0.0112	490 (6.57)
$[\{Re(CO)_3Cl\}_2(bpt)]^-$	314 (6.4)	528 (220)	0.0109	485 (6.41)
$[Ru(bpy)_2(bpt)]^+$	475 (11.3)	675 (160)	0.0126	608 (3.00)
$[Ru(d_8\text{-bpy})_2(bpt)]^+$	475 (11.3)	675 (207)	0.0143	608 (4.49)
$[Ru(bpy)_2(bpt)Re(CO)_3Cl]^+$	440 (16)	635 (267)	0.0030	595 (4.88)
$[Ru(d_8\text{-bpy})_2(bpt)Re(CO)_3Cl]^+$				
Isomer I	440 (16)	635 (430)	0.0038	595 (6.71)
Isomer II	440 (16)	635 (425)	0.0042	595 (6.49)
$[\{Ru(bpy)_2\}_2(bpt)]^{3+}$.	453 (22.6)	648 (100)	0.0020	608 (3.60)
$[Ru(bpy)_3]^{2+}$	452 (12.9)	615 (610)	0.0280	582 (5.09)

Table 4. 4 *Absorption maxima and luminescence properties of the complexes containing the 3,5-bis(pyridin-2-yl)-1,2,4-triazole ligand. τ refers to the emission lifetime while ϕ denotes the radiative quantum yield. [a]Measured in acetonitrile, [b] in deoxygenated acetonitrile, [c] in ethanol:methanol (4:1).*

4.2.4.1 Absorption spectra of the mononuclear complexes

An understanding of the absorption spectra of $[Ru(bpy)_2bpt]^+$, $[Re(CO)_3(Hbpt)Cl]$ and $[Re(CO)_3(bpt)Cl]^-$ is essential before interpretation of the absorption spectra of the dinuclear complexes (Section 4.2.4.1). The absorption spectrum of $[Ru(bpy)_2bpt]^+$ will be discussed firstly. Figure 4. 14 displays the absorption spectra of $[Ru(bpy)_2bpt]^+$ and $[Ru(bpy)_3]^{2+}$. The absorption maximum of $[Ru(bpy)_2bpt]^+$ obtained in these studies (Table 4. 4 and Figure 4. 14) is in agreement with that previously reported by Hage.[15,17]

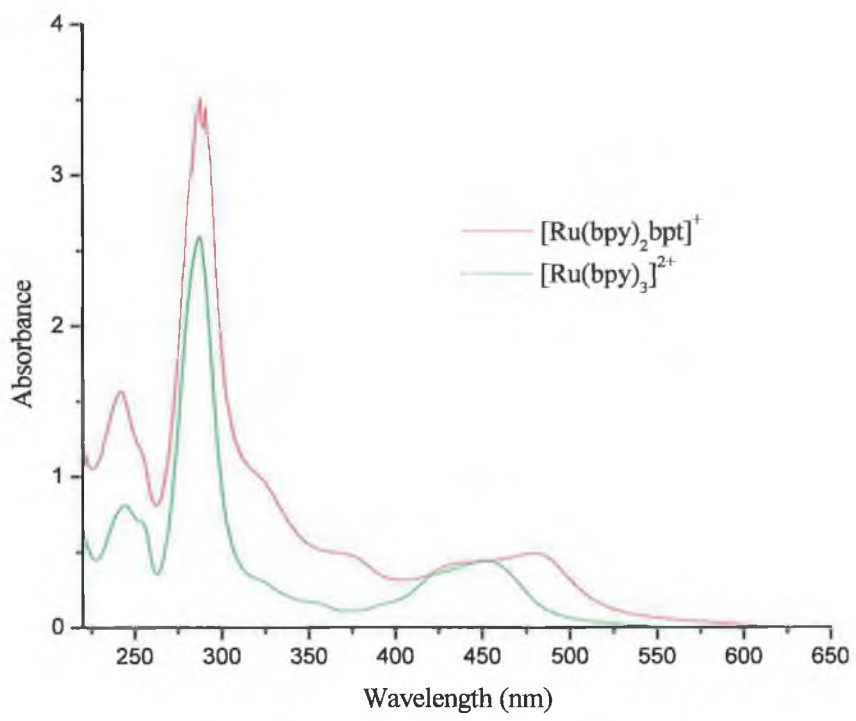

Figure 4. 14 *Absorption spectra of* $[Ru(bpy)_2bpt]^+$ *and* $[Ru(bpy)_3]^{2+}$ *in acetonitrile at 298 K.*

$[Ru(bpy)_3]^{2+}$ has an MLCT ($Ru \rightarrow \pi^*(bpy)$) absorption maximum at 452 nm (Table 4. 4 and Figure 4. 14).[50] The absorption maximum of $[Ru(bpy)_2bpt]^+$ is red shifted by 23 nm to 475 nm when compared to $[Ru(bpy)_3]^{2+}$. Pyridyl-triazole ligands are strong σ-donors.[16] As the bpt^- ligand donates electron density to the metal centre, the energy of the HOMO is increased. Consequently the gap between the HOMO and the LUMO is reduced. Hence a red shift is observed in the absorption maximum of $[Ru(bpy)_2bpt]^+$ compared to $[Ru(bpy)_3]^{2+}$ (see Figure 4. 14). Previous resonance Raman measurements assign the lowest energy absorption band of $[Ru(bpy)_2bpt]^+$ as an $Ru \rightarrow \pi^*(bpy)$ MLCT transition.[18] No $Ru \rightarrow \pi^*(bpt^-)$ transitions were observed in this absorption band in the resonance Raman studies. Deuteriation can affect the vibrational fine structure of absorption spectra, however these differences are only observed at very low temperatures (< 10 K) with high resolution spectroscopic techniques.[51] Hence the absorption maxima of $[Ru(d_8\text{-bpy})_2bpt]^+$ and $[Ru(bpy)_2bpt]^+$ were found to be independent of the level of deuteriation (see Table 4. 4).

The absorption spectra of $[Re(CO)_3(Hbpt)Cl]$ and $[Re(CO)_3(bpt)Cl]^-$ are shown in Figure 4. 15. For $[Re(CO)_3(Hbpt)Cl]$ the lowest absorption maximum occurs at 360 nm. In comparison to the absorption spectra of $[Re(CO)_3(bpy)Cl]$, the pyridyl-triazole complexes synthesised in Chapter 2 and other rhenium complexes containing polypyridyl type ligands, the low energy absorption band in $[Re(CO)_3(Hbpt)Cl]$ is assigned to a ^{1}MLCT transition.[45,52,53] Like the pyridyl-triazole complexes synthesised in Chapter 2, the absorption maximum of $[Re(CO)_3(Hbpt)Cl]$ is found at higher energy compared to that of $[Re(CO)_3(bpy)Cl]$ (Table 4. 4). The Hbpt ligand is a better σ-donor than 2,2'-bipyridyl.[54] Hence the π^* level of the Hbpt ligand is at higher energy compared to 2,2'-bipyridyl. This results in a larger energy gap between the HOMO and the LUMO of $[Re(CO)_3(Hbpt)Cl]$ compared to $[Re(CO)_3(bpy)Cl]$. Consequently the absorption maximum of $[Re(CO)_3(Hbpt)Cl]$ is blue shifted compared to $[Re(CO)_3(bpy)Cl]$.

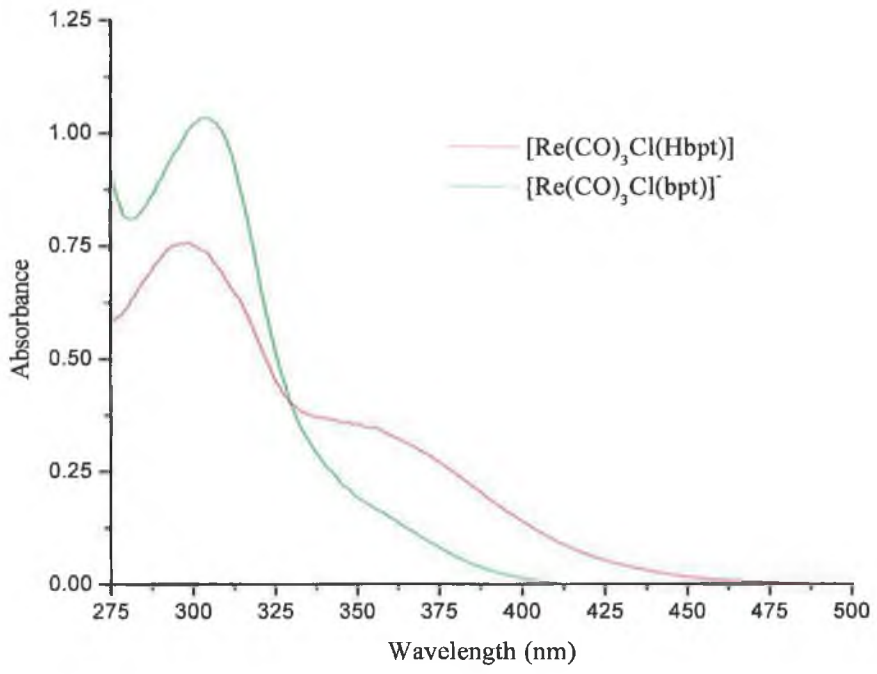

Figure 4. 15 *Absorption spectra of [Re(CO)$_3$(Hbpt)Cl] and [Re(CO)$_3$(bpt)Cl]$^-$ in acetonitrile at 298 K. The spectrum of [Re(CO)$_3$(bpt)Cl]$^-$ was recorded in the presence of triethylamine.*

Figure 4. 3 and Table 4. 4 indicate that the absorption maximum in [Re(CO)$_3$(Hbpt)Cl] depends on whether the triazole ligand is protonated or deprotonated. For the protonated species ([Re(CO)$_3$(Hbpt)Cl]), the absorption maximum is at lower energy than in the deprotonated form ([Re(CO)$_3$(bpt)Cl]$^-$). Such a spectral shift is in agreement with the protonation/deprotonation shifts observed for the pyridyl-triazole complexes synthesised in Chapter 2 (see Table 2.4). For example, the pyridyl-triazole complex [Re(CO)$_3$(Hpytr)Cl] (where Hpytr = 3-(pyridin-2-yl)-1,2,4-triazole) has an absorption maximum of 330 nm, while the deprotonated form [Re(CO)$_3$(pytr)Cl]$^-$ has an absorption maximum of 300 nm. Similarly [Re(CO)$_3$(Hbpt)Cl], has an absorption maximum of 360 nm while [Re(CO)$_3$(bpt)Cl]$^-$ has an absorption maximum of 300 nm. Deprotonation

of the Hbpt ligand generates the negatively charged bpt^- anion, which is a much better σ-donor.[15] The increased σ-donor abilities of the ligand shifts the MLCT band to higher energy. It is likely the MLCT band in $[Re(CO)_3(bpt)Cl]^-$ is obscured by $\pi \rightarrow \pi^*$ transitions associated with the bpt^- ligand (Figure 4. 15). Similar trends were observed with rhenium complexes containing strong σ-donating imidazole type ligands.[55]

4.2.4.2 Absorption spectra of the dinuclear complexes

The absorption spectra of $[\{Re(CO)_3Cl\}_2(Hbpt)]$ and $[Re(CO)_3(Hbpt)Cl]$ are presented in Figure 4. 16. Like the mononuclear analogue, the low energy absorption band of $[Re(CO)_3(Hbpt)Cl]$ is assigned to a ^{1}MLCT transition.

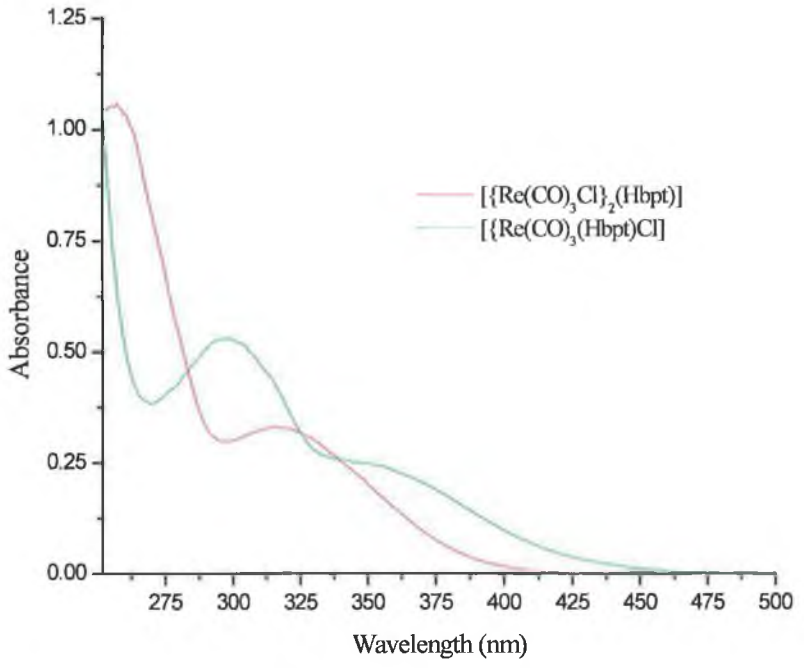

Figure 4. 16 *Absorption spectra of $[\{Re(CO)_3Cl\}_2(Hbpt)]$ and $[Re(CO)_3(Hbpt)Cl]$ in acetonitrile at 298 K.*

For the dinuclear complex the lowest MLCT band is found at higher energy than the corresponding transition in the mononuclear analogue $[Re(CO)_3(Hbpt)Cl]$ (see Figure 4. 16 and Table 4. 1). $[Re(CO)_3(Hbpt)Cl]$ has an absorption maximum at 360 nm, whereas $[\{Re(CO)_3Cl\}_2(Hbpt)]$ has an absorption maximum at 319 nm. This is in contrast to results reported for other dinuclear systems where the absorption maximum is red shifted when compared with the absorption maxima of the mononuclear analogues. [47,48,56,57] In dinuclear complexes containing bridging ligands with low-lying π^* orbitals, attachment of a second $Re(CO)_3Cl$ moiety to the bridging ligand lowers the π^* orbitals of the bridge and a red shift in the MLCT band is observed.[47,48,56] For example the mononuclear complex $[Re(CO)_3(2,3\text{-dpp})Cl]$ (2,3-dpp = 2,3-bis-(2-pyridyl)-pyrazine) has an absorption maximum at 406 nm while the dinuclear complex $[\{Re(CO)_3Cl\}_2(2,3\text{-dpp})]$ has an absorption maximum at 454 nm.[47]

A similar blue shift in the MLCT band has been reported for mononuclear and dinuclear ruthenium complexes containing the bpt^- ligand.[15,17] For example the mononuclear complex $[Ru(bpy)_2bpt]^+$ has an absorption maximum of 475 nm whereas the dinuclear complex $[\{Ru(bpy)_2\}_2bpt]^{3+}$ has an absorption maximum of 453 nm.[15,17] This blue shift has been attributed to the sharing of the negative charge of the triazole upon coordination of the second $Ru(bpy)_2$ unit to the bpt^- ligand. This effect causes a decrease in electron density on the metal centres and a blue shift of the MLCT band. Like the dinuclear complex $[\{Ru(bpy)_2\}_2bpt]^{3+}$, coordination of a second $Re(CO)_3Cl$ fragment to the mononuclear complex $[Re(CO)_3(Hbpt)Cl]$ also results in a sharing of the electron donating ability of the Hbpt ligand between two rhenium(I) metal centres. This stabilises the HOMO, resulting in a larger energy gap between the HOMO and the LUMO in the binuclear complex $[\{Re(CO)_3Cl\}_2(Hbpt)Cl]$ compared to the mononuclear complex $[Re(CO)_3(Hbpt)Cl]$. The larger energy gap between the HOMO and the LUMO manifests itself as a higher energy absorption maximum.

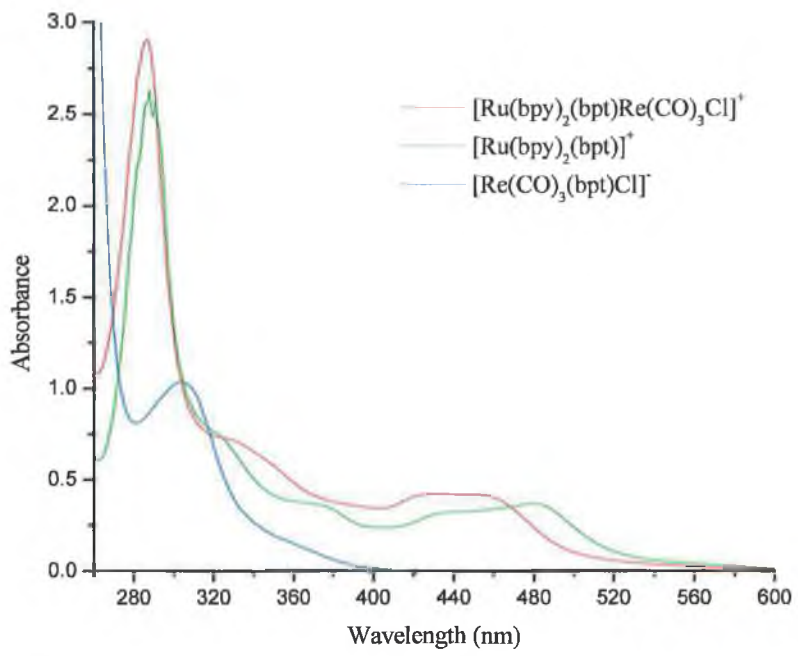

Figure 4. 17 *Absorption spectra of $[Ru(bpy)_2(bpt)Re(CO)_3Cl]^+$, $[Ru(bpy)_2bpt]^+$ and $[Re(CO)_3(bpt)Cl]^-$ in acetonitrile at 298 K. The spectrum of $[Re(CO)_3(bpt)Cl]^-$ was recorded in the presence of triethylamine.*

The absorption spectra of $[Ru(bpy)_2(bpt)Re(CO)_3Cl]^+$, $[Ru(bpy)_2bpt]^+$ and $[Re(CO)_3(bpt)Cl]^-$ are displayed in Figure 4. 17. The absorption maxima of the complexes are summarised in Table 4. 4. As expected, there is no difference in the absorption maxima between $[Ru(bpy)_2(bpt)Re(CO)_3Cl]^+$and its deuteriated analogue $[Ru(d_8\text{-}bpy)_2(bpt)Re(CO)_3Cl]^+$ (see Table 4. 4). The formation of isomers was observed in the ^1H NMR spectra of $[Ru(bpy)_2(bpt)Re(CO)_3Cl]^+$ and $[Ru(d_8\text{-}bpy)_2(bpt)Re(CO)_3Cl]^+$ (Section 4.2.2.2). No differences were observed in the absorption spectra of the two isomers of $[Ru(d_8\text{-}bpy)_2(bpt)Re(CO)_3Cl]^+$. The absorption spectrum of the heteronuclear complex $[Ru(bpy)_2(bpt)Re(CO)_3Cl]^+$ has an absorption band maximum at 440 nm. In comparison to the absorption spectrum of the mononuclear complex $[Ru(bpy)_2bpt]^+$, this absorption is classed as a Ru→π*(bpy) MLCT transition. An Re→π*(bpt^-) transition can be ruled out

as such a transition in the mononuclear derivative is observed at much higher energy (Table 4. 4 and Figure 4. 17). A blue shift of 35 nm was observed in the absorption maximum of $[Ru(bpy)_2(bpt)Re(CO)_3Cl]^+$ compared to the mononuclear complex $[Ru(bpy)_2bpt]^+$. Such a large blue shift has not been observed in other dinuclear Ru(II)/Re(I) complexes. For example Ward and coworkers have synthesised a number of Ru(II)/Re(I) dimers containing the asymmetric ligand 2,2':3',2":6",2"'-quaterpyridine (AB).[58] The heteronuclear complex $[Ru(bpy)_2(AB)Re(CO)_3Cl]^{2+}$ exhibits a ruthenium-based ^{1}MLCT band maximum at 456 nm while the ^{1}MLCT band maximum for the mononuclear complex $[Ru(bpy)_2(AB)]^{2+}$ is observed at 457 nm. As previously discussed, for dinuclear ruthenium complexes containing the bpt^- bridging ligand, coordination of a second $Ru(bpy)_2$ unit to the mononuclear complex $[Ru(bpy)_2bpt]^+$ shifts the absorption maximum from 475 nm to 453 nm.[15] This shift was attributed to a sharing of the negative charge of the triazolate anion upon coordination of the second $Ru(bpy)_2$ unit to the bpt^- ligand. The differences in the absorption maxima of $[Ru(bpy)_2(bpt)Re(CO)_3Cl]^+$ and $[Ru(bpy)_2bpt]^+$ may also be due to a sharing of the electron density of the bpt anion between the $Ru(bpy)_2$ and $Re(CO)_3Cl$ units. This causes a decrease in electron density on the metal centres and results in a blue shift in the Ru→π*(bpy) MLCT transition of $[Ru(bpy)_2(bpt)Re(CO)_3Cl]^+$ compared to $[Ru(bpy)_2bpt]^+$.

A shoulder is observed in the absorption spectrum of $[Ru(bpy)_2(bpt)Re(CO)_3Cl]^+$ at ~ 340 nm (Figure 4. 17). By comparison with the absorption spectrum of $[Re(CO)_3(bpt)Cl]^-$, it is possible this transition could be Re→π*(bpt^-) based. However, ground-state resonance Raman measurements should be performed in the future in order to confirm the exact electronic structure of this shoulder. Both the mononuclear complex $[Ru(bpy)_2bpt]^+$ and the dinuclear complex $[Ru(bpy)_2(bpt)Re(CO)_3Cl]^+$ exhibit intense absorptions between 270 and 295 nm. The position and shape of these bands are characteristic of ligand centred (LC) transitions.[2a]

4.2.4.3 Emission properties of the mononuclear complexes

To enable an understanding of the emission properties of the dinuclear complexes, it is helpful to firstly analyse the emission spectra of the monometallic precursors. The emission spectra of the mononuclear ruthenium complex $[Ru(bpy)_2bpt]^+$ at 298 K and 77 K are shown in (Figure 4. 18). The emission properties of this complex are well understood.[15,17,54] At 298 K and 77 K, emission from $[Ru(bpy)_2bpt]^+$ originates from a ^{3}MLCT state. This ^{3}MLCT state is bpy-based both at 298 K and 77 K. In ruthenium polypyridyl complexes, deuteriation of one of the ligands in a mixed ligand complex will only affect the emission lifetime if the emitting state is based on that ligand.[16,21,59] This is clearly evident for $[Ru(bpy)_2bpt]^+$ and its deuteriated analogue $[Ru(d_8\text{-}bpy)_2bpt]^+$. For $[Ru(bpy)_2bpt]^+$ emission lifetimes of 160 ns (298 K) and 3.00 μs (77 K) were observed. Deuteriation of the 2,2'-bipyridine ligands leads to lifetimes of 200 ns (298 K) and 4.49 μs (77 K). This further supports the conclusion that the emitting state is located on the bpy-ligands.

Note the emission maximum blue shifts on cooling to 77 K (Table 4. 4 and Figure 4. 18). This observed emission temperature dependence is a result of rigidchromism.[54] At 77 K, the solvent dipoles are immobile on the timescale of the excited state and so cannot respond to the change in electronic configuration that accompanies an excitation. Hence the emission maximum blue shifts on cooling to 77 K. In addition to the blue shift on cooling to 77 K, the shape of the spectrum changes to one exhibiting more vibrational structure. Similar vibrational fine-structure has been observed for other ruthenium polypyridine complexes and this fine-structure has been attributed to relaxation via bipyridine-based vibrations.[60]

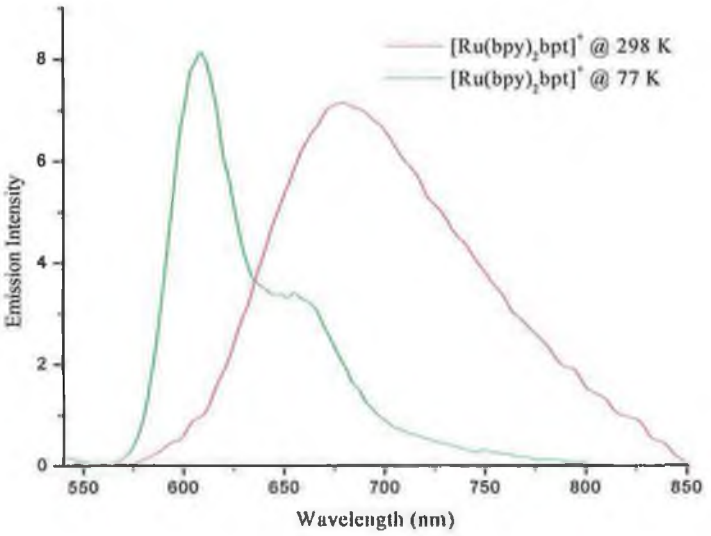

Figure 4. 18 *Emission spectra of $[Ru(bpy)_2bpt]^+$ at 298 K and 77 K. The spectra were obtained at 298 K in acetonitrile and ethanol:methanol 4:1 at 77 K.*

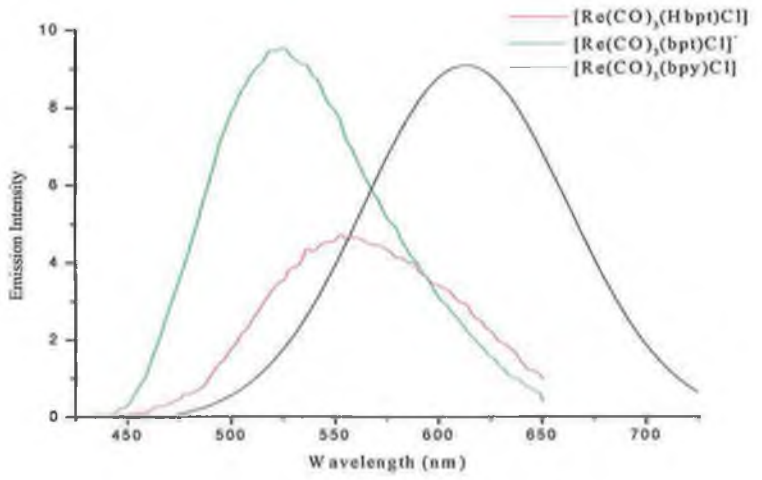

Figure 4. 19 *Emission spectra of $[Re(CO)_3(Hbpt)Cl]$, $[Re(CO)_3(bpt)Cl]^-$ and $[Re(CO)_3(bpy)Cl]$ in acetonitrile at 298 K.*

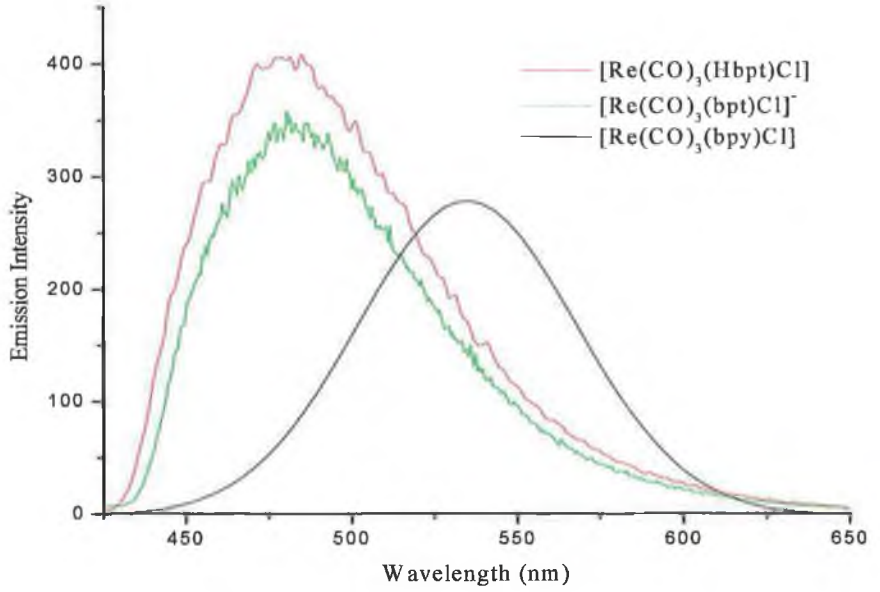

Figure 4. 20 *Emission Spectra at 77 K in ethanol:methanol (4:1) of [Re(CO)$_3$(Hbpt)Cl], [Re(CO)$_3$(bpt)Cl]$^-$ and [Re(CO)$_3$(bpy)Cl].*

Room temperature emission spectra of [Re(CO)$_3$(Hbpt)Cl] and [Re(CO)$_3$(bpt)Cl]$^-$ were recorded in acetonitrile. Figure 4. 19 displays the emission spectra for [Re(CO)$_3$(Hbpt)Cl], [Re(CO)$_3$(bpt)Cl]$^-$ and [Re(CO)$_3$(bpy)Cl] at 298 K. Note the emission maxima of [Re(CO)$_3$(Hbpt)Cl] and [Re(CO)$_3$(bpt)Cl]$^-$ were blue shifted relative to the reference complex [Re(CO)$_3$(bpy)Cl]. The emission maximum of [Re(CO)$_3$(bpt)Cl]$^-$ (λ_{max} = 520 nm) is blue shifted relative to its protonated analogue [Re(CO)$_3$(Hbpt)Cl] (λ_{max} = 540 nm). Such a spectral shift is in agreement with the protonation/deprotonation shifts observed for the pyridyl-triazole complexes synthesised in Chapter 2 (see Table 2. 4). Note, the pyridyl-triazole complex [Re(CO)$_3$(Hpytr)Cl] has an emission maximum of 580 nm, while the deprotonated form [Re(CO)$_3$(pytr)Cl]$^-$ has an emission maximum of 530 nm. The emission observed for [Re(CO)$_3$(Hbpt)Cl] and [Re(CO)$_3$(bpt)Cl]$^-$ was found to be temperature dependent. The emission maxima of both [Re(CO)$_3$(Hbpt)Cl]

and $[Re(CO)_3(bpt)Cl]^-$ shift to higher energy when cooled to 77 K (see Table 4. 1 and Figure 4. 19). It is worth noting the emission spectra of $[Re(CO)_3(Hbpt)Cl]$ and $[Re(CO)_3(bpt)Cl]^-$ are broad and structureless at 77 K (Figure 4. 20). The protonated/deprotonated complexes $[Re(CO)_3(Hbpt)Cl]$ and $[Re(CO)_3(bpt)Cl]^-$ both exhibit emission maxima of 480 nm at 77 K. The emission maxima and lifetimes obtained at 298 K and 77 K are summarised in Table 4. 4.

For both $[Re(CO)_3(Hbpt)Cl]$ and $[Re(CO)_3(bpt)Cl]^-$ the excited state responsible for the luminescence is of MLCT nature. This assignment is based on the following luminescence properties:

i) The position and shape of the emission band at 298 K is consistent with that of $[Re(CO)_3(bpy)Cl]$ and other rhenium(I) complexes assigned as MLCT emitters[45,52]

ii) The luminescence lifetimes and quantum yields are similar to those of $[Re(CO)_3(L)Cl]$ with L = bipyridine type ligand[52,61]

iii) At 77 K the emission spectra are broad and strongly shifted to higher energy compared to the spectra at room temperature[62,63]

iv) The time range of the 77 K emission is typical of Re-based MLCT emitters[64]

In addition, pK_a studies of the pyridyl-triazole complexes $[Re(CO)_3(Hpytr)Cl]$ and $[Re(CO)_3(HBrpytr)Cl]$ (where HBrpytr = 3-(pyridin-2-yl)-5-bromo-1,2,4-triazole) in Chapter 2 show the co-ordinated pyridyl-triazole is less acidic in the excited state than in the ground state i.e. both complexes have a higher pK_a^* compared to the pK_a (see Table 2. 5). This is an important observation; since it shows the triazole ligands actively participate in the emission processes i.e. the electron resides in the pyridyl-triazole after excitation of the complex. Unfortunately $[Re(CO)_3(Hbpt)Cl]$ was insoluble in Britton-Robinson buffer (the solvent used to carry out the pK_a titrations in Chapter 2). Hence no pK_a or pK_a^* values are available for this complex. However, $[Re(CO)_3(Hbpt)Cl]$ exhibited similar protonation/deprotonation shifts to the pyridyl-triazole complexes

$[Re(CO)_3(Hpytr)Cl]$ and $[Re(CO)_3(HBrpytr)Cl]$ at 298 K. Hence it is reasonable to conclude that the Hbpt ligand actively participates in the emission processes i.e. the emission originates from a $^3MLCT(Ru \rightarrow \pi^*(Hbpt))$ state.

As observed for the absorption spectra, the position of the emission maximum is blue shifted with respect to $[Re(CO)_3(bpy)Cl]$ (600 nm) when the Hbpt ligand is both protonated and deprotonated (i.e. 540 nm vs 520 nm in the case of $[Re(CO)_3(Hbpt)Cl]$ compared to $[Re(CO)_3(bpt)Cl]^-$). 2,2'-bipyridine is a better π-acceptor than bpt^-, and hence has a lower π* level.[23,24] This is reflected in the higher Ru(II)/Ru(III) oxidation potential of the mononuclear ruthenium complex $[Ru(bpy)_2bpt]^+$ compared to $[Ru(bpy)_3]^{2+}$.[15] Furthermore, the first reduction potential of $[Ru(bpy)_2bpt]^+$ is 2,2'-bipyridyl based. In addition resonance Raman spectra of $[Ru(bpy)_2bpt]^+$ also suggest that the π*-orbital of 2,2'-bipyridyl is of lower energy compared to that of the corresponding bpt^- level.[17] Hence it seems reasonable to conclude the blue shift in the emission maxima of $[Re(CO)_3(Hbpt)Cl]$ and $[Re(CO)_3(bpt)Cl]^-$ compared to $[Re(CO)_3(bpy)Cl]$ most likely arises from the increased energy of the LUMO of the electron donating triazole ligand compared to 2,2'-bipyridyl. This increases the energy gap between the ground and the ^3MLCT states i.e. a blue shift in the emission maxima is observed. Deprotonation of the triazole further enchances the electron donating ability of the Hbpt ligand.[23,24] Hence the energy gap between the ground and ^3MLCT states increases. Consequently the emission maxima of the deprotonated complexes are blue shifted relative to their protonated analogues and $[Re(CO)_3(bpy)Cl]$.

Longer luminescence lifetimes are observed for $[Re(CO)_3(bpt)Cl]^-$ compared to $[Re(CO)_3(Hbpt)Cl]$ at 77 K and 298 K. The two main factors that control emission lifetimes are:

(i) The energy gap law[65,66]

(ii) The gap between the emitting ^3MLCT state and the deactivating ^3MC state [10,67]

The energy gap law states that the coupling between vibrational levels of the ground and excited state increases as the energy gap between these two levels decreases. A weak coupling between the excited- and ground-state vibrational levels will increase the emission lifetime. The increase in emission lifetime from ~ 20 ns to 48 ns at 298 K upon deprotonation of $[Re(CO)_3(Hbpt)Cl]$ is consistent with the observed increase in the energy gap (as indicated in the blue shift emission maximum from 540 to 520 nm).

4.2.4.4 Emission properties of the dinuclear complexes

The emission spectra for $[\{Re(CO)_3Cl\}_2(Hbpt)]$ and $[\{Re(CO)_3Cl\}_2(bpt)]^-$ at 298 K are presented in Figure 4. 21. For both $[\{Re(CO)_3Cl\}_2(Hbpt)]$ and $[\{Re(CO)_3Cl\}_2(bpt)]^-$, the emitting level can be labelled as ^{3}MLCT in character as both the position and shape of the emission band is similar to the mononuclear complexes $[Re(CO)_3(Hbpt)Cl]$ and $[Re(CO)_3(bpt)Cl]^-$ and other complexes assigned as ^{3}MLCT emitters.[55,68] As observed for the absorption spectra, the emission energy of the dinuclear complex $[\{Re(CO)_3Cl\}_2(Hbpt)]$ is at higher energy than that observed for the mononuclear complex (see Table 4. 4). This can be explained by the sharing of the electron donating ability of the Hbpt ligand between the two $Re(CO)_3Cl$ units. Hence less electron density is present at the metal centre, thus resulting in a stabilisation of the t_{2g} energy level (ground-state). For this reason the energy separation between the ground-state and the ^{3}MLCT state increases and a blue shift in the absorption and emission energies is observed (i.e. 533 nm vs 540 nm in the case of $[\{Re(CO)_3Cl\}_2(Hbpt)]$ compared to $[Re(CO)_3(Hbpt)Cl]$). Note this is in contrast to other examples of bimetallic rhenium carbonyl complexes, which contain a strong π-acceptor ligand bridge. In these examples, coordination of a second $Re(CO)_3Cl$ unit stabilises the π* levels of the bridging ligand resulting in a red shift in the emission maxima of the dinuclear complexes. For example coordination of $Re(CO)_3Cl$ to $[Re(CO)_3(2,3\text{-dpp})Cl]$ (2,3-dpp = 2,3-bis-(2-pyridylpyrazine) shifts the emission maximum from 700 to 790 nm.[47,69]

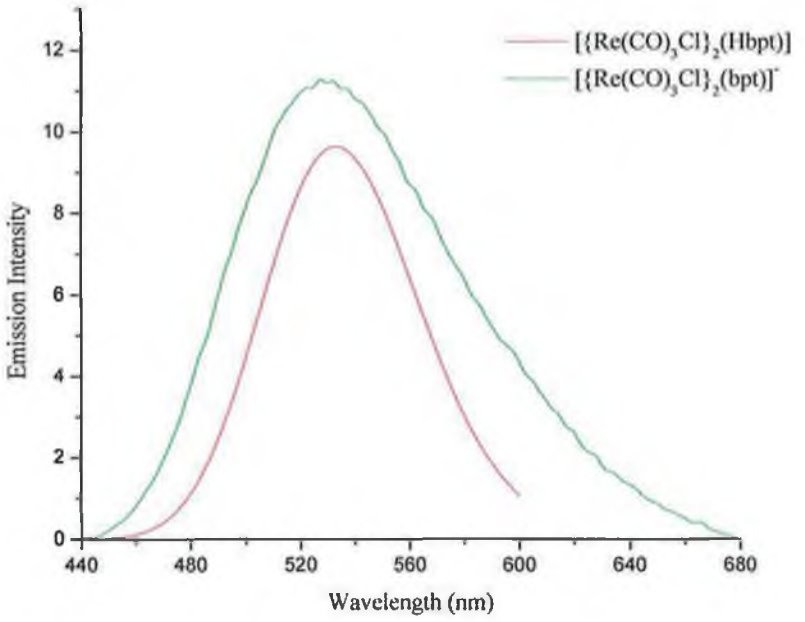

Figure 4. 21 *Emission Spectra at 298 K in acetonitrile of [{Re(CO)$_3$Cl}$_2$(Hbpt)] and [{Re(CO)$_3$Cl}$_2$(bpt)]$^-$.*

Emission spectra of [{Re(CO)$_3$Cl}$_2$(Hbpt)] and [{Re(CO)$_3$Cl}$_2$(bpt)]$^-$ were also recorded at 77 K (Figure 4. 22). A single blue-shifted maximum is observed at 77 K. This shift and lack of vibrational structure is in accord with assignment of these transitions as MLCT in character.[4,52]

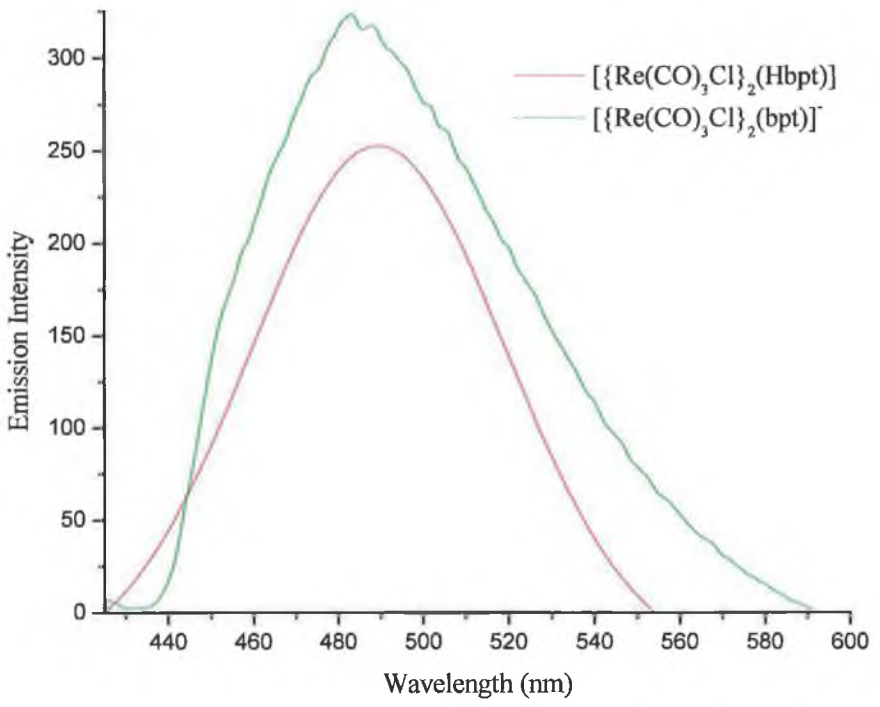

Figure 4. 22 *Emission Spectra at 77 K in ethanol:methanol (4:1) of [{Re(CO)$_3$Cl}$_2$(Hbpt)Cl] and [{Re(CO)$_3$Cl}$_2$(bpt)Cl]$^-$.*

Luminescence lifetimes at 298 K and 77 K are collected in Table 4. 4. The room-temperature luminescence quantum yields are also reported in the table. The lifetimes at 77 K and 298 K of [{Re(CO)$_3$Cl}$_2$(Hbpt)] and [{Re(CO)$_3$Cl}$_2$(bpt)]$^-$ are longer compared to their mononuclear derivatives. A slight increase in the energy gap is observed on coordination of the second Re(CO)$_3$Cl unit to [Re(CO)$_3$(Hbpt)Cl] i.e. the emission maximum blue-shifts from 540 to 533 nm. According to the energy gap law, an increase in the energy gap will increase the emission lifetime. Hence a longer lifetime is observed for [{Re(CO)$_3$Cl}$_2$(Hbpt)] compared to [Re(CO)$_3$(Hbpt)Cl].

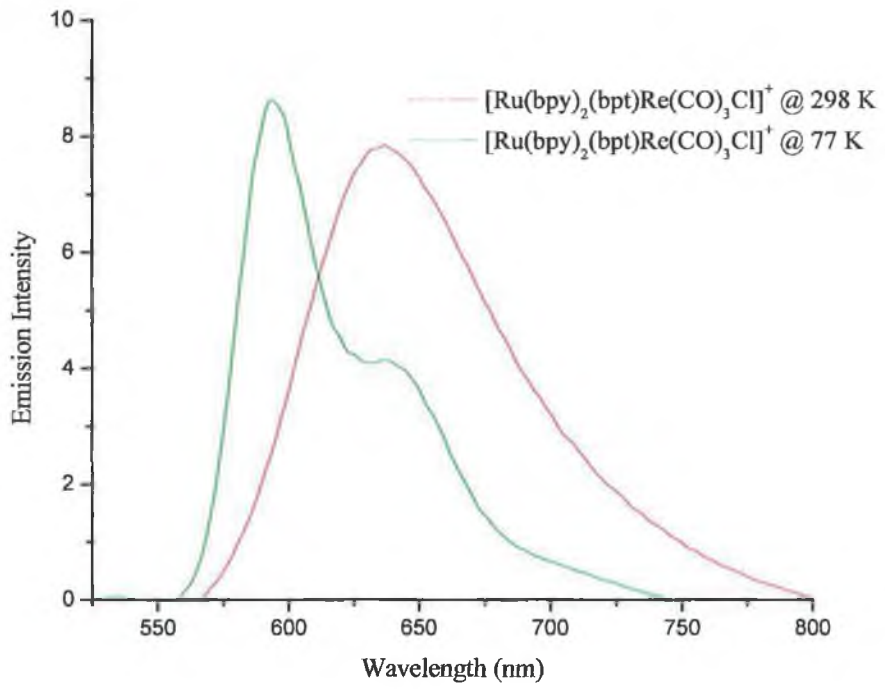

Figure 4. 23 *Emission spectra of $[Ru(bpy)_2(bpt)Re(CO)_3Cl]^+$ at 298 K and 77 K. The spectra were obtained at 298 K in acetonitrile and ethanol:methanol 4:1 at 77 K.*

The emission data of $[Ru(bpy)_2(bpt)Re(CO)_3Cl]^+$ and the two isomers of $[Ru(d_8\text{-}bpy)_2(bpt)Re(CO)_3Cl]^+$ are presented in Table 4. 4. No differences were observed in the emission maxima or lifetimes of the two isomers of $[Ru(d_8\text{-}bpy)_2(bpt)Re(CO)_3Cl]^+$ at 298 K or 77 K. Hence the emission properties of Isomer I and Isomer II will be discussed as $[Ru(d_8\text{-}bpy)_2(bpt)Re(CO)_3Cl]^+$. Figure 4. 23 shows the emission spectra of $[Ru(bpy)_2(bpt)Re(CO)_3Cl]^+$ obtained at 298 K and 77 K. Similar spectra were obtained for the deuteriated complex $[Ru(d_8\text{-}bpy)_2(bpt)Re(CO)_3Cl]^+$.

The heteronuclear complex $[Ru(bpy)_2(bpt)Re(CO)_3Cl]^+$ has an emission maximum of 635 nm while the emission maximum of the mononuclear complex is 675 nm i.e. a blue shift in the emission maximum upon coordination of $Re(CO)_3Cl$ to $[Ru(bpy)_2bpt]^+$ is observed. This is in contrast to other ruthenium(I)/rhenium(I) complexes. For example a red shift in the emission maximum from 638 nm to 646 nm observed upon coordination of $Re(CO)_3Cl$ to $[Ru(dmb)_2(mfibpy)]^{2+}$ (dmb = 4,4'-dimethyl-2,2'-bipyridine; mfibpy = 4-methyl-4'-[1,10]phenanthroline-[5,6-*d*]imidazol-2-yl)bipyridine).[70] This red shift was attributed to a stabilisation of the π^* level of the bridging ligand as a result of coordination of the second metal centre. The blue shift in the emission maximum upon coordination of $Re(CO)_3Cl$ to $[Ru(bpy)_2bpt]^+$ can be evaluated by comparing the luminescence properties of $[Ru(bpy)_2(bpt)Re(CO)_3Cl]^+$ with the dinuclear complex $[\{Ru(bpy)_2\}_2(bpt)]^{3+}$. Likewise a blue shift from 628 nm to 608 nm was observed on coordination of a second $Ru(bpy)_2$ fragment to $[Ru(bpy)_2bpt]^+$.[15] This blue shift was attributed to a sharing of the negative charge of the triazole anion between the two ruthenium metal centres. Thus resulting in a decrease in the electron density on the metal centre leading to an increase in the energy gap between the ground and ^{3}MLCT states. This behaviour causes a blue shift in the emission maximum of $[\{Ru(bpy)_2\}_2(bpt)]^{3+}$ compared to $[Ru(bpy)_2bpt]^+$. The blue shift in the emission maximum of $[Ru(bpy)_2(bpt)Re(CO)_3Cl]^+$ compared to $[Ru(bpy)_2bpt]^+$ may also give rise to an increase in the ground-state and ^{3}MLCT energy gap due to the negative charge of the triazole anion being shared between the two metal centres.

In heteroleptic ruthenium polypyridyl complexes of the form $[Ru(bpy)_2(LL)]^{n+}$ (LL is a bidentate ligand), the excited state may lie on either the bipyridine ligand or LL.[71] Hence the Ru-based lowest excited level in the binuclear complexes $[Ru(bpy)_2(bpt)Re(CO)_3Cl]^+$ and $[Ru(d_8\text{-}bpy)_2(bpt)Re(CO)_3Cl]^+$ could be of Ru→bpy or Ru→bpt$^-$ CT electronic configuration. In $[Ru(bpy)_2(bpt)Re(CO)_3Cl]^+$ and its deuteriated analogue $[Ru(d_8\text{-}bpy)_2(bpt)Re(CO)_3Cl]^+$, the lowest-lying level is tentatively assigned as a ^{3}MLCT (Ru→π^*(bpy)) state. This assignment is based on the following luminescence properties:

(i) The structured emission spectrum at 77 K is similar to that of the bpy-based emitting mononuclear complex $[Ru(d_8\text{-bpy})_2bpt]^+$

(ii) A significant increase in the lifetime is observed at 298 K and 77 K when the bipyridyl ligands are deuteriated

Note vibrational fine-structure has been previously observed for other ruthenium polypyridine complexes at 77 K. This fine-structure has been attributed to relaxation via bipyridine-based vibrations.[2a,60] In previous studies of ruthenium complexes of the form $[Ru(bpy)_2(L)]^+$ (L is a pyridyl-triazole ligand), deuteriation has been used to investigate the location of the excited state.[59,72,73] If the excited state is located on the ligand that has been deuteriated then the excited state lifetime is seen to increase. In $[Ru(bpy)_2(bpt)Re(CO)_3Cl]^+$, deuteriation of the bipyridyl ligands leads to an increase in lifetime from 340 to 430 ns (298 K) and 4.88 μs to 6.71 μs (77 K). This strongly suggests that the excited-state of $[Ru(bpy)_2(bpt)Re(CO)_3Cl]^+$ is bpy-based.

Ward and coworkers have synthesised a number of Ru(II)/Re(I) hetronuclear complexes containing the asymmetric ligand 2,2':3',2":6",2'"-quaterpyridine (AB).[58] The positional isomers $[Re(CO)_3Cl(AB)Ru(bpy)_2]^{2+}$ and $[Ru(bpy)_2(AB)Re(CO)_3Cl]^{2+}$ exhibit either Ru-based or Re-based emission, depending on the coordination sites of the metal. For the heteronuclear complex $[Re(CO)_3Cl(AB)Ru(bpy)_2]^{2+}$ the observed emission at room temperature was assigned to the rhenium(I) metal centre on the basis that its emission energy was similar to that of the mononuclear complex $[Re(CO)_3Cl(AB)]$ and the homodinuclear complex $[\{Re(CO)_3Cl\}_2(AB)]$. For instance $[Re(CO)_3Cl(AB)]$ and $[\{Re(CO)_3Cl\}_2(AB)]$ exhibit rhenium-based emission maxima at 626 nm and 622 nm while the emisison maximum for the heteronuclear complex $[Re(CO)_3Cl(AB)Ru(bpy)_2]^{2+}$ was observed at 623 nm. This is in contrast to $[Ru(bpy)_2(AB)Re(CO)_3Cl]^{2+}$ where ruthenium based emission was observed at 644 nm. For $[Ru(bpy)_2(AB)Re(CO)_3Cl]^{2+}$, excitation at 395 nm (where a significant portion of light is absorbed by the Re- metal centre) or excitation of the

Ru-based metal centre at 456 nm yielded identical luminescence quantum yields (ϕ= 2.7 x 10^{-2}) and emission maximum at 644 nm. Like the heteronuclear complexes containing 2,2':3',2":6",2"'-quaterpyridine, the lowest excited level for $[Ru(bpy)_2(bpt)Re(CO)_3Cl]^+$ and $[Ru(d_8\text{-}bpy)_2(bpt)Re(CO)_3Cl]^+$ can be either Re- or Ru-based. The emission is assigned as Ru-centred in both of these complexes by comparison with the emission properties of $[Re(CO)_3(bpt)Cl]^-$ and $[Ru(bpy)_2bpt]^+$ (see Table 4. 4). Emisison maxima of 520 nm, 675 nm and 635 nm were observed for $[Re(CO)_3(bpt)Cl]^-$, $[Ru(bpy)_2bpt]^+$ and $[Ru(bpy)_2(bpt)Re(CO)_3Cl]^+$. Note Re-based emission from $[Re(CO)_3(bpt)Cl]^-$ occurs at ~115 nm shorter wavelength for $[Re(CO)_3(bpt)Cl]^-$ compared to the heteronuclear complex $[Ru(bpy)_2(bpt)Re(CO)_3Cl]^+$. Like $[Re(CO)_3Cl(AB)Ru(bpy)_2]^{2+}$, the Re-based emission from $[Ru(bpy)_2(bpt)Re(CO)_3Cl]^+$ would be expected to occur at similar wavelength to the analogous mononuclear rhenium(I) complex $[Re(CO)_3(bpt)Cl]^-$. The large energy difference between the emission maxima of $[Re(CO)_3(bpt)Cl]^-$ and $[Ru(bpy)_2(bpt)Re(CO)_3Cl]^+$ does not support Re-based emission from $[Ru(bpy)_2(bpt)Re(CO)_3Cl]^+$.

Furthermore, selective excitation of either the Ru- or Re- based chromophores in $[Ru(bpy)_2(bpt)Re(CO)_3Cl]^+$ can be achieved through excitation wavelengths of 440 and 340 nm respectively. Note at 340 nm, both the Ru- and Re- metal centres absorb, however a significant portion of light is absorbed by the Re- metal centre. Comparison of the luminescence properties under both excitation wavelengths shows the luminescence profiles overlap and the quantum yields are practically identical (ϕ= 0.0036 and 0.0031 for λ_{exc} = 330 nm and 440 nm respectively). Also there is no evidence for a dual exponential decay that would occur if a mixture of Ru- and Re-based emission were occurring. This suggests the lowest lying luminescent centre is Ru-centred in $[Ru(bpy)_2(bpt)Re(CO)_3Cl]^+$. These results indicate the light absorbed by the Re-bpt$^-$ chromophore of $[Ru(bpy)_2(bpt)Re(CO)_3Cl]^+$ is transferred to a ^{3}Ru MLCT state i.e. complete Re→Ru energy transfer takes place. The results also indicate this energy transfer process is temperature independent. The bridging ligand essentialy mediates

energy transfer. Similar Re→Ru energy transfer has been previously reported for other ruthenium/rhenium dinuclear complexes.[69,70,74,75,76]

4.2.5 Electrochemical studies

The electrochemical properties of the complexes are collected in Table 4. 5, together with data for $[Ru(bpy)_3]^{2+}$ and $[Re(CO)_3(bpy)Cl]$ for comparison.

Complex	E (V)					
	Ru (II)/(III)	Re (I)/(II)	Reduction			
$[Re(CO)_3(bpy)Cl]$	—	1.55[b]	-1.29[c]	-1.73[c]	—	—
$[Re(CO)_3(Hbpt)Cl]$	—	1.20[b]	—	—	-1.92[c]	-2.09[c]
$[\{Re(CO)_3Cl\}_2(Hbpt)]$	—	1.40[b]	—	-1.78[c]	-1.90[c]	-2.08[c]
	—	1.55[b]	—	—	—	—
$[Ru(bpy)_2(bpt)Re(CO)_3Cl]^+$	1.09	1.55[b]	-1.41	-1.82[a]	-2.33[a]	—
$[Ru(bpy)_2bpt]^+$	0.92	—	-1.47	-1.70	-2.26	-2.44
$[Ru(bpy)_3]^{2+}$	1.26	—	-1.35	-1.55	-1.80	—

Table 4. 5 *Electrochemical data in acetonitrile with 0.1 M $TBABF_4$ at 100 mV/s scan rate.* [a]*Poorly resolved irreversible sequence of ligand based reductions.* [b]*Anodic peak potential corresponding to an irreversible step.* [c]*Cathodic peak corresponding to an irreversible step.*

The electrochemical behaviour of $[Ru(bpy)_2bpt]^{2+}$ has been discussed previously.[17,54] A reversible Ru(II)/Ru(III) oxidation is observed at 0.85 V. The first and second reduction potentials of $[Ru(bpy)_2bpt]^{2+}$ are assigned to reduction of the coordinated bipyridyl ligands. The two reduction potentials observed at –2.28 V and –2.45 V are associated with the reduction of the bpt^- ligand.[17,54] Note the metal centred oxidation potential of $[Ru(bpy)_2bpt]^{2+}$ is significantly lower than that of $[Ru(bpy)_3]^{2+}$. As explained in Section 4.2.4, the σ-donor ability of the bpt^-

ligand is much stronger than that of bpy. This leads to greater electron density surrounding the ruthenium metal centre of $[Ru(bpy)_2bpt]^{2+}$ compared to $[Ru(bpy)_3]^{2+}$. Hence the ruthenium metal is oxidised at a lower potential in $[Ru(bpy)_2bpt]^{2+}$ in compared to $[Ru(bpy)_3]^{2+}$.

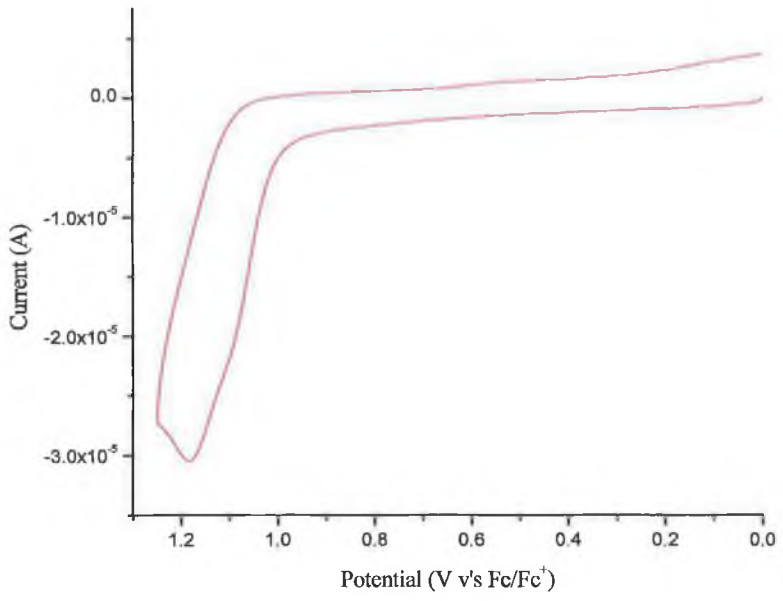

Figure 4. 24 *Cyclic voltammogram of $[Re(CO)_3(Hbpt)Cl]$ in 0.1M $TBABF_4$ in acetonitrile with a scan rate of 100 mV/s.*

The complexes $[Re(CO)_3(Hbpt)Cl]$ and $[\{Re(CO)_3Cl\}_2Hbpt]$ were isolated with a protonated triazole ligand. Upon deprotonation of the triazole with one drop of 0.1 M triethylamine in acetonitrile, poor quality voltammograms were obtained. Hence only the electrochemistry of the protonated complexes, $[Re(CO)_3(Hbpt)Cl]$ and $[\{Re(CO)_3Cl\}_2Hbpt]$ will be discussed. An electrochemically irreversible oxidation was observed at 1.20 V for $[Re(CO)_3(Hbpt)Cl]$ (*Table 4. 5* and *Figure 4. 3*). By comparison with $[Re(CO)_3(bpy)Cl]$ and other rhenium(I) complexes, this irreversible process is assigned to oxidation of the rhenium metal centre (Re(I)/Re(II)).[77,78,79] The Hbpt ligand is a better σ-donor compared to 2,2'-

bipyridyl, therefore the rhenium metal centre is easier to oxidise when coordinated to the Hbpt ligand. Hence the Re(I)/Re(II) oxidation is observed at lower potential for $[Re(CO)_3(Hbpt)Cl]$ compared to $[Re(CO)_3(bpy)Cl]$. Two irreversible reductions were observed at –1.92 and –2.09 V. It is possible these reduction processes correspond to reduction of the Hbpt ligand followed by chloride dissociation as observed for the pyridyl triazole complexes in Chapter 2 and other $[Re(CO)_3(L\text{-}L)Cl]$ type complexes where L-L is a bidentate ligand.[40,8081] A more detailed discussion of the reduction processes of $[Re(CO)_3(Hbpt)Cl]$ cannot be undertaken due to the irreversibility of the reduction waves.

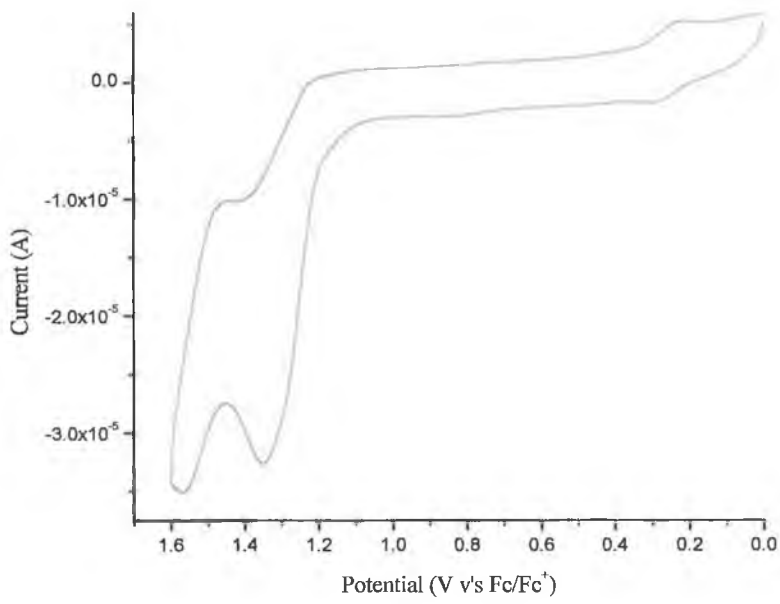

Figure 4. 25 Cyclic voltammogram of $[\{Re(CO)_3Cl\}_2(Hbpt)]$ in 0.1M $TBABF_4$ in acetonitrile with a scan rate of 100 mV/s.

The cyclic voltammogram of the oxidation processes of the rhenium dinuclear complex $[\{Re(CO)_3Cl\}_2(Hbpt)]$ are shown in Figure 4. 25. The first Re(I)/Re(II) couple for the dinuclear complex is observed at 1.33 V. The second Re(I)/Re(II) couple is 250 mV more positive than the first. A number of possibilities can account for this difference in oxidation potentials:

(i) Electrostatic effects: oxidation of the first metal centre increases the charge of the complex and subsequently a higher oxidation potential of the second metal centre will be observed.

(ii) The chemical environments of the two $Re(CO)_3Cl$ moieties are different due to the coordination modes (i.e. N_2 versus N_4).

Previous studies have revealed the N_2 atom of pyridyl-triazole ligands is a better σ-donor site than the N_4 atom.[15] For example, the N_2 bound ruthenium metal centre of $[Ru(bpy)_2(pytr)]^+$ (where pytr = 3-(pyridin-2-yl)-1,2,4-triazole) oxidises at 0.83 V whereas the N_4 bound ruthenium metal oxidises at 0.90 V. Therefore the N_2/N_4 coordination modes of the two metal centres almost certainly contribute to a difference in the oxidation potentials of the two rhenium centres in $[\{Re(CO)_3Cl\}_2(Hbpt)]$. As the N_2 atom has stronger σ-donor properties than the N_4 atom, the $Re(CO)_3Cl$ unit bound at N_2 will most likely be oxidised easier than the N_4 bounded group

Another important point is that the first Re(I)/Re(II) couple of the dinuclear complex is observed at 120 mV higher than the oxidation potential of the Re(I)/Re(II) couple in the mononuclear complex $[Re(CO)_3(Hbpt)Cl]$. Upon coordination of a second $Re(CO)_3Cl$ moiety, the electron density of the Hbpt ligand has to be shared between two $Re(CO)_3Cl$ units. As a result there is less electron density on each metal centre. Hence the first metal-based oxidation is observed at higher oxidation potential for the dinuclear complex compared to the mononuclear complex. The same effect has been observed between the mononuclear $[Ru(bpy)_2bpt]^+$ and dinuclear $[\{Ru(bpy)_2\}_2bpt]^{3+}$ complexes where the first Ru(II)/Ru(III) oxidation of $[\{Ru(bpy)_2\}_2bpt]^{3+}$ is observed at 1.04 V while oxidation of the ruthenium centre in the mononuclear complex $[Ru(bpy)_2bpt]^+$ is observed at 0.85 V.[15,17] A series of irreversible reduction waves were observed at –1.78 V, -1.90 V and –2.08 V. Like the mononuclear rhenium complex $[Re(CO)_3(Hbpt)Cl]$, these reduction processes most likely are a result of reduction of the Hbpt ligand followed by chloride dissociation.

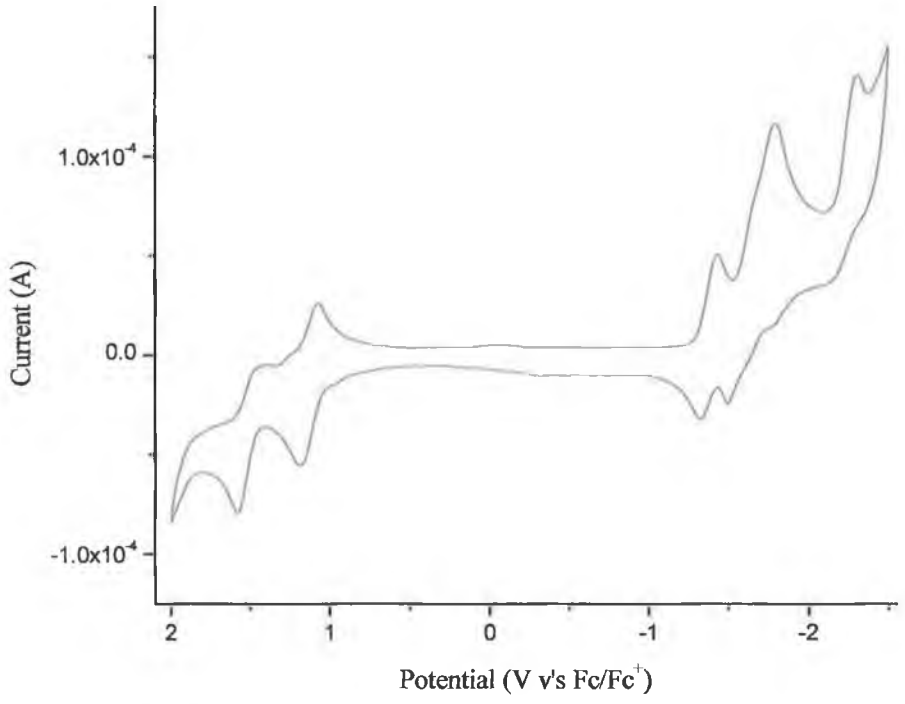

Figure 4. 26 *Cyclic voltammogram of $[Ru(bpy)_2(bpt)Re(CO)_3Cl]^+$ in acetonitrile in 0.1M $TBABF_4$ in acetonitrile with a scan rate of 100 mV/s.*

The cyclic voltammogram of the dinuclear complex $[Ru(bpy)_2(bpt)Re(CO)_3Cl]^+$ is presented in Figure 4. 26. For $[Ru(bpy)_2(bpt)Re(CO)_3Cl]^+$ there are clearly identifiable Ru(II)/Ru(III) and Re(I)/Re(II) couples at 1.09 and 1.55 V. The Ru(II)/Ru(III) couple is fully reversible but for the Re(I)/Re(II) couple, the return wave is less intense than the outward wave. The irreversible nature of the Re(I)/Re(II) couple is typical of rhenium tricarbonyl complexes.[40] It is interesting to note in the $[Ru(bpy)_2(bpt)Re(CO)_3Cl]^+$ complex, the Ru-centred oxidation potential is shifted 170 mV to higher potential compared to the mononuclear $[Ru(bpy)_2bpt]^+$ complex (see Table 4. 5). Upon coordination of the $Re(CO)_3Cl$ unit, the negative charge of the bpt^- ligand is shared between the $Ru(bpy)_2$ and $Re(CO)_3Cl$ moieties. As a result less charge is present on each metal centre. This

results in the ruthenium centre oxidising at a higher oxidation potential. Such differences in oxidation potentials have been observed between the mononuclear $[Ru(bpy)_2bpzt]^+$ and dinuclear $[\{Ru(bpy)_2\}_2bpzt]^{3+}$ complexes (where bpzt is 3,5-di(pyraz-2-yl)-1,2,4-triazole).[82,83] The first Ru(II)/Ru(III) oxidation of $[\{Ru(bpy)_2\}_2bpzt]^{3+}$ is observed at 1.16 V while oxidation of the ruthenium centre in the mononuclear complex $[Ru(bpy)_2bpzt]^+$ is observed at 0.99 V. In the mononuclear complex $[Ru(bpy)_2bpzt]^+$, the negative charge of the bpzt anion is delocalised onto the metal centre through the N_2 of the triazole ring. Addition of a second metal centre results in a delocalisation over two metal centres thus reducing the electron over both and increasing the first oxidation potential of $[\{Ru(bpy)_2\}_2bpzt]^{3+}$ compared to $[Ru(bpy)_2bpzt]^+$.

Deprotonated 1,2,4-triazole ligands have enhanced σ-donor abilities compared to their protonated analogues.[25,36,84] For ruthenium bipyridyl complexes containing 1,2,4-triazole ligands, deprotonation of the triazole ligand causes a significant lowering of the Ru-centred oxidation potentials compared to their protonated derivatives. For example, the metal centred oxidation in $[Ru(bpy)_2bpt]^+$ is 130 mV lower than that of $[Ru(bpy)_2Hbpt]^{2+}$.[17] For the heteronuclear $[Ru(bpy)_2(bpt)Re(CO)_3Cl]^+$ complex, the rhenium centred oxidation wave is at 1.55 V, which is similar to the second rhenium based oxidation in the binuclear $[\{Re(CO)_3Cl\}_2(Hbpt)]$ complex. Note $[\{Re(CO)_3Cl\}_2(Hbpt)]$ was isolated with a protonated triazole lignad in contrast to the heteronuclear $[Ru(bpy)_2(bpt)Re(CO)_3Cl]^+$ complex which contains a negatively charged triazole unit. As a result of the bpt^- anion present in $[Ru(bpy)_2(bpt)Re(CO)_3Cl]^+$, the Re(I)/(II) couple in this complex is expected to occur at lower potential than that in $[\{Re(CO)_3Cl\}_2(Hbpt)]$. There is also a higher charge on the $[Ru(bpy)_2(bpt)Re(CO)_3Cl]^+$ complex compared to $[\{Re(CO)_3Cl\}_2(Hbpt)]$ i.e. +2 compared to 0. Note the overall charge of the complex increases from +1 to + 2 on oxidation of the ruthenium metal centre from Ru(II) to Ru(III). This increased charge makes the rhenium(I) centred oxidation more difficult. For dinuclear ruthenium complexes, metal centred oxidation is more difficult than that for the mononuclear complexes due to the higher charge on the dinuclear

complexes.[10,85,86] The increase in charge on the $[Ru(bpy)_2(bpt)Re(CO)_3Cl]^+$ complex compared to $[\{Re(CO)_3Cl\}_2(Hbpt)]$ probably offsets the proposed deprotonation induced lowering of the Re(I)/Re(II) oxidation potential. Hence the Re(I)/Re(II) couple in $[Ru(bpy)_2(bpt)Re(CO)_3Cl]^+$ is observed at similar potential to the second Re(I)/Re(II) couple in the $[\{Re(CO)_3Cl\}_2(Hbpt)]$ complex.

The reduction processes for $[Ru(bpy)_2(bpt)Re(CO)_3Cl]^+$ are complicated (see Figure 4. 26). The mononuclear complex $[Ru(bpy)_2bpt]^+$ displays a reversible bpy based reduction at –1.47 V.[15] Like $[Ru(bpy)_2bpt]^+$, the quasi-reversible reduction wave observed at –1.41 for the dinuclear complex is mostly likely bpy based. Compared to $[Ru(bpy)_2bpt]^+$, the first reduction potential of $[Ru(bpy)_2(bpt)Re(CO)_3Cl]^+$ is at a slightly less negative value. This most likely results from the fact that the bpt^- ligand has to be shared between two metal centres, thus reducing the electron density on the $Ru(bpy)_2$ fragment. A second bpy based reduction is expected. The second bpy based reduction cannot be clearly identified (see Figure 4. 26) as it is obscured by an irreversible ligand based reduction at –1.82 V. This irreversible ligand based reduction at –1.82 V is most likely bpt^- based. Compared to $[Ru(bpy)_2bpt]^+$, this reduction wave is at a less negative values. When the $Re(CO)_3Cl$ is coordinated to $[Ru(bpy)_2bpt]^+$, the negative charge residing on the bpt anion is shared between the $Re(CO)_3Cl$ and $Ru(bpy)_2$ fragments. This reduction in electron density makes the bpt^- ligand easier to reduce.

4.2.6 Relation between spectroscopic data and electrochemistry

The spectroscopic and electrochemical data for the mononuclear complexes $[Re(CO)_3(Hbpt)Cl]$, $[Re(CO)_3(bpt)Cl]^-$ and $[Ru(bpy)_2(bpt)]^+$ indicate the energy gap i.e. HOMO-LUMO separation is greater for the rhenium metal complexes. This can be substantiated with the following reasons. Firstly, the 1st reduction potential of $[Re(CO)_3(Hbpt)Cl]$ is at a more negative value than the bpy based reduction observed for $[Ru(bpy)_2(bpt)]^+$. The irreversible Re(I)/Re(II) based oxidation is observed at a more positive potential than the Ru(II)/(III) oxidation. Thus the energy gap i.e. the positive difference between the potentials of the first oxidation and the first reduction is greater for the rhenium complexes. Similarly the absorption and emission maxima for $[Re(CO)_3(Hbpt)Cl]$ and $[Re(CO)_3(bpt)Cl]^-$ are observed at higher energy compared to the mononuclear complex $[Ru(bpy)_2(bpt)]^+$. These considerations were used to construct the energy level diagram shown in Scheme 4. 1

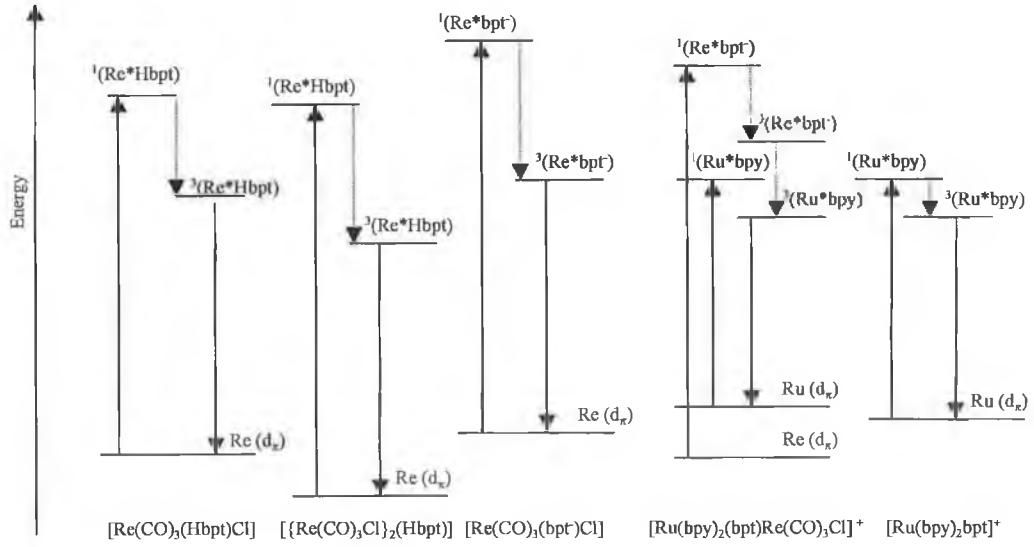

Scheme 4. 1 *Comparison of the ^{1}MLCT absorption maxima and the ^{3}MLCT emission maxima for $[Re(CO)_3(Hbpt)Cl]$, $[Re(CO)_3(bpt)Cl]^-$, $[Ru(bpy)_2(bpt)]^+$ and $[Ru(bpy)_2(bpt)Re(CO)_3Cl]^+$.*

The energy gap is greater for $[\{Re(CO)_3Cl\}_2(Hbpt)]$ compared to $[Re(CO)_3(Hbpt)Cl]$. This is a rare observation, as in bimetallic complexes containing $Re(CO)_3Cl$, the π^* level of the bridging ligand is lowered considerably upon dinucleation.[33,34] This difference in the energy gap between the dinuclear and mononuclear complexes is most likely caused by the weaker σ-donor properties of the dinucleating Hbpt ligand compared to mononucleating Hbpt. This conclusion was based on a number of observations. Firstly, the 1st reduction potential is less negative for $[\{Re(CO)_3Cl\}_2(Hbpt)]$ compared to $[Re(CO)_3(Hbpt)Cl]$. The difference between the values of first oxidation and the first reduction is greater for $[\{Re(CO)_3Cl\}_2(Hbpt)]$. The absorption maximum is at higher energy for $[\{Re(CO)_3Cl\}_2(Hbpt)]$ in contrast to $[Re(CO)_3(Hbpt)Cl]$. Upon coordination of a second $Re(CO)_3Cl$ moiety to $[Re(CO)_3(Hbpt)Cl]$, the electron density of the Hbpt ligand is shared between the two $Re(CO)_3Cl$ units. This lowers the energy of the Hbpt π^* level i.e. the Hbpt ligand is reduced at a less negative potential. But the first rhenium based oxidation is observed at a more positive potential for $[\{Re(CO)_3Cl\}_2(Hbpt)]$ compared to $[Re(CO)_3(Hbpt)Cl]$. Hence the HOMO of the dinuclear complex is at lower energy. The cumulative effect of the change in energy of the HOMO and the LUMO is an increase in the energy gap for $[\{Re(CO)_3Cl\}_2(Hbpt)]$. This is illustrated in Scheme 4. 1.

A very important conclusion is that for $[Ru(bpy)_2(bpt)Re(CO)_3Cl]^+$, a bpy-based first reduction potential has been observed. The first reduction process in metal complexes usually corresponds to the lowest π^* level of that complex. Hence it can be concluded that the lowest energy MLCT band is a $Ru \rightarrow \pi^*(bpy)$ transition. This also suggests that the emitting state of the heteronuclear complex is bpy-based. Deuteriation studies support the assignment of the emission in $[Ru(bpy)_2(bpt)Re(CO)_3Cl]^+$ as being bpy-based.

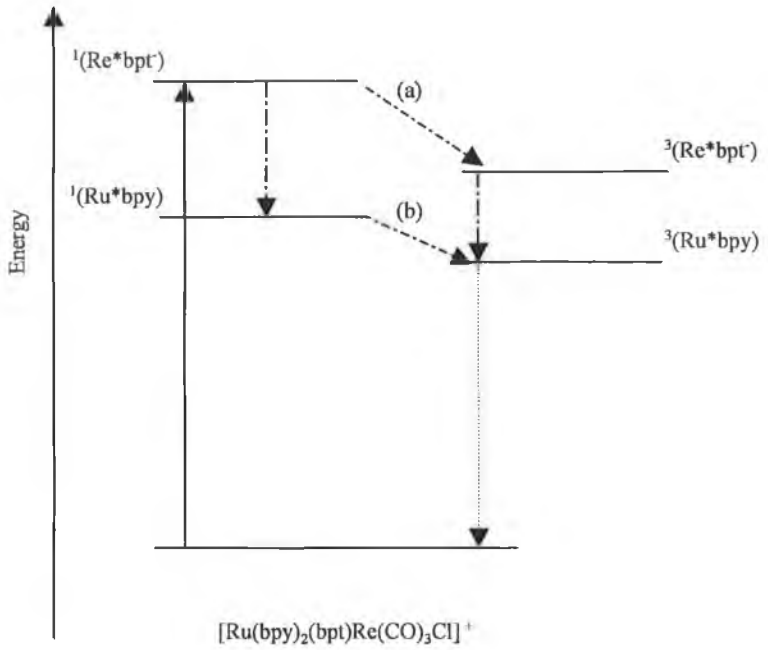

Scheme 4. 2 *Schematic diagram showing rhenium to ruthenium energy transfer.*

As previously discussed, the electrochemical and physical data for $[Re(CO)_3(Hbpt)Cl]$, $[Re(CO)_3(bpt)Cl]^-$ and $[Ru(bpy)_2(bpt)]^+$ indicate the ^{1}MLCT and ^{3}MLCT levels are at higher energy for the rhenium type complexes. Hence it seems reasonable to conclude, the ^{1}MLCT and ^{3}MLCT levels for the Re-based chromophore are at higher energy for $[Ru(bpy)_2(bpt)Re(CO)_3Cl]^+$. The lack of Re-based emission for $[Ru(bpy)_2(bpt)Re(CO)_3Cl]^+$ is ascribed to fast deactivation of the Re-based ^{3}MLCT energy levels, populated after light absorption, in favour of lower lying levels centred on the Ru-fragment i.e. Re→Ru photoinduced energy transfer. This photoinduced energy transfer is depicted in *Scheme 4. 2*. It is also possible, absorption of light leads to population of the Re-based ^{1}MLCT energy level. This rapidly relaxes to the lower energy Ru-based ^{1}MLCT. This is followed by intersystem crossing the Ru-based ^{3}MLCT i.e. route (b) in *Scheme 4. 2*.

4.3 Conclusions

In this chapter the synthesis, characterisation, photophysical and electrochemical properties of a series of rhenium and ruthenium complexes containing the bridging ligand 3,5-bis(pyridin-2-yl)-1,2,4-triazole are reported. The metal ion in the mononuclear complexes are bound to a pyridine ring and the 1,2,4-triazole. The exact coordination mode to the triazole i.e. N_2/N_4 can only be determined by growing crystals suitable for X-ray structure determination. IR studies indicate that in all cases the carbonyl ligands have a facial conformation around the rhenium metal centre. The formation of two geometrical isomers has been observed for the heteronuclear ruthenium/rhenium complex. The isomers of the deuteriated complex $[Ru(d_8\text{-}bpy)_2(bpt)Re(CO)_3Cl]^+$, were successfully isolated. The isomers were studied using NMR spectroscopy. Considerable differences in the ^1H NMR spectra have been observed. The observation of two isomers in the ^1H NMR spectra of $[Ru(bpy)_2(bpt)Re(CO)_3Cl]^+$ and $[Ru(d_8\text{-}bpy)_2(bpt)Re(CO)_3Cl]^+$ may be due to different orientations of the bipyridyl ligands coordinated to the ruthenium(II) metal centre. The electrochemical and electronic properties are however identical for both isomers.

The photophysical properties of these complexes are interesting. Upon coordination of a second metal fragment i.e. $Re(CO)_3Cl$ to the mononuclear complexes, the absorption and emission energies shift to higher energy. This is a rare observation as most other bimetallic complexes containing $Re(CO)_3Cl$, the π^* level of the bridging ligand is lowered considerably upon dinucleation. Although the ligand bridge is asymmetric, dual emission was not observed for $[\{Re(CO)_3Cl\}_2(Hbpt)]$ or $[\{Re(CO)_3Cl\}_2(bpt)]^-$. The observed emission form $[Ru(bpy)_2(bpt)Re(CO)_3Cl]^+$ is bpy-based. The hcteronuclear $[Ru(bpy)_2(bpt)Re(CO)_3Cl]^+$ complex exhibits efficient energy transfer from the Re centre to the Ru centre.

4.4 Experimental

4.4.1 Synthesis of 3,5-bis(pyridin-2-yl)-1,2,4-triazole (Hbpt).

2-Pyridinecarboxylic acid (5.20 g, 43 mmol) and concentrated sulphuric acid ($2cm^3$) were heated at reflux in ethanol for 3 hours. Sodium carbonate was added to neutralise the excess sulphuric acid. Excess hyrdrazine hydrate (3.00g, 60 mmol) was added to this solution. The solution was stirred at 0 °C for 3 hours. The resulting precipitate was filtered and washed with cold ethanol. 2-Cyanopyridine was (3.1 g, 30 mmol) was converted to 2-pyridylmethylimidate by heating at reflux with sodium metal in methanol for 3 hours. The hydrazide was added and the solution was heated for 2 hours. The yellow precipitate was collected under vacuum. 3,5-bis(pyridin-2-yl)-1,2,4-triazole was obtained by heating the hydrazide at reflux in ethylene glycol for 1 hour, Yield 5. 12 g, 23 mmol, 54%. ^{1}H NMR (d_6-DMSO) δ (ppm): 8.76 (d), 8.16 (d), 8.01 (t), 7.52 (t).

4.5 Preparation of the coordination complexes

[$Re(CO)_3$(Hbpt)Cl]

Hbpt (0.07g, 0.332 mmol) was dissolved in 50 ml of toluene. A few drops of trifluroacetic acid were added to this solution. [$Re(CO)_5Cl$] (0.100 g, 0.277 mmol) was added to this acidified toluene solution. This solution was refluxed under an argon atmosphere for 4 hours yielding a yellow solution. The reaction mixture was refrigerated overnight. The resulting yellow precipitate was collected by filtration yielding the desired product. Yield 0.115 g, 0.219 mmol, 79 %. Elemental analysis for $ReC_{15}H_9N_5O_3Cl$: Calculated C, 34.06; H, 1.70; N, 13.25; Found C, 33.73; H, 1.89; N, 12.66; ^{1}H NMR (CD_3CN), δ in ppm: Ring A: H_3: 8.41 (d); H_4: 8.32 (m); H_5: 7.70 (m); H_6: 9.07 (d); Ring B: H_3: 8.46 (d); H_4: 8.25 (m); H_5: 7.70 (m); H_6: 8.82 (d); ν_{CO} (cm^{-1}) in THF: 2022, 1913, 1889.

[{Re(CO)$_3$Cl}$_2$(Hbpt)]

Hbpt (0.06g, 0.277 mmol) was dissolved in 50 cm^3 of toluene. A few drops of trifluroacetic acid were added to this solution. [Re(CO)$_5$Cl] (0.200 g, 0.554 mmol) was added to this acidified toluene solution. This solution was refluxed under an argon atmosphere for 6 hours resulting in a yellow solution. The reaction mixture was refrigerated overnight. The resulting yellow precipitate was collected by filtration yielding the desired product. Yield 0.185 g, 0.223 mmol, 81%. Elemental analysis for $Re_2C_{18}H_9N_5O_6Cl_2$: Calculated C, 25.90; H, 1.08; N, 8.39; Found C, 26.01; H, 1.11; N, 8.25; ^{1}H NMR (CD_3CN), δ in ppm: H_3: 8.23 (m); H_4: 8.23 (m); H_5: 7.60 (m); H_6: 9.03 (d); ν_{CO} (cm^{-1}) in THF: 2029, 1917, 1897.

[Ru(bpy)$_2$(bpt)](PF$_6$).1/2H$_2$O

Hbpt (0.220g, 1mmol) was dissolved in 50 cm^3 ethanol/water (2/1 v/v). 0.250 g (0.500 mmol) of [Ru(bpy)$_2$Cl$_2$].2H$_2$O was added in small portions to the dissolved Hbpt ligand. The purple solution was refluxed for 8 hours. The solvent was removed and the orange residue was dissolved in a small amount of water. A few drops of concentrated NaOH were added to this solution. The complex was precipitated with ammonium hexafluorophosphate. The orange precipitate was collected under vacuum. The complex was dissolved in a minimum volume of acetonitrile and purified by column chromatography on alumina. The first band (N_2 isomer) was eluted with acetonitrile. The N_4 isomer remained on the top of the column and was eluted with methanol. This present study is only interested in the N_2 isomer hence only this isomer was characterised. Yield 0.263 g, 0.175 mmol, 35 %. ^{1}H NMR (CD_3CN), δ in ppm: Ring A: H_3: 8.15 (d); H_4: 7.90 (m); H_5: 7.15 (m); H_6: 7.52 (d); Ring B: H_3: 8.00 (m); H_4: 7.75 (m); H_5: 7.22 (m); H_6: 8.53 (d); bpy: H_3: 8.55 (m); H_4: 7.98 (m); H_5: 7.35 (m); H_6: 7.83 (m).

$[Ru(d_8\text{-bpy})_2(bpt)](PF_6).1/2H_2O$

As for $[Ru(bpy)_2(bpt)](PF_6).1/2H_2O$ except 0.260 g (0.500 mmol) $[Ru(d_8\text{-bpy})_2Cl_2].2H_2O$ was used in place of $[Ru(bpy)_2Cl_2].2H_2O$. Yield 0.326 g, 0.215 mmol, 43 %. ^1H NMR (CD_3CN), δ in ppm: Ring A: H_3: 8.15 (d); H_4: 7.90 (m); H_5: 7.15 (m); H_6: 7.52 (d); Ring B: H_3: 8.00 (m); H_4: 7.75 (m); H_5: 7.22 (m); H_6: 8.53 (d).

$[Ru(bpy)_2(bpt)Re(CO)_3Cl](PF_6).3H_2O$

0.100 g (0.125 mmol) of $[Ru(bpy)_2bpt](PF_6)$ was reacted with 0.050 g (0.139 mmol) of $Re(CO)_5Cl$ in 50 ml of methanol for 6 hours. The solvent was removed. The complex was recrystallised from acetone/ethanol (2/1 v/v). Yield 0.085 g, 0.071 mmol, 57 %. Elemental analysis for$RuReC_{35}H_{27}N_9O_9ClPF_6$: Calculated C, 36.86; H, 2.37; N, 11.06; Found C, 36.74; H, 2.50; N, 10.34; ν_{CO} (cm^{-1}) in THF: 2021, 1912, 1889.

$[Ru(d_8\text{-bpy})_2(bpt)Re(CO)_3Cl](PF_6).3H_2O$

100 mg (0.125 mmol) of $[Ru(d_8\text{-bpy})_2bpt](PF_6)$ was reacted with 0.050 g (0.139 mmol) of $Re(CO)_5Cl$ in 50 cm^3 of methanol for 6 hours. Solvent was removed. Careful recrystallisation from acetone/ethanol (2/1 v/v) yielded three different isomers. Yield 0.097 g, 0.081 mmol, 65 %. $RuReC_{35}H_{11}D_{16}N_9O_9ClPF_6$: Calculated C, 36.34; H, 1.21; N, 10.90; Found C, 37.00; H, 1.50; N, 10.54; ν_{CO} (cm^{-1}) in THF: 2021, 1912, 1889.

4.6 Bibliography

1 V. Balzani, A. Credi, M. Venturi, *Molecular Devices and Machines; A journey into the nanoworld*, VCH, Weinheim **2003**.

2 (a) A. Juris, V. Balzani, F. Barigelletti, S. Campagna, P. Besler, A. von

Zelewsky, *Coord. Chem. Rev.* **1988**, 84, 85. (b) F.R. Keene, *Coord. Chem. Rev.* **1997**, 121, 159.

3 (a) K.E. Splan, M.H. Keefe, A.M. Massari, K.A. Walters, J.T. Hupp, *Inorg. Chem.* **2002**, 41, 619. (b) E.C. Constable, E. Schofield, *Chemm. Commun*, **1998**, 403, (c) M. Fujita, *Chem. Soc. Rev.* **1998**, 27, 417.

4 A. Vlček Jr., *Coord. Chem. Rev.*, **2000**, 200-202, 933.

5 K. Kalyanasundaram, M.K. Nazeeruddin, *Inorg. Chem.*, **1990**, 29, 1888.

6 G. Denti, S. Serroni, S. Campagna, V. Ricevuto, V. Balzani, *Coord. Chem. Rev.*, **1991**, 111, 227.

7 W. Kaim, *Coord. Chem. Rev.*, **2002**, 230, 127.

8 C. Di Pietro, S. Serroni, S. Campagna, M.T. Gandolfi, R. Ballardini, S. Fanni, W.R. Browne, J.G. Vos, *Inorg. Chem.*, **2002**, 41, 2871.

9 S. Baitalik, U.Flörke, K. Nag, *Inorg. Chem.*, **1999**, 38, 3296.

10 F. Weldon, L. Hammarström, E. Mukhtar, R. Hage, E. Gunneweg, J.G. Haasnoot, J. Reeijk, W.R. Browne, A.L. Guckian, J.G. Vos, *Inorg. Chem.*, **2004**, 43, 4471.

11 F. Weldon, PhD. Thesis, Dublin City University, **1998**.

12 V. Balzani, A. Juris, M. Venturi, *Coord. Chem. Rev.*, **1996**, 96, 759.

13 J.P. Sauvage, J.P. Collin, J.C. Chambron, S. Guillerez, C. Coudet, V. Balzani, F. Barigelletti, L. De Cola, L. Flamigni, Chem. Rev., **1994**, 94, 993

14 V. Balzani, L. Moggi, Coord. Chem. Rev., **1990**, 97, 313

15 R. Hage, Ph.D. Thesis, Leiden University, The Netherlands, **1991**

16 S. Fanni, T.E. Keyes, C.M. O'Connor, H. Hughes, R. Wang, J.G. Vos, *Coord. Chem. Rev.*, **2000**, 208.

17 R. Hage, A.H.J. Dijkhuis, J.G. Haasnoot, R. Prins, J. Reedijk, B.E. Buchanan, J.G. Vos, *Inorg. Chem.*, **1988**, 27, 2185.

18 R. Hage, J.G. Haasnoot, D.J. Stufkens, T.L. Snoeck, J.G. Vos, J. Reedijk, *Inorg. Chem.*, **1989**, 28, 1413

19 R.P. Thummel, D. Williamson, C. Hery, *Inorg. Chem.*, **1993**, 32, 1587

20 T.E. Keyes, F. Weldon, E. Muller, P. Pechy, M. Gratzel, J.G. Vos, *J.*

Chem. Soc. Dalton Trans., **1995**, 2705.

21 W.R. Browne, J.G. Vos, *Coord. Chem. Rev.*, **2001**, 219, 761

22 J.F. Geldard, F. Lions, *J. Org. Chem.*, **1965**, 30, 318.

23 M.H. Klingele, S. Brooker, *Coord. Chem. Rev.*, **2003**, 241, 119.

24 J.G. Haasnoot, , *Coord. Chem. Rev.*, **2000**, 200, 131.

25 B.E. Buchanan, R. Wang, J.G. Vos, R. Hage, J.G. Haasnoot, J. Reedijk, *Inorg. Chem.*, **1990**, 29, 3263.

26 H.M. Burke, J.F. Gallagher, M.T. Indelli, J.G. Vos, *Inorg. Chim. Acta.*, **2004**, 357, 2989.

27 M.P. Garcia, M. Martin, L.A. Oro, *Inorg. Chim. Acta.*, **1992**, 191, 221.

28 P.J. Steel, E.C. Constable, *J. Chem. Soc., Dalton Trans.*, **1990**, 1389

29 P.J. Steel, F. Lahousse, C. Marzin, *Inorg. Chem.*, **1983**, 22, 1488

30 E.C. Constable, K.R. Seddon, *J. Chem. Soc., Chem. Commun.*, **1982**, 34

31 A. Llobet, P. Doppelt, T.J. Meyer, *Inorg. Chem.*, **1988**, 27, 514

32 R. Hage, J.P. Turkenburg, R.A.G. DeGraff, J.G. Haasnoot, J. Reedijk, J.G. Vos, *Acta Crystallogr., Sect. C,* **1989**, 45, 381.

33 S. Van Wallendael, R.J. Shaver, D.P. Rillema, B.J. Yoblinski, M. Stathis, T.F. Guarr, *Inorg. Chem.*, **1990**, 29, 1761

34 M.R. Waterland, T.J. Simpson, K.C. Gordon, A.K. Burrell, *J. Chem. Soc., Dalton Trans.*, **1998**, 185

35 A.L. Rheingold, P. Saisuwan, N.C. Thomas, *Inorg. Chim., Acta.*, **1993**, 214, 41.

36 R. Hage, R. Prins, J.G. Haasnoot, J. Reedijk, J.G. Vos, *J. Chem. Soc., Dalton Trans,* **1987**, 1389

37 W.R. Browne, PhD. Thesis, Dublin City University, **2002**.

38 D. Mulhern, PhD. Thesis, Dublin City University, **2003**.

39 S. Frantz, T. Scheiring, J. Fiedler, W. Kaim, *J. Organomet. Chem.*, **2000**, 604, 267.

40 S. Frantz, W. Kaim, J. Fiedler, C. Duboc, *Inorg. Chim. Acta.*, **2004**, 357, 3657.

41 W.R. Browne, C.M. O'Connor, C. Villani, J.G. Vos, *Inorg. Chem.*, **2001**,

40, 5461.

42 T. Scheiring, J. Fiedler, W. Kaim, *Organometallics*, 2001, 20, 1437

43 G.L. Geoffroy, M.S. Wrighton, *Organometallic Photochemistry*, Academic Press: New York, **1979**.

44 W. Kaim, S. Kohlmann, *Inorg. Chem.*, **1987**, 26, 68.

45 M. Wrighton, D.L. Morse, *J. Am. Chem. Soc.*, **1974**, 96, 998.

46 S.M. Fredericks, J.C. Luong, M.S. Wrighton, *J. Am. Chem., Soc.*, **1979**, 101, 7415.

47 S. Van Wallendael, R.J. Shaver, D.P. Rillema, B.J. Yoblinski, M. Stathis, T.F. Guarr, *Inorg. Chem.*, **1990**, 29, 1761.

48 B.J. Yoblinski, M. Stathis, T.F. Guarr, *Inorg. Chem.*, **1992**, 31, 5.

49 B. Kumar Panda, S. Sengupta, A. Chakravorty, *J. Organomet. Chem.*, **2004**, 1780.

50 A. Juris, V. Balzani, F. Barigelletti, S. Campagna, P. Besler, A. von Zelewsky, *Coord. Chem. Rev.*, **1988**, 84, 85.

51 W. Humbs, H. Yersin, J. Strasser, *Topics Curr. Chem.*, **1997**, 191, 154.

52 L.A. Worl, R. Duesing, P. Chen, L. Della Ciana, T.J. Meyer, *J. Chem. Soc., Dalton Trans.* **1991**, 849.

53 L. Yang, A. Ren, J. Feng, X. Liu, Y. Ma, M. Zhabg, X. Liu, J. Shen, H. Zhang, *J. Phys. Chem. A*, **2004**, 108, 6797.

54 F. Barigelletti, L. De Cola, V. Balzani, R. Hage, J.G. Haasnoot, J. Reedijk, J.G. Vos, *Inorg. Chem.*, **1989**, 28, 4344.

55 M. Leirer, G. Knör, A. Vogler, *Inorg. Chim. Acta*, **1999**, 288, 150.

56 T.J. Simpson, K.C. Gordon, *Inorg. Chem.*, **1995**, 34, 6323.

57 S.E. Page, A. Flood, K.C. Gordon, *J. Chem. Soc., Dalton Trans.* **2002**, 1180.

58 D.A. Bardwell, F. Bargelletti, R.L. Cleary, L. Flamigni, M. Guardigli, J.C. Jeffery, M.D. Ward, *Inorg. Chem.*, **1995**, 34, 2438.

59 T.E. Keyes, F. Weldon, E. Müller, P. Pechy, M. Grätzel, J.G. Vos, *J. Chem. Soc., Dalton Trans.* **1995**, 2705.

60 R.S. Lumpkin, E.M. Kober, L. Worl, Z. Murtaza, T.J. Meyer, *J. Phys.*

Chem., **1990**, 94, 239.

61 A. Juris, S. Campagna, I. Bidd, J.M. Lehn, R. Ziessel, *Inorg. Chem.,* **1988**, 27, 2438.

62 A.A. Marti, G. Mezei, L. Maldonado, G. Paralitici, R. G. Raptis, J.L. Colon, *Eur. J. Inorg. Chem.,* **2005**, 118.

63 W. Kaim, H.E.A. Kramer, C. Vogler, J. Rieker, *J. Organomet. Chem.,* **1989**, 367, 107.

64 D.J. Stufkens, A. Vlček Jr., *Coord. Chem. Rev.,* **1998**, 177, 127.

65 E.M. Kober, J.V. Caspar, R.S.. Lumpkin, T.J. Meyer, *J. Phys. Chem.,* **1986**, 90, 4007.

66 J.V. Caspar T.J. Meyer, *J. Phys. Chem.,* **1983,** 87, 952.

67 R. Wang, J.G. Vos, R.H. Schmehl, R. Hage, *J. Am. Chem. Soc.,* **1992,** 114, 1964.

68 J.V. Caspar T.J. Meyer, *J. Phys. Chem.,* **1983,** 87, 952.

69 K. Kalyanasundaram, M.K. Nazeeruddin, *J. Chem. Soc. Dalton Trans.,* **1990**, 1657.

70 B. Gholamkhass, H. Mametsuka, K. Koike, T. Tanabe, M. Furue, O. Ishitani, *Inorg. Chem.,* **2005**, 44, 2326.

71 C.G. Coates, P.L. Callaghan, J.J. McGarvey, J.M. Kelly, P.E. Kruger, M.E. Higgins, *J. Raman Spect.* **2000**, 31, 283.

72 T.E. Keyes, C.M. O'Connor, U. O'Dwyer, C.G. Coates, P. Callaghan, J.J. McGarvey, J.G. Vos, *J. Phys. Chem. A,* **1999**, 103, 8915.

73 W.H. Henry, W.R. Browne, K.L. Ronayne, N.M. O'Boyle, J.G. Vos, J.J. McGarvey, *J. Mol. Structure,* **2005**, 735-736, 123.

74 D.A. Bardwell, F. Bargelletti, R.L. Cleary, L. Flamigni, M. Guardigli, J.C. Jeffery, M.D. Ward, *Inorg. Chem.,* **1995**, 34, 2438.

75 A. Vogler, J. Kisslinger, *Inorg. Chim. Acta.,* **1986**, 115, 193.

76 R. Sahai, D.P. Rillema, R. Shaver, S. Van Wallendael, D.C. Jackman, M. Boldaji, *Inorg. Chem.,* **1989**, 28, 1022.

77 J.C. Luong, L. Nadgo, M.S. Wrighton, *J. Am. Chem. Soc.,* **1978**, 100, 5790.

78 S. Frantz, J. Fiedler, I. Hartenbach, T. Schleid, W. Kaim, *J. Organomet. Chem.*, **2004**, 3049.

79 M. Bakir, J.A.M. McKenzie, *J. Chem. Soc., Dalton Trans.* **1997**, 3571.

80 B.P. Sullivan, C.M. Bolinger, D.C. William, W.J. Vining, T.J. Meyer, *J. Chem. Soc., Chem. Commun.*, **1985**, 1414.

81 A. Klein, C. Vogler, W. Kaim, *Organometallics*, **1996**, 15, 236.

82 J.M. de Wolf, R. Hage, J.G. Haasnoot, J. Reedijk, J.G. Vos, *New J. Chem.*, **1991**, 15, 501.

83 W.R. Browne, C.M. O'Connor, H.P. Hughes, R. Hage, O. Walter, M. Doering, J.F. Gallagher, J.G. Vos., *J. Chem. Soc., Dalton Trans.* **2002,** 4048.

84 W.R. Browne, F. Weldon, A. Guckian, J.G. Vos, *Collect., Czech. Chem. Commun.*, **2003**, 68, 1467.

85 M.D. Ward *J. Chem. Soc., Dalton Trans.* **1993**, 1321

86 M.D. Ward *J. Chem. Soc., Dalton Trans.* **1994**, 3095

Chapter 5

Methylation of ruthenium triazole complexes

Chapter 5 discusses the methylation of the ruthenium(II) bipyridyl complex containing the pyrazyl triazole ligand 3-(pyrazin-2-yl)-5-phenyl-1,2,4-triazole. Selective deuteriation of the bipyridyl ligands and the triazole ligand was also employed. Comparison of the ^{1}H NMR spectra of the deuteriated and undeuteriated complexes was found to aid structural characterisation of the complexes. The photophysical and electrochemical properties of all complexes have also been examined. Wavelength dependent ground-state resonance Raman measurements were carried out to elucidate the electronic transitions in the compounds.

5.1 Introduction

Chapter 5 describes the synthesis, methylation and characterisation of a ruthenium(II) pyrazyl-triazole complex and two deuteriated analogues. Earlier work on similar compounds indicates that methylation takes place at the triazole ring, which removes the negative charge on this moiety.[1] This would be advantageous for the preparation of $[Ru(bpy)_2LM(CO)_5]$ type complexes (where bpy = 2,2'-bipyridyl; L = substituted 3-(pyridin-2-yl)-1,2,4-triazole ligand; M = Cr, Mo or W), since they are destabilised by negatively charged ligands.

Ruthenium(II) polypyridyl complexes, because of their suitable photophysical and redox properties have received a great deal of attention as building blocks to synthesise supramolecular assemblies.[2,3,4,5,6] $[Ru(bpy)_3]^{2+}$ is the most extensively studied of the myriad of ruthenium(II) polypyridyl complexes, with the first reported emission from this complex made by Paris and Brandt in 1959.[7] Since then the interest in $[Ru(bpy)_3]^{2+}$ has flourished, with numerous reports concerning its photophysical and photochemical properties.[4,8,9] $[Ru(bpy)_3]^{2+}$ is not the most suitable complex for use as a photosensitiser, as population of the metal centered (^{3}MC) excited state results in photodecomposition of the complex. Van Houten and Watts found that the ^{3}MC excited state of $[Ru(bpy)_3]^{2+}$ is thermally populated following population of the ^{3}MLCT.[10]

For this reason, attempts have been made to enhance the ground and excited state properties of $[Ru(bpy)_3]^{2+}$ by varying the ligands coordinated to the ruthenium metal centre. Ligands may be classed on the basis of their σ-donor and π-acceptor properties. "Class B" ligands (σ-donors) donate electron density to the metal centre, causing lower oxidation potentials and more negative reduction potentials, while "Class A" ligands (π-acceptors) remove electron density from the metal centre of the metal complex giving rise to higher oxidation potentials and low reduction potentials. 2,2'-bipyridine (bpy),[11] 2,2'-bipyrazine (bpz)[12] and 1,10-phenanthroline (phen)[13] are examples of strong π-acceptor ligands. Imidazoles,[14] pyrazoles[15] and triazoles[16] have all been employed as strong σ-donor ligands.

Complexes containing ligands which are better π acceptors than 2,2'-bipyridine have lower lying ^{3}MLCT excited states than $[Ru(bpy)_3]^{2+}$. These types of ligands are usually weaker σ-donors than bipyridine. Hence the ligand field splitting is reduced in their metal complexes, making the ^{3}MC excited state more accessible which leads to photodissociation. In contrast "Class B" ligands (strong σ-donors, weak π-acceptors) have the reverse effect on the ground and excited state properties. Their strong σ-donor capacities result in larger ligand-field splitting, raising the energy of the ^{3}MC excited state and thus reducing photodecomposition. Due to their strong σ-donor capabilities, the ligands possess π* levels of much higher energy than bpy and as a result higher energy absorption would be required for MLCT excitation into such ligands. High energy absorption is undesirable for supramolecular assemblies, consequently mixed ligand complexes of these ligands, where they participate as spectator ligands, forms the basis of interest in "Class B" ligands.

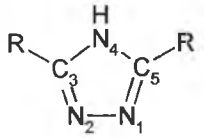

Figure 5. 1 *Stucture of a substituted 1,2,4-triazole.*

By combining "Class A" and "Class B" ligands, it is possible to generate a system that has the photostability of σ-donor ligands and the low energy absorptions of π-acceptor ligands. Substituted 1,2,4-triazoles (Figure 5. 1) are an example of how this may be achieved. When the triazole is deprotonated, a negative charge resides on the triazole. This negative charge enhances the σ-donor capabilities of the ligand. The presence of a pyridine or a pyrazine ring in the "3" or the "5" position of the triazole results in a bidentate ligand containing strong σ-donor (triazole) and strong π-acceptor (pyrazine/pyridine) components. The first

reported ruthenium(II) complex containing a 1,2,4-triazole was reported in 1983.[17] Since then a wide range of 1,2,4-triazoles have been synthesised and studied.[18,19]

Coordination of a ruthenium(II) metal centre to a 1,2,4-triazole ligand may occur at either of the two non-equivalent nitrogens on the triazole ring (Figure 5. 2).[20] These coordination isomers are referred to as the "N_2" isomer and the "N_4" isomer. The N_2 isomer and N_4 isomer in Ru(II) complexes incorporating 1,2,4-triazole ligands exhibit different redox potentials and absorption and emission maxima. The extent of N_2/N_4 coordination in ruthenium(II) complexes is governed by the size of the substituents on the C_5 position.[21] Bulky substituents such as a phenyl, thiol, methyl or Br group favour the formation of the N_2 isomer in ruthenium(II) complexes.[22]

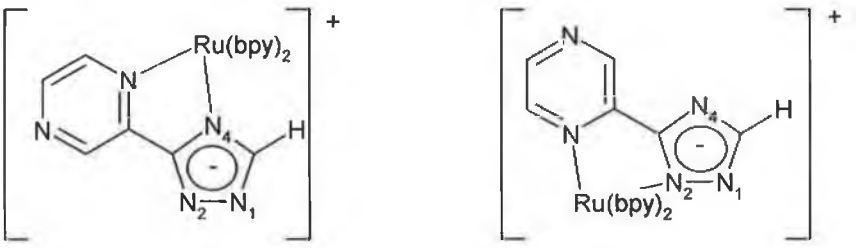

N_4 Isomer N_2 Isomer

Figure 5. 2 *The two possible modes of coordination of a ruthenium(II) metal centre to the pyrazyl-triazole ligand, 3-(pyrazin-2-yl)-1,2,4-triazole (Hpztr).*

N-Methylated triazoles are of interest for the comparison between neutral and negatively charged 1,2,4-triazole containing bridges. In the traditional route to these complexes, the N-methylated ligand is prepared first and subsequently used to prepare the appropriate metal complex.[18,21] When the methyl group is located on the N_1 position of the triazole ring, the N_4 isomer is predominantly formed. In an alternative synthetic approach to such complexes, the direct methylation of the appropiate precursor metal complex with trimethyl oxonium tetrafluroborate was

investigated (Figure 5. 3). Methylation occurred predominantly at the N_1 position for both pyrazine and pyridine triazole complexes irrespective of the size of the group in the "5" position.[1]

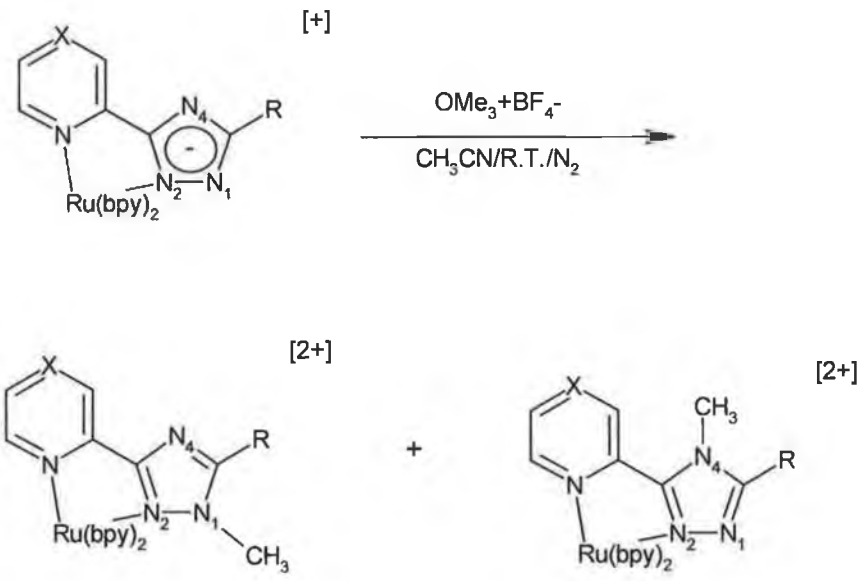

1)	X=C, R=H	2)	X=C, R=Me
3)	X=C, R=Br	4)	X=C, R= p-tolyl
5)	X=N, R=H	6)	X=C, R= o-hydroxyphenyl
7)	X=C, R=9,10,-phenothiazine	8)	X=C, R= p-chloromethoxyphenyl

Figure 5. 3 *Methylation of Ru(II) 1,2,4-triazole complexes.*[1]

In this chapter a methylated ruthenium(II) pyrazyl-triazole complex and two deuteriated analogues are synthesised and characterised. The ruthenium complexes were methylated using a similar synthetic route as that used by Fanni and co-workers.[1] Selective deuteriation of ligands in heteroleptic Ru(II) polypyridyl complexes simplifies complicated ^{1}H NMR spectra.[23] Hence selective deuteriation of the ligands in the methylated complexes will aid interpretation of the ^{1}H NMR spectra. The electrochemical, absorption and emission properties of the methylated complexes have also been investigated.

Furthermore, wavelength dependent ground-state resonance Raman (rR) measurements were carried out in order to elucidate the electronic transitions in the absorption spectra. The deuteriated complexes were employed to aid interpretation of these spectra. The structures and abbreviations of the ligands and complexes cited in this chapter are shown in Figure 5. 4.

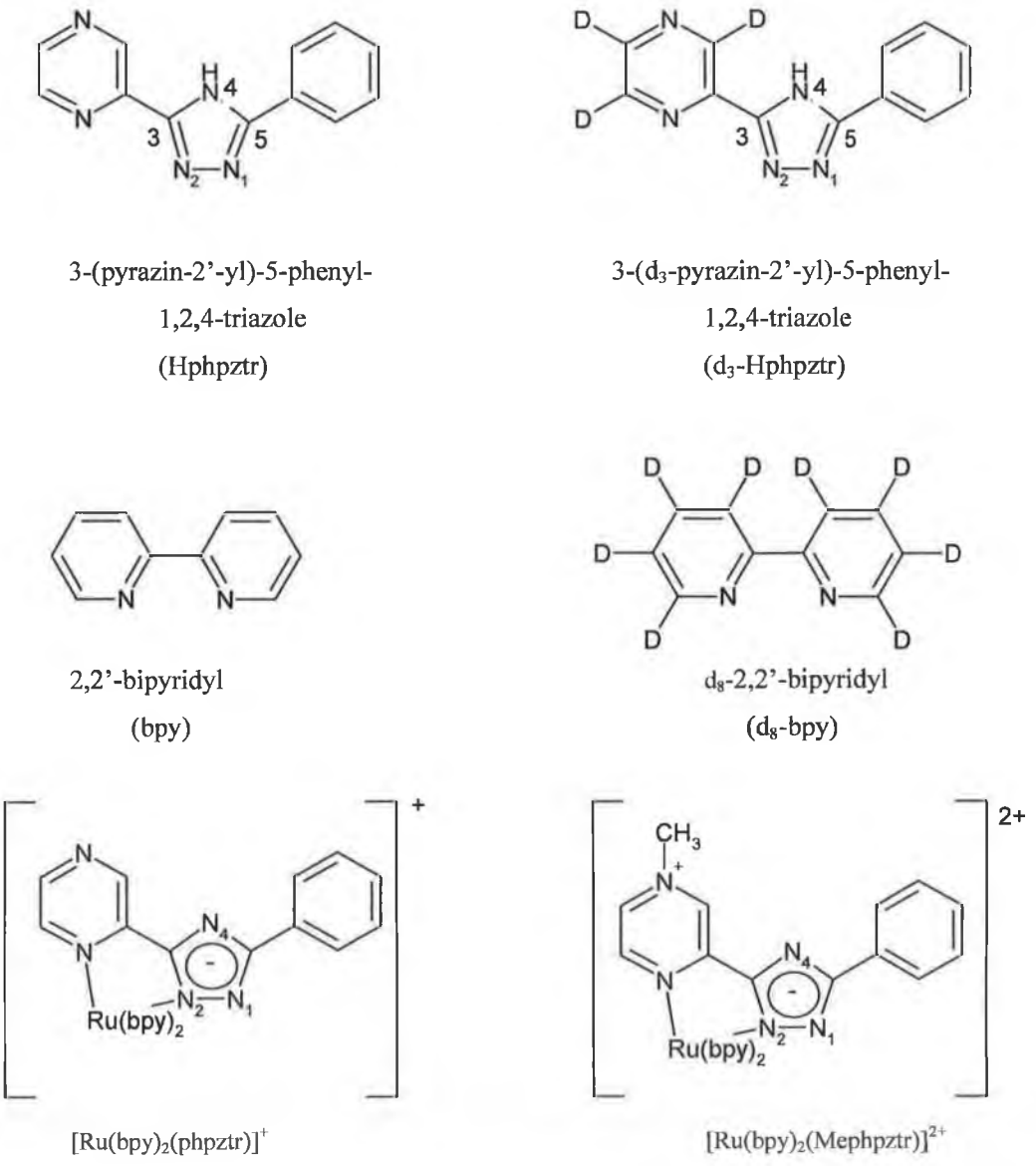

Figure 5. 4 *Structures of the ligands and complexes and their abbreviations as cited throughout this chapter.*

5.2 Results and Discussion

5.2.1 Synthetic methods

The ligand Hphpztr was prepared as previously reported.[22] The mononuclear complex $[Ru(bpy)_2(phpztr)]^+$ (see Figure 5. 4) was prepared by reacting the Hphpztr ligand in a 1:1 ratio with $[Ru(bpy)_2Cl_2].2H_2O$ according to a previously established procedure.[22] The crude complex $[Ru(bpy)_2(phpztr)]^+$ contains both N_2 and N_4 isomers (Figure 5. 5). Hence the complex was purified by column chromatography on alumina. The N_2 isomer was eluted first with acetonitrile. The N_2 isomer was subsequently recrystallised from water:acetone (1:1). 2 M NaOH was added to this solution to ensure the triazole ligand was fully deprotonated. Since this study is concerned with the N_2 isomer of $[Ru(bpy)_2(phpztr)]^+$, the purification and characterisation of the N_4 isomer will not be discussed any further. $[Ru(d_8\text{-}bpy)_2(phpztr)]^+$ was synthesised and purified as for $[Ru(bpy)_2(phpztr)]^+$ with one major change; $[Ru(d_8\text{-}bpy)_2Cl_2].2H_2O$ was used instead of $[Ru(bpy)_2Cl_2].2H_2O$. $[Ru(bpy)_2(d_3\text{-}phpztr)]^+$ was prepared in a similar manner except the ligand d_3-Hphpztr was used in place of Hphpztr.

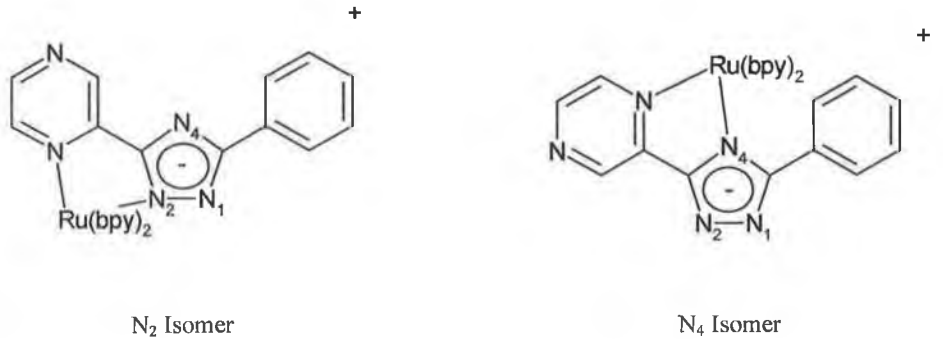

N_2 Isomer N_4 Isomer

Figure 5. 5 *The two possible coordination isomers of* $[Ru(bpy)_2(phpztr)]^+$.

The methylation reactions were carried out according to a synthetic route developed by Fanni and co-workers.[1] All reactions were carried out under nitrogen and were protected from light exposure due to the possibility of photodecomposition. Studies by Fanni and co-workers showed that methylation of $[Ru(bpy)_2(pztr)]^+$ (where pztr = 3-(pyrazin-2-yl)-1,2,4-triazole) occurs at both of the non-equivalent nitrogens on the triazole ring.[1] ^{1}H NMR studies showed the formation of the N_1 and N_4 isomers in the ratio of 70:30. However, for the methylated complexes reported in this chapter, ^{1}H NMR studies (Section 5.2.3) indicate a single isomer was obtained in each case. During the methylation reaction, the solution changed from orange to a dark purple colour. This is a surprising observation as other ruthenium(II) bipyridyl complexes containing a methylated 1,2,4-triazole ligand are generally orange in colour.[24] Fanni and coworkers did not comment upon such a colour change.[1] To determine the nature of the products obtained from the methylation reactions, detailed electrochemical, absorption, emission and wavelength dependent resonance Raman studies were carried out.

5.2.2 Mass spectrometry

The complexes were studied using electrospray mass spectrometry. This method involves analysing an ionised aerosol of the particular complex. An aerosol of the complex is formed by passing the complex in solution (acetonitrile) through a fine needle held at 80 eV at 300 °C. Since this is a soft ionisation technique and fragmentation patterns are not observed with this approach, the complex remains intact and its molecular weight may be determined. Table 5. 1 lists the observed and theoretical molecular ions for each methylated complex and the unmethylated complex $[Ru(bpy)_2(phpztr)]^+$. For all of the ruthenium complexes, the molecular ion appears minus the PF_6 counter ion. Figure 5. 6 shows a mass spectrum of $[Ru(bpy)_2(Mephpztr)]^{2+}$ which is typical of the spectra obtained for the methylated complexes. Methylation results in the formation of a doubly charged fragment, which occurs at the m/z value corresponding to half of the value that

would be expected for a +1 fragment. The doubly charged $[Ru(bpy)_2(Mephpztr)]^{2+}$ molecular ion is clearly visible at 325.4 m/z.

$[Ru(bpy)_2(phpztr)]^+$, $[Ru(d_8\text{-}bpy)_2(phpztr)]^+$ and $[Ru(bpy)_2(d_3\text{-}phpztr)]^+$ have been previously synthesised and characterised.[22] Mass spectroscopy and elemental analysis confirmed the presence of a negative charge on the triazole ligand. As these complexes have been fully characterised, the mass spectrum of $[Ru(bpy)_2(phpztr)]^+$ was only obtained. Table 5. 1 confirms $[Ru(bpy)_2(phpztr)]^+$ has been synthesised as a singly charged complex, thus indicating the presence of a negative charge on the triazole.

Complex	Observed (m/z)	Theoretical (m/z)
$[Ru(bpy)_2(phpztr)]^+$	636.1	636.0
$[Ru(bpy)_2(Mephpztr)]^{2+}$	325.4	325.0
$[Ru(d_8\text{-}bpy)_2(Mephpztr)]^{2+}$	333.4	333.0
$[Ru(bpy)_2(d_3\text{-}Mephpztr)]^{2+}$	326.8	326.5

Table 5. 1 *Observed and theoretical m/z values for the complexes investigated.*

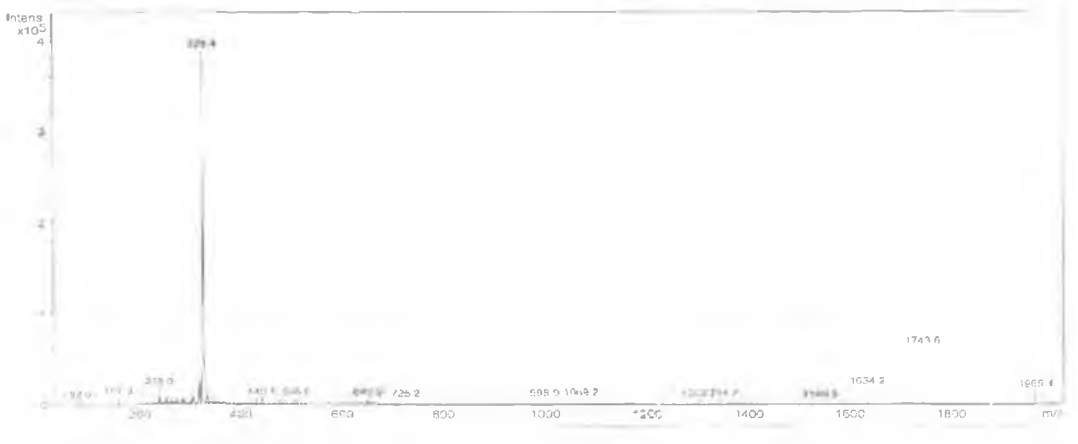

Figure 5. 6 *Mass spectrum of $[Ru(bpy)_2(Mephpztr)]^{2+}$ in acetonitrile.*

There are three possible methylation sites on $[Ru(bpy)_2(phpztr)]^+$, $[Ru(d_8\text{-}bpy)_2(phpztr)]^+$ and $[Ru(bpy)_2(d_3\text{-}phpztr)]^+$ (two on the triazole and one on the pyrazine). Methylation of the triazole or the pyrazine forms a ruthenium complex with an overall charge of +2.[18] The mass spectra data of $[Ru(bpy)_2(Mephpztr)]^{2+}$, $[Ru(d_8\text{-}bpy)_2(Mephpztr)]^{2+}$ and $[Ru(bpy)_2(d_3\text{-}Mephpztr)]^{2+}$ listed in Table 5. 1 confirm the synthesis of a doubly charged complex. Although the mass spectroscopy data indicate that methylation has taken place, the location of the methyl group is still uncertain. The complexes were therefore further investigated with ^1H NMR spectroscopy.

5.2.3 NMR spectroscopy

As ruthenium complexes are diamagnetic low-spin d^6 metal complexes, NMR spectroscopy has been an important technique in the elucidation of the structures of ruthenium polpyridyl complexes.[25,26,27] While the spectrum of the ligand was straightforward to interpret, spectra of the complexes proved to be much more complex, requiring both two dimensional NMR (COSY) experiments and deuteriation studies in order to fully explain the spectra. The numbering system employed in the ^1H NMR discussion is described in Figure 5. 7. The relevant ^1H NMR data of all complexes are presented in Table 5. 2. The coordination-induced shifts (c.i.s. = $\delta_{complex} - \delta_{ligand}$) are in parentheses. The chemical shifts of the 2,2'-bipyridyl protons for $[Ru(bpy)_2(phpztr)]^+$, $[Ru(bpy)_2(d_3\text{-}phpztr)]^+$, $[Ru(bpy)_2(Mephpztr)]^{2+}$ and $[Ru(bpy)_2(d_3\text{-}Mephpztr)]^{2+}$ have been omitted, because they fall in the normal range for these systems.

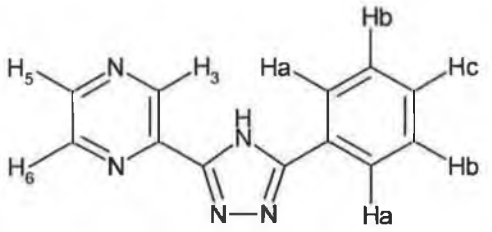

3-(pyrazin-2-yl)-5-phenyl-1,2,4-triazole
(Hphpztr)

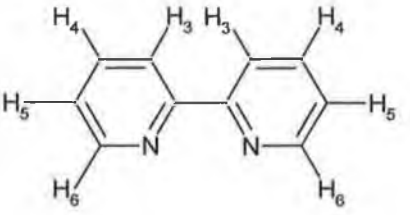

2,2'-bipyridyl
(bpy)

Figure 5. 7 *Structures of ligands discussed in this section, including the numbering system employed in the assignment of ^1H NMR peaks.*

Before discussing the ^1H NMR spectra of the methylated complexes, the ^1H NMR spectra of the reference complexes $[Ru(bpy)_2(phpztr)]^+$, $[Ru(d_8\text{-}bpy)_2(phpztr)]^+$ and $[Ru(bpy)_2(d_3\text{-}phpztr)]^+$ (see Figure 5. 8) will be briefly summarised. Ruthenium (II) bipyridyl complexes incorporating asymmetric 1,2,4-triazole ligands display complicated ^1H NMR spectra with considerable overlap of the ^1H NMR signals.[18,28] This is clearly evident in the ^1H NMR spectrum of $[Ru(bpy)_2(phpztr)]^+$, which has a total of 24 aromatic protons. However, deuteriation in $[Ru(d_8\text{-}bpy)_2(phpztr)]^+$ and $[Ru(bpy)_2(d_3\text{-}phpztr)]^+$ greatly simplifies the ^1H NMR spectra. In the absence of the 2,2'-bipyridine resonances in $[Ru(d_8\text{-}bpy)_2(phpztr)]^+$ and the pyrazine resonances in $[Ru(bpy)_2(d_3\text{-}phpztr)]^+$, it is possible to identify all of the resonances associated with the $phpztr^-$ ligand. The H_3 proton of the pyrazine ring is observed at 9.29 ppm and is coupled to the H_5 proton (J = 1.6 Hz), which is in agreement with the ^1H NMR spectra of $[Ru(bpz)_3]^{2+}$ (bpz = 2,2'-bipyrazine) and other pyrazyl-triazole complexes.[18, 29] The H_6 proton is more strongly coupled to the H_5 proton (J = 3.3 Hz) and appears as a doublet at 8.25 ppm. The splitting pattern of the H_5 proton is complicated, as it is coupled with the H_6 proton (J = 3.3 Hz) and with the H_3 proton (J = 1.6 Hz).

Complex	H_3	H_5	H_6	H_a	H_b	H_c	Me
$[Ru(bpy)_2(phpztr)]^+$	9.29	7.60	8.25	7.95	7.36	7.31	—
	(-0.10)	(-1.06)	(-0.41)	(-0.16)	(-0.18)	(-0.18)	—
$[Ru(d_8\text{-}bpy)_2(phpztr)]^+$	9.29	7.60	8.25	7.95	7.36	7.31	—
	(-0.10)	(-1.06)	(-0.41)	(-0.16)	(-0.18)	(-0.18)	—
$[Ru(bpy)_2(d_3\text{-}phpztr)]^+$	—	—	—	7.95	7.36	7.31	—
	—	—	—	(-0.16)	(-0.18)	(-0.18)	—
$[Ru(bpy)_2(Mephpztr)]^{2+}$	9.13	7.97	8.32	7.96	7.41	7.38	4.25
	(-0.26)	(-0.69)	(-0.34)	(-0.15)	(-0.13)	(-0.11)	—
$[Ru(d_8\text{-}bpy)_2(Mephpztr)]^{2+}$	9.13	7.97	8.32	7.96	7.41	7.38	4.25
	(-0.26)	(-0.69)	(-0.34)	(-0.15)	(-0.13)	(-0.11)	—
$[Ru(bpy)_2(d_3\text{-}Mephpztr)]^{2+}$	—	—	—	7.96	7.41	7.38	4.25
	—	—	—	(-0.15)	(-0.13)	(-0.11)	—

Table 5. 2 *^1H NMR data for the ruthenium(II) bipyridyl complexes discussed in this chapter. All data was obtained in d_3-acetonitrile. Values in parenthesis are the coordinated induced shifts relative to the free ligands.*

Three signals corresponding to H_a, H_b and H_c of the monsubstituted phenyl ring of phpztr$^-$ are observed at 7.95, 7.36 and 7.31 ppm in the ^1H NMR spectra of $[Ru(bpy)_2(phpztr)]^+$, $[Ru(d_8\text{-}bpy)_2(phpztr)]^+$ and $[Ru(bpy)_2(d_3\text{-}phpztr)]^+$ (see Table 5. 2 and Figure 5. 6). The H_a proton is coupled to the H_b proton, hence it is observed as a doublet. As H_b is coupled to both H_a and H_c, it is observed as a doublet of doublets, at 7.36 ppm. H_c is coupled to H_b, therefore H_c is observed as a triplet at 7.31 ppm.

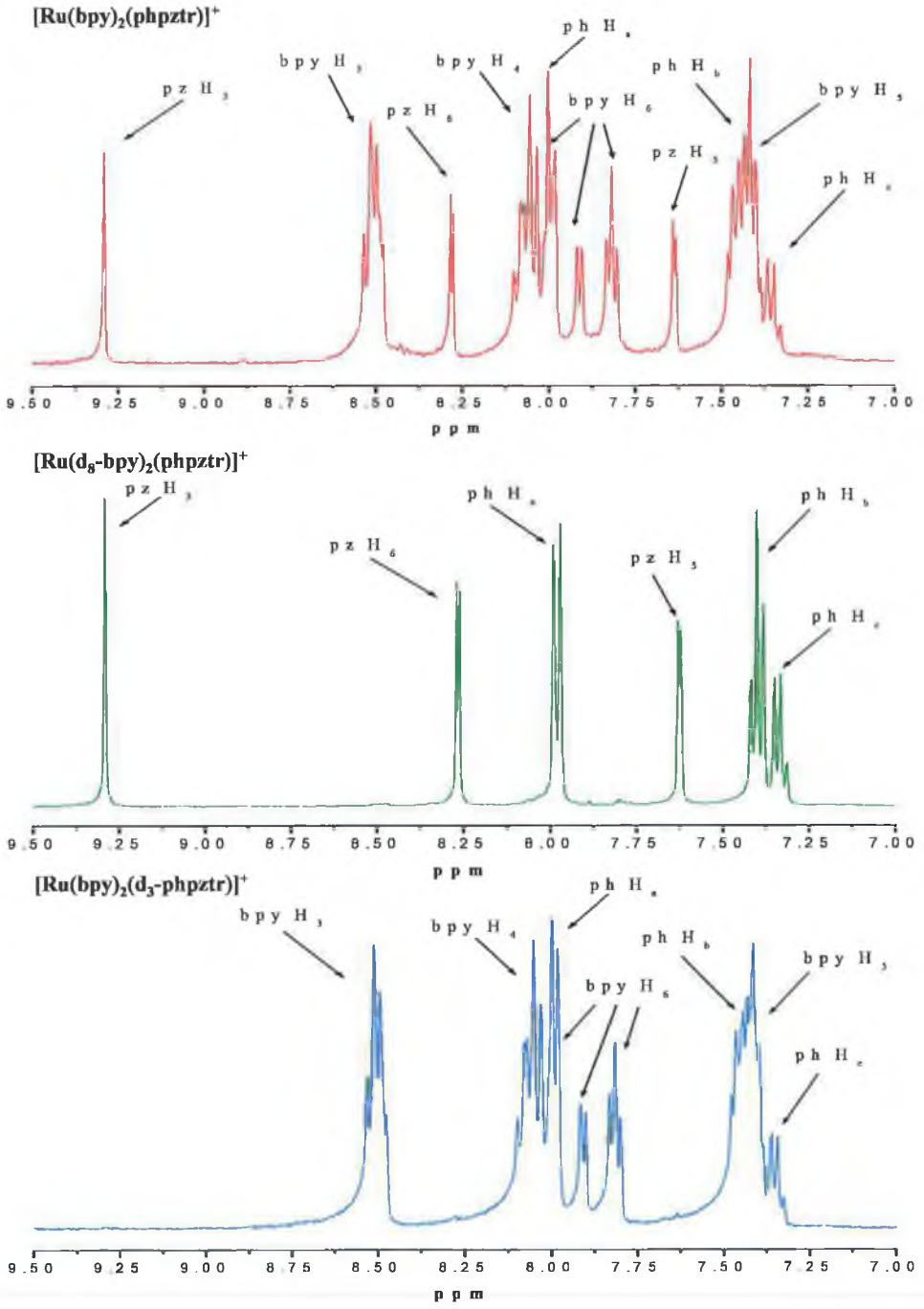

Figure 5. 8 *^1H NMR spectra of the aromatic region of $[Ru(bpy)_2(phpztr)]^+$, $[Ru(d_8\text{-}bpy)_2(phpztr)]^+$ and $[Ru(bpy)_2(d_3\text{-}phpztr)]^+$ in d_3-acetonitrile.*

Negative c.i.s. values were observed for all of the phpztr$^-$ protons in $[Ru(bpy)_2(phpztr)]^+$, $[Ru(d_8\text{-}bpy)_2(phpztr)]^+$ and $[Ru(bpy)_2(d_3\text{-}phpztr)]^+$. These negative c.i.s. values are attributed to:

(i) Metal-to-ligand π-back donation between the ruthenium metal centre and the pyrazine ring.

(ii) Delocalisation of electron density form the negatively charged triazole ring to the strong π-accepting pyrazine ring.

(iii) Through space anisotropy effects i.e. since the H6 proton is directed above a pyridine ring of an adjacent bpy ligand.

The ^{1}H NMR spectra of the aromatic region of $[Ru(bpy)_2(Mephpztr)]^{2+}$, $[Ru(d_8\text{-}bpy)_2(Mephpztr)]^{2+}$ and $[Ru(bpy)_2(d_3\text{-}Mephpztr)]^{2+}$ are presented in Figure 5. 9. The ^{1}H NMR spectrum of $[Ru(d_8\text{-}bpy)_2(phpztr)]^+$ is included for comparative purposes. Displayed in Figure 5. 10 is the ^{1}H NMR spectrum of $[Ru(bpy)_2(Mephpztr)]^{2+}$ with an expansion of the methyl region. The spectra show only one set of signals, thus indicating the presence of only one isomer for all complexes. $[Ru(bpy)_2(d_3\text{-}Mephpztr)]^{2+}$ has 27 inequivalent protons (Figure 5. 10) whose spectral signals are observed between 4.20 and 9.20 ppm. Many of the signals in the aromatic region were found to overlap. Complete assignments were made with the aid of two dimensional (COSY) spectra and by comparison with the ^{1}H NMR spectra of the selectively deuteriated $[Ru(d_8\text{-}bpy)_2(Mephpztr)]^{2+}$ and $[Ru(bpy)_2(d_3\text{-}Mephpztr)]^{2+}$ complexes. The chemical shifts of the Mephpztr protons of $[Ru(bpy)_2(Mephpztr)]^{2+}$, $[Ru(d_8\text{-}bpy)_2(Mephpztr)]^{2+}$ and $[Ru(bpy)_2(d_3\text{-}Mephpztr)]^{2+}$ are summarised in Table 5. 1.

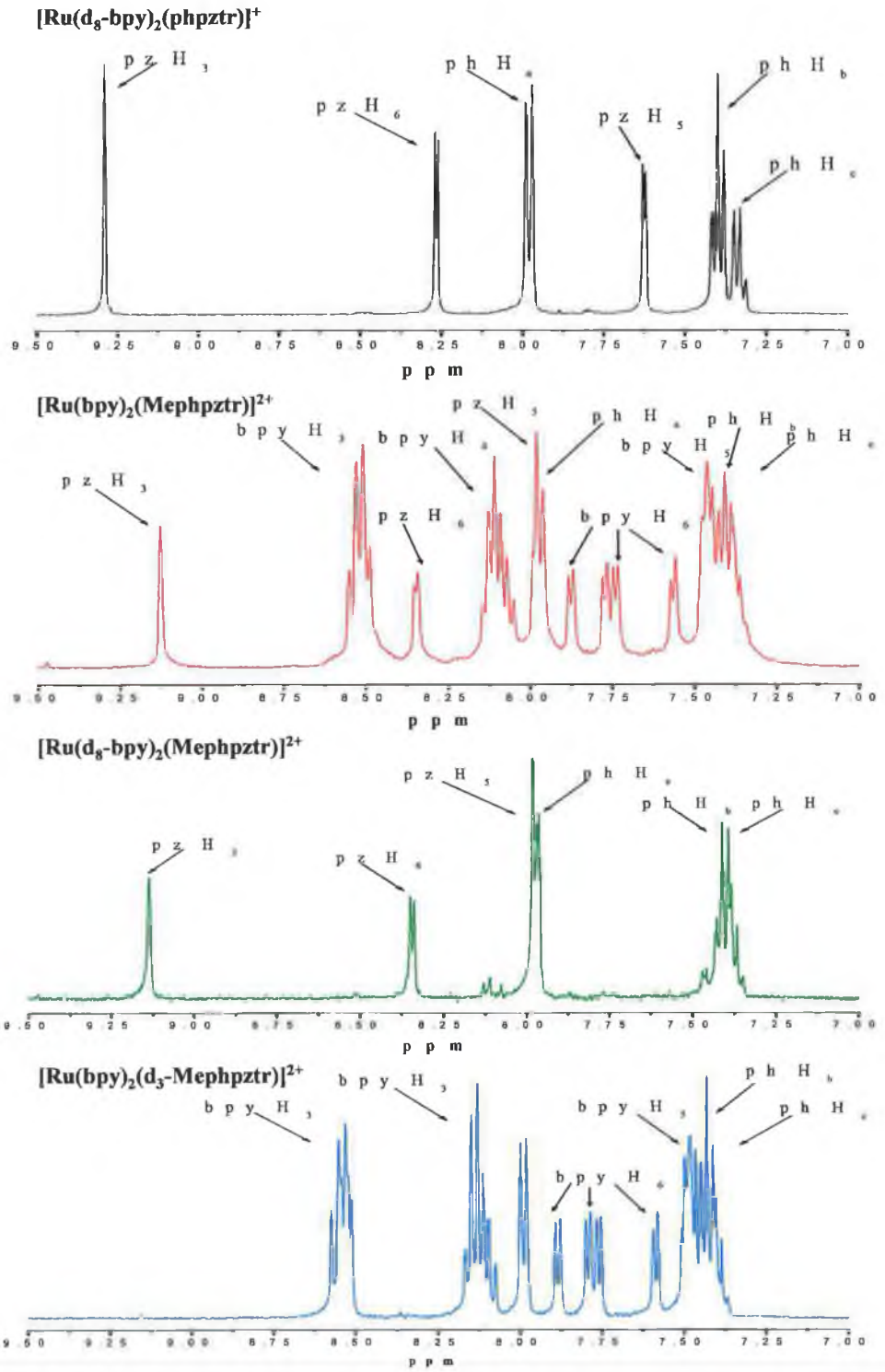

Figure 5. 9 *^{1}H NMR spectra of the aromatic region of $[Ru(d_8\text{-bpy})_2(phpztr)]^+$ $[Ru(bpy)_2(Mephpztr)]^{2+}$, $[Ru(d_8\text{-bpy})_2(Mephpztr)]^{2+}$ and $[Ru(bpy)_2(d_3\text{-Mephpztr})]^{2+}$ in d_3-acetonitrile.*

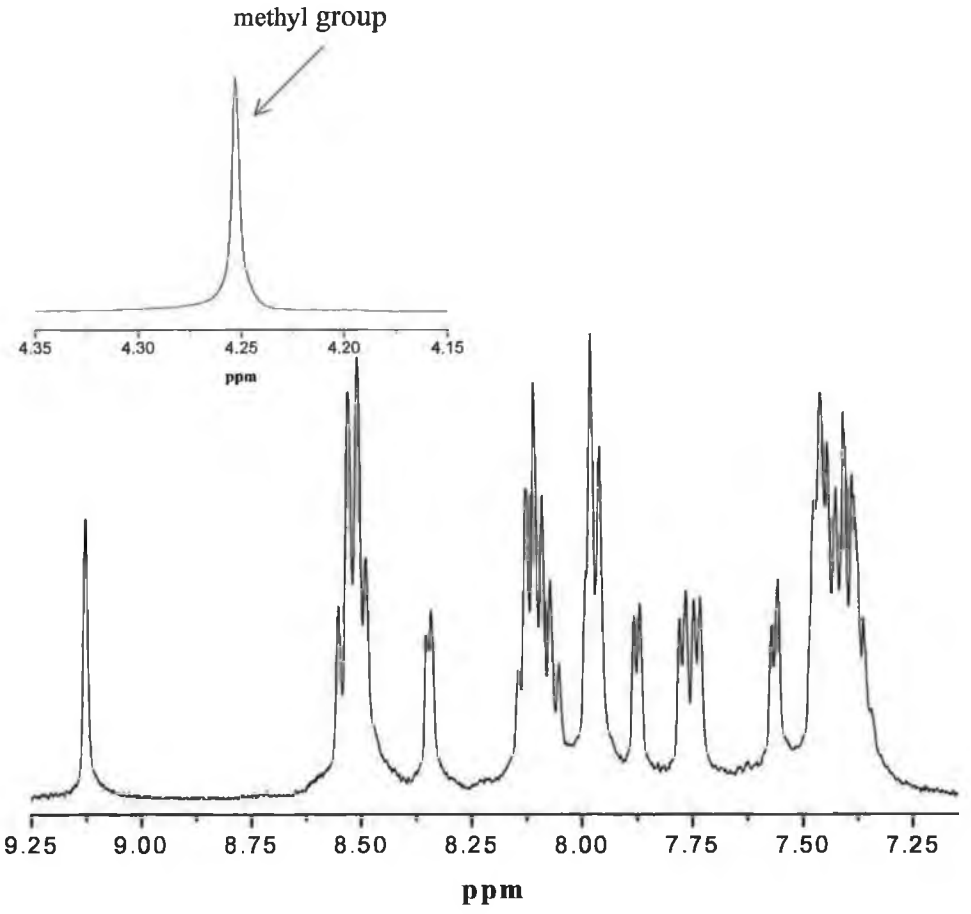

Figure 5. 10 *^{1}H NMR spectrum of $[Ru(bpy)_2(Mephpztr)]^{2+}$ in d_3-acetonitrile. The inset shows a close up of the methyl group.*

It is immediately clear from the spectra in Figure 5. 9, that by introduction of d_8-bpy, it is easier to indentify the pyrazyl-triazole protons. Thus, the H_3 proton is assigned to the singlet resonance at 9.13 ppm. $J_{3,5}$ and $J_{5,6}$ coupling is observed (see Figure 5. 11), and so the H_5 proton can be distinguished from the H_6 proton. Hence the doublet at 8.32 ppm is assigned to H_6, while the multiplet at 7.97 ppm contains the H_5 proton. These protons are absent in the ^{1}H NMR spectrum of $[Ru(bpy)_2(d_3\text{-}Mephpztr)]^{2+}$, which contains a deuteriated pyrazine ring. H_b on the phenyl ring is coupled to both H_c and H_a. Hence the multiplet with an integration

of 3 observed at 7.41 ppm is assigned to H_b (see Figure 5. 9 and Figure 5. 11). H_a is observed at 7.96 ppm.

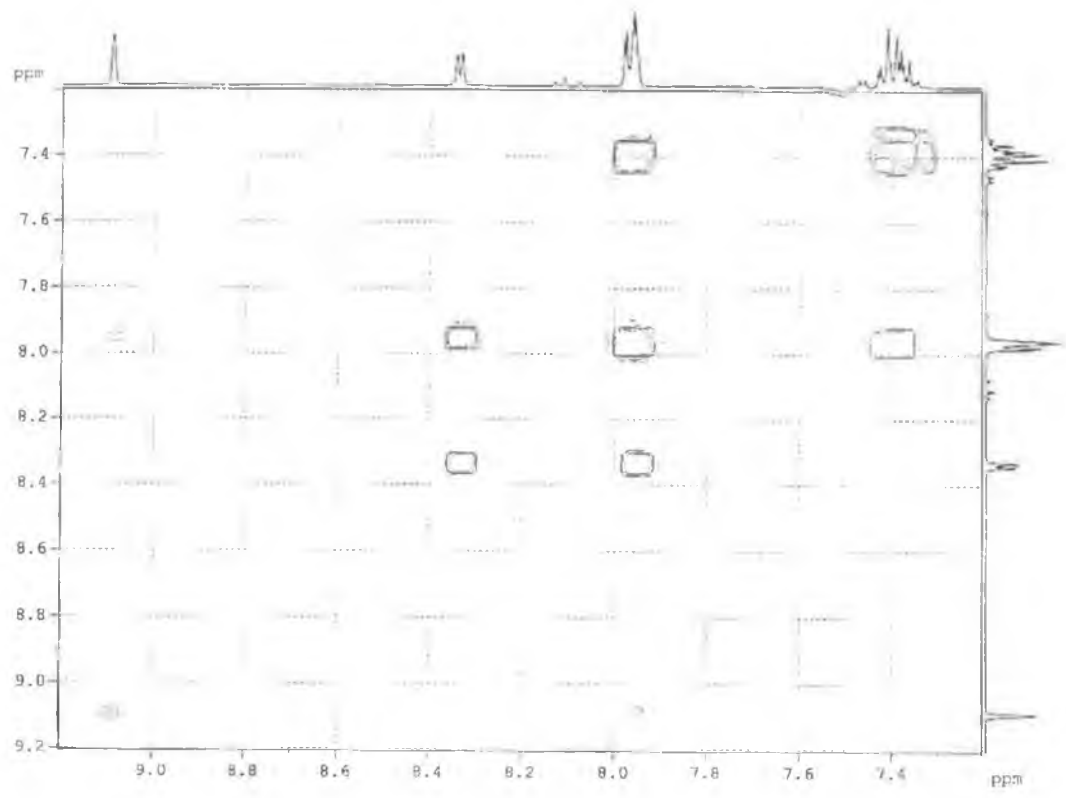

Figure 5. 11 *^1H COSY of the aromatic region of $[Ru(d_8\text{-bpy})_2(Mephpztr)]^{2+}$ in d_3-acetonitrile.*

As pointed out above, methylation of $[Ru(bpy)_2(pztr)]^+$ (pztr is 3-(pyrazin-2-yl)-1,2,4-triazole) may occur at either of the two non-equivalent nitrogens on the triazole ring (Figure 5. 12). These methylated isomers are referred to as the "N_1-Me" isomer and the "N_4-Me" isomer. The ^1H NMR spectra for this reaction shows the formation of both the N_1-Me and the N_4-Me isomers in the ratio of 70:30. The methyl group of N_1-Me was observed at 3.17 ppm, whilst that of N_4-Me was found at 4.26 ppm.[1] The "N_1-Me" isomer and the "N_2-Me" isomer in Ru(II) complexes incorporating 1,2,4-triazole ligands have exhibited different

redox potentials and absorption and emission maxima.[18,30] Hence identification of the methylation site of $[Ru(bpy)_2(phpztr)]^+$ is particularly important.

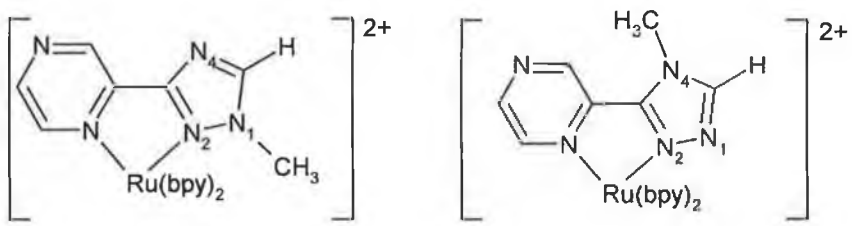

N_1-Me

N-Me δ: 3.17 ppm

N_4-Me

N-Me δ: 4.26 ppm

Figure 5. 12 *The two possible products of methylation of* $[Ru(bpy)_2(pztr)]^+$.

The formation of these isomers was also anticipated for $[Ru(bpy)_2(Mephpztr)]^{2+}$ and its deuteriated analogues. However, for these complexes the formation of a single isomer was observed. The singlet associated with the methyl substituent was found at 4.25 ppm for all three complexes. In contrast, the singlet associated with the methyl group of N_1-Me $[Ru(bpy)_2(Mepztr)]^{2+}$ was observed at 3.17 ppm. For this reason, it is unlikely the "N_1-Me" isomer of $[Ru(bpy)_2(Mephpztr)]^{2+}$, $[Ru(d_8\text{-bpy})_2(Mephpztr)]^{2+}$ and $[Ru(bpy)_2(d_3\text{-Mephpztr})]^{2+}$ was formed. The methyl group of the "N_4-Me" isomer of $[Ru(bpy)_2(Mepztr)]^{2+}$ was found at 4.26 ppm which is comparable to that of $[Ru(bpy)_2(Mephpztr)]^{2+}$, $[Ru(d_8\text{-bpy})_2(Mephpztr)]^{2+}$ and $[Ru(bpy)_2(d_3\text{-Mephpztr})]^{2+}$. This may suggest methylation of the N_4 position of the 1,2,4-triazole has occurred. However, as noted in Section 5.2.1, the three Mephpztr complexes are purple in colour whereas ruthenium complexes containing methylated 1,2,4-triazoles are orange.[30,31,32] However, in concentrated sulphuric acid, $[Ru(bpy)_2(phpztr)]^+$ and other ruthenium complexes of the form $[Ru(bpy)_2(L)]^+$ (L= pyrazyl-triazole ligand) can be protonated on the non-coordinating nitrogen of the pyrazine ring yielding a purple coloured solution with a λ_{max} of ~ 535 nm.[18,20,31] As $[Ru(bpy)_2(Mephpztr)]^{2+}$ and

its deuteriated analogues have λ_{max} at 545 nm (Section 5.2.4), it seems likely that methylation of the nitrogen of the pyrazine ring has occurred.

It is well established that in pyrazyl-triazole ligands, the pyrazine fragment is a poorer σ-donor and better π-acceptor than the 1,2,4-triazole.[16,18] Hence for the methylated complexes, the methyl substituent is expected to resonate significantly further upfield than the methyl group in the "N_4-Me" isomer of $[Ru(bpy)_2(Mepztr)]^{2+}$. As previously discussed, the methyl resonances for both sets of complexes are observed at $\delta \sim 4.25$. Previous studies of ruthenium bipyridyl complexes containing a negatively charged pyrazyl-triazole ligand have suggested a considerable degree of delocalisation of the negative charge on the triazole ring onto the pyrazine, thus increasing the electron density on the pyrazine fragment.[31] It is likely a similar interaction is occurring between the negatively charged triazole and the methylated pyrazine in $[Ru(bpy)_2(Mephpztr)]^{2+}$, $[Ru(d_8\text{-}bpy)_2(Mephpztr)]^{2+}$ and $[Ru(bpy)_2(d_3\text{-}Mephpztr)]^{2+}$. Hence the methyl group of these complexes resonates at a similar chemical shift to that of the N_4-Me isomer of $[Ru(bpy)_2(Mepztr)]^{2+}$.

H_3 of $[Ru(bpy)_2(Mephpztr)]^{2+}$ is observed at 9.13 ppm whilst H_3 of $[Ru(bpy)_2(phpztr)]^{+}$ is observed at 9.29 ppm. Methylation produces a positively charged nitrogen on the pyrazine ring of $[Ru(bpy)_2(Mephpztr)]^{2+}$. As previously discussed, the electron rich deprotonated triazole ring offloads electron density onto its substituents. This electron delocalisation is felt most by the H_3 on the pyrazine. Hence the H_3 proton of $[Ru(bpy)_2(Mephpztr)]^{2+}$ is shifted upfield relative to $[Ru(bpy)_2(phpztr)]^{+}$ (see Table 5. 2 and Figure 5. 9). Note for the methylated complex $[Ru(bpy)_2(Mepztr)]^{2+}$, methylation of the triazole ring results shifts the H_3 proton from 9.17 to 9.47 ppm.[18] A very peculiar observation is that for $[Ru(bpy)_2(Mephpztr)]^{2+}$, the H_5 and H_6 protons of the pyrazine have been shifted downfield compared to $[Ru(bpy)_2(phpztr)]^{+}$. As previously discussed, the methyl group and H_3 of $[Ru(bpy)_2(Mephpztr)]^{2+}$ experiences the effect of electron delocalisation between the triazole and the methylated pyrazine. This is

apparently not of importance for the H_5 and H_6 protons, but it is unclear why a different behaviour is observed for these protons.

The pH dependence of $[Ru(d_8\text{-bpy})_2(Mephpztr)]^{2+}$ was also investigated using ^1H NMR spectroscopy (Figure 5. 13). The pH dependence of the ^1H NMR spectra were monitored in D_2O. pH adjustments were made by adding 75 µl of 2 M NaOH or 2 M H_2SO_4 to a 100 cm^3 volume of the dissolved complex. In the solvent system used, the methyl group is observed at 4.55 ppm compared to the D_2O solvent peak at 4.70 ppm. As the pH increased, the D_2O solvent peak eventually masked the singlet due to the methyl group. Consequently, the chemical shift of the H_3 singlet was monitored as a function of pH.

The effect of pH on the ^1H NMR spectrum of $[Ru(d_8\text{-bpy})_2(Mephpztr)]^{2+}$ is shown in Figure 5. 13. At pH 1.00, the H_3 proton of $[Ru(d_8\text{-bpy})_2(Mephpztr)]^{2+}$ resonates at 9.48 ppm. This gradually shifts to lower field with increasing pH. The ^1H NMR spectrum at a pH of 9.50 clearly shows the presence of two species. However, at pH 12 there is only one set of signals, thus indicating only one species is present in solution. The ^1H NMR spectrum of $[Ru(d_8\text{-bpy})_2(phpztr)]^{+}$ was also obtained at pH 12 (see Figure 5. 13). The ^1H NMR spectra of $[Ru(d_8\text{-bpy})_2(phpztr)]^{+}$ and $[Ru(d_8\text{-bpy})_2(Mephpztr)]^{2+}$ are similar at pH 12. Hence it is reasonable to deduce that loss of the methyl group is the most reasonable explanation for the observed ^1H NMR spectral changes with increasing pH.

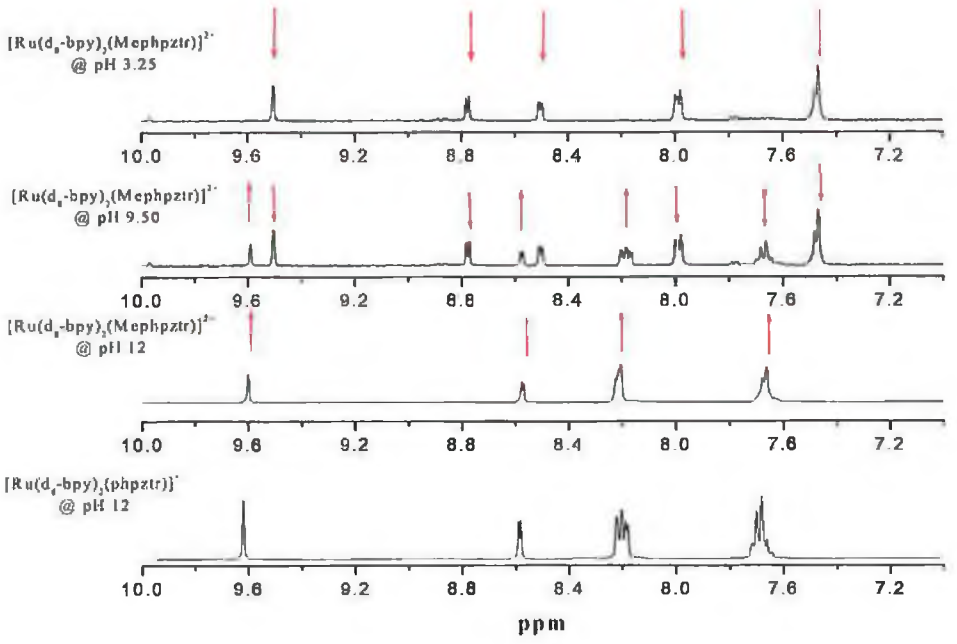

Figure 5. 13 *pH dependent ^1H NMR spectral changes of $[Ru(d_8\text{-}bpy)_2(Mephpztr)]^{2+}$. A ^1H NMR of $[Ru(d_8\text{-}bpy)_2(phpztr)]^{+}$ at pH 12 is also included.*

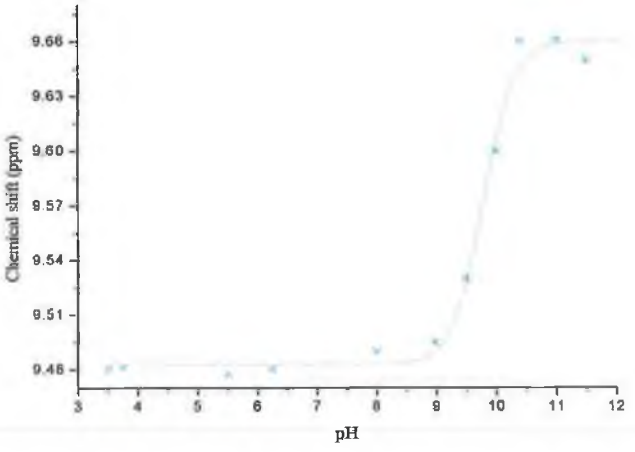

Figure 5. 14 *Chemical shift of the H_3 proton versus pH for $[Ru(d_8\text{-}bpy)_2(Mephpztr)]^{2+}$.*

A plot of the chemical shift of the H_3 singlet against pH, results in a curve (see Figure 5. 14), which allows the pH inflection point (pH_i) to be determined. A pH_i value of 9.80 was obtained. Hence loss of the methyl group from $[Ru(d_8\text{-bpy})_2(Mephpztr)]^{2+}$ occurs at a pH of 9.80.

5.2.4 Absorption and emission properties

Absorption and emission data for all complexes synthesised in this chapter are presented in Table 5. 3. The table also contains data for $[Ru(bpy)_3]^{2+}$.

Complex	Absorption	Emission	
	$\lambda_{max}{}^a/(\varepsilon \times 10^4)$	298 K[a] (77 K)[c]	$\tau_{298\ K}$ (ns)[b]
$[Ru(bpy)_2(phpztr)]^+$	450 (1.19)	670 (610)	217[d]
$[Ru(d_8\text{-bpy})_2(phpztr)]^+$	450 (1.18)	670 (610)	270[d]
$[Ru(bpy)_2(d_3\text{-phpztr})]^+$	450 (1.14)	670 (610)	210[d]
$[Ru(bpy)_2(Hphpztr)]^{2+}$	445 (1.31)	655 (600)	570[d]
$[Ru(d_8\text{-bpy})_2(Hphpztr)]^{2+}$	445 (1.28)	655 (600)	565[d]
$[Ru(bpy)_2(d_3\text{-Hphpztr})]^{2+}$	445 (1.35)	655 (600)	560[d]
$[Ru(bpy)_2(H_2phpztr)]^{3+}$	535 (1.22)	—(—)	—(—)
$[Ru(bpy)_2(Mephpztr)]^{2+}$	545 (1.05)	—(—)	—(—)
$[Ru(d_8bpy)_2(Mephpztr)]^{2+}$	545 (1.00)	—(—)	—(—)
$[Ru(bpy)_2(d_3\text{-Mephpztr})]^{2+}$	545 (1.07)	—(—)	—(—)
$[Ru(bpy)_2(HMephpztr)]^{3+}$	535 (1.15)	—(—)	—(—)
$[Ru(d_8\text{-bpy})_2(HMephpztr)]^{3+}$	535 (1.18)	—(—)	—(—)
$[Ru(bpy)_2(d_3\text{-HMephpztr})]^{3+}$	535 (1.16)	—(—)	—(—)
$[Ru(bpy)_3]^{2+}$	452 (1.30)	620 (580)	610

Table 5. 3 *Absorption and luminescence properties of the ruthenium pyrazyl-triazole complexes. τ refers to the emission lifetime. Data for $[Ru(bpy)_3]^{2+}$ is also included for evaluation purposes. [a]Data in acetonitrile, [b] in deoxygenated acetonitrile and [c] in ethanol/methanol(4:1). [d]Reference [34].*

The UV-Vis absorption and emission spectra of all complexes were found to be independent of the level of deuteration. This is not unexpected as deuteration can affect vibrational fine structure of absorption and emission spectra, these differences are only observed at very low temperatures (< 10 K) with high-resolution spectroscopic techniques.[33]

The data obtained for the reference complex $[Ru(bpy)_2(phpztr)]^+$ are in agreement with earlier studies.[22,34] The absorption spectra of $[Ru(bpy)_2(phpztr)]^+$, $[Ru(bpy)_2(Hphpztr)]^{2+}$ and $[Ru(bpy)_2(H_2phpztr)]^{3+}$ are shown in Figure 5. 15. In the UV-Vis absorption spectrum of $[Ru(bpy)_2(phpztr)]^+$, a broad band is observed in the visible part of the spectrum at 450 nm. Ground-state resonance Raman measurements at 457.9 nm have assigned this low energy absorption band to an $Ru\rightarrow\pi^*(bpy)$ MLCT transition.[22,34] No evidence for a $Ru\rightarrow\pi^*(phpztr^-)$ transition was observed in the resonance Raman studies at 457.9 nm. The intense absorption band at 285 nm is assigned to a ligand centred (π-π^*) transition. The ^{1}MLCT absorption band of $[Ru(bpy)_2(Hphpztr)]^{2+}$ at 430 nm is blue shifted compared to the corresponding absorption in $[Ru(bpy)_2(phpztr)]^+$. This arises form a change in the σ-donor/π-acceptor properties of the pyrazyl-triazole ligand on protonation of the triazole moiety. Since protonation results in a reduction of the electron density on the 1,2,4-triazole ring, the ligand becomes a weaker σ-donor and better π-acceptor than the deprotonated form.[16] This results in a stabilisation of the HOMO of $[Ru(bpy)_2(Hphpztr)]^{2+}$ compared to $[Ru(bpy)_2(phpztr)]^+$. A larger energy gap now exists between the HOMO and the LUMO of $[Ru(bpy)_2(Hphpztr)]^{2+}$, which manifests itself as a higher energy λ_{max}. A similar trend was observed for the pyrazyl-triazole complexes $[Ru(bpy)_2(pztr)]^+$ and $[Ru(bpy)_2(Hpztr)]^{2+}$ (pztr = is 3-(pyrazin-2-yl)-1,2,4-triazole).[18] $[Ru(bpy)_2(pztr)]^+$ has an absorption maximum at 456 nm while the protonated complex $[Ru(bpy)_2(Hpztr)]^{2+}$ has an absorption maximum at 440 nm. The blue shift in the absorption maximum of $[Ru(bpy)_2(Hpztr)]^{2+}$ compared to $[Ru(bpy)_2(pztr)]^+$ was attributed to a stabilisation of the HOMO on protonation of the complex.

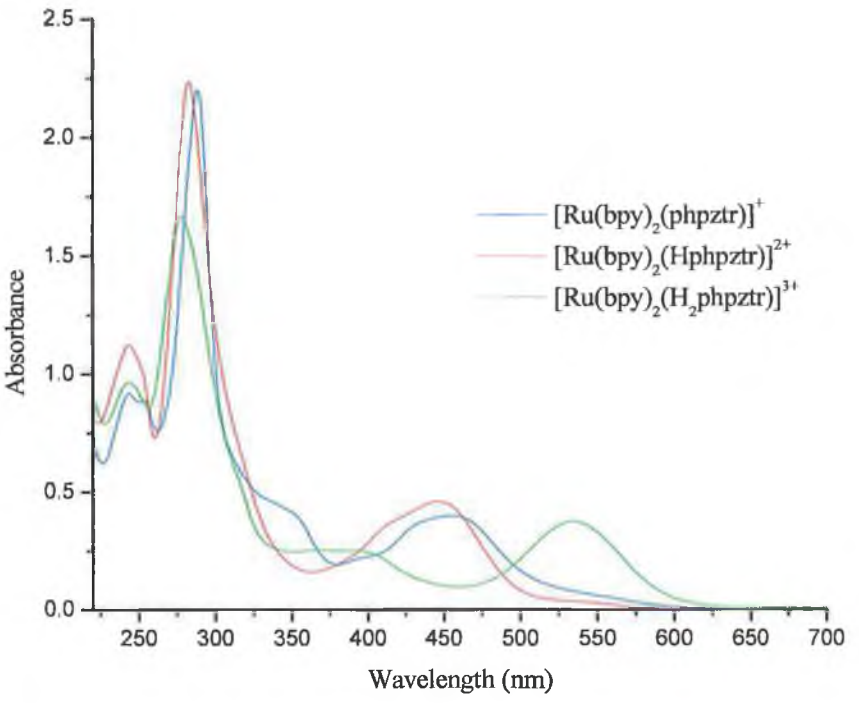

Figure 5. 15 *Absorption spectra of $[Ru(bpy)_2(phpztr)]^+$, $[Ru(bpy)_2(Hphpztr)]^{2+}$ and $[Ru(bpy)_2(H_2phpztr)]^{3+}$ in acetonitrile. The absorption spectrum of $[Ru(bpy)_2(Hphpztr)]^{2+}$ was obtained in the presence of trifluoroacetic acid, while the absorption spectrum of $[Ru(bpy)_2(H_2phpztr)]^{3+}$ was obtained in the presence of concentrated sulphuric acid.*

For ruthenium(II) bipyridyl complexes incorporating a pyrazyl-triazole based ligand, the non-coordinating nitrogen of the pyrazine ring can also be protonated.[18,31] For this second protonation step considerable changes are observed in the UV-Vis absorption spectrum of with the appearance of an absorption band at ~540 nm. This is illustrated in the absorption spectrum of the doubly protonated complex $[Ru(bpy)_2(H_2phpztr)]^{3+}$ which is purple in colour and exhibits a λ_{max} at 535 nm (see Table 5. 3 and Figure 5. 15). The positive charge on the pyrazine ring of $[Ru(bpy)_2(H_2phpztr)]^{3+}$ increases the π-acceptor character of the pyrazyl-triazole ligand by lowering the π* energy level. A smaller energy

gap now exists between the HOMO and the LUMO. Hence the λ_{max} of $[Ru(bpy)_2(H_2phpztr)]^{3+}$ is red shifted compared to $[Ru(bpy)_2(Hphpztr)]^{2+}$ and the deprotonated complex $[Ru(bpy)_2(phpztr)]^{+}$.

Figure 5. 16 shows the absorption spectra of $[Ru(bpy)_2(Mephpztr)]^{2+}$ and $[Ru(bpy)_2(HMephpztr)]^{3+}$. The spectrum of $[Ru(bpy)_2(H_2phpztr)]^{3+}$ is also included for comparative purposes. By comparison with the absorption spectra of other ruthenium polypyridyl complexes[32,35] and that of the unmethylated starting material $[Ru(bpy)_2(phpztr)]^{+}$, the absorption band at 545 nm in $[Ru(bpy)_2(Mephpztr)]^{2+}$ is assigned to an ^{1}MLCT transition. This absorption band is red shifted by 90 nm when compared to the same band in $[Ru(bpy)_2(phpztr)]^{+}$. Methylation results in the presence of a positive charge on the pyrazine ring, which enhances the π-acceptor capabilities of the pyrazine moiety. Hence the methylated complexes have lower π* orbitals compared to their corresponding starting materials. As a result the ^{1}MLCT band of $[Ru(bpy)_2(phpztr)]^{+}$ is red shifted when methylated. A similar trend was observed on protonation of the pyrazine ring of $[Ru(bpy)_2(phpztr)]^{+}$ with concentrated sulphuric acid. In this case an absorption band appears at 535 nm.

The absorption spectrum of $[Ru(bpy)_2(Mephpztr)]^{2+}$ was also recorded in the presence of trifluoroacetic acid (see Table 5. 3 and Figure 5. 16). The ^{1}MLCT absorption band of $[Ru(bpy)_2(HMephpztr)]^{3+}$ at 535 nm is blue shifted compared to the corresponding absorption in $[Ru(bpy)_2(Mephpztr)]^{2+}$. This blue shift of the ^{1}MLCT band in the presence of acid is most likely due to protonation of the triazole ring as there are no other vacant protonation sites on the complex. On protonation of the triazole ring the σ-donation ability of the triazole ring is reduced due to the removal of the negative charge, thus lowering the energy of the metal d orbitals (due to the reduction in the electron density on the metal centre). Consequently the energy separation between the HOMO and LUMO increases. Hence the ^{1}MLCT absorption band is blue shifted.

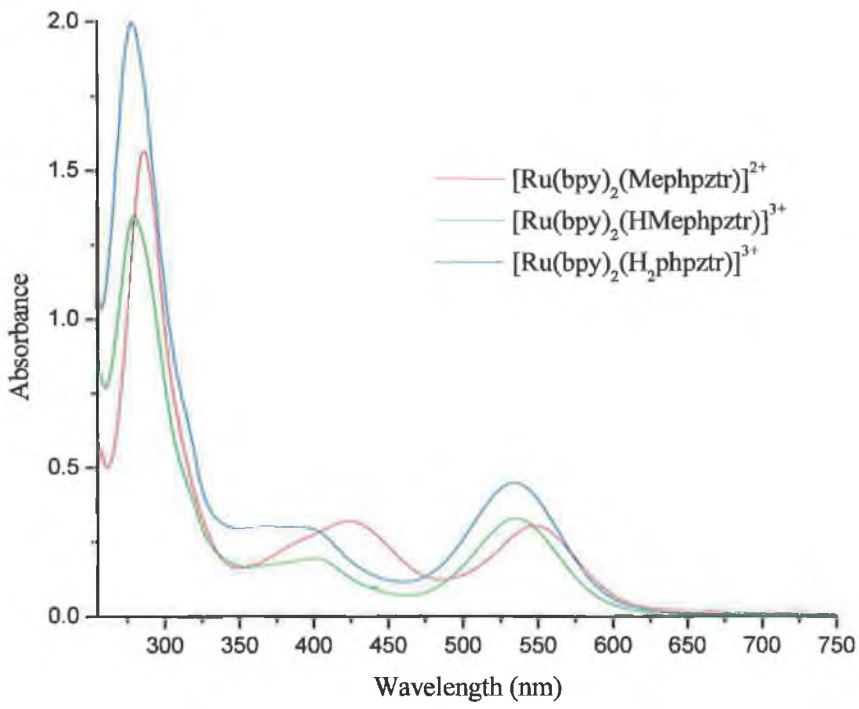

Figure 5. 16 *Absorption spectra of* $[Ru(bpy)_2(Mephpztr)]^{2+}$, $[Ru(bpy)_2(HMephpztr)]^{3+}$ *and* $[Ru(bpy)_2(H_2phpztr)]^{3+}$ *in acetonitrile. The absorption spectrum of* $[Ru(bpy)_2(HMephpztr)]^{3+}$ *was obtained in the presence of trifluoroacetic acid, while the absorption spectrum of* $[Ru(bpy)_2(H_2phpztr)]^{3+}$ *was obtained in the presence of concentrated sulphuric acid.*

Room temperature emission spectra of $[Ru(bpy)_2(phpztr)]^{+}$ and $[Ru(bpy)_2(Hphpztr)]^{2+}$ were recorded in acetonitrile. The emission spectra of $[Ru(bpy)_2(phpztr)]^{+}$ and $[Ru(bpy)_2(Hphpztr)]^{2+}$ are shown in Figure 5. 17. At 298 K, the emission from $[Ru(bpy)_2(phpztr)]^{+}$ originates from a ^{3}MLCT state. $[Ru(bpy)_2(phpztr)]^{+}$ has been studied using excited state resonance Raman spectroscopy.[22] The spectra show clearly that the excited state is bpy-based with bands for bpy^- at 1211 and 1285 cm^{-1}.

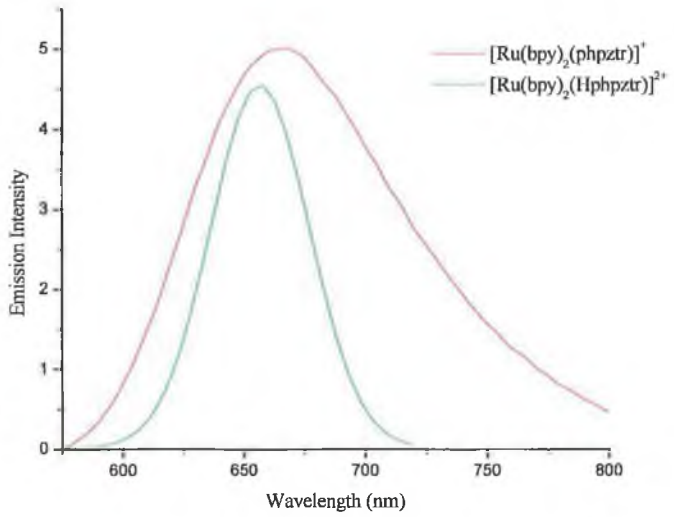

Figure 5. 17 *Emission Spectra of* $[Ru(bpy)_2(phpztr)]^+$ *and* $[Ru(bpy)_2(Hphpztr)]^{2+}$ *in acetonitrile at 298 K. The emission spectrum of* $[Ru(bpy)_2(Hphpztr)]^{2+}$ *was obtained in the presence of trifluoroacetic acid*

In ruthenium polypyridyl complexes, deuteriation of one of the ligands in a mixed ligand complex will only affect the emission lifetime if the emitting state is based on that ligand.[36,37] This is clearly evident for $[Ru(bpy)_2(phpztr)]^+$ and its deuteriated analogues $[Ru(d_8\text{-}bpy)_2(phpztr)]^+$ and $[Ru(bpy)_2(d_3\text{-}phpztr)]^+$. For $[Ru(bpy)_2(phpztr)]^+$ an emission lifetime of 217 ns was observed at 298 K. Deuteration of the bpy ligand leads to an emission lifetime of 270 ns whilst deuteration of the pyrazine ring has little effect on the emission lifetime (Table 5. 3). These observations confirm the assignment of the lowest ^{3}MLCT state as being bpy based. As observed for the absorption spectra, the emission maximum of the protonated complex $[Ru(bpy)_2(Hphpztr)]^{2+}$ is blue shifted compared to $[Ru(bpy)_2(phpztr)]^+$ (see Table 5. 3 and Figure 5. 17). Protonating the triazole ring reduces its σ-donating abilities, thus decreasing electron density on the metal centre. The HOMO level is stabilised, thus increasing the energy gap between the

ground and the ^{3}MLCT states. Hence the emission maximum of $[Ru(bpy)_2(Hphpztr)]^{2+}$ is blue shifted compared to that of $[Ru(bpy)_2(phpztr)]^+$. The ^{3}MLCT emission band of $[Ru(bpy)_2(Hpztr)]^{2+}$ at 658 nm is blue shifted compared to the corresponding emission in $[Ru(bpy)_2(pztr)]^+$ at 668 nm.[18] This blue shift was ascribed to the weaker σ-donor properties of the Hpztr ligand, leading to reduced electron density on the metal centre, and as a consequence increasing energy gap.

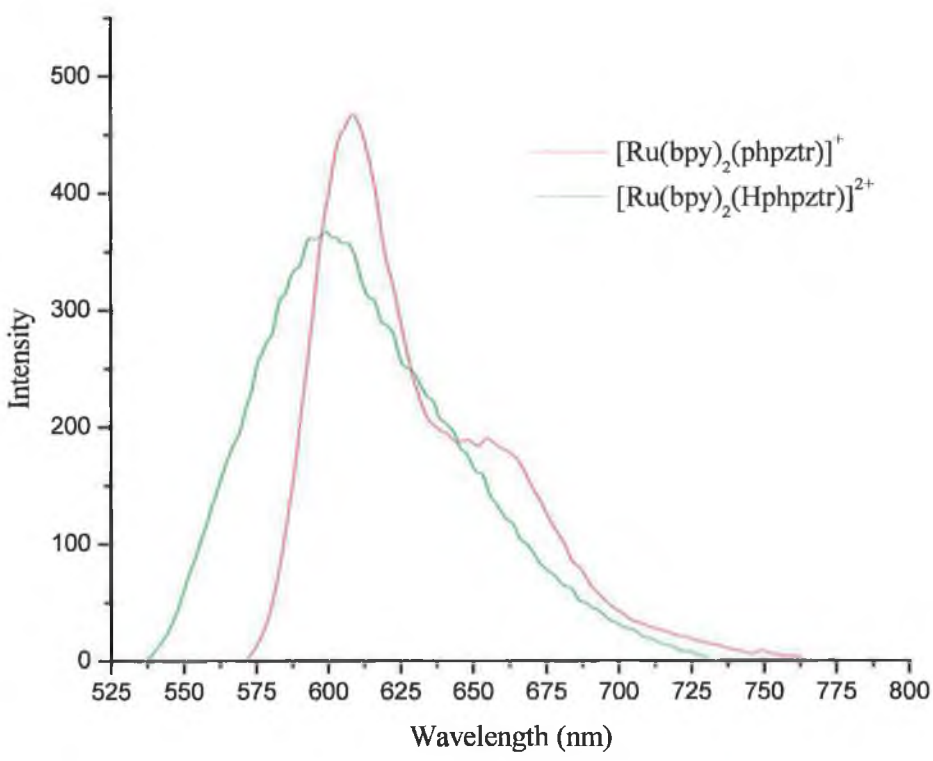

Figure 5. 18 *Emission Spectra of $[Ru(bpy)_2(phpztr)]^+$ and $[Ru(bpy)_2(Hphpztr)]^{2+}$ in ethanol:methanol (4:1) at 77 K. The emission spectrum of $[Ru(bpy)_2(Hphpztr)]^{2+}$ was obtained in the presence of trifluoroacetic acid.*

The emission spectra of $[Ru(bpy)_2(phpztr)]^+$ and $[Ru(bpy)_2(Hphpztr)]^{2+}$ at 77 K are displayed in Figure 5. 18. $[Ru(bpy)_2(phpztr)]^+$ has an emission maximum at 610 nm while the emission maximum of $[Ru(bpy)_2(Hphpztr)]^{2+}$ is observed at 610 nm. At 77 K, the emission from $[Ru(bpy)_2(phpztr)]^+$ and the protonated complex $[Ru(bpy)_2(Hphpztr)]^{2+}$ originates from a ^{3}MLCT state. There is a blue shift in the emission maxima of $[Ru(bpy)_2(phpztr)]^+$ and $[Ru(bpy)_2(Hphpztr)]^{2+}$ at 77 K when compared to the maxima of the complexes at 298 K (Table 5. 3). This observed emission temperature dependence is a result of rigidchromism.[38] At 298 K, the solvent dipoles will adopt a configuration that stabilises the ^{3}MLCT, whereas at 77 K the solvent dipoles are immobile on the timescale of the excited state and so cannot respond to the change in electronic configuration that accompanies an excitation.

No emission was detected from $[Ru(bpy)_2(H_2phpztr)]^{3+}$ or the methylated complexes $[Ru(bpy)_2(Mephpztr)]^{2+}$ and $[Ru(bpy)_2(HMephpztr)]^{3+}$ at 298 K or 77 K (see Table 5. 3). This observation can be rationalised by considering the two main factors that control the emission properties of ruthenium(II) polypyridyl complexes:

(i) The energy gap between the ground state and the ^{3}MLCT state (the energy gap law).[39,40,41]

(ii) The energy gap between the ^{3}MLCT state and the deactivating ^{3}MC state.[42,43,44]

The absorption studies suggest a smaller energy gap exists between the ground and the ^{1}MLCT state of $[Ru(bpy)_2(H_2phpztr)]^{3+}$ and the methylated complex $[Ru(bpy)_2(Mephpztr)]^{2+}$. Previous studies of ruthenium (II) systems have found a decrease in the energy of the ^{1}MLCT state is also reflected in the energy of the ^{3}MLCT.[4] Hence the energy of the ^{3}MLCT is lower for $[Ru(bpy)_2(Mephpztr)]^{2+}$ and $[Ru(bpy)_2(H_2phpztr)]^{3+}$ compared to $[Ru(bpy)_2(phpztr)]^+$. As a result the energy separation between the ground and the ^{3}MLCT states is reduced for $[Ru(bpy)_2(H_2phpztr)]^{3+}$ and the methylated complexes $[Ru(bpy)_2(Mephpztr)]^{2+}$

and $[Ru(bpy)_2(HMephpztr)]^{3+}$. This has important consequences, as according to the energy gap law the closer the two energy levels are the larger the rate of nonradiative deactivation. Hence $[Ru(bpy)_2(H_2phpztr)]^{3+}$, $[Ru(bpy)_2(Mephpztr)]^{2+}$ and $[Ru(bpy)_2(HMephpztr)]^{3+}$ do not emit. The energy gap law has accounted for enhanced rates of nonradiative deactivation in ruthenium polypyridyl complexe.[22,45,46] For example the ^{3}MLCT (λ_{max} = 678 nm) of $[Ru(dmb)(bpy(COOEt)_2)(dpp)]^{2+}$ (dmb = 4,4'-dimethyl-2,2'-bipyridine; dpp = 2,3-bis(2-pyridyl)pyrazine) decays with a lifetime of 788 ns while the ^{3}MLCT (λ_{max} > 850 nm) of $[Ru(dmb)(bpy(COOEt)_2)(dpb)]^{2+}$ (dpb = 2,3-bis(2-pyridyl)benzoquinoxaline) decays with a lifetime of 98 ns.[46] The ligand based reduction potentials of $[Ru(dmb)(bpy(COOEt)_2)(dpp)]^{2+}$ and $[Ru(dmb)(bpy(COOEt)_2)(dpb)]^{2+}$ are – 0.96 V and –0.75 V respectively. The authors concluded that the energy gap for $[Ru(dmb)(bpy(COOEt)_2)(dpb)]^{2+}$ is smaller relative to the ruthenium complex $[Ru(dmb)(bpy(COOEt)_2)(dpp)]^{2+}$. Hence the rate of nonradiative deactivation is greater for $[Ru(dmb)(bpy(COOEt)_2)(dpb)]^{2+}$ compared to $[Ru(dmb)(bpy(COOEt)_2)(dpp)]^{2+}$.

As well as lowering the π^* energy level, methylation/protonation of $[Ru(bpy)_2(phpztr)]^+$ decreases the σ-donor capacity of the pyrazyl-triazole ligand. Consequently the ligand field splitting is decreased, which favours thermal population of the nonradiative e_g^* (^{3}MC) state. It is also possible the excited states of $[Ru(bpy)_2(H_2phpztr)]^{3+}$, $[Ru(bpy)_2(Mephpztr)]^{2+}$ and $[Ru(bpy)_2(HMephpztr)]^{3+}$ decay via a ^{3}MC excited state while $[Ru(bpy)_2(phpztr)]^+$ and $[Ru(bpy)_2(Hphpztr)]^{2+}$ do not efficiently populate this state at 298 K or 77 K. As a result $[Ru(bpy)_2(phpztr)]^+$ and $[Ru(bpy)_2(Hphpztr)]^{2+}$ were found to emit, while no emission was detected from $[Ru(bpy)_2(H_2phpztr)]^{3+}$, $[Ru(bpy)_2(Mephpztr)]^{2+}$ or $[Ru(bpy)_2(HMephpztr)]^{3+}$. A decrease in luminescence lifetimes from 142 ns to 2 ns upon protonation of the pyridyl-triazole ligand in $[Ru(bpy)_2(pytr)]^+$ (pytr = 3-(pyridin-2-yl)-1,2,4-triazole) has been attributed to population of a non-radiative ^{3}MC decay path arising from the decrease in the MLCT/MC gap on protonation.[47]

5.2.5 Acid base properties

As observed in Section 5.2.4, the absorption spectra of $[Ru(bpy)_2(Mephpztr)]^{2+}$ and $[Ru(bpy)_2(phpztr)]^{+}$ are pH dependent. The ground-state acid-base chemistry of the complexes was investigated using UV/Vis absorption spectroscopy. The pH dependence of the absorption spectra was monitored in Britton-Robinson buffer. pH adjustments were made by adding 75 μl of 2 M NaOH or 2 M H_2SO_4 to a 100 cm^3 volume of the dissolved complex. The effect of pH on the absorption spectrum of $[Ru(bpy)_2(Mephpztr)]^{2+}$ is displayed in Figure 5. 19. Figure 5. 20 shows the effect of pH on the absorption spectrum of $[Ru(bpy)_2(phpztr)]^{+}$ for comparative purposes. The absorption spectra for both complexes show isosbestic points, indicating that only one pH dependent process is occurring. There is clearly a different pH trend for $[Ru(bpy)_2(Mephpztr)]^{2+}$ compared to $[Ru(bpy)_2(phpztr)]^{+}$. For $[Ru(bpy)_2(Mephpztr)]^{2+}$, no pH changes were observed in the pH range 1-7. However, in the pH range 7-12 the absorption spectrum clearly alters (see Figure 5. 19). At pH 7.00 in Britton-Robinson buffer $[Ru(bpy)_2(Mephpztr)]^{2+}$ exhibits a λ_{max} at 550 nm. This blue shifts with increasing pH. In addition the colour of the solution changes from purple to orange with increasing pH. A plot of change in absorbance (monitored at 550 nm) against pH results in curve with only one inflection point (see Figure 5. 19).

For $[Ru(bpy)_2(phpztr)]^{+}$, pH changes were only observed in the pH range 1-5. At pH 1.00 in Britton-Robinson buffer, $[Ru(bpy)_2(phpztr)]^{+}$ exhibits a λ_{max} at 446 nm. This gradually shifts to 455 nm with increasing pH. Note the solution of $[Ru(bpy)_2(phpztr)]^{+}$ remains orange throughout the pH titration. A plot of absorbance (monitored at 446 nm) against pH results in a curve with only one inflection point. $[Ru(bpy)_2(Mephpztr)]^{2+}$ was found to have a pH inflection point (pH_i) of 9.9 while a pH_i of 3.0 was observed for $[Ru(bpy)_2(phpztr)]^{+}$. A pH_i of 9.8 for $[Ru(bpy)_2(Mephpztr)]^{2+}$ was also determined using ^1H NMR spectroscopy (see Section 5.2.3).

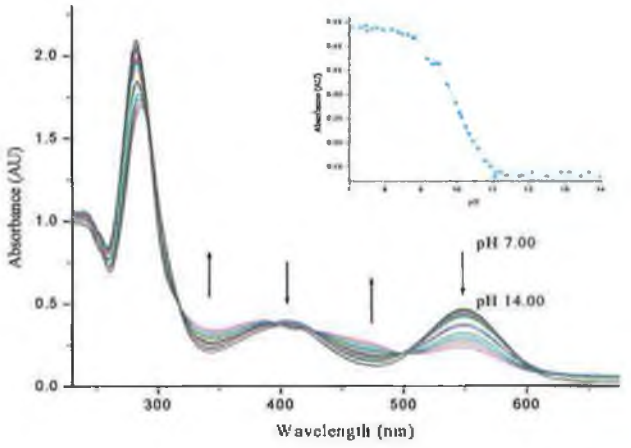

Figure 5. 19 *pH dependence of the absorption spectra of* $[Ru(bpy)_2(Mephpztr)]^{2+}$ *in Britton-Robinson buffer. Inset shows a plot of intensity versus increasing pH, with fitted curve.*

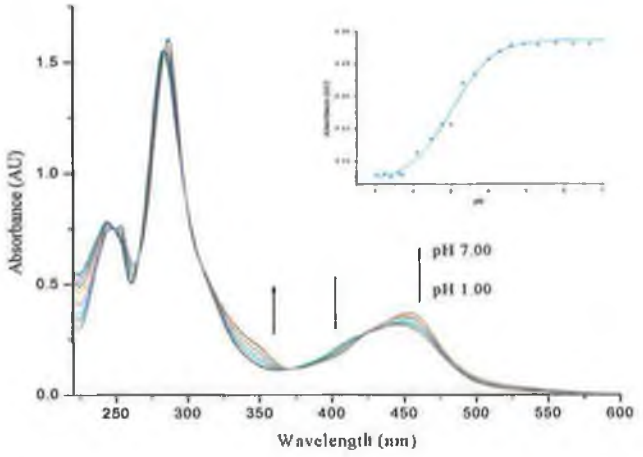

Figure 5. 20 *pH dependence of the absorption spectra of* $[Ru(bpy)_2(phpztr)]^{+}$ *in Britton-Robinson buffer. Inset shows a plot of intensity versus increasing pH, with fitted curve.*

The graphs of absorbance against pH for the pyrazyl-triazole complexes $[Ru(bpy)_2(pztr)]^+$ and $[Ru(bpy)_2(bpzt)]^+$ (where pztr = 3-(pyrazin-2-yl)-1,2,4-triazole and bpzt = 3,5-di(pyrazin-2-yl)-1,2,4-triazole) yield pH inflection points of 3.7 and 2.0 respectively.[18,48] For these complexes, the pH inflection point is also the pK_a of the complex. The pK_a is attributed to protonation/deprotonation of the triazole ring. The pH_i value of 3.0 obtained for $[Ru(bpy)_2(phpztr)]^+$ is similar to the previously obtained value of 3.7 for $[Ru(bpy)_2(pztr)]^+$. Hence its is reasonable to conclude that the pH_i is also the pK_a of $[Ru(bpy)_2(phpztr)]^+$. The acid/base behaviour observed for $[Ru(bpy)_2(phpztr)]^+$ can be explained by protonation/deprotonation of the triazole moiety as indicated in Equation 5. 1.

$$[Ru(bpy)_2(Hphpztr)]^{2+} \leftrightarrow [Ru(bpy)_2(phpztr)]^+ + H^+ \qquad \textbf{5. 1}$$

There is one protonation site on the triazole ring of $[Ru(bpy)_2(Mephpztr)]^{2+}$, however, no spectral changes were observed in the pH range 1-7. This is an unusual observation as changes in the absorption spectra of coordinated ruthenium pyrazyl-triazole complexes are observed in the region of pH 1.00 to pH 4.50.[31] The pH dependent ^1H NMR studies of $[Ru(d_8\text{-bpy})_2(Mephpztr)]^{2+}$ (Section 5.2.3), indicate loss of the methyl group at high pH yielding the unmethylated complex $[Ru(d_8\text{-bpy})_2(phpztr)]^+$. Hence loss of the methyl group is the most reasonable explanation for the observed spectral changes of $[Ru(bpy)_2(Mephpztr)]^{2+}$ in basic solution. This explanation also compliments the observed colour change of $[Ru(bpy)_2(Mephpztr)]^{2+}$ from purple to orange as $[Ru(bpy)_2(phpztr)]^+$ is also orange coloured at high pH. To the best of my knowledge there is only one other example pH dependent studies on a methylated ruthenium polypyridyl complex. Ward and co-workers carried out pH dependent absorption studies on $[Ru(bpy)_2(Me\text{-}QP)]^{2+}$ (Me-QP is mono-methylated 2,2':3',2'':6'',2''' quaterpyridine) in the pH range 0-8. Like $[Ru(bpy)_2(Mephpztr)]^{2+}$ no spectral changes were observed in this pH range.[49] The pH dependence of $[Ru(bpy)_2(Me\text{-}QP)]^{2+}$ was not studied at higher pH.

The acidity of a coordinated 1,2,4-triazole ligand is strongly dependent on substituents of the triazole ring.[16] For example, an electron donating methyl group increases the pK_a to 4.2, while the presence of an electron withdrawing bromine group can reduce the pK_a value to 1.4.[50,51] In all cases the acid/base behaviour of pyrazyl-triazole complexes can be explained in terms of protonation/deprotonation of the triazole moiety. Deprotonated pyrazyl-triazole complexes have the ability to offload electron density from the 1,2,4-triazole onto the neighbouring pyrazine ring. When the pyrazine ring is methylated, a positive charge exists on the nitrogen, which enhances the π-acceptor abilities of the pyrazine ring. It is possible that the triazole ring offloads more electron density onto the pyrazine ring in $[Ru(bpy)_2(Mephpztr)]^{2+}$ compared to the unmethylated complex $[Ru(bpy)_2(phpztr)]^{+}$. It is possible the triazole ring in the methylated complexes becomes a "better" acid with a much lower pK_a value. Therefore it is possible that the pK_a exists below pH 1.

5.2.6 Electrochemistry

Cyclic voltammetry (CV) was applied to study the redox properties of the methylated ruthemium complexes. CV measurements were carried out according to procedures in the literature.[52] The measurements were all obtained in dry acetonitrile containing 0.1 M TEAP (tetraethyl ammonium perchlorate) and are reported versus saturated calomel electrode. The results for all oxidations and reductions are summarised in Table 5. 4. Figure 5. 21 shows a CV of $[Ru(bpy)_2(Mephpztr)]^{2+}$. The CV of $[Ru(bpy)_2(Mephpztr)]^{2+}$ is typical of the methylated complexes. The redox processes are *quasi-reversible*, with peak-to-peak separations of 60-100 mV. Note, the degree of deuteriation has no effect on oxidation or reduction potentials (see Table 5. 4).

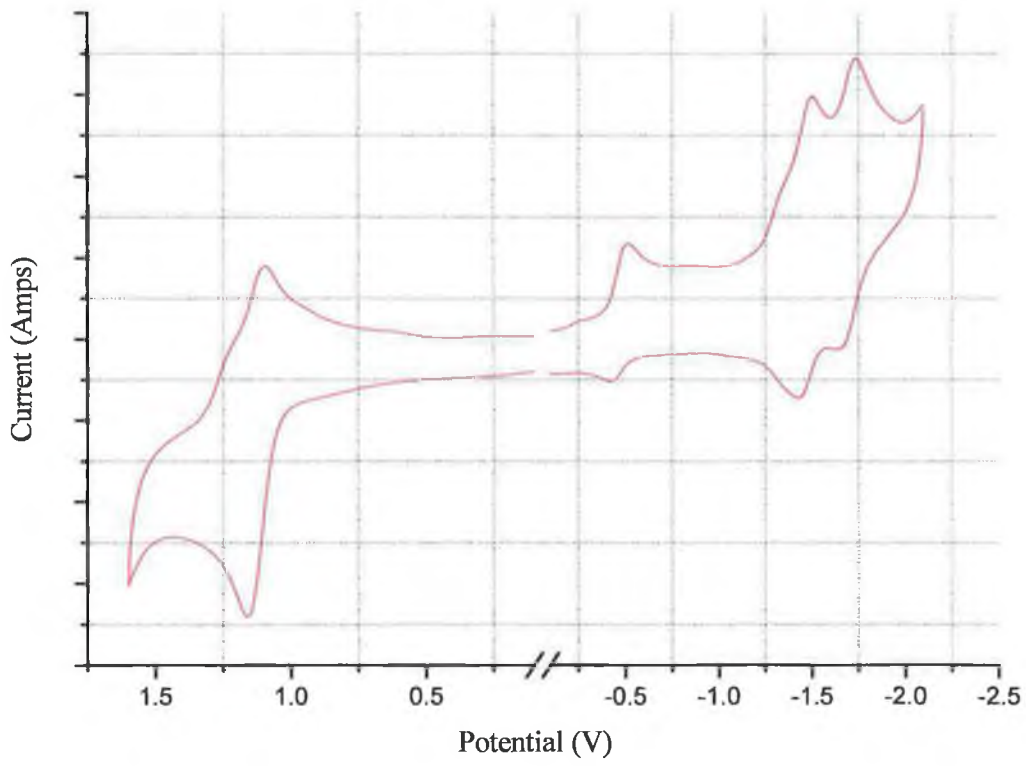

Figure 5. 21 *Cyclic voltammogram of the oxidation of* $[Ru(bpy)_2(Mephpztr)]^{2+}$ *in 0.1 M TEAP in acetonitrile with a scan rate of 100 mV/s.*

Assignment of redox processes is relatively straightforward by comparison with previously reported 1,2,4-triazole complexes. The Ru(II)/Ru(III) redox couple for ruthenium bipyridyl complex containing a deprotonated pyrazyl-triazole ligand is found at ~ 0.95 V.[50,53,54] $[Ru(bpy)_2(Mephpztr)]^{2+}$, $[Ru(d_8\text{-}bpy)_2(Mephpztr)]^{2+}$ and $[Ru(bpy)_2(d_3\text{-}Mephpztr)]^{2+}$ exhibit a Ru(II)/(III) based oxidation at 1.12 V, compared to a value of 0.93 V for $[Ru(bpy)_2(phpztr)]^{+}$ (see Table 5. 4). The nature of the ligands surrounding the ruthenium metal centre greatly influences the oxidation potential. $[Ru(bpy)_2(Mephpztr)]^{2+}$, $[Ru(d_8\text{-}bpy)_2(Mephpztr)]^{2+}$ and

$[Ru(bpy)_2(d_3\text{-Mephpztr})]^{2+}$ are better π-acceptors than $[Ru(bpy)_2(phpztr)]^+$. Hence the ruthenium metal centre of these complexes is more difficult to oxidise. This explains the increased Ru(II)/Ru(III) oxidation potential compared to $[Ru(bpy)_2(phpztr)]^+$.

Complex	$E_{(1/2)}$ (V)			
	Ru (II/III)	Reduction		
$[Ru(bpy)_2(Mephpztr)]^{2+}$	1.12	-0.47	-1.46	-1.72
$[Ru(bpy)_2(Mephpztr)]^{2+}$	1.13	-0.48	-1.46	-1.72
$[Ru(bpy)_2(Mephpztr)]^{2+}$	1.12	-0.48	-1.46	-1.72
$[Ru(bpy)_2(phpztr)]^+$	0.93	—	-1.45	-1.65

Table 5. 4 *Electrochemical data in acetonitrile with 0.1 M TEAP at 100 mV/s scan rate.*

The redox waves at ~ -1.4 and –1.7 V are typical of bpy-based reductions and therefore are assigned so.[4] The methylated complex $[Ru(bpy)_2(Me\text{-}QP)]^{2+}$ (where Me-QP is mono-methylated 2,2':3',2'':6'',2''' quaterpyridine) showed a weak irreversible reduction at – 1.39 V.[49] By comparison with $[bpy\text{-}Me]^+$, this was assigned to reduction of the methylated site. It is possible that the bipyridyl-based reduction at –1.48 V obscures the methyl based reduction in this series of methylated complexes.

A third reduction peak is observed at – 0.48 V for the methylated complexes. This was not observed for the unmethylated $[Ru(bpy)_2(phpztr)]^+$ complex. This is most likely due to reduction of the electron poor methylated pyrazine moiety. Other Ru(II) pyrazyl triazole complexes with a methyl group on the triazole exhibit a pyrazine-based reduction at –1.26 V.[31] The more positive reduction peak observed for the methylated complexes further confirms that the pyrazine rather than the triazole ring is methylated.

5.2.7 Raman spectroscopy

In a resonance Raman (rR) experiment, a sample is irradiated with laser light at various wavelengths. If excitation takes place near an allowed electronic transition, the symmetrical stretching modes of the ligand show enhanced Raman intensities.[55,56] Resonance Raman spectroscopy has been useful in assigning MLCT transitions of mixed-ligand ruthenium complexes.[54,57,58] Excitation into an allowed [Ru $\rightarrow$ π^*] transition in mixed ligand complexes gives rise to enhancement of the symmetrical stretching modes of the ligand involved in the transition.[59,60] Hence it is possible to characterise which ligand is involved in the lowest energy MLCT band by using rR spectroscopy. Different electronic transitions within one absorption band can be detected and identified by studying the wavelength dependence of the rR spectra.

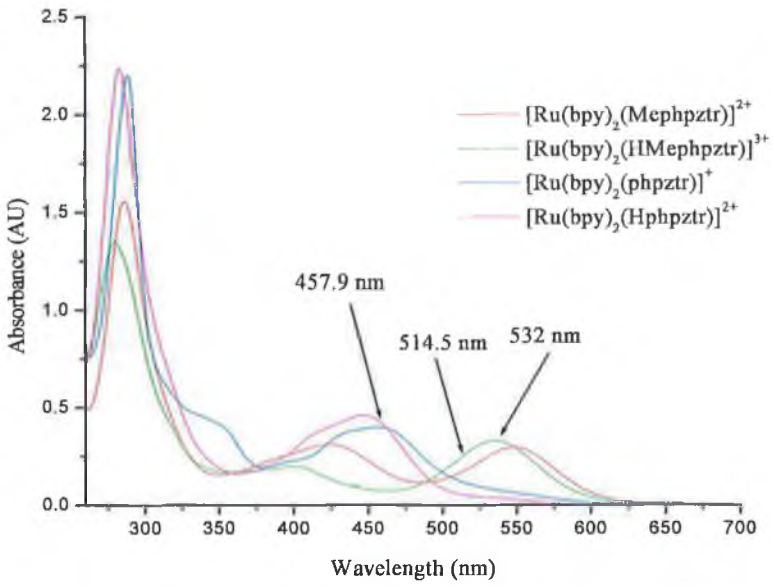

Figure 5. 22 *Absorption spectra of* $[Ru(bpy)_2(Mephpztr)]^{2+}$, $[Ru(bpy)_2(HMephpztr)]^{3+}$ $[Ru(bpy)_2(phpztr)]^{+}$ *and* $[Ru(bpy)_2(Hphpztr)]^{2+}$ *in acetonitrile. The arrows indicate the rR excitation wavelengths.*

Ground-state rR studies of $[Ru(bpy)_2(Mephpztr)]^{2+}$ and $[Ru(bpy)_2(HMephpztr)]^{3+}$ were carried in CD_3CN at excitation wavelengths of 457.9, 514.5 and 532 nm. Note rR spectra of $[Ru(bpy)_2(HMephpztr)]^{3+}$ were obtained in the presence of hydrochloric acid. Selected deuteriation of ligands in ruthenium(II) polypyridyl complexes assists in the assignment of rR spectra on the basis of the isotopic shifts.[61,,62] Hence the ground state rR spectra of $[Ru(d_8\text{-}bpy)_2(Mephpztr)]^{2+}$ and $[Ru(bpy)_2(d_3\text{-}Mephpztr)]^{2+}$ and their protonated analogues were also studied. The three excitation wavelengths are shown in Figure 5. 22 in relation to the absorption spectra of the complexes.

Ground-state rR studies of $[Ru(bpy)_2(phpztr)]^{+}$ and $[Ru(bpy)_2(Hphpztr)]^{2+}$ have been examined in CD_3CN at excitation wavelengths of 457.9 nm and 514.5 nm.[22,34] These results will be briefly summarised. Following excitation of $[Ru(bpy)_2(Hphpztr)]^{2+}$ at 457.9 nm, features attributable to bpy based vibrations are observed 1610, 1565, 1494, 1429, 1320, 1277 and 1175 cm^{-1}. Some weak pyrazine based features at 1534 and 1193 cm^{-1} were observed. The assignment of these bands was made from the isotopic shifts observed in the spectra of $[Ru(d_8\text{-}bpy)_2(Hphpztr)]^{2+}$ and $[Ru(bpy)_2(d_3\text{-}Hphpztr)]^{2+}$ and by comparison with the rR spectra of $[Ru(bpy)_3]^{2+}$.[63,64,65] Following excitation of $[Ru(bpy)_2(phpztr)]^{+}$ at the same wavelength, the spectral features observed are bpy in nature. Excitation of $[Ru(bpy)_2(Hphpztr)]^{2+}$ and $[Ru(bpy)_2(phpztr)]^{+}$ at 514.5 nm led to bpy based excitation features at 1610, 1565, 1494, 1429, 1320, 1277 and 1175 cm^{-1}. Upon excitation of $[Ru(bpy)_2(H_2phpztr)]^{3+}$ at 532 nm pyrazine based features were detected at 1633, 1472, 1171, 1140 cm^{-1}.[34] These results indicate that the low energy bands in the absorption spectra of $[Ru(bpy)_2(phpztr)]^{+}$ and $[Ru(bpy)_2(Hphpztr)]^{2+}$ originate from $[Ru\rightarrow\pi^*(bpy)]$ transitions whilst the low energy absorption band of $[Ru(bpy)_2(H_2phpztr)]^{3+}$ is due to an $[Ru\rightarrow\pi^*$(pyrazyl-triazole)] transition.

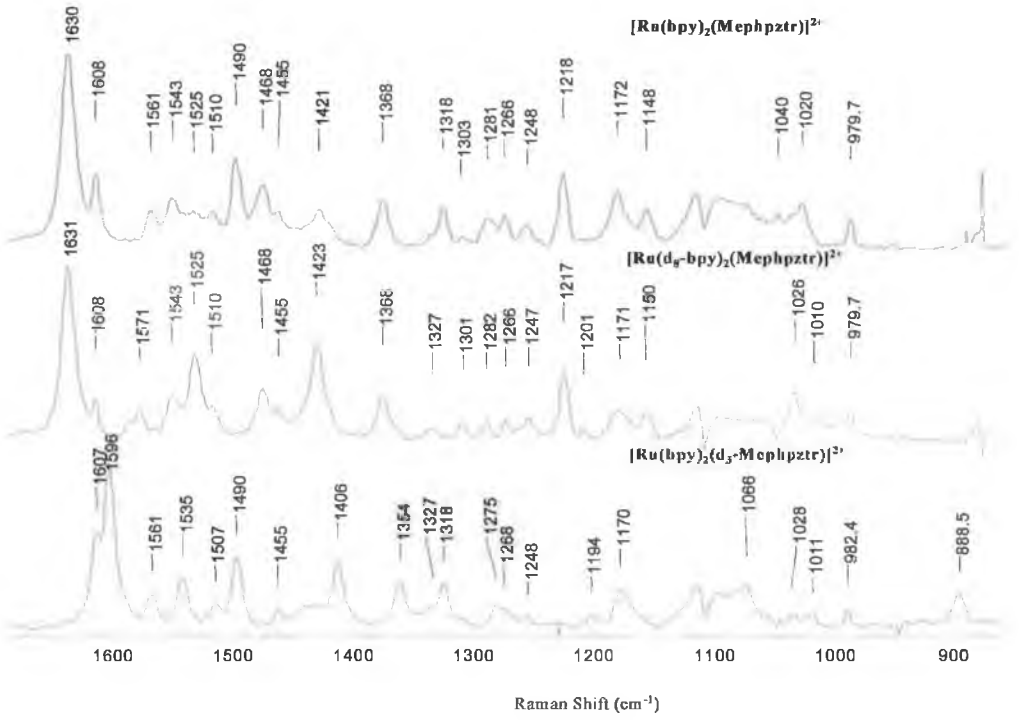

Figure 5. 23 *Ground state resonance Raman spectra of* $[Ru(bpy)_2(Mephpztr)]^{2+}$, $[Ru(d_8\text{-}bpy)_2(Mephpztr)]^{2+}$ *and* $[Ru(bpy)_2(d_3\text{-}Mephpztr)]^{2+}$ *in* CD_3CN *at 457.9 nm.*

Figure 5. 23 shows the three spectra from samples of $[Ru(bpy)_2(Mephpztr)]^{2+}$, $[Ru(d_8\text{-}bpy)_2(Mephpztr)]^{2+}$ and $[Ru(bpy)_2(d_3\text{-}Mephpztr)]^{2+}$ following excitation at 457.9 nm in CD_3CN. Excitation features attributable to bpy modes are observed at 1608, 1561, 1490 and 1318 cm^{-1} in the spectra of $[Ru(bpy)_2(Mephpztr)]^{2+}$ and $[Ru(bpy)_2(d_3\text{-}Mephpztr)]^{2+}$. These peaks are shifted to 1573, 1524, 1424, 1250 cm^{-1} in the spectrum of $[Ru(d_8\text{-}bpy)_2(Mephpztr)]^{2+}$.[66] There are additional features present at 1630, 1468, 1368, 1218, and 1148 cm^{-1} in the spectra of $[Ru(bpy)_2(Mephpztr)]^{2+}$ and $[Ru(d_8\text{-}bpy)_2(Mephpztr)]^{2+}$ which are attributed to the vibrational modes of the pyrazine.[59,67,68] These vibrations were not observed in the rR sprectrum of $[Ru(bpy)_2(d_3\text{-}Mephpztr)]^{2+}$ which contains a deuterated pyrazine. Excitation of $[Ru(bpy)_2(HMephpztr)]^{3+}$, $[Ru(d_8\text{-}bpy)_2(HMephpztr)]^{3+}$ and $[Ru(bpy)_2(d_3\text{-}HMephpztr)]^{3+}$ at 457.9 nm yielded poor quality spectra, thus

making a detailed analysis of the spectra impossible. Modes associated with both the bipyridyl and pyrazyl-triazole ligands were enhanced using an excitation wavelength of 457.9 nm. This suggests that the feature at 425 nm is a mixture of both [Ru → π*(bpy)] and [Ru → π*(pyrazyl-triazole)] transitions.

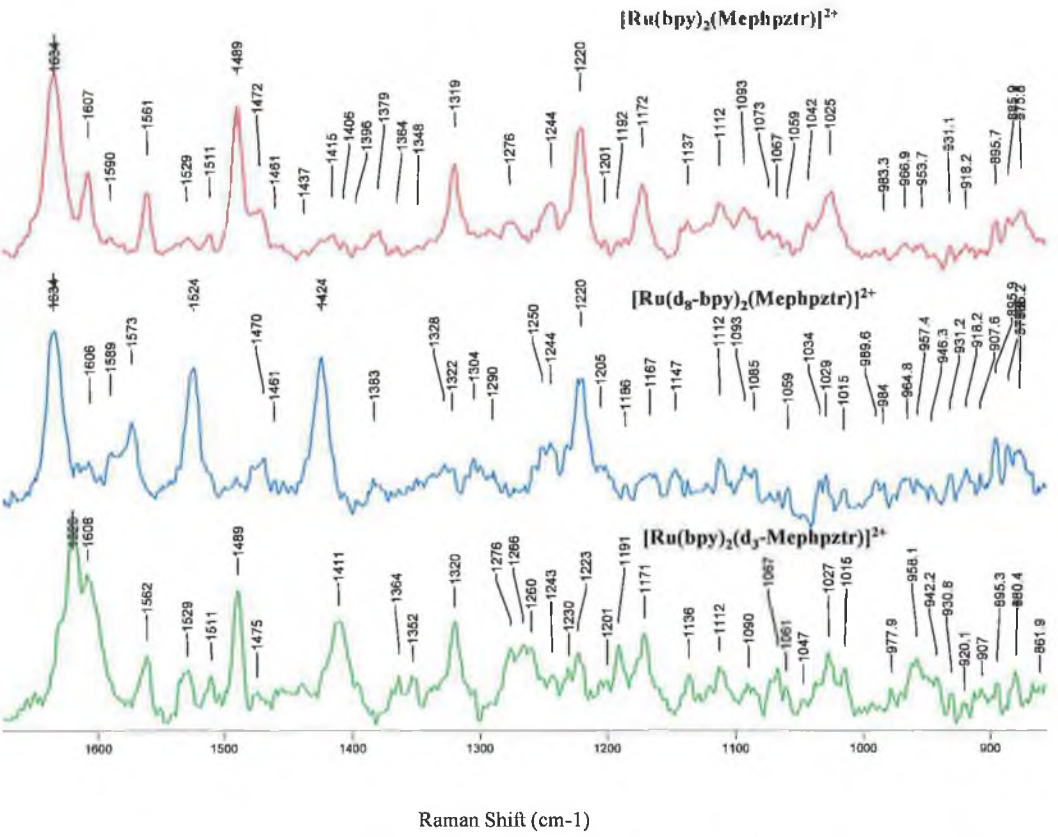

Figure 5. 24 *Ground state resonance Raman spectra of $[Ru(bpy)_2(Mephpztr)]^{2+}$, $[Ru(d_8\text{-}bpy)_2(Mephpztr)]^{2+}$ and $[Ru(bpy)_2(d_3\text{-}Mephpztr)]^{2+}$ in H_2O at 514.5 nm.*

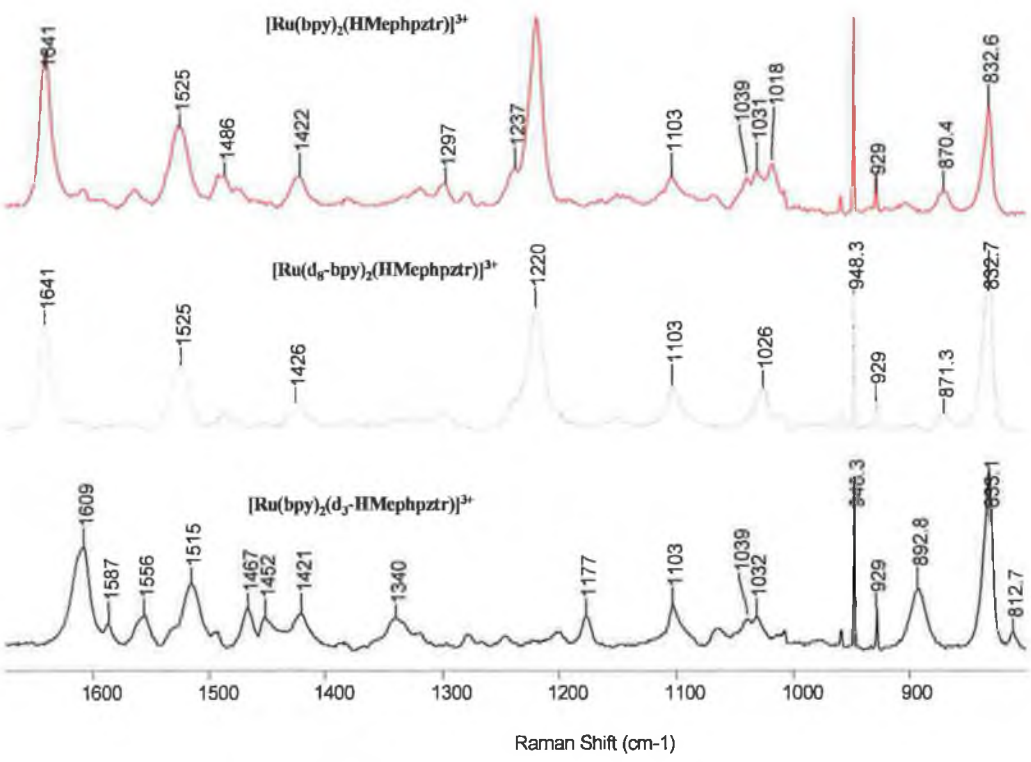

Figure 5. 25 *Ground state resonance Raman spectra of* $[Ru(bpy)_2(HMephpztr)]^{3+}$, $[Ru(d_8\text{-}bpy)_2(HMephpztr)]^{3+}$ *and* $[Ru(bpy)_2(d_3\text{-}HMephpztr)]^{3+}$ *in HCl at 514.5 nm.*

Ground-state rR spectra obtained for $[Ru(bpy)_2(Mephpztr)]^{2+}$ and $[Ru(bpy)_2(d_3\text{-}Mephpztr)]^{2+}$ (Figure 5. 24) recorded 514.5 nm show bands at 1607, 1562, 1489 and 1320 cm^{-1}, characteristic of the bpy ligands. These bands were shifted to 1573, 1524, 1424 and 1250 cm^{-1} in the spectrum of $[Ru(d_8\text{-}bpy)_2(Mephpztr)]^{2+}$, which contains deuteriated bpy ligands. Two additional bands at 1634 and 1220 cm^{-1} present in the spectra of $[Ru(bpy)_2(Mephpztr)]^{2+}$ and $[Ru(d_8\text{-}bpy)_2(Mephpztr)]^{2+}$ are assigned to a pyrazine-associated vibration. These bands are shifted to 1620 and 1191 cm^{-1} when the pyrazine ring is deuterated ($[Ru(bpy)_2(d_3\text{-}Mephpztr)]^{2+}$). Following excitation of $[Ru(bpy)_2(HMephpztr)]^{3+}$ and $[Ru(d_8\text{-}bpy)_2(HMephpztr)]^{3+}$ (Figure 5. 25) at 514.5 nm, features attributable to pyrazine based vibrations are observed at 1641, 1520, 1240, and 1219 cm^{-1}.

These features are absent when the pyrazine ring is deuterated ($[Ru(bpy)_2(d_3\text{-}HMephpztr)]^{3+}$). No evidence for any bpy modes are present in the spectra. From the ground-state rR studies at 514.5 nm, it can be concluded that the MLCT transition of $[Ru(bpy)_2(Mephpztr)]^{2+}$ consists of an overlap between [Ru → π*(pyrazyl-triazole)] and [Ru → π*(bpy)] transitions while the[Ru → π*(pyrazyl-triazole)] transitions become more apparent for $[Ru(bpy)_2(HMephpztr)]^{3+}$.

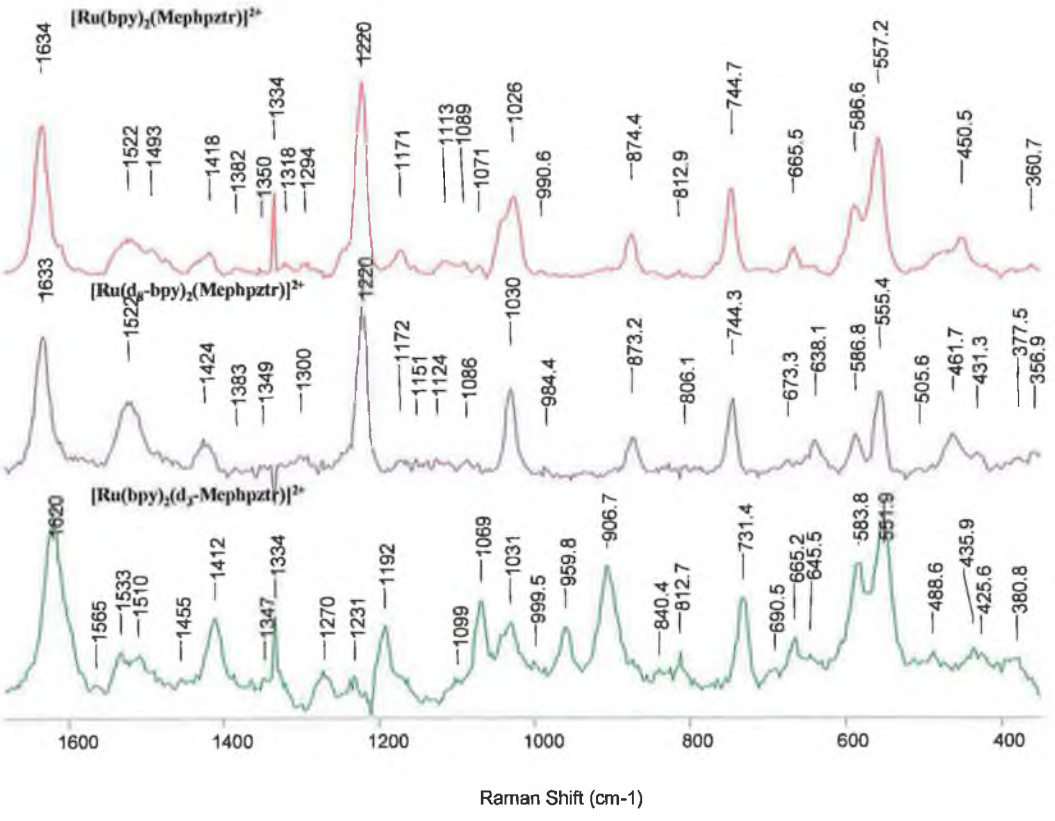

Figure 5. 26 *Ground state resonance Raman spectra of $[Ru(bpy)_2(Mephpztr)]^{2+}$, $[Ru(d_8\text{-}bpy)_2(Mephpztr)]^{2+}$ and $[Ru(bpy)_2(d_3\text{-}Mephpztr)]^{2+}$ in H_2O at 532 nm.*

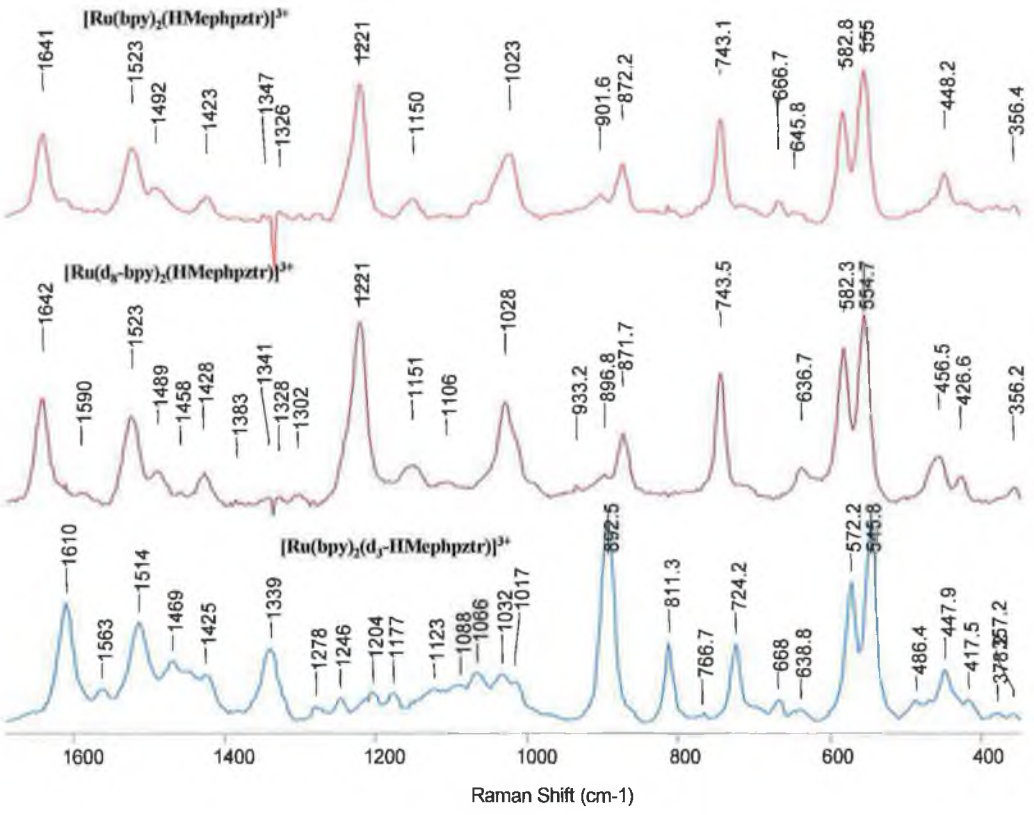

Figure 5. 27 *Ground state resonance Raman spectra of* $[Ru(bpy)_2(HMephpztr)]^{3+}$, $[Ru(d_8\text{-}bpy)_2(HMephpztr)]^{3+}$ *and* $[Ru(bpy)_2(d_3\text{-}HMephpztr)]^{3+}$ *in HCl at 532 nm.*

Displayed in Figure 5. 26 are the rR spectra of $[Ru(bpy)_2(Mephpztr)]^{2+}$, $[Ru(d_8\text{-}bpy)_2(Mephpztr)]^{2+}$ and $[Ru(bpy)_2(d_3\text{-}Mephpztr)]^{2+}$ following 532 nm. Bands assigned to the pyrazyl-triazole ligand are observed at 1641, 1523, 1221, 1028, and 743 cm^{-1}. These bands were sensitive to deuteriation of the pyrazine in the pyrazyl-triazole i.e. the bands are shifted to 1412, 1192, 907 and 731 cm^{-1} in the rR spectrum of $[Ru(bpy)_2(d_3\text{-}Mephpztr)]^{2+}$ following excitation at 532 nm. For $[Ru(bpy)_2(HMephpztr)]^{3+}$, $[Ru(d_8\text{-}bpy)_2(HMephpztr)]^{3+}$ and $[Ru(bpy)_2(d_3\text{-}HMephpztr)]^{3+}$ an similar spectral features were observed (see Figure 5. 27). Analysis of the ground-state rR spectra of $[Ru(bpy)_2(Mephpztr)]^{2+}$ and $[Ru(bpy)_2(HMephpztr)]^{3+}$ reveals that the enhanced bands are pyrazyl-triazole based vibrations.

The three excitation wavelengths used to acquire rR data span the absorption spectrum of $[Ru(bpy)_2(Mephpztr)]^{2+}$ (Figure 5. 22). With excitation at 532 nm, a wavelength nearly coincident with the maximum of the low energy electronic transition of the complex, modes associated with the coordinated pyrazyl-triazole ligand are selectively enhanced. Such behaviour provides convincing evidence for assignment of this lower energy electronic transition to that associated with an [Ru $\rightarrow$ π^*(pyrazyl-triazole)] transition. Although there is a general increase in the intensities of bpy associated modes in the spectra acquired with progressively higher energy excitations (i.e. 514.5 nm and 457.9 nm), it is clear that several of the pyrazyl-triazole modes are also enhanced with these excitaion wavelengths. This behaviour differs from that observed for the unmethylated complex $[Ru(bpy)_2(phpztr)]^+$, where the low energy electronic transition is predominantly bpy based. The most reasonable interpretation of the behaviour observed here is that methylation of $[Ru(bpy)_2(phpztr)]^+$ has lowered the π^* level compared to that of the bpy ring. Hence the low energy electronic transition of $[Ru(bpy)_2(Mephpztr)]^{2+}$ is pyrazyl-triazole based.

5.3 Conclusions

Monomethylation of $[Ru(bpy)_2(phpztr)]^+$, $[Ru(d_8\text{-}bpy)_2(phpztr)]^+$ and $[Ru(bpy)_2(d_3\text{-}phpztr)]^+$ was confirmed by ^1H NMR spectroscopy, elemental analysis and mass spectroscopy. Methylation could in principle occur at the pyrazine ring or either of the nitrogens on the triazole ring but it is clear from the ^1H NMR spectra that only one isomer is present. Methylation of $[Ru(bpy)_2(phpztr)]^+$, $[Ru(d_8\text{-}bpy)_2(phpztr)]^+$ and $[Ru(bpy)_2(d_3\text{-}phpztr)]^+$ has occurred on the pyrazine ring. This can be substantiated for by number of reasons: Firstly, the absorption maximum of $[Ru(bpy)_2(Mephpztr)]^{2+}$ and its protonated analogue $[Ru(bpy)_2(HMephpztr)]^{3+}$ are at similar energy to that of $[Ru(bpy)_2(H_2phpztr)]^{3+}$, for which it was already concluded that a protonated pyrazine is present. Secondly, ground-state resonance Raman studies provide convincing evidence for assignment of the lower energy electronic transition of

the methylated complexes to that associated with an [Ru → π*(pyrazyl-triazole)] transition. In addition, the first reduction potential of $[Ru(bpy)_2(Mephpztr)]^{2+}$ is less negative than the first reduction potential of $[Ru(bpy)_2(phpztr)]^{+}$ Note the first potential of $[Ru(bpy)_2phpztr]^{2+}$ is assigned to reduction of the coordinated bipyridyl ligand. This further confirms methylation has lowered the π* level of the complex. The oxidation potential of $[Ru(bpy)_2(Mephpztr)]^{2+}$ complexes is 190 mV higher than that found in the corresponding unmethylated complex $[Ru(bpy)_2(phpztr)]^{+}$, thus indicating that the methylated product $[Ru(bpy)_2(Mephpztr)]^{2+}$ contains a weaker σ-donor ligand.

5.4 Experimental

5.4.1 Ligand Synthesis

3-(pyrazin-2'-yl)-5-phenyl-1,2,4-triazole (Hphpztr)

Hydrazine hydrate (2.37g, 47 mmol) was slowly added to a solution of 2-cyanopyrazine (5 g, 47 mmol) in 20 $cm^3$of ethanol. The reaction mixture was gently heated to 40 °C . After the formation of a yellow solution the heat was turned off and the reaction was left stirring overnight. The yellow precipitate was filtered under vacuum and washed with ethanol. Benzoyl chloride (6.60g, 47 mmol) was added dropwise to a stirred solution of 4 cm^3 of triethylamine and the pyrazin-2-yl amidrazone in 20 cm^3 of dry THF. The yellow suspension was stirred for three hours at room temperature. The yellow crystals were filtered under vacuum and left drying overnight. The crystals were dissolved in ethylene glycol and refluxed for three hours. The ethylene glycol solution was allowed cool to room temperature. 10 cm^3 of water was added to the solution to aid precipitation. The white triazole ligand precipitated overnight and was collected under vacuum. The triazole was recrystallised twice from ethanol to yield a fine white powder. Yield: 5.92 g, (56 %, 26 mmol). ^{1}H NMR d_6-DMSO, δ in ppm: 9.35 (s, 1H, pz H_3), 8.79 (dd, 1 H, pz H_5), 8.76 (d, 1H, pz H_6), 8.11 (d, 2H, ph-H_2/H_6), 7.54 (dd, 2H, ph-H_3/H_5), 7.49 (t, 1H, ph H_4).

[D_3]-3-(pyrazin-2'-yl)-5-phenyl-1,2,4-triazole (d_3-Hphpztr)

Dr. W.R. Browne provided the ligand d_3-Hphpztr.

5.4.2 Preparation of the complexes

[$Ru(bpy)_2(phpztr)]PF_6$

0.25 g (0.5 mmol) of $[Ru(bpy)_2Cl_2].2H_2O$ was added to an equimolar amount of Hphpztr dissolved in 100 cm^3 ethanol/water (1/1 v/v). The purple solution was refluxed for 8 hours. The solvent was removed and the orange residue was dissolved in a small amount of water. A few drops of concentrated NaOH were added to this solution. The complex was precipitated with ammonium hexafluorophosphate. The orange precipitate was collected under vacuum. The complex was dissolved in a minimum volume of acetonitrile and purified by column chromatography on alumina. The first band (N_2 isomer) was eluted with acetonitrile. The N_4 isomer remained on the top of the column and was eluted with methanol. This work is only interested in the N_2 isomer hence only this isomer was characterised. Yield 0.167 g (0.215 mmol, 44 %). ^1H NMR spectroscopy in CD_3CN: 9.29 (1H, d), 8.47 (4H, m), 8.25 (1H, d), 8.04 (4H m), 7.96 (3H, m) 7.88 (1H, d), 7.80 (2H, dd), 7.60 (1H, d), 7.40 (7H, m). Mass spec. Mol^+ (calculated for $RuC_{32}H_{24}N_9$: 636) found: 636.1 m/z.

[$Ru(d_8\text{-}bpy)_2(phpztr)]PF_6$

This complex was prepared and purified as described for $[Ru(bpy)_2(phpztr)]PF_6$, except $[Ru(d_8\text{-}bpy)_2Cl_2].2H_2O$ was used instead of $[Ru(bpy)_2Cl_2].2H_2O$. Yield 0.90 g (0.115 mmol, 23%). ^1H NMR spectroscopy in CD_3CN: 9.29 (1H, d), 8.25 (1H, d), 7.96 (3H, m), 7.60 (1H, d), 7.33 (H, dd).

$[Ru(bpy)_2(d_3\text{-phpztr})]PF_6$

This compound was prepared and purified as described for $[Ru(bpy)_2(phpztr)]PF_6$, except d_3-Hphpztr was used instead of Hphpztr. Yield 0.148 g (0.19 mmol, 38%). ^{1}H NMR spectroscopy in CD_3CN: 8.47 (4H, m), 8.04 (4H m), 7.96 (3 H, m) 7.88 (1H, d), 7.80 (2H, dd), 7.40 (7H, m).

$[Ru(bpy)_2(Mephpztr)](PF_6)_2$

An excess of Me_3OBF_4 was added under argon to 38.7 mg (0.05 mmol) of $[Ru(bpy)_2phpztr]PF_6$ and 28 mg (0.21mmol) of Na_2CO_3 in 10 cm^3 of dry acetonitrile in one portion at room temperature. The resulting purple solution was stirred for 1 h. The solvent was removed under vacuum. The residue was dissolved in the minimum amount of water and precipitated with conc. NH_4PF_6 solution and recrystallised from acetone/water (50/50 v/v). Yield 38 mg (0.04 mmol, 82%). ^{1}H NMR in CD_3CN; 9.15 (1H, s, pzH3), 8.55 (4H, m, bpyH3), 8.37 (1H, d, pzH5), 8.01 (4H, m bpyH4), 7.98 (3H, m, pz H6/phH2/H5,), 7.89 (1H, d, bpyH6), 7.80 (1H, d, bpyH6), 7.66 (1H, d, bpyH6) 7.58 (1H, d, bpyH6) 7.45 (7H, m, bpyH5 and phH3/H4/H5), 4.25 (3H, s, Me). Mass spec. Mol^{2+} (calculated for $RuC_{33}H_{27}N_9$: 325) found: 325.4 m/z. Elemental analysis (calculated for $RuC_{33}H_{27}N_9P_2F_{12}$) C: 42.13% (41.89%), H: 2.87 % (2.31 %), N: 13.40% (13.21 %).

$[Ru(d_8\text{-bpy})_2(Mephpztr)](PF_6)_2$

As for $[Ru(bpy)_2(Mephpztr)](PF_6)_2$ except an excess of Me_3OBF_4 was added to 35 mg (0.044 mmol) of $[Ru(d_8\text{-bpy})_2phpztr]PF_6$ Yield 31.5 mg (.033 mmol, 76 %). ^{1}H NMR in CD_3CN. 9.15 (1H, s, pzH3), 8.36 (1H, d, 3 Hz, pzH5), 7.80 (3H, m, phH2/H5, pzH6), 7.44 (3H, m, phH3/H4/H5), 4.25 (3H, s, Me). Mass spec. Mol^{2+} (calculated for $RuC_{33}H_{11}N_9D_{16}$: 333) found: 333.4 m/z. Elemental analysis calculated for $RuC_{33}H_{11}N_9D_{16}P_2F_{12}$ (found) C: 41.42 % (40.12 %), H: 2.82 % (2.35 %), N: 13.18 % (13.48 %).

[Ru(bpy)$_2$(d_3-Mephpztr)]PF_6.

As for[Ru(bpy)$_2$(Mephpztr)](PF_6)$_2$ except an excess of Me_3OBF_4 was added to 40 mg (0.05 mmol) of [Ru(bpy)$_2$$d_3$-phpztr]$PF_6$ Yield 39 mg (0.042 mmol, 84 %). ^{1}H NMR in CD_3CN. 8.44 (4H, m, bpyH3), 8.01 (4H, m bpyH4), 7.89 (2H, d, phH2/H5,),7.78 (1H, d, bpyH6), 7.69 (1H, d, bpyH6), 7.65 (1H, d, bpyH6) 7.48 (1H, d, bpyH6) 7.44 (7H, m, bpyH5 and phH3/H4/H5), 4.15 (3H, s, Me). Mass spec. Mol^{2+} (calculated for $RuC_{33}H_{24}N_9D_3$: 326.5) found: 326.9 m/z. Elemental analysis calculated for $RuC_{33}H_{24}N_9D_3$ P_2F_{12} (found) C: 41.99% (40.45 %), H: 2.86 % (2.51 %), N: 13.36 % (12.87 %).

5.5 Bibliography

1 S. Fanni, S.Murphy, J.S. Killeen, J.G. Vos, *Inorg. Chem.*, **2000**, 39, 1320.

2 V. Balzani, A. Credi, M. Venturi, *Molecular Devices and Machines; A journey into the nanoworld*, VCH, Weinheim **2003**.

3 F.R. Keene, *Coord. Chem. Rev.* **1997**, 121, 159.

4 A. Juris, V. Balzani, F. Barigelletti, S. Campagna, P. Besler, A. von Zelewsky, *Coord. Chem. Rev.* **1988**, 84, 85.

5 (a) K.E. Splan, M.H. Keefe, A.M. Massari, K.A. Walters, J.T. Hupp, *Inorg. Chem.* **2002**, 41, 619. (b) E.C. Constable, E. Schofield, *Chemm. Commun*, **1998**, 403, (c) M. Fujita, *Chem. Soc. Rev.* **1998**, 27, 417.

6 A. Vlček Jr., *Coord. Chem. Rev.*, **2000**, 200-202, 933.

7 J.P. Paris and W. W. Brandt, *J. Am. Chem. Soc.*, **1959**, *81*, 5001

8 K. Kalyanasundaram, *Coord. Chem. Rev.*, **1982**, *46*, 159.

9 K. Kalyanasundaram, *Photochemistry of Polypyridine and Porphyrin Complexes*, Academic Press, London, **1992.**

10 J. Van Houton, R. J. Watts, *J. Am. Chem. Soc.*, **1976**, 98, 4853

11 S. D. Ernst, W. Kaim, *Inorg. Chem.* **1989**, 28, 1520

12 D. P. Rimella, G. Allen, T. J. Meyer, D. Conrad, *Inorg. Chem.*, **1983**, 22, 1617.

13 F. Barigelletti, A. Juris, V. Bazani, P. Belser, A. Von Zelewski, *Inorg. Chem.*, **1987**, 4115

14 S. Rau, T. Buttner, C. Temme, M. Ruben, H. Gorls, D. Walther, M. Duati, S. Fanni, J.G. Vos, *Inorg. Chem*, **2000**, 39, 1621.

15 P.J. Steel, F. Lahousse, C. Marzin, *Inorg. Chem.,* **1983**, 22, 1488

16 S. Fanni, T. E. Keyes, C. M. O'Connor, H. Hughes, R. Wang, J. G. Vos, *Coord. Chem. Rev.* **2000**, 208, 77

17 J. G. Vos, J. G. Haasnoot, *Inorg. Chim. Acta.,* **1983,** 71, 155

18 R. Hage Ph.D. Thesis, Leiden University, **1991.**

19 W.R. Browne, C.M. O'Connor, H.P. Hughes, R. Hage, O. Walter, M. Doering, J.F. Gallagher, J.G. Vos, *J. Chem. Soc., Dalton Trans,* **2002,** 4048

20 B.E. Buchanan, R.Wang, J.G. Vos, R. Hage, J.G. Haasnoot, J. Reedijk, *Inorg. Chem,* **1990**, 29, 3263.

21 R. Hage, R. Prins, J.G. Haasnoot, J. Reedijk, J.G. Vos, *J. Chem. Soc., Dalton Trans,* **1987**, 1389

22 W.R. Browne, PhD. Thesis, Dublin City University, **2001.**

23 R.P. Thummel, D. Williamson, C. Hery, *Inorg. Chem.,* **1993**, 32, 1587

24 F. Weldon, PhD. Thesis, Dublin City University, **1998**.

25 P.J. Steel, F. Lahouse, D. Lerner, C. Marzin, *Inorg. Chem.,* **1983**, 22, 1488.

26 G. Orellana, C. Alvarez Ibarra, J. Santoro, *Inorg. Chem.,* **1988**, 27, 1025.

27 P.J. Steel, E.C. Constable, *J. Chem. Soc.,* **1990**, 1389.

28 R. Hage, A.H.J. Dijkhuis, J.G. Haasnoot, R. Prins, J. Reedijk, B.E. Buchanan, J.G. Vos, *Inorg. Chem.*, **1988**, 27, 2185.

29 R.J. Crutchley, A.B.P. Lever, *Inorg. Chem.,* **1982**, 21, 2276.

30 S. Fanni, F.M. Weldon, L. Hammarström, E. Mukhtar, W.R. Browne, T.E. Keyes, J.G. Vos, *Eur. J. Inorg. Chem.,* **2001**, 529.

31 H.A. Nieuwenhuis, J.G. Haasnoot, R. Hage, J. Reedijk, T.L. Snoeck, D.J. Stufkens, J.G. Vos, *Inorg. Chem.,* **1991**, 30, 48.

32 B.E. Buchanan, R. Degn, J.M. Pavon, Velasco, H. Hughes, B.S. Creaven,

C. Long, J.G. Vos, R.A. Howie, R. Hage, J.H. van Demen, J.G. Haasnoot, J. Reedijk, *J. Chem. Soc.*, **1992**, 1177.

33 W. Humbs, H. Yersin, J. Strasser, *Topics Curr. Chem.*, **1997**, 191, 154.

34 W.R. Browne, P. Passaniti, M.T. Gandolfi, R. Ballardini, C.M. O'Connor, M. Maestri, W. Henry, C.G. Coates, C. Brady, J.J. McGarvey, J.G. Vos, *Submitted to Photochemical and Photobiological Sciences.*

35 L. De Cola, P. Besler, *Coord. Chem Rev.*, **1998**, 177, 301.

36 W.R. Browne, J.G. Vos, *Coord. Chem. Rev.*, **2001**, 761.

37 T.E. Keyes, F. Weldon, E. Müller, P. Pechy, M. Grätzel, J.G. Vos, *J. Chem. Soc., Dalton Trans.* **1995**, 2705.

38 N.H. Damrauer, J.K. McCusker, *Inorg. Chem.*, **1999**, 38, 4268.

39 J.V. Caspar T.J. Meyer, *J. Phys. Chem.*, **1983,** 87, 952.

40 E.M. Kober, J.V. Caspar, R.S. Lumpkin, T.J. Meyer, *J. Phys. Chem.*, **1986**, 90, 3722.

41 L.D. Ciana, W.J. Dressick, D. Sandrini, M. Maestri, M. Ciano, *Inorg. Chem.*, **1990**, 29, 2792..

42 M. Haga, *Inorg. Chim. Acta.*, **1980**, *45*, 183.

43 A.M. Bond and M. Haga, *Inorg. Chem.*, **1986**, *25*, 4507.

44 P. Day and N. Saunders, *J. Chem. Soc., A*, **1967**, 1536.

45 M. Duati, S. Tasca, F.C. Lynch, H. Bohlen, J.G. Vos, S. Stagni, M.D. Ward, *Inorg. Chem.*, **2003**, *42*, 8377.

46 J.A. Treadway, B. Loeb, R. Lopez, P.A. Anderson, F.R. Keene, T.J. Meyer, *Inorg. Chem.*, **1996**, *35*, 2242.

47 R. Wang, J.G. Vos, R.H. Schmehl, R. Hage, *J. Am. Chem. Soc.*, **1992**, 114, 1964.

48 W.R. Browne, C.M. O'Connor, H.P. Hughes, R. Hage, O. Walter, M. Doering, JF. Gallagher, J.G. Vos, *J. Chem. Soc., Dalton Trans.*, **2002**,

49 M. Guardigli, L. Flamigni, F. Barigelletti, C.S.W. Richards, M.D. Ward, *J. Phys. Chem.*, **1996**, 100, 10620

50 C. Di Pietro, S. Serroni, S. Campagna, M.T. Gandolfi, R. Ballardini, S. Fanni, W.R. Browne, J.G. Vos, *Inorg. Chem.*, **2002**, 41, 2871.

51 J.G. Vos, *Polyhedron,* **1992**, 11, 2285

52 A.E. Kaifer, M. Gomez-Kaifer, *Supramolecular Electrochemistry*, **1999** Wiley-VCH, Weinheim, Germany.

53 W.R. Browne, F. Weldon, A. Guckian, J.G. Vos, *Collect. Czech, Chem. Commun,* **2003**, 68, 1467.

54 W.R. Browne, N.M. O'Boyle, W. Henry, A.L. Guckian, S. Horn, T. Fett, C.M. O'Connor, M. Duati, L. De Cola, C.G. Coates, K.L. Ronayne, J.J. McGarvey, J.G. Vos, *J. Am. Chem. Soc.,* **2005**, 127, 1229.

55 C.N. Banwell, E.M. McCash, *Fundamentals of Molecular Spectroscopy 4th Edition,* McGraw Hill, **1994**, Chapter 4.

56 E.I. Solomon, A.B.P. Lever, *Inorganic Structure and Spectroscopy, Vol. 1*, Wiley-VCH, Weinheim, Germany, **1999**, Chapter 7.

57 W.R. Browne, R. Hage, J.G. Vos, *Coord. Chem. Rev.,* **2006**, 250, 1653

58 C.G. Coates, T.E. Keyes, H.P. Hughes, P.M. Jayaweera, J.J. McGarvey, J.G. Vos, *J. Phys. Chem. A,* **1998**, 102, 5013.

59 G.D. Danzer, J.A. Golus, J.R. Kincaid, *J. Am. Chem. Soc.,* **1993**, 115, 8643.

60 J.S. Gardner, D.P. Strommen, W.S. Szulbinski, H. Su, J.R. Kincaid, *J. Phys. Chem. A,* **2003**, 107, 351.

61 C.G. Coates, P.L. Callaghan, J.J. McGarvey, J.M. Kelly, P.E. Kruger, M.E. Higgins, *J. Raman Spect.* **2000**, 31, 283.

62 T.E. Keyes, C.M. O'Connor, U. O'Dwyer, C.G. Coates, P. Callaghan, J.J. McGarvey, J.G. Vos, *J. Phys. Chem. A*, **1999**, 103, 8915.

63 R.F. Dallinger, W.H. Woodruff, *J. Am. Chem. Soc.,* **1979**, 101, 4391.

64 P.G. Bradley, N. Kress, B.A. Hornberger, R.F. Dallinger, W.H. Woodruff, *J. Am. Chem. Soc.,* **1981**, 103, 7441.

65 D.P. Strommen, P.K. Mallick, G.D. Danzer, R.S. Lumpkin, J.R. Kincaid, *J. Phys. Chem.,* **1990**, 94, 1357.

66 P.K. Mallick, G.D. Danzer, D.P. Strommen, J.R. Kincaid, *J. Phys. Chem.,* **1988**, 92, 5628.

67 G.D. Danzer, J.R. Kincaid, *J. Phys. Chem.,* **1990**, 94, 3976.

68 D.J. Stufkens, T.L. Snoeck, A.B.P. Lever, *Inorg. Chem.*, **1988,** 27, 953.

Chapter 6

Experimental procedures

This chapter details the experimental methods and procedures used in this thesis. A brief description of the instrumentation involved in the measurements detailed in the previous chapters is also provided along with an explanation of the source and nature of the chemical materials used in these studies.

6.1 Materials and reagents

The synthetic reagents employed during the course of these studies were purchased from Sigma-Aldrich and no further purification was undertaken. All solvents used were of HPLC grade or better and used as received unless otherwise stated. The solvents utilised for spectroscopic and electrochemical studies were all of spectrophotometric grade. *Cis*-$Ru(bpy)_2Cl_2.2H_2O$ and its deuteriated analogue were synthesised via literature methods and obtained in a pure form from Complex Solutions (DCU).[1,2,,3] The ligand d_3-Hphpztr (Chapter *5*) was supplied and synthesised by Dr. Wesley Browne (DCU).

6.2 NMR Spectroscopy.

The ^{1}H-NMR and ^{1}H COSY spectra were recorded on a Bruker AC400 (400 MHz) NMR spectrometer. Deuteriated solvents (d_6-DMSO, d_6-acetone or d_3-acetonitrile) were employed for these measurements unless otherwise stated. The chemical shifts were recorded relative to TMS and spectra were converted from their free induction decay (FID) profiles using XWIN-NMR software.

6.3 Column chromatography

Column chromatography purification was performed on neutral alumina (Al_2O_3, 150 mesh). Generally, a 100 % solution of acetonitrile was used as the mobile phase. However, occasionally 5-10% MeOH was added in order to aid elution.

6.4 Absorption Spectroscopy

The UV/Vis spectra presented in this thesis were carried out on a Shimadzu *UV3100* UV/Vis-NIR spectrophotometer, which was interfaced to an Elonex *PC575* desktop computer. The spectra were obtained in the ultraviolet region in

the wavelength range 200 to 800 nm. The data obtained were initially acquired on a UVPC graphics program before being converted to an ASCII format and processed using Microcal Origin *6.0* software. All samples were measured in dichloromethane or acetonitrile in 1 cm path-length quartz cuvettes. The pH of the complexes was adjusted to 8.5 via the addition of triethylamine in order to obtain the deprotonated data.

6.5 Emission spectroscopy

The emission spectra presented in this thesis were obtained on a Perkin-Elmer *LS50B* luminescence spectrometer which was linked to a Dell *PC166* desktop computer. Low temperature measurements were taken at 77K by surrounding the samples in liquid nitrogen in a vacuumed cryostat environment. Excitation and emission slit widths of 10 nm were used for all measurements except at low temperature, where an emission slit width of 2.5 nm was used. All of the spectra were generated initially on Perkin-Elmer FL Winlab custom built software and were processed further using Microcal Origin *6.0* software. Room temperature measurements were carried out in dichloromethane or acetonitrile while at 77K measurement were performed in ethanol:methanol (4:1). The pH of the complexes was adjusted to 8.5 by the addition of triethylamine in order to generate the deprotonated data. All samples were prepared with an optical density of approximately 0.1 at the employed excitation wavelength in order to overcome the consequences of the inner filter effect.[4]

6.6 Emission quantum yield measurements

Quantum yield measurements were carried out in accordance with Parker and Rees' methodology.[5] $[Ru(bpy)_3]^{2+}$ was used as the reference and hence the reference and the sample were excited at a wavelength at which the absorption of $[Ru(bpy)_3]^{2+}$ and that of the sample were the same. The samples were all prepared with an optical density circa approximately 0.1 as concentrated samples can cause errors in these calculations and it is therefore necessary to examine the

emissions in the linear region where the concentration is proportional to the luminescence.[4] Emission quantum yields were evaluated by comparing areas under the corrected emission spectra according to the following equation:

$$\Phi_s = \frac{A_r F_s n_s^2}{A_r F_r n_r^2} \Phi_r \qquad \textbf{6. 1}$$

where $[Ru(bpy)_3]^{2+}$ has an established quantum yield (Φ_r) of 0.028 in aqueous, deoxygenated solution. *r* and *s* indicate reference and sample, *F* is the integrated area of the emission spectrum with the wavelength in cm^{-1}, A is the absorbance at the excitation wavelength, *n* is the refractive index of the solvent and Φ is the quantum yield of emission. The area under the emission spectrum of each sample was calculated using Microcal Origin 6.0 software and the relative quantum yield was hence calculated. Quantum yield measurements for the complexes in Chapter's 2 and 3 were carried out in dichloromethane. The quantum yields were calculated using Equation 6. 1 with values of 1.424 and 1.344 for the refractive indices of dichloromethane and acetonitrile. Measurements in Chapter 4 were obtained in acetonitrile and therefore it was not necessary to correct for the refractive index of the solvent.

6.7 IR Spectroscopy

Infra red spectra were recorded on a Perkin Elmer 2000 FT-IR spectrometer in 0.1 mm sodium chloride liquid solution cells. Spectra were recorded in spectroscopic grade THF. Measurements were also performed in 2 % (v/v) triethylamine in THF in order to generate spectra for the deprotonated complexes.

6.8 Acid-Base measurements

All ground state and excited state pK_a measurements reported in this thesis were carried out in aqueous Britton-Robinson buffer. The samples were firstly

dissolved in a small amount (~ 0.5 ml) of acetonitrile prior to dilution in the buffer solution. pH adjustments were made by adding 75 μl of 2 M NaOH or 2 M H_2SO_4 to a 100 cm^3 volume of the dissolved complex. The pH of the solution was monitored using a Corning 240 digital pH meter. Absorption and emission spectra were accordingly obtained over a range of pH values. The pK_a was determined from the changes in the absorption spectra of the complexes examined using the Henderson-Hasslebach equation (Equation 6. 2).[6] A plot of change in absorbance against pH results in a sigmoidal shaped curve with only one inflection point. The pH inflection point (pH_i) is also the pK_a of the complex. The inflection points were determined from the best-fit sigmoidal curve calculated using Microcal Origin *6.0* software.

$$pH = pK_a + \log_{10}([HA]/[A^-]) \qquad \textbf{6. 2}$$

Isobestic points from the absorption spectra indicated a wavelength value at which the concentrations of both the protonated and deprotonated species are equal. These values were subsequently used as the excitation wavelengths for determination of the excited state pK_a (pK_a^*). A plot of emission against pH results in a curve which allows the excited state inflection point (pH_i^*) to be determined. The inflection points (pH_i^*) were determined from the best-fit sigmoidal curve calculated using Microcal Origin *6.0* software.

$$pK_a^* = pH_i^* + \log(\tau_a/\tau_b) \qquad \textbf{6. 3}$$

Unlike the ground-state titrations, pH_i^* does not equal pK_a^*. This is due to the protonated and deprotonated species having different luminescence lifetimes. The pK_a^* can be calculated from pH_i^* and the lifetimes of the protonated (τ_a) and deprotonated (τ_b) species using Equation 6.3.[7]

$$pK_a^* = pK_a + \{0.625(\nu_b - \nu_a)/T\} \qquad \textbf{6. 4}$$

Another method of calculating pK_a^* is with Försters equation, as detailed in Equation 6. 4.[8] Försters equation relates pK_a^* to the ground-state pK_a and the emission maxima (in wavenumbers) of the protonated (ν_a) and deprotonated (ν_b) species for a given temperature, T.

6.9 Luminescence lifetimes

Transient emission data were generated using a Q-switched Nd-YAG spectrum laser system. The data were plotted and analysed with the aid of Sigma Plot 8.0 software. All measurements were obtained in acetonitrile or dichloromethane at room temperature and EtOH / MeOH 4:1 (v/v) at 77 K. Samples were prepared with an optical density of 0.4 absorption units in order to counteract the consequences of the inner filter effect. The lifetimes were calculated at the emission maxima. The pH was controlled via the addition of either triethylamine (TEA) or trifluoroacetic acid (TFA). When necessary solutions were degassed by bubbling argon through the solution for 15 minutes.

6.10 Single Photon Counter

The lifetimes of samples (< 100 ns) were determined using an Edinburgh Instruments nf900 ns flashlamp interfaced to a CD900 TAC photon counter in DCU with assistance from Dr.'s Fiona Killard and Andrea McNally. The samples were excited using 337 nm as excitation wavelength and the lifetimes were collected in the maxima of the emission. Samples were degassed by bubbling argon through the sample for 15 minutes Lifetime errors are estimated to be less than 8 %.

6.11 Electrochemical measurements

Cyclic voltammetry (CV) was carried out using a CH Instruments CHI Version 2.07 software controlled potentiostat (CH Instruments Memphis 660). CV's of the complexes from Chapter's 2, 3 and 4 were obtained in a 0.1 M solution of

tetrabutylammonium tetrafluoroborate ($TBABF_4$) in anhydrous acetonitrile. The solution was purged with N_2 (10 min) and a N_2 atmosphere was maintained throughout the experiment. The three electrodes employed consisted of a platinum disc (working, 2 mm diameter), platinum wire (counter) and an Ag/Ag^+ (acetonitrile + 10 mM $AgNO_3$ + 0.1 M $TBABF_4$) half-cell reference. The instrument was calibrated using the Fc/Fc^+ couple at an equivalent molarity to the sample being tested.

Measurements of the complexes from Chapter 5 were carried out in anhydrous acetonitrile with 0.1 M TEAP as the supporting electrolyte. Tetraethylammoniumperchlorate (TEAP) was prepared by dissolving a 1 M of TEAB (tetraethylammoniumbromide) in water. Perchloric acid was added dropwise until precipitation of the white perchlorate salt ceased. The product was collected by filtration and redissolved in hot water, neutralised with NaOH and then recrystallised from hot water. A 3 mm glassy carbon electrode encased in Teflon was used as the working electrode, a platinum wire as the counter electrode and a saturated calomel electrode (SCE) was utilised as the reference electrode. A platinum wire was used as the reference electrode. Each sample was deaerated prior to scanning and a N2 atmosphere was maintained throughout the measurement.

Extensive pre-treatment of the working electrodes were preformed prior to each CV. Pre-treatment generally consisted of polishing of the electrode surface with decreasing grades of alumina polish (1 μm, 0.5 μm) in distilled water with finely graded polishing pads in a figure of eight motion. Excess alumina particles on the surface of the electrodes were removed by sonication in distilled water for 10 min periods. The electrodes were then allowed to air dry. A CV of the solvent was obtained prior to each electrochemical measurement in order to ensure that all the peaks noted in the CVs were due to the sample being examined.

6.12 Elemental analysis

C, H, N elemental analysis was carried out at the Microanalytical Laboratory of University College Dublin. These analyses were obtained using an Exador analytical CE440 instrument.

6.13 Mass Spectrometry

Mass spectra were carried out by Mr. Maurice Burke at the National Centre for Sensor Research at Dublin City University. The spectra were recorded with a Bruker-EsquireLC_00050 electrospray ionisation mass spectrometer.

6.14 Resonance Raman measurements

Resonance Raman measurements were carried out with Dr. Wesley Browne in Queens University Belfast. Ground-state spectra were obtained using a Spectra Physics Argon Laser at 457 nm, 514 nm, 532 nm and 514.5 nm. Samples were held in an NMR tube and spun to reduce localised sample heating and thermal decomposition. All measurements were carried out in d_3-acetonitrile, unless otherwise stated. Protonation of samples was achieved using trifluoroacetic acid.

6.15 Bibliography

1 E. C. Constable, J. Lewis, *Inorg. Chem. Acta.,* **1983,** 70, 251.

2 B. P. Sullivan, D. J. Salmon and T. J. Meyer, *Inorg Chem.*, **1978**, 17, 3334.

3 W. R. Browne, C. M. O'Connor, J. S. Killeen, A. L. Guckian, M. Burke, P. James, M. Burke, J. G. Vos, *Inorg. Chem.*, **2002**, 41, 4245.

4 J.R. Lakowicz, *Principles of Fluorescence Spectroscopy, Second Edition,* Kluwer Academic Publications, New York.

5 C.A. Parker and W.T. Rees., *Analyst*, **1960**, 85, 587.

6 P. W. Atkins, *General Chemistry, International Student Edition*, **1989**, Scientific American Books, New York.

7 J. F. Ireland and P. A. H. Wyatt, *Adv. Phys. Org. Chem.*, **1976**, 12, 131

8 J. G. Vos, *Polyhedron* **1992**, 11, 2285.

Chapter 7

Conclusions and future work

This chapter summaries the synthetic work presented in this thesis. The properties of the mononuclear and dinuclear complexes are reviewed with suggestions of future studies, which might answer queries arising from this work.

7.1 Conclusions

Chapter 1 provides an introduction to the area of supramolecular chemistry. The topics discussed in Chapter 1 have been limited to those that are relevant to this thesis as the area of inorganic and supramolecular chemistry is now so large. The development of this area of chemistry is outlined and its relevance to this thesis is highlighted. The "parent" complex of many of the complexes discussed in this thesis [$Re(CO)_3(bpy)Cl$] is introduced, and its importance to the area of inorganic chemistry is highlighted. The thesis can be divided in to two projects. The first involves the synthesis and characterisation of a series rhenium(I) tricarbonyl complexes and is discussed in Chapters 2, 3 and 4. The second project (Chapter 5) studies the methylation of a ruthenium(II) pyrazyl-triazole complex.

In Chapter 2, a range of substituted pyridyl-triazole ligands were synthesised. The complexes of these ligands were also prepared and characterised by spectroscopic and electrochemical means. It was found that the properties of the pyridyl triazole complexes are altered when compared with those of [$Re(CO)_3(bpy)Cl$], the traditional rhenium(I) polypyridyl photosensitiser. These new complexes were found to have interesting pH dependent properties, due to the presence of the triazole. In both the protonated and deprotonated forms of the pyridyl-triazole complexes the absorption and emission maxima are blue-shifted with respect to [$Re(CO)_3(bpy)Cl$]. This is attributed to the change in the σ-donor nature of the triazole compared to 2,2-bipyridyl. With the exception of [$Re(CO)_3(Hthpytr)Cl$] and the deprotonated form [$Re(CO)_3(thpytr)Cl]^-$ (at 77 K) the emitting level was labelled as ^{3}MLCT in character for all of the pyridyl-triazole complexes. Ground and excited state pKa studies on two of the complexes also reach the same conclusion. For the complexes [$Re(CO)_3(Hthpytr)Cl$] and [$Re(CO)_3(thpytr)Cl]^-$ at 77 K, the emitting level has mixed MLCT and LC character. In addition, the oxidation potential of the rhenium(I) centre in each of the pyridyl-triazole complexes has been reduced significantly with respect to [$Re(CO)_3(bpy)Cl$].

A similar series of ligands and complexes based on pyrazyl-triazoles was also prepared and characterised in Chapter 3. The presence of the strongly π-accepting pyrazine results in a red shift of both the absorption and emission spectra when compared to the corresponding pyridyl-triazole complexes. Luminescent lifetime measurements indicate that the excited state is classed as a ^{3}MLCT emitter at both 77 and 298 K. Again, pH dependent properties were found. Deprotonation of the triazole results in a blue shift of the absorption and emission maxima. pK_a titrations showed a an increase in the pK_a in the excited state, pointing to the fact that the excited state is located on the pyrazyl-triazole. Longer lifetimes were observed for the deprotonated complexes with respect to the protonated forms. This behaviour was attributed to inefficient population of the non-radiative ^{3}MC excited state as a result of the enhanced σ-donor ability of the deprotonated form. From the electrochemical studies, it was seen that the oxidation potential of the metal centre is generally ~ 200mV higher for the pyrazyl-triazole complexes when compared to the analogous pyridyl-triazole complexes. This is due mainly to the weaker σ-donor/stronger π-acceptor properties of pyrazine over pyridine.

Chapter 4 details the synthesis of a mononuclear rhenium(I) complex, a homo-nuclear rhenium(I) dinuclear complex and hetero-nuclear ruthenium(II)-rhenium(I) dinuclear complex, all containing the Hbpt ligand. The complexes were characterised by IR and ^{1}H NMR spectroscopy. The complexes exhibited three bands in the carbonyl region of the IR spectra. Assignment of proton resonances in the ^{1}H NMR spectra of the mononuclear rhenium(I) and the homo-nuclear rhenium(I) dinuclear complex complexes were made by comparison with the pyridyl-triazole complexes synthesised in Chapter 2 and with the aid of two dimensional (COSY) techniques. The characterisation of the ruthenium(II)-rhenium(I) dinuclear complex was complicated by the fact that two isomers were formed. Assignment of the bpt$^-$ protons in the ^{1}H NMR of the ruthenium(II)-rhenium(I) dinuclear complex was aided by deuteriation of the 2,2'-bipyridyl rings. ^{1}H NMR studies suggest that the formation of isomers may be due to the different orientation of the bipyridyl ligands coordinated to the ruthenium metal centre. The photophysical properties of the mononuclear and dinuclear

complexes were also studied. Upon coordination of a second metal fragment i.e. $Re(CO)_3Cl$ to the mononuclear complexes, the absorption and emission maxima are blue shifted. For all of the complexes, the emitting level was labelled as ^{3}MLCT in character. In the case of the mono- and dinuclear rhenium(I) complexes, the excited state is located on the triazole ligand. However, for the ruthenium(II)-rhenium(I) dinuclear complex, the excited state is located on the bipyridyl ligand. This assignment is based on the following properties:

(i) The structured emission spectrum at 77 K is similar to that of the bipyridyl based emitting mononuclear complex $[Ru(bpy)_2bpt]^+$

(ii) A significant increase in the lifetime is observed at 298 K and 77 K when the bipyridyl ligands are deuteriated

(iii) The first reduction potential of the complex is bpy-based

For the ruthenium(II)-rhenium(I) complex, the absorption and emission properties indicate intercomponent energy transfer from the rhenium(I) metal centre to the ruthenium(II) metal centre.

Chapter 5 discusses the methylation of the ruthenium(II) bipyridyl complex $[Ru(bpy)_2phpztr]^+$, where phpztr is 3-(pyrazin-2-yl)-5-phenyl-1,2,4-triazole. The ^{1}H NMR spectrum of the methylated complex shows only one set of signals, thus indicating the presence of one isomer. Assignments of the protons in the ^{1}H NMR of the methylated complex were aided by partial deuteriation of the 2,2'-bipyridyl and the pyrazine rings. ^{1}H NMR studies indicate that methylation has occurred on the pyrazine ring. The photophysical and electrochemical properties of all complexes were also examined. The absorption maximum of the methylated complex was red shifted with respect to that of $[Ru(bpy)_2phpztr]^+$. Methylation of the pyrazyl-triazole ligand was found to quench emission from $[Ru(bpy)_2phpztr]^+$. This behaviour was attributed to efficient population of the non-radiative ^{3}MC excited state as a result of the enhanced π-acceptor ability of the methylated complex. Wavelength dependent ground-state resonace Raman studies were also carried out in order to elucidate the electronic transitions in the absorption spectra.

With excitation at 532 nm, a wavelength nearly coincident with the maximum of the low energy electronic transition of the methylated complex, modes associated with the coordinated pyrazyl-triazole ligand are selectively enhanced. Such behaviour provides convincing evidence for assignment of this lower energy electronic transition to that associated with an [Ru $\rightarrow$ π^*(pyrazyl-triazole)] transition. Although there is a general increase in the intensities of bpy associated modes in the spectra acquired with progressively higher energy excitations (i.e. 514.5 nm and 457.9 nm), it is clear that several of the pyrazyl-triazole modes are also enhanced with these excitation wavelengths. The effect of pH on the ^{1}H NMR and absorption spectra of the methylated complex was also examined. Loss of the methyl group was observed at high pH. Electrochemical studies indicate the oxidation potential of the methylated complexe is 190 mV higher than that found in the unmethylated complex $[Ru(bpy)_2(phpztr)]^+$, thus indicating that the methylated product $[Ru(bpy)_2(Mephpztr)]^{2+}$ contains a weaker σ-donor ligand. Chapter 6 provides details of experimental procedures used in this thesis.

7.2 Future work

Chapter 2:

Longer lifetimes were observed for the deprotonated complexes with respect to the protonated forms. This behaviour was attributed to inefficient population of the non-radiative ^{3}MC. Temperature dependent lifetime and emission studies in both acidic and basic media of these complexes should be carried out in order to ascertain the role of the ^{3}MC state. Emission was detected from both the ^{3}MLCT and $^3\pi\pi^*$ states for $[Re(CO)_3(Hthyptr)Cl]$ and $[Re(CO)_3(thyptr)Cl]^-$. Time-resolved IR and resonance Raman studies should be carried out in order to confirm the exact nature of the dual emission observed in $[Re(CO)_3(Hthyptr)Cl]$ and $[Re(CO)_3(thyptr)Cl]^-$.

Chapter 3:

Temperature dependent lifetime studies should be carried out in order to establish the non-radiative decay paths in the pyrazyl-triazole complexes. Time resolved resonance Raman studies should be conducted in order to ascertain if the excited state is localised over the pyrazyl-triazole ligand or the pyrazine moiety.

Chapter 4:

The separation of the isomers of $[Ru(d_8\text{-bpy})_2(bpt)Re(CO)_3Cl]^+$ and $[Ru(bpy)_2(bpt)Re(CO)_3Cl]^+$ using chromatograpy should be explored. For the ruthenium(II)-rhenium(I) dinuclear complex, the excited state is located on the bipyridyl ligand. In order to unambiguously define the location of the excited state, further studies, such as resonance Raman spectroscopy are necessary.

Chapter 5:

No crystals of the methylated complexes suitable for X-ray analysis were obtained. Future work in this area is recommended to confirm the location of the methyl group on the pyrazine ring. DFT studies in order to compared the electronic structure of the methylated complex with that of the unmethylated complex.

Appendix A Dinuclear ruthenium(II)/tungsten(0) tetracarbonyl complexes

A.1 Synthesis

In this section the attempted synthesis of two new dinuclear $[Ru(bpy)_2LW(CO)_4]$ type complexes (where bpy = 2,2'-bipyridyl; L = 3-(pyrazin-2-yl)-5-(pyridin-2-yl)-1,2,4-triazole or 3-bis-(2-pyridyl)-pyrazine) are described. The structures and abbreviations for the ligands and complexes cited in this section are shown in

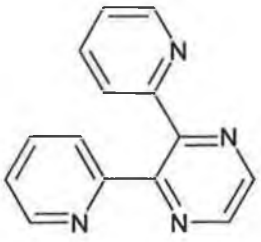

2,3-bis-(2-pyridyl)-pyrazine
2,3-dpp

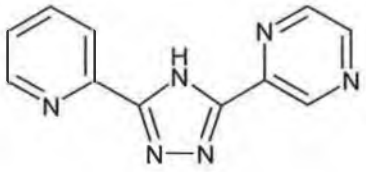

3-(pyrazin-2-yl)-5-(pyridin-2-yl)-1,2,4-triazole
Hppt

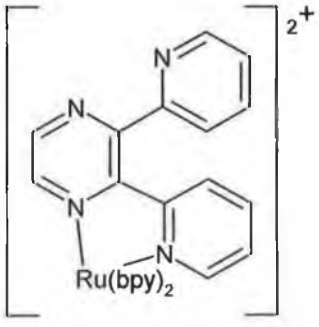

$[Ru(bpy)_2(2,3\text{-}dpp)]^{2+}$

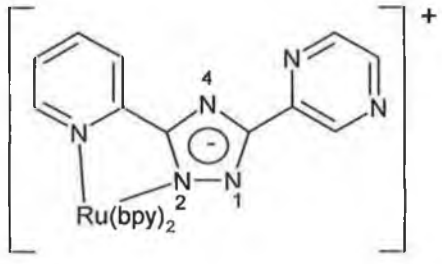

$[Ru(bpy)_2(ppt)]^{+}$

Figure A. 1 *Structures of the ligands and complexes as cited throughout this section.*

A.1.1 Preparation of the ligands

The syntheses of the ligands were carried out following literature methods. The synthetic method followed for the synthesis of the 2,3-dpp ligand was similar to that of Case and coworkers.[1] Synthesis of the Hppt ligand was carried out according to the procedure adopted by Dr. Christine O' Connor.[2] Other routes for the synthesis of this ligand exist but were not investigated.

A.1.2 Preparation of the mononuclear complexes

The mononuclear complex $[Ru(bpy)_2(2,3\text{-dpp})]^{2+}$ was prepared following literature procedures.[3] A stirring suspension of $[Ru(bpy)_2Cl_2].2H_2O$ in ethanol/water (2/1 v/v) was slowly added to the a 2 fold excess of the 2,3-dpp ligand in ethanol. The reaction mixture was refluxed for eight hours. Solvent was removed and the resulting material was dissolved in the minimum amount of acetone/water (2/1 v/v). Purification was carried out on a Sephadex C-25 ion exchange column. The chloride form of the complex was eluted with 0.1 M NaCl. The complex was precipitated using NH_4PF_6 and then recrystallised from acetone/water (1/1 v/v).

The mononuclear complex $[Ru(bpy)_2(ppt)]^+$ (see Figure A. 1) was prepared by reacting the Hppt ligand in a 2:1 ratio with $[Ru(bpy)_2Cl_2].2H_2O$ according to a previously established procedure.[4] The $[Ru(bpy)_2(ppt)]^+$ mononuclear complexes form four different coordination isomers due to the various coordination sites of the Hppt ligand. Two of the isomers are bound via the N_4 of the 1,2,4-triazole and are formed in small amounts. The two major isomers are bound via the N_1 and N_2 of the triazole ligand.

---

1 F.H. Case, E. Koft, *J. Org. Chem.*, **1959**, 905.

2 C.M. O'Connor, PhD. Thesis, **2000**, Dublin City University.

3 G. Denti, S. Campagna, L. Sabatino, S. Serroni, M. Ciano, V. Balzani, *Inorg. Chem.*, **1990**, 29, 4750.

4 W.R. Browne, C.M. O'Connor, H.P. Hughes, R. Hage, M. Doering, J.F. Gallagher, J.G. Vos, *J. Chem. Soc., Dalton Trans,* **2002**, 4048

Recrystallisation of the crude product from acetone/water (2/1 v/v) yields the N_1 and N_2 isomers. The isomers were separated by column chromatography on a neutral alumina column. The N_2 isomer eluted off the column using 100% acetonitrile, while the N_1 isomer eluted off using 100% methanol. The N_2 isomer was subsequently recrystallised from water:acetone (1:1). 2 M NaOH was added to this solution to ensure the triazole ligand was fully deprotonated. Since this study is concerned with the N_2 isomer of $[Ru(bpy)_2(ppt)]^+$, the purification and characterisation of the N_1 isomer will not be discussed any further.

A.1.3 Preparation of the dinuclear complexes

A solution of dry THF was purged with argon in a photolysis well. $W(CO)_6$ was dissolved in the THF and irradiated with UV light from a Hg lamp (see Figure A. 2). The reaction was followed by IR. The characteristic band of $W(CO)_6$ at 1978 cm^{-1} gradually disappeared and was replaced by bands at 2076, 1935 and 1900 cm^{-1}.

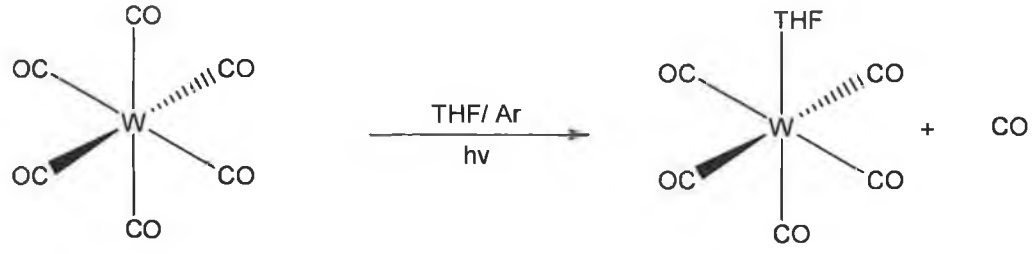

Tungsten Hexacarbonyl

Figure A. 2 *Reaction of tungsten hexacarbonyl with THF.*

The heteronuclear complexes $[Ru(bpy)_2(2,3\text{-dpp})W(CO)_4]^{2+}$ and $[Ru(bpy)_2(ppt)W(CO)_4]^+$ were prepared by reacting molar equivalents of the mononuclear ruthenium complex and $W(CO)_5THF$ under an argon atmosphere. The reaction was monitored using IR spectroscopy. The reaction was complete when there was no evidence of any $W(CO)_5$ in the IR spectrum. Note the reactions were protected from sunlight in order to eliminate photodecomposition.

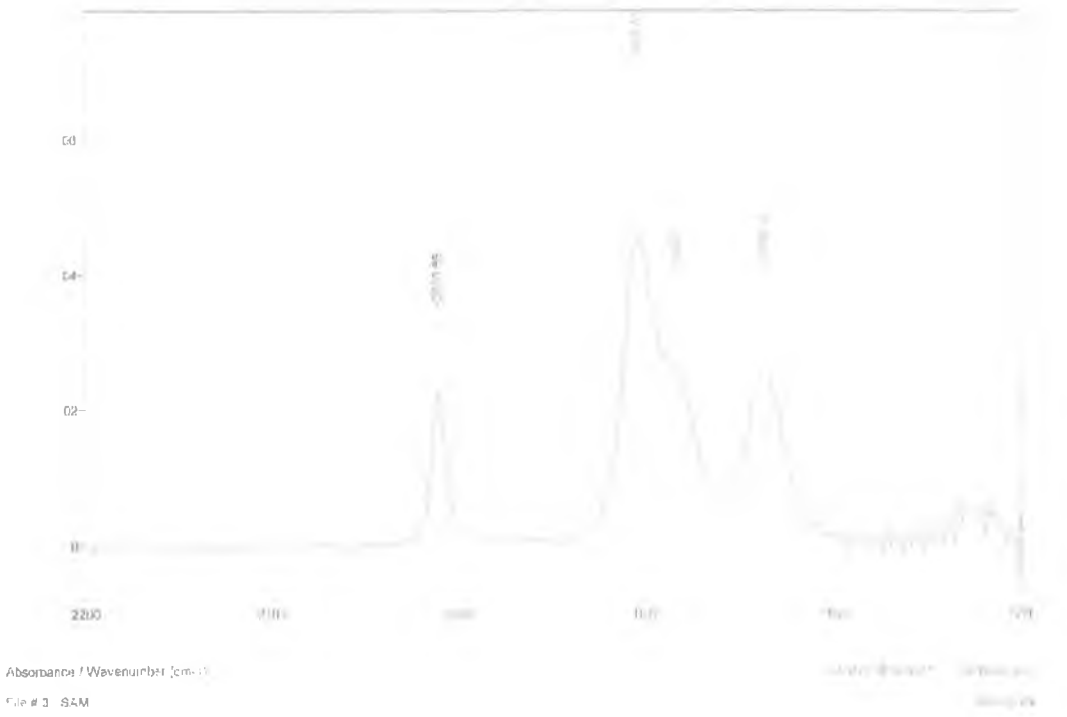

Figure A. 3 *IR spectrum (CO-stretching region) of* $[Ru(bpy)_2(2,3\text{-dpp})W(CO)_4]^{2+}$ *in THF at 298 K.*

Complex	$\nu_{(CO)}$ cm^{-1}			
$[Ru(bpy)_2(2,3\text{-dpp})W(CO)_4]^{2+}$	2010	1902	1883	1836
$[Ru(bpy)_2(ppt)W(CO)_4]^{+}$	2012	1900	1880	1830

Table A. 1 *IR data for the carbonyl stretching of the metal complexes. All measurements are in THF.*

The IR spectral data of the complexes in THF are presented in Table A. 1. Figure A. 1 shows the IR spectra of $[Ru(bpy)_2(2,3\text{-dpp})W(CO)_4]^{2+}$ The CO bands in these spectra are typical of the dinuclear complexes synthesised in this section. The formation of the

pentacarbonyl complexes $[Ru(bpy)_2(2,3\text{-dpp})W(CO)_5]^{2+}$ and $[Ru(bpy)_2(ppt)W(CO)_5]^{+}$ was anticipated, however the IR spectra in the carbonyl region show four CO stretching frequencies characteristic of substituted tetracarbonyl complexes.[5,6] Figure A. 4 outlines the proposed structures of the tetracarbonyl complexes $[Ru(bpy)_2(2,3\text{-dpp})W(CO)_4]^{2+}$ and $[Ru(bpy)_2(ppt)W(CO)_4]^{+}$

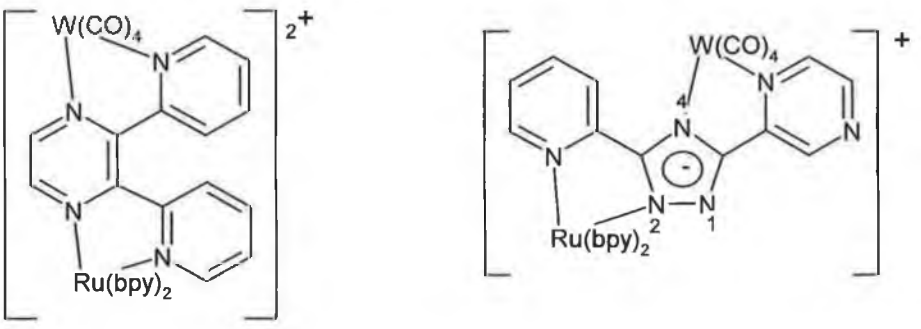

Figure A. 4 *Proposed structures of the dinuclear complexes* $[Ru(bpy)_2(2,3\text{-dpp})W(CO)_4]^{2+}$ *and* $[Ru(bpy)_2(ppt)W(CO)_4]^{+}$

^{1}H NMR spectra of the dinuclear complexes revealed the presence of unreacted starting material i.e. the mononuclear complex. Attempts to purify the complexes with an alumina column proved unsuccessful.

5 R.R. Ruminski, I. Wallace, *Polyhedron*, **1987**, 6, 1673.

6 M.H.B. Stiddard, *J. Chem. Soc.*, **1962**, 4712.

A.1.4 Experimental

A.1.4.1 Preparation of the ligands

2,3-bis-(2-pyridyl)-pyrazine

A solution of ethylenediamine (0.600 g; 0.010 mol) in ethanol (5 cm^3) was added slowly to a solution of 2,2'-pyridil (2.100 g; 0.010 mol) in ethanaol (30 cm^3). This solution darkened in colour. The mixture was refluxed for 1 hour. Pale yellow crystals separated on cooling. The yellow precipitate (2,3-bis-(2-pyridyl)-5,6-dihydropyrazine) was filtered and washed with cold ethanol. The 2,3-bis-(2-pyridyl)-5,6-dihydropyrazine in mesitylene (15 cm^3)was refluxed with 0.100 g of palladium/charcoal catalyst overnight. The mixture was filtered while hot. The product precipitated on cooling of the mesitylene and was collected under vacuum. The 2,3-bis-(2-pyridyl)-pyrazine was recrystallised from ethanol to yield a fine white powder. Yield: 0.770 g, 0.003 mol, 33 %. ^1H NMR (d_6-DMSO), δ in ppm : pyH_3: 7.84 (m); pyH_4: 7.84 (m); pyH_5: 7.33 (m); pyH_6: 8.23 (d); pzH_5: 8.77 (s)

3-(pyridin-2-yl)-5(pyrazin-2-yl)-1,2,4-triazole

15.000 g (0.12 mol) 2-pyrazylcarboxylic acid was dissolved in 90 cm^3 ethanol and 15 cm^3 concentrated H_2SO_4 and heated under reflux for 3 hours. The solution was neutralised with a saturated solution of Na_2CO_3 and then filtered to remove side products. Most of the ethanol was removed and the remaining solution was extracted with dichloromethane to yield a yellow product. The fractions were dried over $MgSO_4$. The dichloromethane was evaporated off to yield the ester, which crystallised after a few minutes. 9.600 g (0.063 mol) of the ester was reacted with an equimolar amount of hydrazine monohydrate. The ester was dissolved in ethanol and then dropped into the hydrazine monohydrate and the pyrazylhydrazide crystalised out overnight in the freezer (-4^0C). The pyrazylhydrazide was filtered and weighed. An equimolar amount of 2-cyanopyridine (as to the pyrazylhydrazide) was weighed out and dissolved in 30

cm^3 of methanol and 0.7 g sodium and was heated under reflux for 3 hours to form pyridyl-imidate. The pyrazylhydrazide was added to the solution and heated for 15 min. The precipitate (yellow intermediate) was heated under reflux for 1 hour in a minimal quantity of ethylene glycol to yield the Hppt ligand. The ligand (white) was recrystallised in hot ethanol. Yield: 5.600g, 0.025 mol, 21 %. ^{1}H NMR (d_6-DMSO), δ in ppm : (Pyrazine ring) H_3, 9.33 (s); H_5 and H_6, 8.72 (m); (Pyridine ring) H_3, 8.17 (d); H_4, 8.01ppm(t); H_5, 7.54 (t); H_6, 8.77 (d).

A.1.4.2 Preparation of the coordination complexes

$[Ru(bpy)_2(2,3\text{-}dpp)](PF_6)_2$

Cis-$[Ru(bpy)_2Cl_2].2H_2O$ (520 mg;1 mmol) and 2,3-dpp ligand (470 mg; 2 mmol) were heated under reflux for 8 hours in 40 cm^3 ethanol and 10 cm^3 water. The solution was evaporated to dryness and the residue then dissolved in the minimum amount of water:acetone 5:3 (v/v). The solution was chromatographed on a Sephadex-CM C-25 ion exchange column. Elution with 0.05 M NaCl yielded a pale brown fraction which was subsequently discarded. -$[Ru(bpy)_2(2,3\text{-}dpp)]$ was eluted using 0.1 M NaCl solution. The solution was evaporated to dryness and the residue then dissolved in 10 cm^3 of water and precipitated by addition of aqueous NH_4PF_6. The complex was recrystallised in a mixture of acetone: water 2:1 (v/v). Yield 53 % (0.490 g; 0.524 mmol).

$[Ru(bpy)_2(ppt)]PF_6$

Cis-$[Ru(bpy)_2Cl_2].2H_2O$ (520 mg;1 mmol) and Hppt ligand (224 mg; 2 mmol) were heated under reflux for 8 hours in 40 cm^3 ethanol and 10 cm^3 water. The solution was evaporated to dryness and the residue then dissolved in 10 cm^3 water and precipitated by addition of aqueous NH_4PF_6. This resulted in a mixture of two isomers. The complex was recrystallised in a mixture of acetone: water 2:1 (v/v). The isomers were separated

by column chromatography on a neutral alumina column. The N_2 isomer eluted off the column using 100% acetonitrile, and the N_1 isomer eluted off using 100% methanol. Yield of combined fractions: 0. 444 g (48%).

A.1.4.3 Preparation of the dinuclear complexes

$W(CO)_5THF$ was obtained by photolysing 0.050 g (0.142 mmol) of tungsten hexacarbonyl in 250 cm^3 of dry THF under an argon atmosphere. The $W(CO)_5THF$ and an equimolar amount of the appropriate metal complex were stirred under argon. As the reaction time progressed the colour of the solution changed from orange to deep purple. The reaction was complete when there was no evidence of any $W(CO)_5$ in the IR spectrum. Attempts to purify the complexes with an alumina column and acetonitrile as eluent proved unsuccessful.

Appendix B Poster Presentations

"Methylation of Coordinated Ruthenium Triazole Complexes."
Poster presentation: 55th Irish Universities Colloquium, University of Limerick, June 2004.

"Synthesis and Characterisation of Rhenium Triazole Complexes."
Poster presentation: 3rd Euchem Conference on Nitrogen Ligands in Organometallic Chemistry and Homogeneous Catalysis, Camerino, Italy, September 2004.

"Synthesis and Photophysical properties of Rhenium and Ruthenium Triazole Complexes."
Poster presentation: 16th International Symposium on the Photophysics and Photochemistry of Coordination Compounds, California, July 2005.

Methylation of Coordinated Ruthenium Triazole Complexes

C. Brennan[a], M. T. Pryce[a], J.G. Vos[a], W.R. Browne[b], J.J. McGarvey[c]

[a]School of Chemical Sciences / NCSR, Dublin City University, Dublin 9, Ireland
[b]Department of Organic and Molecular Inorganic Chemistry, University of Groningen, Groningen, The Netherlands
[c]School of Chemistry, Queen's University Belfast, Belfast, Northern Ireland

It is well known that Ruthenium(II) polypyridyl complexes are particularly suitable for the construction of supramolecular assemblies for the development of photochemically driven molecular devices. The spectroscopic, photochemical and electrochemical properties of these types of complexes can be both manipulated and tuned synthetically. In this contribution, direct methylation of Ruthenium (II) triazole complexes are discussed.

Results and Discussion

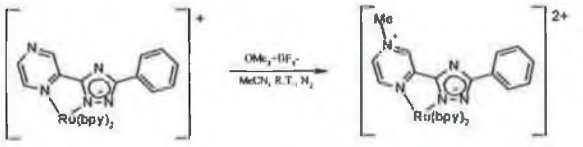

Fig.1: Reaction and conditions employed for the methylation of $[Ru(bpy)_2(phpztr)]^+$ (phpztr = 2-(5-Phenyl—[1,2,4]triazol-3-yl)-pyrazine).

Complex	UV/Vis λ_{max} (nm)	Emission (298 K) λ_{max} (nm)	Ru(II)/Ru(III) (ΔE_a, V)	Reduction (ΔE_a, V)
$[Ru(bpy)_2(Mephpztr)]^{2+}$	545	-	1.14	-0.48 -1.44 -1.71
$[Ru(bpy)_2(phpztr)]^+$	453	670	0.93	- -1.45 -1.65
$[Ru(bpy)_2(Hphpztr)]^{2+}$	440	650	1.09	Not observed

Table 1: UV/vis, emission and electrochemical data for all compounds in this study (UV/vis measurements were obtained in acetonitrile, electrochemical measurements were carried out in 0.1 M TEAP).

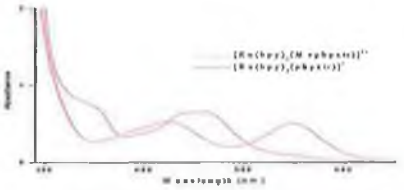

Fig.2: Electronic absorption spectra in acetonitrile at 298 K.

Outlined in figure 1 are the complexes synthesised and characterised in this study. Methylation of the pyrazine ring has the ability to lower the π^* acceptor orbitals on the pyrazine moiety. Interestingly the low energy ^{1}MLCT band on $[Ru(bpy)_2(Mephpztr)]^{2+}$ is red shifted compared to the starting material $[Ru(bpy)_2(phpztr)]^+$ (table 1 and figure 2). Methylation of the pyrazine ring is proposed from the electrochemical studies where an increase in the oxidation potential and a third reduction peak is observed for the methylated complexes relative to the starting material. The ground state resonance Raman studies indicate that the low energy ^{1}MLCT is pyrazine based (figure 4). The low energy ^{1}MLCT of the starting material $[Ru(bpy)_2(phpztr)]^+$ is predominently bipyridine based.[1] This suggests that the location of the ^{1}MLCT is switched from bipyridyl to pyrazine as a result of the methylation. The methylated complex $[Ru(bpy)_2(Mephpztr)]^{2+}$ has a pK_a of 10.04 (figure 3). This pK_a may be due to deprotonation of the methyl group. Further work is on going to confirm this interesting observation. In an earlier study by Fanni and co-workers using the same conditions and similar complexes, methylation occurred on the triazole ring.[2] Suprisingly in our study, methylation occurs at the pyrazine ring.

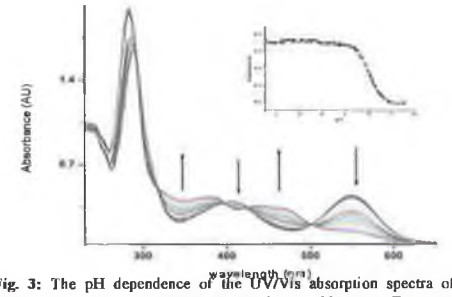

Fig. 3: The pH dependence of the UV/vis absorption spectra of $[Ru(bpy)_2(Mephpztr)]^{2+}$ in an aqueous Britton-Robinson Buffer at pH 6-11 (Inset, a plot of intensity v's increasing pH at 550 nm.)

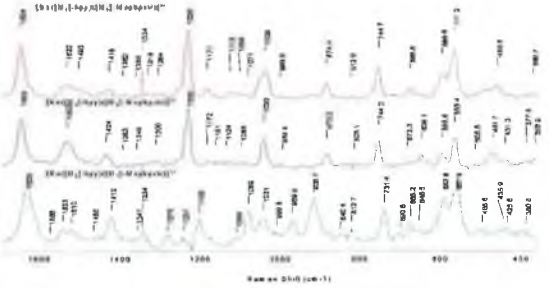

Fig. 4:Ground state resonance Raman spectra of $[Ru(bpy)_2(Mephpztr)]^{2+}$ and its isotopomers in H_2O at 532 nm.

References: 1) W.R. Browne, *PhD*., Thesis **2002**, Dublin City University
2) S. Fanni, S. Murphy, J.S. Kileen, J.G. Vos, *Inorg. Chem*., **2000**, 39, 1320

Acknowledgements: We would like to thank Enterprise Ireland, the HEA and Louth County Council for financial support

Synthesis and Characterisation of Rhenium Triazole Complexes.

C. Brennan, M. T. Pryce, J.G. Vos

School of Chemical Sciences/ National Centre for Sensor Research
Dublin City University, Dublin 9, Ireland
e-mail: claire.brennan5@mail.dcu.ie

Introduction

Rhenium(I) carbonyl polypyridyl complexes have received much interest because of their spectroscopic, photophysical, photochemical and electrochemical properties. These properties are of particular use in the construction of supramolecular assemblies and in the development of photochemically driven molecular devices. In this contribution the synthesis and characterisation of a series of rhenium complexes containing triazole ligands (*figure 1*) are discussed.

Structures

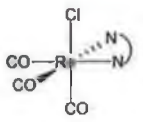

fac-[Re(CO)$_3$Cl(1,2,4-triazole)]

Where N-N is:

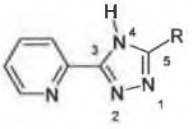

L_1 R=H (Hpytr)

L_2 R=phenyl (Hphpytr)

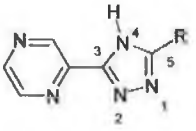

L_3 R=H (Hpztr)

L_4 R=phenyl (Hphpztr)

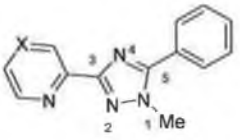

L_5 X=CH (Mephpytr)

L_6 X=N (Mephpztr)

Fig.1:Structures of the complexes synthesised.

Synthesis

Outlined in figure 1 are the structures, numbering and abbreviations of the ligands presented in this study. The complexes under investigation were synthesised by reacting [Re(CO)$_5$Cl] with an equimolar amount of the ligand in toluene for 4 hours at reflux temperature. In principle two coordination modes are possible for the triazole ligands, i.e. through the N_2 or the N_4. Surprisingly ^{1}H NMR studies showed evidence for only one isomer. Furtherwork is ongoing to confirm which nitrogen on the triazole ligand is coordinated to the rhenium centre.

References

1) G.J. Stor *et al, Organometallics*, **1994**, 2641

2) D.J. Stufkens, A. Vlcek Jr., *Coord. Chem. Rev.*, **1998**, 127

3) I. Costa, *et al, J. Organomet. Chem.*, **2000**, 267

Spectroscopic Data

Complex	ν_{CO}(cm^{-1})[a]	λ_{abs} (nm)	λ_{em} (nm)	τ (ns)	λ_{em} (nm)	τ (μs)
[Re(CO)$_3$Cl(L$_1$)]	2020, 1917, 1893	390	600	5.4	530	2.38
[Re(CO)$_3$Cl(L$_2$)]	2021, 1917, 1892	330	580	51	493	9.35
[Re(CO)$_3$Cl(L$_3$)]	2023, 1922, 1894	355	559	29	497	5.25
[Re(CO)$_3$Cl(L$_4$)]	2026, 1926, 1898	390	-	-	530	4.85
[Re(CO)$_3$Cl(L$_5$)]	2027, 1928, 1901	395	570	50	540	6.43
[Re(CO)$_3$Cl(L$_6$)]	2023, 1918, 1890	350	537	735	489	16.17
[Re(CO)$_3$Cl(L$_6$)]	2026, 1927, 1898	395	625	149	540	9.74

Table 1 Spectroscopic data for the [Re(CO)$_3$Cl(1,2,4-triazole)] complexes. Data for [Re(CO)$_3$Cl(bpy)] is included for comparison. [a]Data in THF, [b]In dichloromethane and in [c]ethanol:methanol 4:1.

Discussion of Results

The spectroscopic data of the complexes synthesised and characterised are presented in table 1. The IR frequencies are consistent with the facial isomer for all complexes studied.[1] Absorption and emission spectra of [Re(CO)$_3$Cl(L$_2$)] are shown in *figure 1*. The absorption spectra are similar to those already published for similar Re complexes.[2] Hence the lowest energy absorption band is assigned to the MLCT transition [Re→Lπ^*]. This low energy ^{1}MLCT band is clearly sensitive to the nature of the polypyridine ligand as the band on the pyrazine triazoles are red shifted relative to the analagous pyridine complexes as pyrazine has lower π^* orbitals. This is reflected in the shifts in the CO bands for the *fac*-[Re(CO)$_3$Cl] moieties. For example the high frequency band at 2021 cm^{-1} present in the IR spectrum of [Re(CO)$_3$Cl(L$_1$)] shifts to 2026 cm^{-1} in the pyrazine equivalent [Re(CO)$_3$Cl(L$_2$)]. All of the complexes with the exception of [Re(CO)$_3$Cl(L$_2$)] luminesce at 298K and 77K. [Re(CO)$_3$Cl(L$_1$)] is found to only emit at 77K. The emitting level can be labelled as ^{3}MLCT in character as the position and shape of the emission band is consistent with that previously reported for similar complexes assigned as MLCT emitters.[3]

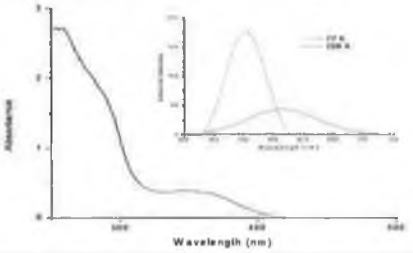

Fig.2: Absorption and Emission spectra of [Re(CO)$_3$Cl(L$_2$)]

Acknowledgements

We would like to thank Enterprise Ireland and Louth County Council for financial assistance.